UNIVERSITÄT
DUISBURG
ESSEN

Open-Minded

Analysis of biomarkers in liquid biopsies for prognostic and diagnostic testing in patients with retinoblastoma and uveal melanoma

Inaugural-Disseration

zur Erlangung des Doktorgrades

Dr. rer. nat.

der Fakultät für

Biologie

an der

Universität Duisburg-Essen

vorgelegt von

Nicole Barwinski

aus Essen

Dezember 2022

DOI: 10.17185/duepublico/78361
URN: urn:nbn:de:hbz:465-20230519-070730-7

Die der vorliegenden Arbeit zugrunde liegenden Experimente wurden am Institut für Humangenetik der Universität Duisburg-Essen und in der Kinderklinik III des Universitätsklinikums Essen durchgeführt.

1. Gutachter: Prof. Dr. Dietmar Lohmann

2. Gutachterin: Prof^{in}. Dr^{in}. Anke Hinney

Vorsitzender des Prüfungsausschusses: Prof. Dr. Ralf Küppers

Tag der mündlichen Prüfung: 19.04.2023

Die Arbeit muss Spaß machen. Dann wächst man in fast jede Aufgabe hinein.

Hans-Dietrich Genscher

Für meine Eltern und meinen Mann.

Table of Contents

1 Introduction

1.1 The biomarker concept

1.1.1 Definition

The field of biomarker research is wide and has experienced a growing interest in recent years. A search in the NIH *RePORT* database with the keyword "biomarker" resulted in 107,785 projects funded with more than 58 billion dollars in total and around 1.2 million publications (accessed under http://projectreporter.nih.gov/reporter.cfm on 30th of August 2022).

Interest in biomarker research has increased in diverse medical fields, raising the need for standardized terminology (Ptolemy and Rifai 2010; Califf 2018). In 2016, the FDA and NIH of the United States founded a biomarkers definitions working group, a task force to develop a definition of biomarkers and any related terms. This group published a resource called BEST (Biomarkers, EndpointS, and other Tools), wherein they define a biomarker as "A defined characteristic that is measured as an indicator of normal biological processes, pathogenic processes, or biological responses to an exposure or intervention, including therapeutic interventions. Biomarkers may include molecular, histologic, radiographic, or physiologic characteristics. A biomarker is not a measure of how an individual feels, functions, or survives." (FDA-NIH Biomarker Working Group 2016). The definition uses the term "characteristic", which is quite open and able to cover the diverse kinds of biomarkers that will be described in the next chapter in more detail. Biomarkers can be of qualitative (e.g. presence of a surface marker) or quantitative nature (e.g. the amount of extracellular vesicles).

The high number of projects and publications dealing with biomarkers emphasizes their important role in many diverse application fields (visualized in figure 1, page 15). A broad spectrum of biomarkers has already been identified, but the discovery of new biomarkers remains an integral part of the field intending to identify new targets for the early detection of cancer or other diseases like Alzheimer's. The results of biomarker testing are also used as input for machine learning. Algorithms are developed to investigate if certain biomarker signatures are associated with the activity or severity of diseases (Cirillo and Valencia 2019; Sharma et al. 2019; McIntyre et al. 2014). Of note, the field of clinical trials is already represented in biomarker research projects (see figure 1), and this highlights the contribution of biomarker testing for developing procedures in precision medicine. Another major part of the studies deals with biomarkers derived from characteristics of DNA. Often, the aim is to perform genetic profiling to develop a personalized treatment based on genetic variants or other features of the patient's genome. Plenty of biomarkers are already used in clinical settings for prediction, diagnosis, and treatment decisions. Especially for prevalent types of cancer like breast cancer, colon cancer, non–small cell lung cancer (NSCLC), or leukemia, several biomarkers are already used for decision-making in routine patient care (Selleck, Senthil, and Wall 2017).

Figure 1: Word Cloud of the fields of biomarker research. Generated from the results of the search on the NIH *RePORT* database with the keyword "biomarker" using the R package `wordcloud`.

1.1.2 Categories and sources of biomarkers

The FDA-NIH Biomarker Working group has developed a classification of biomarkers that is based on the intended use. With this goal-oriented perspective, they structured the huge variety of biomarker applications and identified seven different categories of biomarkers (FDA-NIH Biomarker Working Group 2016):

- susceptibility/risk biomarker: "A biomarker that indicates the potential for developing a disease or medical condition in an individual who does not currently have clinically apparent disease or the medical condition."
- diagnostic biomarker: "A biomarker used to detect or confirm presence of a disease or condition of interest or to identify individuals with a subtype of the disease."
- monitoring biomarker: "A biomarker measured repeatedly for assessing status of a disease or medical condition or for evidence of exposure to (or effect of) a medical product or an environmental agent."
- prognostic biomarker: "A biomarker used to identify likelihood of a clinical event, disease recurrence or progression in patients who have the disease or medical condition of interest."

- predictive biomarker: "A biomarker used to identify individuals who are more likely than similar individuals without the biomarker to experience a favorable or unfavorable effect from exposure to a medical product or an environmental agent."
- response biomarker: "A biomarker used to show that a biological response, potentially beneficial or harmful, has occurred in an individual who has been exposed to a medical product or an environmental agent."
- safety biomarker: "A biomarker measured before or after an exposure to a medical product or an environmental agent to indicate the likelihood, presence, or extent of toxicity as an adverse effect."

A biomarker can be a single measurand (cf. Glossary on page 185) or a set of measurands, i.e., several discrete measurements that constitute a signature. Many different analytes (cf. Glossary) may serve as biomarkers, but biomolecules like proteins or nucleic acids are the most prominent ones. However, characteristics of any chemical substance or even physical quantities may be used as biomarkers. Biomolecules that are used as biomarkers are frequently contained in higher structures such as extracellular vesicles or circulating tumor cells.

It is essential that a biomarker is accessible, and the aim to obtain biomarkers with minimally invasive procedures has increased in the past years. Biomarker discovery is often driven by the intention to replace tissue biopsies with less invasive sample collection procedures. Primary samples that can be obtained with minimally invasive procedures include blood, urine, liquor, or other body fluids. Collecting such body fluids and analysis of the biomarker they contain is often subsumed under the term liquid biopsy.

1.1.3 Liquid biopsies

Liquid biopsies provide the opportunity to detect, analyze and monitor diseases based on samples from various body fluids (Poulet, Massias, and Taly 2019). More than ten years ago, liquid biopsies of circulating tumor cells (CTCs) were introduced, but since then, the field has grown rapidly (Alix-Panabières and Pantel 2021). Most liquid biopsies are complex fluids that contain a wide spectrum of potential biomarkers. Figure 2 (page 17) shows this complexity for whole blood, which is made up of a cellular and a cell-free component. The following work will focus mainly on the latter component, which contains extracellular vesicles and cell-free nucleic acids as its two main subcomponents. Each of these contains several biomolecules like DNA derived from extracellular vesicles (EV-DNA) or cell-free DNA (cfDNA), and these hold many biomarkers like disease-specific genetic variants or can show allelic imbalance as an indicator of a disease process. Figure 2 also shows the terminology used in this work with definitions provided in the Glossary (8.5 on page 185).

To date, tissue samples are still the gold standard source of biomarkers, especially for patients with cancers. However, liquid biopsies can overcome several disadvantages of tissue sampling

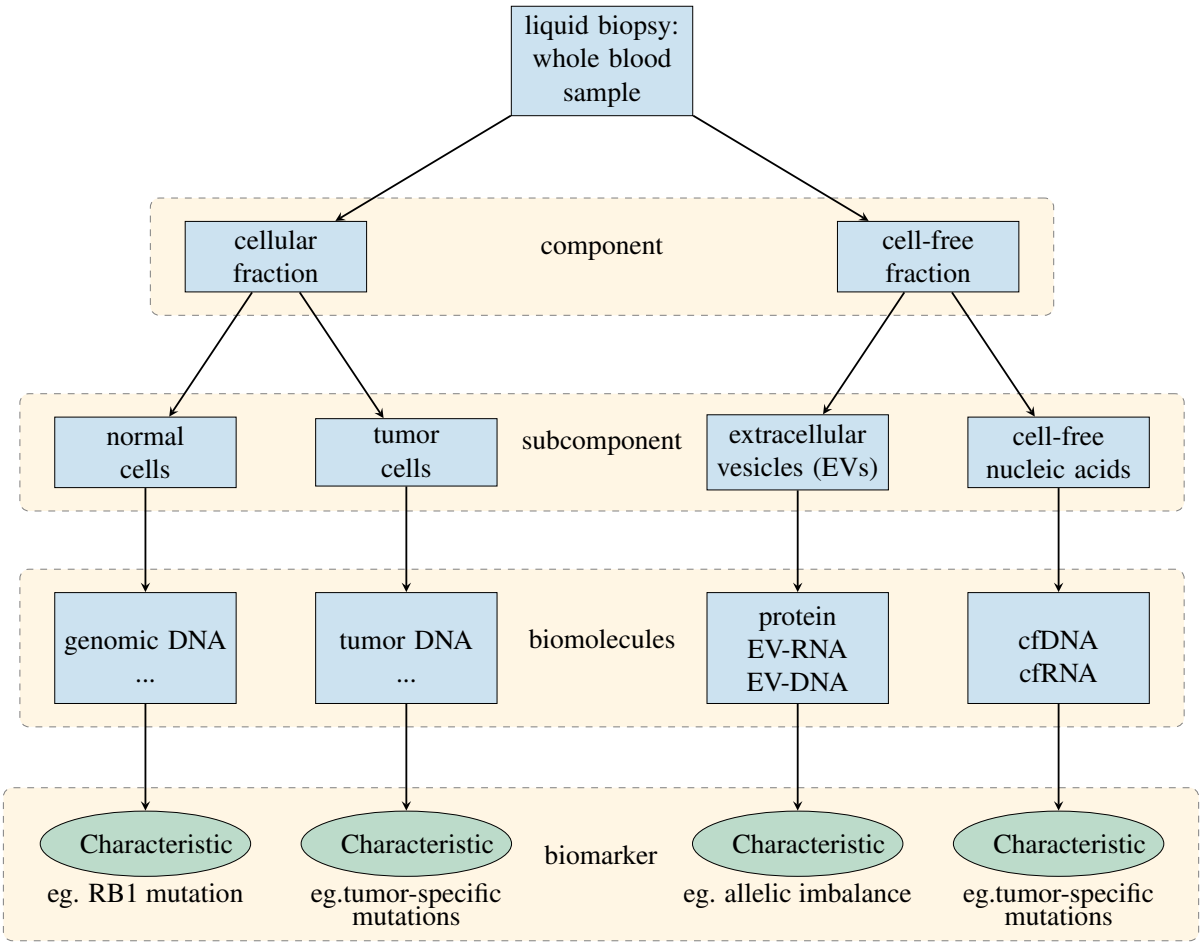

Figure 2: Characteristics that can be measured by analysis of components contained in a liquid biopsy from blood. cf-DNA: cell-free DNA; cfRNA: cell-free RNA; EV-DNA: DNA derived from extracellular vesicles; EV-RNA: RNA derived from extracellular vesicles.

and provide new diagnostic opportunities. In contrast to tumor tissue, liquid biopsies are easier to obtain and almost always available. Specifically, this is true for peripheral blood, the body fluid most commonly used for laboratory testing (Möhrmann et al. 2018).

Liquid biopsy examinations are already part of clinical applications, especially for patients with advanced-stage cancer (Ignatiadis, Sledge, and Jeffrey 2021). The presence of cell-free tumor DNA (ctDNA) in cell-free DNA (cfDNA) from plasma is widely used as a biomarker for the early detection of many kinds of tumors (Alix-Panabières and Pantel 2021). One example of a predictive biomarker obtained by a liquid biopsy can be found in the field of NSCLC. Previously, mutational analysis of the genes *BRAF* and *EGFR* has been performed based on tumor DNA from tissue biopsies. Today, mutations in *KRAS* detected in cell-free DNA from blood are used to predict therapy response as these genetic markers are known to indicate resistance against several drugs (Riely, Marks, and Pao 2009; McCormick 2020; Möhrmann et al. 2018). Next generation sequencing (NGS) plays an important role in enabling such multi-marker analysis and, thereby personalized medicine.

Liquid biopsies entail several challenges, and specific requirements need to be fulfilled. They mostly contain low levels of tumor-derived subcomponents, and this leads to an increased risk of false negatives (further described in chapter 1.4). Strict guidelines for sample collection are needed, especially if the timeframe available for analysis is short and storage is difficult, as is the case for cfDNA (Poulet, Massias, and Taly 2019).

In conclusion, liquid biopsies hold many advantages over tissue biopsies and unlock new possibilities for treatment and disease monitoring as well as personalized medicine. Before implementation of liquid biopsies in clinical practice, validation is needed. However, requirements for sufficient validation are complex (Ilié and Hofman 2016).

1.1.4 Extracellular vesicles (EVs)

In the following, the definition and biogenesis of extracellular vesicles (EVs), the types of biomolecules they contain, and their classification into subtypes are described. Examples of their use as a source of characteristics that can be used as biomarkers for diagnosis, prognosis, or treatment monitoring with a special focus on cancer are presented.

1.1.4.1 Definition of EVs

EVs are a heterogeneous population of small phospholipid bilayer-bound structures secreted by almost all cell types (Gustafson, Veitch, and Fish 2017). They are mediators of cell-to-cell communication and transport cargo from a donor cell to a recipient cell. The cargo they contain is diverse and includes proteins, lipids, various nucleic acid species, and some metabolites (Yáñez-Mó et al. 2015). EVs play a role in regulating physiological and pathophysiological processes such as coagulation or immune response (Becker et al. 2016).

EVs display surface markers specific to the parental cell type (Hermann et al. 2022). These are used to engage with receptors on their recipient cell (Ginini et al. 2022). EVs are taken up via different mechanisms, including endocytosis, direct fusion, or binding of surface proteins like tetraspanins to the cell membrane (Gustafson, Veitch, and Fish 2017). They can evoke diverse responses in recipient cells, such as inflammation and increased oxidative stress, or they can affect specific pathways (Akbar et al. 2019).

1.1.4.2 Biogenesis and classification

EVs can be further classified into subtypes depending on their biogenesis and mode of secretion. They can be found in nearly every multicellular species, and release mechanisms are evolutionary conserved. The best-studied subtypes of extracellular vesicles are exosomes, microvesicles, and apoptotic bodies.

Exosomes are less than 150 nm in size and arise from the endosomal system (Gurunathan et al. 2019). The biogenesis starts with the in-budding of endosomes to form multivesicular bodies (MVBs, also called multivesicular endosomes (MVEs)) which contain intraluminal vesicles (ILVs) (Gurunathan et al. 2019; Raposo and Stoorvogel 2013). The MVB fuses with the plasma membrane and releases the ILVs into the extracellular space as exosomes via exocytosis (Gurunathan et al. 2019). The size of the ILVs is causative for the size of the exosomes (cf. figure 3). As a result of their origin, exosomes contain endosome-associated proteins and membrane proteins like tetraspanins (Raposo and Stoorvogel 2013; Gurunathan et al. 2019).

EVs often comprise exosomes and **microvesicles** (MVs) (Raposo and Stoorvogel 2013). The latter are $100 - 1,000$ nm in size and are secreted by outward budding and fission of the plasma membrane, as shown in figure 3 (Gurunathan et al. 2019; Yáñez-Mó et al. 2015). In contrast to exosomes, MVs directly bud from the plasma membrane without the participation of the endosomal system (Raposo and Stoorvogel 2013; Yáñez-Mó et al. 2015). Exosomes and MVs often have a common composition that makes it very hard to distinguish between them after EV isolation. When originating from cancer cells, they are called oncosomes and can be bigger in size (van Niel, D'Angelo, and Raposo 2018).

Apoptotic bodies are large, membrane-surrounded fragments of dying cells that are 1-5 µm in size (Gurunathan et al. 2019). When a cell undergoes apoptosis, the cell membrane blebs, forming a thin membrane protrusion, and finally, apoptotic bodies are generated (Caruso and Poon 2018).

Because of the overlapping characteristics of all three major subclasses of EVs, a classification based on size, morphology, or cargo composition, which would allow the differentiation of different EV subtypes after isolation, is not possible. However, the classification of EVs is of great interest as there are differences in functionality between the subclasses that are not yet fully understood (Doyle and M. Z. Wang 2019).

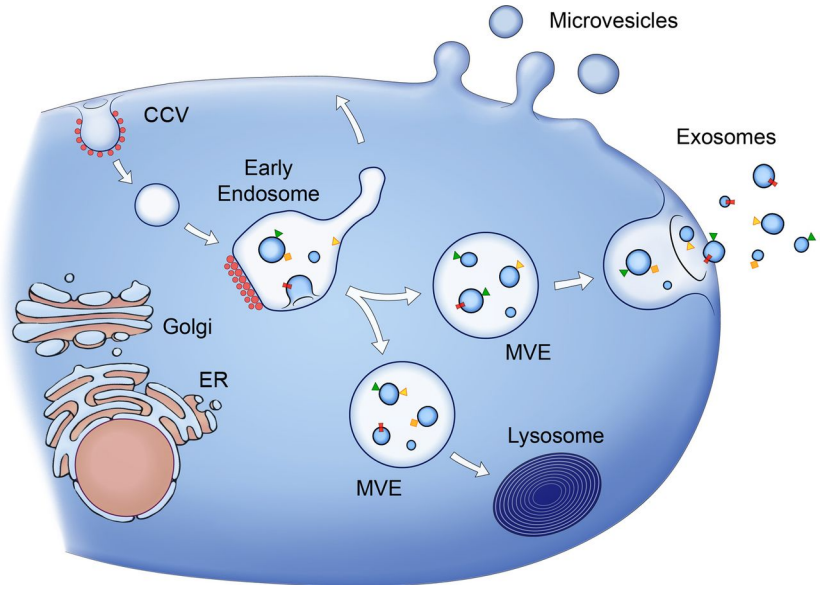

Figure 3: Biogenesis of different EV subtypes. Taken from Raposo and Stoorvogel 2013 with permission (license ID 1294469-1). CCV: clathrin-coated vesicles; MVE: multivesicular endosome; ER: endoplasmic reticulum

1.1.4.3 Analysis of EV-DNA

Interest in the analysis of DNA from EVs (EV-DNA) started with the initial findings of Thakur et al., who investigated EVs derived from cultured cells, and the study by Kahlert et al. who analyzed serum from cancer patients in 2014 (Thakur et al. 2014; Kahlert et al. 2014). Many studies followed, and today, it is widely accepted that DNA is part of the EV cargo. However, most of the biomarker studies on EVs focused on other biomolecules like RNA or proteins. Recently, a group even claimed that there is no DNA in small EVs but that the majority of the DNA detected in EV studies is associated with non-vesicular particles (Jeppesen et al. 2019). Zhang et al. confirmed the existence of these non-vesicular particles but stated that small EVs also contain DNA (H. Zhang et al. 2018). The mechanism of loading DNA into vesicles is unresolved, as is the function of EV-DNA or its effect on a recipient cell (Malkin and Bratman 2020; García-Silva, Gallardo, and Peinado 2021; Ghanam et al. 2022). But what has been shown is that the inhibition of exosome secretion leads to an accumulation of DNA in the cytosol and puts the cell into a senescence-like state. This, in turn, suggests that shedding DNA into exosomes is an important process for the preservation of cell homeostasis (Takahashi et al. 2017).

The concentration of DNA present in EVs remains a matter of debate. One study showed a median DNA concentration in plasma exosomes of 4.9 ng/ml plasma, measured by fluorescent dye-based quantification. The authors also investigated the copy number of a target gene by droplet digital PCR and found a median number of 1,560 copies/ml plasma (Fernando et al. 2017). The DNA content apparently differs significantly between EVs derived from cancer cells and those derived from healthy cells (Ghanam et al. 2022).

There are reports on different DNA species and origins as listed in table 1. Reports on single-stranded DNA preceded that of double-stranded DNA (dsDNA), and later, mitochondrial DNA

Table 1: Types and sources of EV-DNA. Taken from Kawamura et al. 2017, modified, licensed under CC BY-NC 4.0. dsDNA: double-stranded DNA; ssDNA: single-stranded DNA; mtDNA: mitochondrial DNA; EV: extracellular vesicle.

EV source	Type of DNA detected	Characteristics of DNA extracted from EV	Reference
Astrocytes, glioblastomas	mtDNA	Majority on outer surface of EV	Guescini et al. 2009
Medulloblastomas	ssDNA	Amplified *c-Myc* oncogene sequences	Balaj et al. 2011
Various cancer cell lines	dsDNA	Identification of driver mutations such as BRAF and EGFR	Thakur et al. 2014
ras-driven cancer cells	dsDNA	H-*ras* DNA, histone-bound	Lee et al. 2014
ras-driven cancer cells	dsDNA	No permanent transformation of recipient cells	Lee et al. 2016
hMSC transduced with Arabidopsis thaliana DNA	dsDNA	Majority on outer surface of EV, horizontal transfer of Arabidopsis thaliana DNA	Fischer et al. 2016

(mtDNA) was identified in EVs (Balaj et al. 2011; Cai et al. 2016). However, it remains unclear how mtDNA is packed into vesicles and which function it holds (Malkin and Bratman 2020). In plasma from prostate cancer patients Lázaro-Ibáñez, Sanz-Garcia, et al. showed that there is DNA in all EV subtypes with different kinds of DNA and composition between EV subpopulations (Lázaro-Ibáñez, Sanz-Garcia, et al. 2014).

DNA in different EV subtypes

Apoptotic bodies originate from cells undergoing apoptosis or necrosis. It is very well known that they contain very fragmented genomic dsDNA of a very characteristic length (around $160 - 180$ base pairs) (Bortner, Oldenburg, and Cidlowski 1995). This is the case because during apoptosis, endonucleases cut the dsDNA inside the nucleus between the nucleosomes. This results in DNA fragments equal to the DNA that is wrapped around a nucleosome (Wyllie 1980). These nucleosomes are packed into apoptotic bodies (Bortner, Oldenburg, and Cidlowski 1995). If the cellular turnover rates are very high and there is an increased number of cell deaths, apoptotic bodies are even released into circulation and, therefore, have been detected in blood (Holdenrieder et al. 2001). Apoptosis is one of the main events where DNA leaves the intracellular space. However, there is increasing evidence that DNA can also be actively secreted in the form of nucleosomes or DNA-protein complexes (Thierry et al. 2016; Holdenrieder et al. 2001).

Several studies have shown that besides apoptotic bodies, there are large EVs which are often called oncosomes or large oncosomes in cancer research (Minciacchi, Freeman, and Di Vizio 2015; Di Vizio et al. 2012). These vesicles are $1 - 10$ µm in size and, according to several

studies, show an enrichment of dsDNA compared to smaller vesicles. It has been found that the fragment length of this DNA is more than two million basepairs which suggests that it contains the entire genome of a parental cell, including tumor-specific alterations in case of a cancerous origin (Vagner et al. 2018; Di Vizio et al. 2012; Hager et al. 2012). Exosomes contain smaller dsDNA fragments with a size of 100 bp to 20 kbp. There is evidence that tumor-derived exosomes can also carry whole genomes of their parental cells, but these findings were not observed *in vivo* (Kahlert et al. 2014; T. H. Lee, Chennakrishnaiah, Meehan, et al. 2016). Others observed fragments of up to 4 kbp in exosome-derived DNA (Lázaro-Ibáñez, Lässer, et al. 2019; Vagner et al. 2018; Malkin and Bratman 2020).

DNA loading mechanisms, functions and location of EV-DNA

One common hypothesis regarding EV-DNA loading mechanisms is that DNA is packed into vesicles during the formation of ILVs where cytosolic DNA is thought to be encapsulated into these structures together with proteins, lipids, and cytosol (Elzanowska, Semira, and Costa-Silva 2021). Another DNA loading pathway that was proposed is via micronuclei, structures enclosed by a nuclear membrane that arise if a failure during mitosis leads to acentric chromosomes or chromatid fragments that are not included in the daughter cell. This tiny nucleus-like structure is highly unstable and can occasionally break down, releasing its content to the cytoplasm during cell division where it might be transported into MVBs with the help of tetraspanins (Fenech et al. 2011; Kisurina-Evgenieva, Sutiagina, and Onishchenko 2016; Harding et al. 2017; Bakhoum et al. 2018). Yokoi et al. found that induced genomic instability leads to an increase in the number of micronuclei and an increase in DNA amount, which supports the previous findings (Yokoi et al. 2019).

In 2017 Takahashi et al. proposed that EVs serve to maintain homeostasis, remove harmful DNA from the cytosol and thereby avoid apoptosis (Takahashi et al. 2017). Several groups investigated the location of DNA in relation to the vesicle, performing experiments treating EVs with DNAse and membrane-disrupting detergents. They found that a small part of the DNA is inside the vesicle but the majority is located on the surface (Thakur et al. 2014; Lázaro-Ibáñez, Lässer, et al. 2019; Németh et al. 2017).

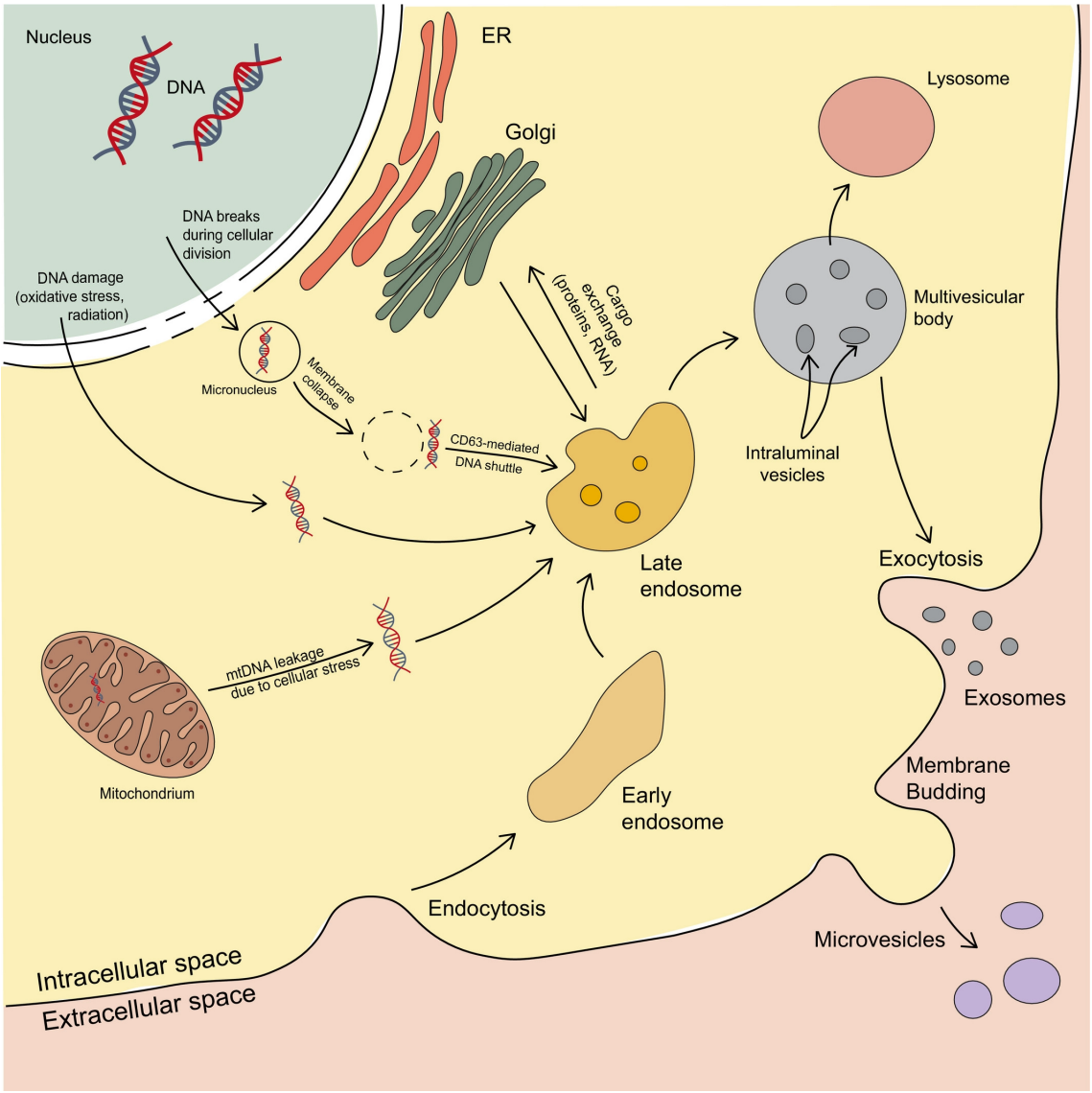

Figure 4: Mechanisms of loading DNA into extracellular vesicles. Taken from Elzanowska, Semira, and Costa-Silva 2021, licensed under CC BY 4.0. Components of the cytoplasm can be incorporated into microvesicles during their generation via membrane budding. Exosomes arise from intraluminal vesicles of multivesicular bodies derived from endosomes. DNA that has escaped the nucleus or mitochondriom due to stress-induced damage and is hence exposed to cytoplasm can be shuttled to intraluminal vesicles or be integrated into microvesicles. mtDNA: Mitochondrial DNA; ER: Endoplasmatic Reticulum.

1.1.4.4 EV biomarker studies with a focus on cancer research

The field of EV research established only recently. Although EVs have been known since the 1980s, it took around 20 years until research on EVs expanded rapidly. The number of publications, patents, grants, and start-up companies related to EV research grew tremendously, as did biomarker research in general (Couch et al. 2021; Roy, Hochberg, and Jones 2018).

EVs are already being used as biomarker containing components in various research fields like cancer research, autoimmune diseases, or neurodegenerative diseases (Yáñez-Mó et al. 2015; Kawamura et al. 2017). Still, a lot of basic research needs to be done to further characterize EVs and their physiological functions. Research on EVs strongly depends on technical developments. Technical limitations, in addition to the heterogeneity of EVs, slow down the progression of biomarker discovery and especially validation. Methods used for EV biomarker studies use heterogeneous analytical principles and, therefore, there is a high level of heterogeneity between EV studies (Gandham et al. 2020). To address the increasing need for standardization, the international society for extracellular vesicles published the MISEV (Minimal Information for Studies of Extracellular Vesicles) guidelines in 2014 (updated in 2018) to provide guidance in standardization and enhance the reproducibility of studies (Witwer et al. 2017).

Especially in cancer research, various EV-derived biomarkers are used for prognostic and diagnostic testing, disease monitoring, prediction of the best treatment, and treatment monitoring (Wit et al. 2019; Hu, Wolfram, and Srivastava 2021). For example, there is evidence that alterations in the composition of the EV cargo promote tumor growth and metastasis and contribute to the tumor microenvironment (Becker et al. 2016; B. Li et al. 2022). Tumor-derived EVs that express EpCAM and cytokeratin but not CD45 and that do not contain DNA are associated with poor overall survival of patients with NSCLC and thus can serve as a prognostic biomarker (Wit et al. 2019). Another example is the analysis of the identity of EV-derived MicroRNAs. This biomarker is used for the early prediction of metastatic disease in patients with colorectal cancer (Miguel Pérez et al. 2020).

1.1.4.5 Liquid biopsy examinations based on EVs and their biomolecules

Although most body fluids have been shown to contain EVs, primary samples used for liquid biopsy examinations based on characteristics of EVs are mainly blood and urine and, for some applications, cerebrospinal fluid (Hu, Wolfram, and Srivastava 2021). This qualifies EVs as a perfect liquid biopsy component. All cells present in blood or lining blood vessels can secrete EVs into the bloodstream (Yáñez-Mó et al. 2015). The number of EVs and their cargo composition are distinct depending on the origin and pathological state of the secreting cell. Therefore, blood can contain EVs from pathological cells like tumor cells, which has been confirmed by several studies (Caby et al. 2005; Vagner et al. 2018). All this makes blood a suitable source for EVs and EV-derived biomolecules whose characteristics can serve as diagnostic or prognostic biomarkers. To retrieve EVs from blood, either plasma or serum can be used. Serum contains

a higher number of vesicles, but most of them are platelet-derived and released during clotting processes. By contrast, plasma is a more suitable matrix for EV analysis as it is not affected by such bias introduced by sample collection (Witwer et al. 2017).

Another body fluid that can be used to obtain EVs is urine. EVs isolated from urine (also called uEVs) have a high potential to serve as a liquid biopsy component. uEVs contain proteins as well as nucleic acids that can be used as sources of biomarkers for the risk stratification of patients with a wide variety of mainly nephrological diseases such as chronic renal insufficiency or the nephrotic syndrome (Droste and Büscher 2020; Karpman, Ståhl, and Arvidsson 2017; Erdbrügger and Le 2016).

EV-DNA extracted from several kinds of body fluids has been widely used for mutation detection in patients with cancer. In several tumor entities, tumor-specific characteristics have been detected in EV-DNA, which can be used as biomarkers (Malkin and Bratman 2020, Table 3). For example, Möhrmann et al. showed that in patients with advanced cancers, the proportion of mutant alleles in EV-DNA correlates with the survival or time to treatment failure and that low amounts of EV-DNA, in general, are correlated with partial response and stable disease (Möhrmann et al. 2018).

1.1.4.6 EV isolation and enrichment: technical aspects

Evolving fields are in need of standardization and guidelines. This is especially true if the analytical procedures required are elaborate. EVs are very small and, therefore, difficult to isolate with high specificity and difficult to visualize and quantify. The heterogeneity of EV types and a lack of nomenclature guidelines lead to further confusion (Willms et al. 2018). With the MISEV guidelines, a first and essential step towards standardization was made (Witwer et al. 2017).

The choice of EV isolation or enrichment method is very important for further applications because it highly influences the EV subpopulations that are isolated or enriched. Starting with ultracentrifugation as the gold standard further technologies were developed for EV isolation including size exclusion chromatography (SEC) using self-made or commercially available columns, ultrafiltration, precipitation with polyethylenglycol (PEG), or tangential flow filtration. For analysis of EV-DNA, it is essential to define the subpopulation to be isolated because, as explained above, different subpopulations are known to contain different amounts and types of DNA (Lázaro-Ibáñez, Lässer, et al. 2019). For each analytical application, the optimum EV isolation method has to be determined.

1.1.5 Cell-free DNA

The term cell-free DNA (cfDNA) describes DNA fragments present in body compartments outside of cells, such as body fluids. Currently, there is no unified terminology and the terms cell-free DNA, circulating DNA, cell-free circulating DNA, or extracellular DNA are all used

in literature to describe DNA located outside of cells. Bronkhorst et al. aimed to harmonize the terminology and, according to their suggestions, the term cell-free DNA with the abbreviation cfDNA will be used in this thesis with further specification depending on the source the cfDNA is derived from (Bronkhorst et al. 2021).

Cell-free DNA was discovered in 1948, but its potential as a source of characteristics that can be used as biomarkers has been investigated only in the last two decades (Bronkhorst et al. 2021; Mandel and Metais 1948). Every body fluid contains cfDNA, but levels vary, with blood having the highest number of DNA fragments per volume. Because of this and the easy accessibility, blood is the most commonly used body fluid for cfDNA analysis. However, other body fluids might be preferred depending on the intended use. In oncology, body fluids that are in direct contact with a tumor often contain high levels of cell-free tumor DNA (ctDNA) (Tivey et al. 2022).

1.1.5.1 Origins and characteristics of cfDNA

The cells from which cfDNA originates and the processes that result in the release of DNA into body fluids are diverse and only partially understood (Thierry et al. 2016; Otandault et al. 2019). In general, cfDNA can be of nuclear as well as of mitochondrial origin (Thierry et al. 2016; Kustanovich et al. 2019; Otandault et al. 2019). Within body fluids, cfDNA can either be part of molecular complexes like nucleosomes or be associated with EVs (encapsulated or attached to their surface), and thus protected from the continuous nuclease activity in the bloodstream (Thierry et al. 2016; Kustanovich et al. 2019; Otandault et al. 2019). Most cfDNA molecules are double-stranded or partly single-stranded as the result of degradation (Otandault et al. 2019; Sanchez et al. 2021).

The presence of cfDNA is not restricted to patients (Kustanovich et al. 2019). It appears that the release of cfDNA serves some functions in physiological processes. However, levels of cfDNA are often increased in patients with cancer and other diseases, suggesting an increased release of cfDNA during pathological processes (Bettegowda et al. 2014; Mouliere and Thierry 2012; Thierry et al. 2016).

Apoptosis is the primary origin of cell-free DNA. Per day, $50-70$ million cells undergo apoptotic death and may release DNA into the bloodstream depending on their location in the body (Grabuschnig et al. 2020; Kustanovich et al. 2019; Sanchez et al. 2021). The genomic DNA in the nucleus is wrapped around histone octamers and stabilized by histone 1 to form a structure called nucleosome (Thierry et al. 2016). Single nucleosomes are connected by linker regions (Thierry et al. 2016). In the process of apoptosis, a caspase activated DNAse cleaves the double-stranded DNA at the inter-nucleosomal linker regions (Grabuschnig et al. 2020). Later, the cell undergoes phagocytosis, a process during which lysosomal DNAse II further trims the DNA into smaller fragments (Thierry et al. 2016; Grabuschnig et al. 2020).

The stretch of DNA wrapped around a histone comprises $180-200$ bp (Bortner, Oldenburg, and Cidlowski 1995). This size and multiples of it are characteristic for DNA-fragments re-

leased by apoptotic processes and, therefore, this characteristic size distribution is also called the 'apoptotic ladder' (Bortner, Oldenburg, and Cidlowski 1995). Based on this specific nucleosome fragmentation pattern, it has been estimated that $67.5 - 80\,\%$ of cfDNA in the blood is nicked into mononucleosomes, indicating its apoptotic origin. Around $10\,\%$ are packed into Di-nucleosomes (Sanchez et al. 2021). By contrast, tumor-derived cfDNA is known to be more fragmented with less than 145 bp in size, whereas necrosis, a process of passive cell death, leads to much bigger fragments with a size of around 10 kbp (Kustanovich et al. 2019; Grabuschnig et al. 2020; Sanchez et al. 2021; Thierry et al. 2016). This is important when choosing the way of blood draw for a particular biomarker assay because serum collection enhances the release of necrotic DNA, leading to a bias in the composition of cfDNA (Kustanovich et al. 2019).

The main physiological processes leading to cfDNA release are hematopoietic cell death and erythroblast enucleation (Grabuschnig et al. 2020; Thierry et al. 2016). It has been shown that the nucleosome footprint in healthy individuals corresponds to a hematopoietic origin, with around $55\,\%$ of cfDNA derived from leucocytes and around $30\,\%$ originating from erythrocyte progenitors. This finding is further supported by analysis of methylation patterns (Kustanovich et al. 2019; Moss et al. 2018; Tivey et al. 2022). Another possible origin of cfDNA is NETosis, a cell death program of activated neutrophils that leads to chromatin decondensation and cell lysis, resulting in the release of neutrophil extracellular DNA traps, shortly NETs. These NETs are formed to catch and kill pathogens. However, there is also a vital NETosis process where the neutrophils form NETs but stay viable (Thierry et al. 2016; Kustanovich et al. 2019).

cfDNA can also result from active secretion during many different processes. These include vital NETosis, espulsion of nuclei, egestion of mitochondrial DNA, or release of virtosomes. Virtosomes are nucleoprotein complexes synthesized and spontaneously secreted by non-dividing cells like lymphocytes (Gahan and Stroun 2010).

The role of cfDNA in healthy individuals remains largely unknown, and hypotheses range from cfDNA being just a byproduct or even a waste molecule to cfDNA playing roles in the maintenance of cell homeostasis or mediation of immunomodulatory or proinflammatory effects (Kustanovich et al. 2019). As it has been shown that cfDNA can penetrate host cells, it was suggested that these DNA fragments might be able to change some aspects of the behavior of these host cells (Otandault et al. 2019).

1.1.5.2 Liquid biopsy examinations based on cfDNA

Many project investigations have shown that cfDNA is a biomolecule that can serve as a biomarker, and some applications are even routine use. The cfDNA contained in body fluids is obtained by taking samples (liquid biopsy samples), and the complete process that includes the analysis of the relevant characteristics (biomarkers) of these cfDNA fragments is defined as liquid biopsy examination. Improved technologies for the analysis of low-abundance DNA fragments, such as NGS and Droplet Digital PCR, have widened the scope of liquid biopsy

examinations. These technologies permit highly sensitive analysis of multiple genetic characteristics in parallel. With short turnaround times and parallel processing of large sample batches, the prerequisites for use in routine clinical care are fulfilled (Wan et al. 2017).

Most studies using cfDNA determine the presence of specific genetic alterations, such as oncogenic mutations, that can serve as biomarkers for early detection, prognosis, treatment monitoring, or detection of treatment resistance. Other studies focus on epigenetic characteristics (methylation states), copy number aberrations, or gene expression patterns that can be detected in cfDNA and serve as biomarkers. Specifically, epigenetic markers currently are of increased interest as they are often consistent over many samples and, therefore, epigenetic characteristics are more generalizable compared to genetic features, which often show a high degree of variability (Rahat et al. 2020; Keller et al. 2021).

One of the first examples where cfDNA was used as an analytical target for a biomarker examination is autoimmune diseases. The first study was published in 1966 and showed that the level of cfDNA is a diagnostic biomarker for systemic lupus erythematosus. Since then, quantitative as well as qualitative changes of cfDNA are used to determine the inflammatory activity of this disease. Advances in technology and the disease processes showed that mechanisms like NETosis are the source of the increased cfDNA levels in this condition (Duvvuri and Lood 2019). Another example where cfDNA levels are used as a biomarker is transplantation, where donor-derived cfDNA detected in the recipient of the organ after transplantation can be used for early detection of organ rejection. Here, the big advantage of this method is that it can detect rejection far earlier than any procedures based on a histologic examination that has been performed previously (Gielis et al. 2015).

Since 1977 it is known that levels of cfDNA are increased in cancer patients (Leon et al. 1977). Fragments of cell-free DNA derived from tumor cells are called ctDNA. It is not fully understood why cfDNA levels are increased in cancer patients. CTCs are a putative source but are unlikely to be the primary source because of their low abundance. One source of ctDNA is cell death via apoptosis and other mechanisms, which are increased in cancer. Additionally, cfDNA is cleared rapidly from the circulation in healthy individuals, but cancer patients show reduced clearance leading to the accumulation of cfDNA (Kustanovich et al. 2019). It has been shown that ctDNA levels during treatment can correlate with the outcome (Kamat et al. 2010). Furthermore, it has been shown that cell-free DNA secreted by tumor cells reflects its cell of origin carrying several features/characteristics like tumor-specific mutations. Information on the cellular origin facilitates finding the location of the affected tissue and can be a powerful tool in the early diagnosis of cancer (Kustanovich et al. 2019).

In prostate cancer, for example, a copy number instability score is calculated based on copy number aberration analyses in cfDNA and used to discriminate between prostate cancer patients, patients with benign prostatic disease, and healthy individuals. In addition, changes in this score in follow-up investigations can be used to predict therapy response (Oellerich et al. 2017). In NSCLC, both ctDNA levels and specific mutant variants are used as biomarkers. ctDNA levels contain information on disease progression, therapy response, and progression-free survival.

For patients carrying the mutation $BRAF^{V600E}$, it has been found that the detection of the additional mutation $NRAS^{Q61}$ predicts shorter progression-free and overall survival. The use of these biomarkers allows earlier detection compared with routine radiological scans. Moreover, as sample taking is minimally invasive and analyses have a short turnaround, biomarker testing allows treatment monitoring at short intervals (Váraljai et al. 2019).

The first biomarker assay that was approved by the FDA as a companion diagnostics in patients with cancer was the *EGFR* mutation test that is based on Realtime PCR. This test targets several mutations in the *EGFR* gene and is used for the prescription of *EGFR* inhibitors to NSCLC patients if no tumor tissue biopsy is available (Kwapisz 2017). Outside of cancer and the most famous biomarker assay based on cfDNA overall is the NIPT (Non-Invasive Prenatal Testing) test. In 1997 Lo et al. showed that the blood of pregnant women contains fetal DNA (Lo et al. 1997). In this assay, fetal DNA is detected in the blood of the mother during pregnancy and analyzed for aneuploidies of chromosomes 13, 18, and 21. In 2011 NIPT was introduced into clinical practice. Recently, genome-wide screening for copy number alterations and inherited monogenic disorders based on fetal DNA analysis is offered to pregnant women as well (Brady et al. 2016; Alberry et al. 2021; Hartwig et al. 2017).

1.2 Diagnostic biomarker in retinoblastoma

1.2.1 Epidemiology of retinoblastoma

Retinoblastoma is a very rare cancer (one case per $15,000 - 20,000$ live births worldwide) but is the most common intraocular malignant neoplasm in childhood. It accounts for 9.2 % of all cancers of children under one year of age (Kaatsch 2018). In Germany, 0.4 of 100,000 children get diagnosed with retinoblastoma per year (Zentrum für Krebsregisterdaten und Gesellschaft der epidemiologischen Krebsregister in Deutschland e.V. 2021).

Retinoblastoma is most often discovered because of leukocoria, an abnormal white reflection from the retina. This also becomes visible in flashlight photos and is often recognized by parents. The disease is curable if diagnosis and treatment are within 3-6 months after the first signs of leukocoria (Dimaras et al. 2012). Other first signs of retinoblastoma are strabismus, poor visual tracking, glaucoma, or inflammation (Dimaras et al. 2012).

Retinoblastoma can affect one or both eyes (unilateral or bilateral retinoblastoma, respectively). Around 35 % of all cases are bilateral. There is a heritable and a non-heritable form of retinoblastoma. In Germany, 45 % of all cases are heritable retinoblastomas, and most of them have bilateral tumors (cf. table 2). The age at diagnosis of the heritable form is earlier than that of the non-heritable form of retinoblastoma.

In high-income countries with a good healthcare system, such as Germany, almost all children with retinoblastoma survive (Global Retinoblastoma Study Group 2020). In low and middle-income countries, which worldwide have the highest prevalence (more than 80 % of all retinoblastoma cases), the survival rate is only $30 - 60$ % because of the higher proportion of patients with disseminated and metastatic disease, which most often are fatal (Schaiquevich et al. 2022; Dimaras et al. 2012; Global Retinoblastoma Study Group 2020). The age at diagnosis for patients from high-income countries is 14.1 months (median), but for patients from low-income countries, it is 30.5 months (median), and this can explain the higher frequency of patients with advanced disease stages at the time of diagnosis (Global Retinoblastoma Study Group 2020).

1.2.2 Molecular genetics of retinoblastoma

Retinoblastoma originates from retinal progenitor cells (Friend et al. 1986). Development of retinoblastoma is initiated by biallelic inactivation of the tumor suppressor gene *RB1,* which encodes for the pRB protein (Cavenee et al. 1983; Dick and Rubin 2013). The heritable form

Table 2: Retinoblastoma cases by type and laterality in Germany. Data taken from Reschke et al. 2021, licensed under CC BY 4.0. Patients with missing data were excluded.

	Bilateral	Unilateral	Total
Heritable	35 %	10 %	45 %
Non-heritable	0 %	55 %	55 %
Total	35 %	65 %	100 %

of this disease is an autosomal dominant tumor predisposition syndrome that is caused by heterozygosity for an inactivated *RB1* allele.

1.2.2.1 The *RB1* gene in heritable and nonheritable retinoblastoma

The RB transcriptional co-repressor 1 (*RB1*) gene is located on the long arm of chromosome 13, consists of 27 exons, and spans 200 kbp. It has a promotor region without a typical TATA box, and transcription can be initiated at three different sites (F. D. Hong et al. 1989). It encodes for only one functional transcript (ENST00000267163.6) that is translated into the nuclear phosphoprotein pRB (Lees et al. 1991). It has been shown that the inactivation of this tumor suppressor gene is an important step in tumorigenesis not only of retinoblastoma but also of several other cancers (Flores and Goodrich 2022; Berman et al. 2008; Di Fiore et al. 2013).

According to Knudson's "two-hits-hypothesis", only two genetic events are required to trigger retinoblastoma development (Knudson 1971). Later it was shown that each "hit" causes a loss of function of one allele at the *RB1* locus. The first hit can be inherited, arise during gametogenesis, or as a somatic event (Knudson 1971; Friend et al. 1986; Cavenee et al. 1983). Patients with heritable retinoblastoma are heterozygous for an affected allele, and one additional somatic event (second hit) that causes loss of the other allele leads to the development of a retinoblastoma tumor focus (cf. figure 5). Non-heritable retinoblastoma develops if two sequential somatic events affect both alleles of the *RB1* locus, as shown in the lower part of figure 5 (Cavenee et al. 1983). Familial retinoblastoma is a subgroup of heritable retinoblastoma, where one or more relatives are affected because of a heritable *RB1* variant. According to current estimates, 4.7 % of all patients from all countries and 8.4 % of patients from high-income countries have a positive family history (Global Retinoblastoma Study Group 2020).

The mutational events that lead to the loss of function of the *RB1* gene are very heterogenous in nature and location. The spectrum of alterations comprises small alterations such as nonsense, frameshift, splice site, or missense mutations, in-frame deletions, or mutations of the promotor region. Most pathogenic alterations lead to a premature termination codon and result in a reduced amount of a truncated protein that is essentially non-functional. On the other end of the spectrum are large deletions of the whole *RB1* and flanking genomic regions. The most common second genetic event that leads to loss of the normal allele and thus initiation of retinoblastoma is loss of heterozygosity (LOH) (Hagstrom and Dryja 1999).

1.2.2.2 Loss of heterozygosity

Second hits at tumor suppressor loci are often accompanied by LOH. This phenomenon was first discovered in retinoblastoma but is found in many cancer entities (Cavenee et al. 1983). It can be caused by one of several events, as shown in Figure 6. Some of these events are copy number neutral, including mitotic recombination, gene conversion, or chromosomal nondisjunction if followed by subsequent duplication or deletion. Other chromosomal events like

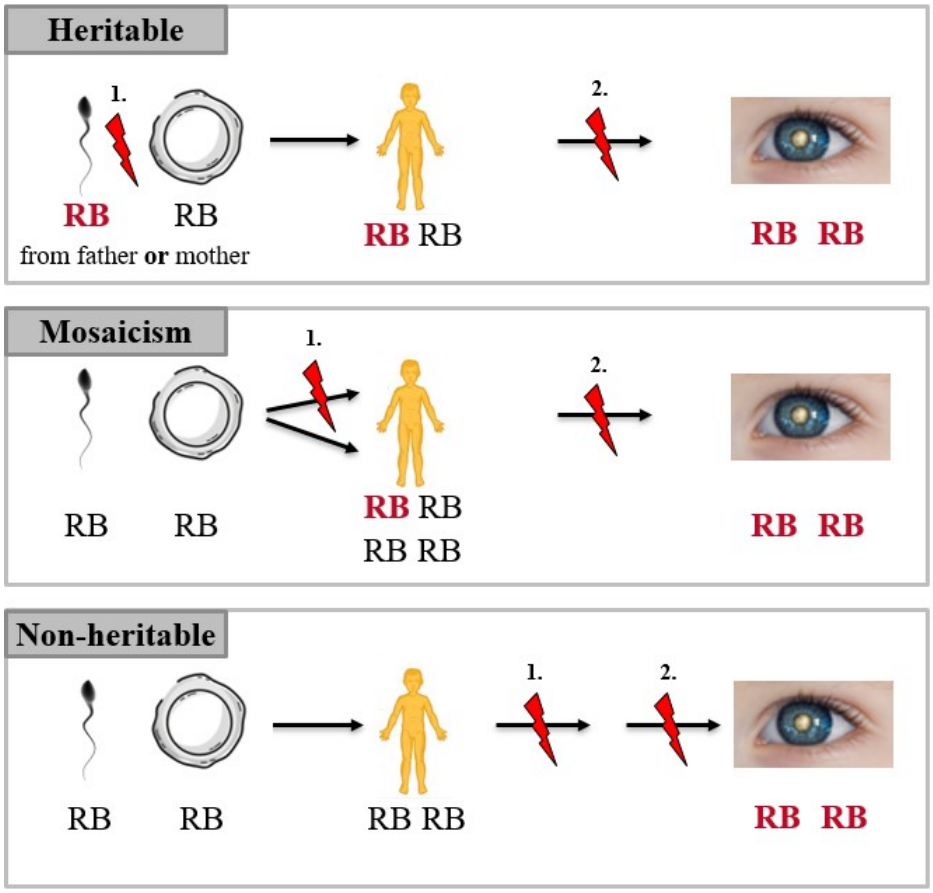

Figure 5: Biallelic inactivation of RB1. Picture taken from `https://www.kinderaugenkrebsstiftung.de/`. Flashes indicating genetic events ("hits").

non-disjunction, partial deletion, or chromosome loss result in a change of the gene dosis (Hagstrom and Dryja 1999; Cavenee et al. 1983; Saeki et al. 2011).

1.2.2.3 CpG-methylation and imprinting

Hypermethylation of the *RB1* promoter can also be a genetic event leading to loss of function of an *RB1*$^{-}$ allele. This epigenetic alteration is not heritable. Concerning epigenetic features, it has to be noted that the *RB1* locus is imprinted, as it shows parent-of-origin dependent gene expression. Imprinting of the *RB1* gene is linked to DNA methylation at the CpG island 85, which is part of a pseudogene located in intron 2 of the *RB1* gene. It is methylated on the maternal chromosome but unmethylated on the paternal allele. This CpG island functions as a weak promotor for an alternative transcript expressed from the paternal allele, and this results in skewed gene expression in favor of the maternal allele (Kanber et al. 2009).

1.2.2.4 Mosaicism

In 1979, Carlson and Desnick proposed that some patients with sporadic retinoblastoma have mutational mosaicism (Carlson and Desnick 1979). Analysis of family history can help to detect mosaicism and led to the assumption that the frequency of mosaicism is about 10 % (Sippel

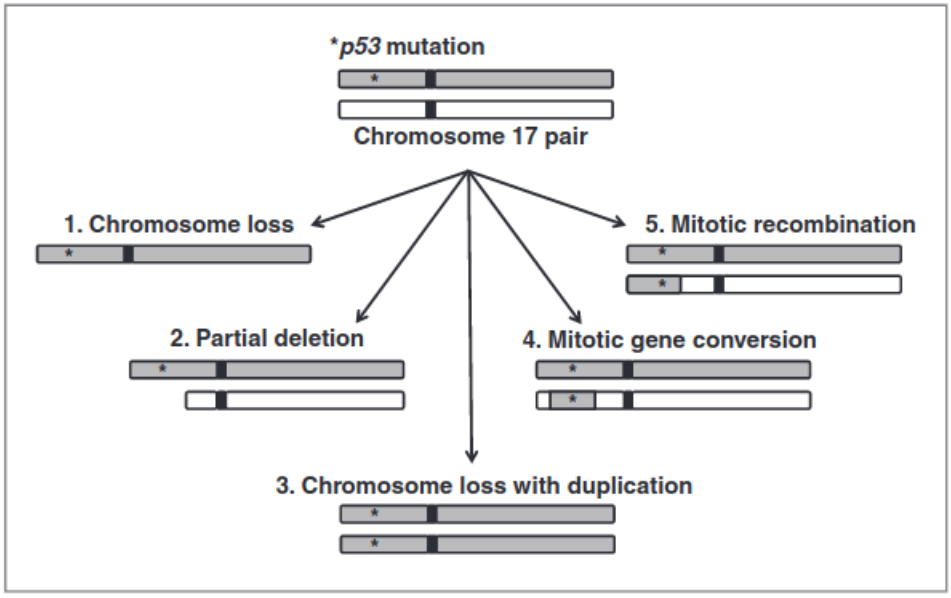

Figure 6: Mechanisms that lead to LOH. Figure taken from Saeki et al. 2011 with permission (license number 5437571211432).

et al. 1998). In 2020 an even higher proportion of mosaic patients was supposed, 14 % of patients with bilateral and 38 % with unilateral retinoblastoma showed high-level mosaicism (Rodríguez-Martín et al. 2020). Using ultra-deep NGS, even low-level mosaicism ($10-15$ %) could be detected in 19 % of unilaterally affected patients (Rodríguez-Martín et al. 2020). Mosaicism occurs due to a mutational event in an early embryonic but postzygotic cell leading to the presence of the mutated allele only in a fraction of all somatic cells (Sippel et al. 1998). Such a mutational event can also happen prezygotic in germ cells of a patient's parent, leading to recurrence risk in siblings (germline mosaicism) (Sippel et al. 1998).

1.2.2.5 Function of the pRB protein

The pRB protein is almost ubiquitously expressed and comprises 928 amino acids. The most important and highly conserved structural domain of pRB is the pocket domain which consists of the two subdomains A and B (C. Lee et al. 2002). In addition, there are the two less conserved domains RB-N (bipartite amino-terminal region), consisting of the subdomains RB-N_C, RB-N_N, and RB-C. They form alpha helices connected by linker regions that contain phosphorylation target sites ((Rubin et al. 2005; Burke, Deshong, et al. 2010; Burke, Hura, and Rubin 2012). The complete 3D Structure has been resolved by AlphaFold (Jumper et al. 2021; Varadi et al. 2022).

In cells with normal *RB1,* dephosphorylated pRB binds the transcription factor E2F, repressing its activity and thereby regulating different cell-growth-related processes, most prominently the cell-cycle transition from G1 to S-phase. Phosphorylated by CDKs pRB leads to the release of E2F, allowing the cell-cycle transition into S-phase. Phosphorylation, as a posttranslational modification in general, enables inter-regional interactions resulting in protein conformation

changes that rule the function (Rubin 2013; Dick and Rubin 2013). Loss of function of pRB leads to uncontrolled proliferation and therefore contributes to tumorigenesis.

1.2.2.6 Copy number variation as a driver of retinoblastoma development

In $3-4\,\%$ of retinoblastomas, all approaches to detect *RB1* genetic alterations fail with current methods. Mutations that would remain undetected are, for example, chromosomal rearrangements or intronic mutations. However, some tumors, mainly those diagnosed very early, do not show any *RB1* alteration but copy number variations at the *MYCN* locus. As these are very rare cases, more research into these genetically exceptional tumors is needed (Rushlow et al. 2013).

1.2.2.7 Variable phenotypic expression

Heritable predisposition to retinoblastoma shows variable phenotypic expression. The spectrum of expression ranges between two extremes. On the one hand, there are multiple independent tumors arising in both eyes of a patient. On the other hand, there is incomplete penetrance (a reduced likelihood that a phenotype is expressed if a particular genotype is present), in other words, the presence of a genetic predisposition but no development of retinoblastoma.

In families with incomplete penetrance, patients often show less severe phenotypes. Incomplete penetrance has been associated with partial inactivation of the pRB protein. Such variant alleles have been shown to lead to a defect in protein-binding activity, but the variant protein could still undergo phosphorylation, which mitigates the oncogenic effect (Otterson et al. 1997). Other variants with incomplete penetrance affect transcription factor binding sites in the promotor region and reduce transcriptional activity (Sakai et al. 1991).

1.2.3 Second primary malignancies

Survivors of heritable retinoblastoma are at risk of developing second primary neoplasms later in life, these entities can be benign or malignant (Draper, Sanders, and Kingston 1986). These tumors can occur at various sites like bones, skin, lungs, brain, or others. Osteosarcomas are the most frequent type of second primary malignancy (SPM), followed by soft tissue sarcomas (Temming, Arendt, Viehmann, Eisele, Le Guin, Schündeln, Biewald, Astrahantseff, et al. 2017; Temming, Arendt, Viehmann, Eisele, Le Guin, Schündeln, Biewald, Mäusert, et al. 2016). SPMs are a major cause of early death of retinoblastoma patients, with survival at 40 years after diagnosis of only $79.5\,\%$ for patients with stage zero or one tumors (Temming, Arendt, Viehmann, Eisele, Le Guin, Schündeln, Biewald, Mäusert, et al. 2016). SPMs predominantly occur in survivors of bilateral retinoblastoma, but also unilaterally affected patients with a positive family history are at an increased risk to develop SPMs.

1.2.3.1 Risk factors for SPMs

The main risk factor for SPMs is genetic predisposition. The incidence rate of SPMs for patients with heritable retinoblastoma, which make up around half of all Rb-patients, is 8.4 per $1,000$ person years (95 % CI $6.3 - 11.1$) (Ketteler, Hülsenbeck, et al. 2020). The type of the pathogenic *RB1* variant also influences the incidence of SPMs (Ketteler, Hülsenbeck, et al. 2020; Dommering et al. 2012). For patients with somatic mosaicism for a pathogenic *RB1* allele, the incidence rate for SPM development appears to be considerably lower, with 2.1 per $1,000$ person years (95 % CI: 0.0–11.4). However, current studies include only few patients with somatic mosaicism, and therefore, risk estimations are imprecise (Ketteler, Hülsenbeck, et al. 2020). Patients with incomplete penetrance variants rarely develop SPMs (Ketteler, Hülsenbeck, et al. 2020).

The retinoblastoma treatment patients receive substantially influences the risk for SPMs (Abramson et al. 1984). The choice of therapy depends on several factors, including laterality at the time of presentation, genetic predisposition, size and location of the tumor, tumor progression, level of metastasis, age, and more. In high-income countries, most patients present with intraocular retinoblastoma that is confined within the eye and can often be cured by eye-preserving treatment. Therefore, the focus of treatment for these patients has shifted from saving the life to preserving vision and improving quality of life (Global Retinoblastoma Study Group 2020).

In low-income countries, however, extraocular retinoblastoma is quite frequent. Due to delayed diagnosis, retinoblastomas expand outside the eye and may infiltrate the choroid, the optical nerve, or even the central nervous system. These patients need to be enucleated, followed by adjuvant therapy. Enucleation is the removal of the eye with the tumor.

Retinoblastomas are very radiation sensitive, and therefore, external beam radiation therapy (EBRT) has been the eye-preserving therapy of choice for many years. It has been almost entirely replaced by chemotherapy because it has been shown that patients who received EBRT have a threefold higher risk for SPM development, mainly in the periorbital region within the irradiation field (Temming, Viehmann, et al. 2015). It is assumed that the radiation increases the risk of a mutation of the second *RB1* allele leading to the development of osteosarcomas or other SPMs (Chauveinc et al. 2001; Lefèvre et al. 2001). Nevertheless, EBRT is still an essential tool to treat relapses that do not respond to other therapies. EBRT using protons has been shown to have fewer side effects and is probably associated with a lower risk of second cancers compared to classical EBRT techniques and is therefore increasingly used (Daumann et al. 2020; Ketteler, Yiallouros, and Ch. Jurklies 2022).

Another eye-preserving therapy is chemotherapy. Systemic chemotherapy describes the intravenous delivery of chemotherapeutic agents distributed to all body compartments. It has been shown that systemic chemotherapy increases the risk for SPMs by 1.8-fold, being the most dominant risk factor for tumor growth outside the periorbital region. There are concerns that topoisomerase inhibitors, widely used as chemotherapeutic agents, induce SPMs, and it has been found that they increase the risk for leucemia, but further investigation, especially on the

impact of localized chemotherapy, is needed (Temming, Arendt, Viehmann, Eisele, Le Guin, Schündeln, Biewald, Astrahantseff, et al. 2017; Temming, Viehmann, et al. 2015).

Local chemotherapies aim to avoid or at least reduce the side effects of systemic chemotherapy. In intraarterial chemotherapy, the chemotherapeutic agent is directly administered into the arteria opthalmologica. A few studies have shown a high effectiveness of this treatment and mild side effects, but further data are needed, and, as of now, the long-term effects remain unknown (Daumann et al. 2020; Ketteler, Yiallouros, and Ch. Jurklies 2022).

1.2.3.2 Early detection of SPMs: The need for a diagnostic biomarker

There is a high need for a lifelong screening for survivors of heritable Rb. A risk stratification and screening protocol according to patient specific risk factors for SPM development which is primarily the therapy they received, is required. Screening can be performed by whole body MRT screening. However, this is too costly to be performed frequently and is marred by false positive findings. A molecular biomarker, ideally a non-invasive liquid biopsy examination, is desirable to enable early diagnosis of SPMs, lower the emotional stress for patients and families and ultimately reduce mortality (Temming, Arendt, Viehmann, Eisele, Le Guin, Schündeln, Biewald, Astrahantseff, et al. 2017). Although the genetic mechanisms of SPM development in carriers of *RB1* variants appear to be diverse, some genetic features of these SPMs, as well as parallels between retinoblastoma and SPM development, have been discovered (Friend et al. 1986; Açikbas et al. 2002; Benedict, Fung, and Murphree 1988; Lefèvre et al. 2001).

Osteosarcomas are the most frequent type of SPM (Wadayama et al. 1994). The mutational landscape of these tumors is highly heterogenous, with mutations found in 388 genes and somatic copy number alterations being more frequent than small variations (Kovac et al. 2015; Wu and Livingston 2020). *RB1* and *TP53* were found to be the main driver genes in 87 % of all osteosarcomas (Kovac et al. 2015). Alterations in *TP53* were found in $75-90$ % of the patients, alterations in the *RB1* gene occured in $50-78$ % of all osteosarcomas (Wu and Livingston 2020). LOH at the RB1 locus was detected in 62.9 % of osteosarcomas ($n = 63$) (Wadayama et al. 1994).

Furthermore, it has been found that heritable retinoblastoma predisposes to osteosarcoma and that almost all Rb-patients who developed osteosarcoma are heterozygous carriers of *RB1* mutations. Conversely, LOH within the *RB1* gene has even been proposed as a biomarker for early prediction of osteosarcoma (Feugeas et al. 1996). The second most frequent SPM entity is leiomyosarcoma. Zhai et al. found that six of 20 tumors showed LOH at the *RB1* locus (Zhai et al. 1999).

Taken together, as genetic alterations in SPMs are very heterogeneous, there are only very few common features that can be used as a biomarker to detect SPMs. LOH at the *RB1* gene locus is not only the most common event for the second hit that leads to retinoblastoma development, but it is also likely to be the most common alteration in the most common SPMs in patients with heritable retinoblastoma. This assumption is reasonable because the same molecular

mechanism triggers the development of Rb and SPMs (Friend et al. 1986; Açikbas et al. 2002; Benedict, Fung, and Murphree 1988; Lefèvre et al. 2001). Consequently, allelic imbalance at the *RB1* locus caused by LOH is a candidate biomarker for the early detection of SPMs in patients with heritable retinoblastoma. Potentially, this molecular characteristic could be detected in the cell-free components, such as EV-DNA or cf-DNA.

1.3 Diagnostic and prognostic biomarkers in uveal melanoma

1.3.1 Epidemiology and management of uveal melanoma

Uveal melanoma (UM) arises from melanocytes within the choroidal plexus, ciliary body, and iris of the eye, but apart from the cell type of origin, there are very few similarities between uveal and cutaneous melanoma (Van Raamsdonk, Griewank, et al. 2010). UM is a rare cancer accounting for only 5 % of all melanomas, but it is the most common intraocular tumor in adulthood (A. D. Singh, Turell, and Topham 2011). Most patients of UM are between 50 and 70 years of age (median 62 years) and slightly more often male than female (Jager et al. 2020; Aronow, Topham, and A. D. Singh 2018). In the United States, the age-adjusted incidence accounts for 5.2 cases per million. In Europe, the standardized incidence ranges from less than 2 to more than 8 cases per million. The numbers are highest in the north and decrease towards the south (Virgili et al. 2007). The main reason for this gradient is that fair skin and light-colored eyes, which are more frequent in northern Europe, are risk factors for uveal melanoma. Accordingly, studies on the population of the United States have shown that black people are rarely affected (Aronow, Topham, and A. D. Singh 2018). Other risk factors are melanocytoma, *BAP1* tumor predisposition syndrome, congenital ocular melanocytosis, or the rare dysplastic nevus syndrome. In contrast to retinoblastoma, patients with uveal melanoma are nearly exclusively unilaterally affected (Jager et al. 2020; Bornfeld et al. 2018). Around 50 % of the patients develop metastatic disease, which is fatal for nearly all of them (Fallico et al. 2021; Nathan et al. 2021).

Initial symptoms are highly dependent on the position of the tumor within the eye. Peripheral tumors mostly remain unrecognized for months or years, while tumors located at the posterior pole have an early effect due to their proximity to the macula. Typical symptoms are lens displacement, secondary glaucoma, or visual field defects (Bornfeld et al. 2018). Treatment options are plaque brachytherapy or proton beam irradiation, while advanced-stage tumors need to be enucleated. There is no treatment for metastatic disease that would significantly increase the lifespan of patients (Schefler and R. S. Kim 2021). UM can be diagnosed by clinical examination with the help of imaging technologies. The concurring opinion is that patients who develop metastasis later in the disease course already had micrometastasis at the time of treatment, but currently, there is no method allowing earlier detection of metastasis. Although there is usually no need for any invasive sampling of tumor tissue in terms of diagnosis, it is necessary for prognostic testing (Frizziero et al. 2019; Bornfeld et al. 2018).

1.3.2 Molecular genetics of uveal melanoma

Since 1996 it is known that more than half of the UM tumors show monosomy of chromosome 3 and that this chromosomal aberration is associated with metastasis and prognosis (Prescher et al. 1996). Other frequent chromosomal anomalies are gains of chromosome 8 or parts of 8q and gains of 6p or losses of 6q (Prescher et al. 1996). $3-5$ % of tumors show isodisomy 3,

which results from the loss of one copy of chromosome 3 and the duplication of the remaining one (White, McNeil, and Horsman 1998; Gallenga et al. 2022).

A genetic feature present in the vast majority (83 %) of UMs is a somatic mutation in one of the paralogue genes *GNAQ* and *GNA11*, both family members of the heterotrimeric G protein subunit alpha. Mutations occur exclusively in codons 209 (exon 5) or 183 (exon 4) of one of these genes encoding for G protein-coupled receptors (GPCR) and result in UM-specific changes of the conserved catalytic glutamine at position 209 (Van Raamsdonk, Bezrookove, et al. 2009; Van Raamsdonk, Griewank, et al. 2010; Gallenga et al. 2022). As a result, the proto-oncogenes *GNAQ* or *GNA11* are turned into oncogenes causing the MAP Kinase, PI3K/AKT, or YAP/TAZ pathway to be upregulated and promoting tumor progression. Constitutive activation of the MAP-Kinase pathway is known to play an important role in tumorigenesis of nearly all melanoma and nevi. Furthermore, it is considered an early event in UM development as it activates multiple pathways involved in cell growth and proliferation (Van Raamsdonk, Bezrookove, et al. 2009; Van Raamsdonk, Griewank, et al. 2010; Gallenga et al. 2022).

Mutations leading to GNAQ NP_002063.2 (p.Gln209Pro^Leu^Tyr) occur in 45 % of all uveal melanomas, and 22 % of UM metastases. Mutations in *GNA11* leading to GNA11 NP_002058.2 (p.Gln209Pro^Leu^Tyr) are less abundant in primary UMs (32 %) but more abundant in metastatic disease with 57 %. Mutations in codon 183 of one of the genes are comparatively rare, occurring in only 6 % of all tumors. Even though activating mutations in *GNA11* induce spontaneous metastatic spread in mouse models and although both genes are known to increase the number of intradermal melanocytes in mice, the particular mutation seems not to affect the survival of the UM patients (Van Raamsdonk, Bezrookove, et al. 2009; Van Raamsdonk, Griewank, et al. 2010; Gallenga et al. 2022; Decatur et al. 2016; Bauer et al. 2009).

The *BAP1* gene located on 3p21 encodes the BRCA1-associated protein 1 and is known to be a tumor suppressor gene. The ubiquitin C-terminal hydrolase (UCH) domain of BAP1 is involved in cell-cycle regulation, cell death, and differentiation (Han, Purwin, and Aplin 2021). Together with ASXL1, BAP1 forms the polycomb group repressive deubiquitinase complex, which plays a role in stem cell pluripotency and is involved in several developmental processes. It has been found that *BAP1* shows inactivating mutations in around 84 % of all metastasizing UM tumors and that those tumors exclusively showed monosomy 3. The mutations detected were loss of function mutations leading either to a premature stop codon or affecting the UCH domain of BAP1 (Harbour et al. 2010).

Martin et al. found mutations in one of the genes *EIF1AX* or *SF3B1* in 77 % of the tumors with disomy 3 and in 62 % of the tumors that showed only partial loss of heterozygosity of chromosome 3. *EIF1AX* encoding for the Eukaryotic Translation Initiation Factor 1A is located on the X chromosome, *SF3B1* is located on 2q33 and encodes for subunit 1 of the splicing factor 3b protein complex. Mutations in *EIF1AX* were mostly hemizygous missense mutations leading to a change of function by causing mainly in-frame changes (amino acid substitutions or short deletions) affecting the N-terminal part of the protein leaving the core protein unchanged (Martin-Marcos et al. 2017). Although the gene is located on a gonosome, men are not signifi-

cantly more frequently affected than women, which can be explained by mutations in this gene that always occur on the active X chromosome in females. In *SF3B1*, most of the mutations occurred within the region of HEAT repeats and were missense mutations leading to a change of the amino acid arginine at position 625. The protein encoded by this gene is an essential component of both spliceosomes and plays a key role in binding of these to the intron near the branch point. It is suggested that mutations in HEAT repeats lead to alternative splicing of many target genes but do not affect the general functionality of the protein complex (Martin et al. 2013).

1.3.3 Classification of uveal melanoma

In 2003, Tschentscher et al. were the first to describe two distinct entities of uveal melanoma that can not be distinguished by clinicopathological features (Tschentscher et al. 2003). Shortly thereafter, Onken et al. agreed to this concept. (Onken, Worley, Ehlers, et al. 2004). The tumor classes they described are highly correlated with prognosis. Patients having class one tumors have an excellent prognosis with a 92-month survival rate of around 95 % and a low risk of metastasis (Thomas et al. 2012; Onken, Worley, Ehlers, et al. 2004). Patients with class two tumors, on the contrary, have a poor prognosis, around 70 % die from metastasis within one year after diagnosis (Thomas et al. 2012). The tumor class can be distinguished based on several biomarkers as shown in figure 7 (page 41) and described subsequently.

The most prominent discriminator of both UM classes is the chromosome 3 status which has been previously described to be a reliable marker for prognosis. The loss of one chromosome 3 copy which is characteristic for class two tumors, likely occurrs very early in tumorigenesis, being one step of a two-step mutational mechanism typical for the inactivation of tumor suppressor genes (Tschentscher et al. 2003).

The mutation pattern differs between the two classes as well. Mutations in *EIF1AX* and *SF3B1* mainly occur in class one tumors, while *BAP1* inactivating mutations have been detected in 84 % of the class two tumors (Gallenga et al. 2022). The mutually exclusive occurrence of mutations in *EIF1AX* or *SF3B1* implicates substitutional effects of the mutations in these genes (Tschentscher et al. 2003).

Another feature associated with UM tumor class is the expression pattern, as reported by Tschentscher et al. The group found 34 genes to be upregulated by at least 3-fold and the transcript of eight genes to be completely absent when comparing the expression pattern in monosomy 3 tumors with the pattern in disomy 3 tumors (cf. figure 7).

Also, the methylation pattern is highly correlated with the tumor class (Robertson et al. 2017). For example, tumors with monosomy 3 and *BAP1* defects show a unique methylation profile with an inverse correlation between hypermethylation and *BAP1* mRNA expression (Robertson et al. 2017; Bakhoum et al. 2018).

Taken together, the tumor class can serve as a prognostic biomarker for clinical predictive testing and prediction of metastatic death.

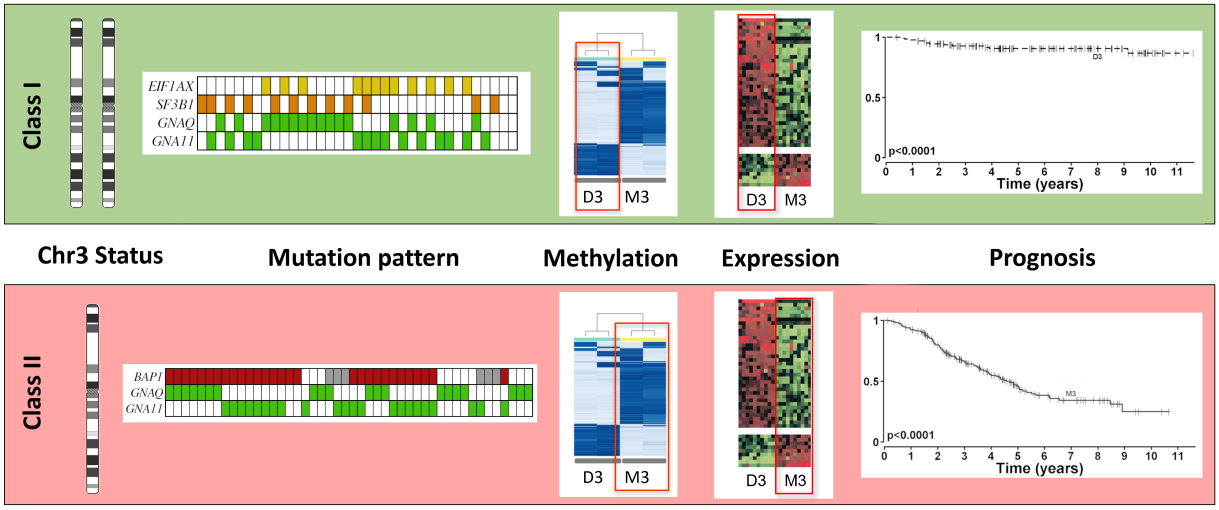

Figure 7: Classification of uveal melanomas. Data for the scheme of mutation pattern taken from Decatur et al. (2016), white boxes: no mutation, grey boxes: missing data; coloured boxes: mutation present. Graph of prognosis and scheme of expression pattern taken from Tschentscher et al. (2003) with permission (license number 5431911462841). Methylation pattern received from Michael Zeschnigk, unpublished data generated by Whole Genome Bisulfite Sequencing (WGBS), further data taken from Martin et al. (2013) and Harbour et al. (2010). D3: Disomy 3; M3: Monosomy 3; *BAP1*: Gene encoding BRCA1 associated protein-1; *GNAQ*: Gene encoding G protein subunit alpha Q; *GNA11*: Gene encoding G protein subunit alpha 11; *EIF1AX*: Gene encodding eukaryotic translation initiation factor 1A X-linked; *SF3B1*: Gene encoding splicing factor 3b subunit 1.

1.3.4 Tissue sampling for prognostic testing of UM

In most cases, the diagnosis of primary UM can be reliably made based on clinical features independent from histopathological analysis of tumor tissue. For detection of metastasis, liver function tests are performed as UM metastasis can be found nearly exclusively in the liver, but these tests have low sensitivity and can detect metastasis only at relatively advanced stages (Jin and Burnier 2021). Although prognosis currently has no effects on therapy management, most patients want to know their prognosis. For this purpose, tumor material is needed. Therefore, a tumor sample must be taken before therapy for tumors subjected to eye-preserving treatment. Transscleral or transvitreal tissue biopsies are the gold standard because they usually have a high cell yield (Frizziero et al. 2019; Schefler and R. S. Kim 2021).

Conventional methods to obtain tissue biopsies can have several side effects, like iatrogenic ocular morbidity or extraocular seeding, especially in cases of inadequate sampling. Consequently, they might worsen the outcome, which would be a considerable trade-off for prognostication only. However, the technique has evolved with the development of fine needle aspiration (FNA). One study that investigated the risks and side effects of FNA biopsies did not find iatrogenic extensions of the tumor and described the risk of extraocular dissemination as minimal but tested only ten patients in total (R. S. Kim et al. 2017). Another study observed intraarterial hemorrhage in 14 % of the patients (Sellam et al. 2016). In contrast to conventional biopsies, FNA biopsies sometimes fail to yield enough material for downstream analysis, especially if the tumor thickness is low. It has been reported that only around 80 % of the biopsies taken yield sufficient cellular material for genetic analysis (Augsburger, Corrêa, and Trichopoulos 2013;

Frizziero et al. 2019). This issue can be overcome by using a special forceps as described in Akgul et al. Tissue sampling with this forceps yields enough material for histological examination and rarely causes complications (Akgul et al. 2011)

1.3.5 Non invasive sources of biomarkers for diagnosis and prognosis of uveal melanoma

Prognostic, as well as diagnostic biomarkers, are already widely used in UM research and clinical routine. Mutations in *GNAQ* or *GNA11* are used as diagnostic biomarkers to confirm the diagnosis of UM. The tumor class, mainly determined by chromosome 3 status, is used as a prognostic marker. Clinical routine diagnostic, as well as prognostic testing, depends on the availability of tumor tissue which in the majority of tumors needs to be obtained by biopsy. A less invasive liquid biopsy is needed to provide a prognostic test that is safe and convenient for the patients (Frizziero et al. 2019). Such a test could also be helpful for monitoring treatment and tumor evolution, including possibly acquired therapy resistances.

cfDNA has been shown to be a good analytical target for a prognostic biomarker test for UM. Metz et al. showed that mutations in *GNAQ* or *GNA11,* which prove the presence of ctDNA, can be detected by ultra-deep amplicon NGS (C. H. D. Metz et al. 2013). Based on this marker, it was examined at which time points ctDNA can be detected in the blood of UM patients after treatment of the primary tumor for early diagnosis of metastasis. 135 patients were followed for up to 41 months, and blood was drawn at several time points. ctDNA has been detected in 17 of 21 patients who developed metastasis but not at the time of diagnosis. This suggests that at the time of diagnosis, the amount of ctDNA is insufficient in most patients for classification of UM. In 10 patients, ctDNA levels increase was detected prior to the clinical diagnosis of metastasis (Le Guin, Bornfeld, et al. 2021). Another study investigating levels of ctDNA after eight weeks of treatment found that the absence of ctDNA after this time correlates with progression-free survival (Cabel et al. 2017). However, a test based on the absence of a feature holds many challenges concerning sensitivity and specificity, especially in terms of false negatives.

Other subcomponents that have been shown to be sources of characteristics that can be used as biomarkers for liquid biopsy examinations are CTCs and extracellular vesicles. Many studies have examined the function of CTCs in the development of metastasis and analyzed their usability for biomarker analysis, but the detection and isolation of CTCs remain challenging as the abundance is usually very low. The prognostic value of CTCs remains unclear, but their proliferation is thought to contribute to metastasis. There are only a few studies on extracellular vesicles in UM, and in all studies sample sizes were small. EVs were found to be increased in UM patients, and miRNAs were detected in exosomes derived from vitreous humor (Ragusa et al. 2015; Jin and Burnier 2021). Further characterization of these vesicles, their release and uptake mechanism is needed to understand the role of EVs in UM and to evaluate whether they can serve as a analytical target for biomarker examinations (Jin and Burnier 2021).

As described previously, any body fluid can be a source of a biomarker, with blood being the most commonly used. In intraocular tumors like UM or Rb, aqueous humor or vitreous body

aspirate are of particular interest as they are in proximity to the tumor and have relatively low amounts of cell-free DNA by themselves. Hence, there have already been many investigations to find biomarkers in these body fluids. Two studies performed cytokine analysis in aqueous humor, one found a correlation between interleukin 6 and tumor thickness or serious retinal detachment (Midena et al. 2020). The other even found three prognostic clusters based on cytokine expression that correlate with several features such as staging or chromosome 3 status (Wierenga et al. 2019). Additionally, other protein markers like S-100, vascular endothelial growth factor, or HLA (human leukocyte antigen) have been investigated in aqueous humor and found to be related to prognosis (Jin and Burnier 2021).

The group of Jesse Berry has investigated cfDNA in aqueous humor and found sufficient levels of ctDNA for genetic analyses. ctDNA levels were highly variable depending on several clinical features such as radiation therapy or type of UM (ciliar body UM or choroidal UM). Somatic copy number alterations were successfully detected in post-radiation samples of ciliar body UM by shallow whole genome sequencing. The authors proposed that the low level of necrosis in UM patients might cause the low abundance of ctDNA in some patients (Im et al. 2022). It has been shown that vitreous body aspirate is also a possible source of cfDNA for mutation detection and determination of allelic fractions (Bonzheim et al. 2022).

1.4 Common requirements and overview of the analytical process

Developing a biomarker examination and validating this examination for the intended use in clinical routine is very challenging (Goossens et al. 2015; Califf 2018). In most kinds of primary samples, the abundance of cfDNA and EVs is very low, and therefore, methods with low a level of detection (LoD) are needed to achieve the levels of analytical sensitivity and specificity that are required for meaningful results. When developing and validating a test procedure, it is important to be aware of the wide spectrum of factors and error sources that can have an effect on analytical accuracy (Figure 8). In the following sections, the factors and sources of error that are most relevant for the biomarker examinations presented here (printed bigger in figure 8) will be discussed.

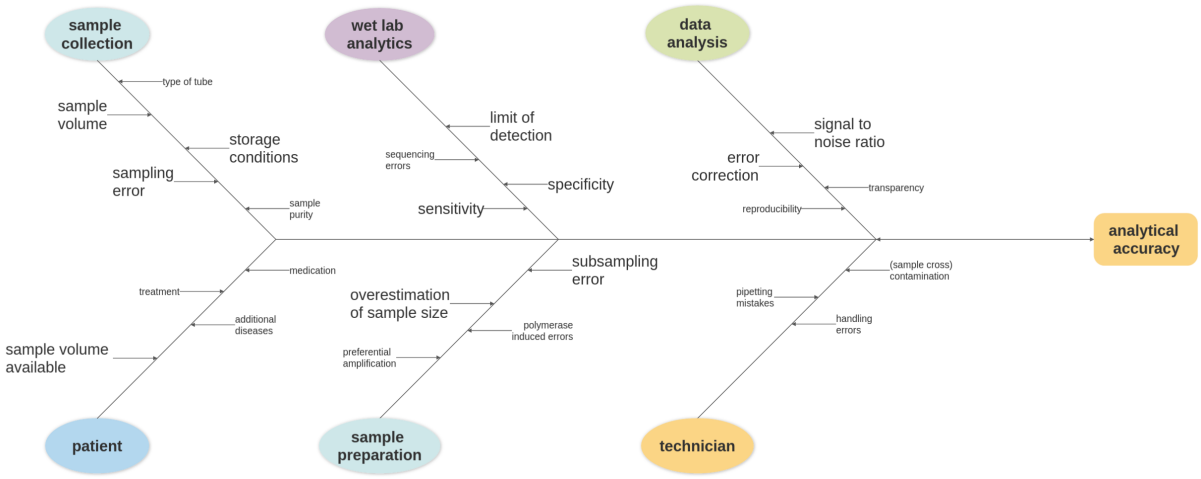

Figure 8: Graph of process. Graph showing factors that influence the analytical accuracy of a biomarker examination. Sources of these factors are shown in colored fields. Larger font sizes emphasize those factors that are most relevant in the context of this study and will be further described in the text.

1.4.1 Sample collection from patients

There is a wide spectrum of primary samples that can be used for biomarker examinations, with the most common ones being liquid biopsies. In terms of sample collection, three major parameters influence the analytical accuracy, these are the volume of the primary sample, storage conditions, and sampling error.

An insufficient **sample volume** leads to low analytical accuracy because of the low number of molecules available for analysis. However, the **sample volume available** from a patient is often limited by nature and/or due to ethical concerns like the amount of blood that can be obtained from small children. High levels of background DNA increase the required DNA input, for example, Ginkel et al. reported that 1 ml Plasma contained 2 to 422 copies of a mutated allele but 7,667 to 156,667 copies of the wildtype allele resulting in a fractional abundance down to 0.01 % which would be one genome equivalent of 10,000 requiring at least 66 ng of input DNA (Ginkel et al. 2017).

Storage conditions also influence the amount of a component or subcomponent of a liquid biopsy that is available for analysis. It has been observed that cfDNA in EDTA blood samples degrades rapidly, with a half-life of only a few minutes up to several hours (Meddeb, Pisareva, and Thierry 2019; Sato et al. 2018; Kustanovich et al. 2019). However, using blood collection tubes containing preservatives and low-bind reaction tubes can help to overcome this issue. This is especially helpful if blood from small children is used for liquid biopsy because the specific circumstances of the sample collection often preclude cfDNA isolation immediately after blood draw.

For the detection of rare variants, the **sampling error** is also relevant for analytical accuracy (Willey et al. 2021). How representative a random sample is for the original distribution depends on the ratio of positives in that original distribution. If a biomolecule of interest, like a specific cfDNA variant, is infrequent in the bloodstream, then the likelihood of obtaining a detectable number of the respective molecules is low. The same effect applies to the determination of allelic ratios. If the amount of cfDNA molecules obtained is comparably low, then the proportion of variant reads obtained does not accurately reflect the proportion in the bloodstream.

1.4.2 Sample preparation and wet lab analytics — Generating raw data on biomarkers

When generating raw data on biomarkers, the **limit of detection** (LoD), as well as the **sensitivity** and **specificity** of the method, are key for high analytical accuracy. Additionally, these parameters highly influence the suitability of the assay for the intended use. If the sensitivity and LoD are too low, a biomarker can not serve for early detection or prognosis. The LoD as well as the sensitivity, are directly influenced by the number of genome equivalents (GEs) obtainable from the primary sample.

The sampling error described in the last section is propagated every time a sample is drawn from a greater whole. This **subsampling error** applies when isolating cfDNA from the primary sample or drawing a sample for PCR or library preparation. Blomquist et al. proved that statistic sampling effects occur when subjecting DNA to the preanalytical process as well as when inserting a part of the preanalytical product into the analytical process (Blomquist et al. 2015). They proposed that stochastic sampling is a major challenge for the clinical implementation of liquid biopsies.

The parameters LoD and sensitivity, as well as the degree of subsampling error, are primarily determined by the choice of the analytical method. In the following, the two most commonly used methods for biomarker examination based on DNA, Droplet Digital PCR (ddPCR) and Next Generation Sequencing (NGS), will be discussed.

1.4.2.1 Droplet Digital PCR and Next Generation Sequencing

In the following, the two techniques, ddPCR and NGS, their strengths and weaknesses will be described. The LoD and sensitivity of these techniques will be pointed out. Lastly, they will

be compared regarding their suitability for detecting low-level ctDNA on the background of cfDNA in the context of liquid biopsy examination.

Droplet digital PCR

ddPCR was developed in 2011 with the aim to improve sensitivity, specificity, and limit of detection of (quantitative) Realtime PCR (Hindson et al. 2011). The major advantage of ddPCR compared to conventional PCR methods is the physical separation of the reaction into thousands of discrete measurements. DNA template molecules are enclosed in nanoliter-sized droplets. Ideally, each droplet would contain only one DNA molecule or none, but in fact, some droplets contain multiple DNA molecules. In order to correct for this issue, the number of target molecules present in the original sample is determined based on Poisson's law, and the fluorescence data is fitted to the Poisson distribution.

Droplets containing a DNA template emit fluorescence due to the hybridization of a fluorescently labeled probe to the given DNA template. Variant and wildtype alleles can be distinguished based on the wavelength resp. the color of the fluorescence signal. Depending on the instrument, up to four colors and their combinations can be detected. This allows a maximum of two variants to be detected simultaneously. Due to the separation of template molecules prior to PCR amplification, this technique is expected to allow precise counting of GEs without PCR-induced bias (Salk, Schmitt, and Loeb 2018).

One performance issue of the ddPCR is the so-called "rain", a phenomenon that causes that some droplets can not be clearly classified as positive or negative. The threshold of fluorescence intensity separating positive and negative signals is set by the software of the detector based on different calculations, but in some cases, especially if there is a lot of rain, it is not well determined and needs to be set manually. Rain, in general, leads to a loss of specificity (Jacobs, Goetghebeur, and Clement 2014).

The LoD is mostly specified by the minimal allelic fraction that can be detected and ranges from 0.01 % to 0.1 % (Volckmar et al. 2018; Guo et al. 2019; Dong et al. 2018) and is highly dependent on the assay as well as on the source, quality, and amount of DNA input. For liquid biopsies in routine diagnostic, the sensitivity ranges between 61 % and 82 %, but in study settings, higher sensitivities have been reported (Volckmar et al. 2018; Olmedillas-López, García-Arranz, and García-Olmo 2017). It has been shown that a shift from 2 ng to more than 5 ng increases the sensitivity of this method from 46.7 % to 82.6 %, which is concordant with other reports showing that the sensitivity declines with decreasing levels of input DNA (Olmedillas-López, García-Arranz, and García-Olmo 2017; Y. Zhang et al. 2017).

Next generation sequencing

Many different NGS techniques are available, but the most popular and commonly used one is sequencing by synthesis developed by Illumina (cf. 2.2.13 for method description). For rare variant detection, amplicon or hybridization capture sequencing is usually performed.

NGS is prone to errors that can arise from various sources (Barbany et al. 2019; Salk, Schmitt, and Loeb 2018). One source of errors is the sequencing process itself, the overall sequencing error of conventional NGS is about 1 %, however, for Illumina sequencers, error rates of $0.25 - 0.8$ %, have been reported (Salk, Schmitt, and Loeb 2018). Sequencing errors mainly result from different types of crosstalk like color crosstalk (an overlap of emission spectra of the dyes), crosstalk between sequencing cycles (due to nucleotide synthesis that is out of synchronization because of inverted repeats or patterns including many GGC sequence motives) or spatial crosstalk (an overlap of signals from adjacent clusters) (R. R. Singh 2020; B. Wang et al. 2017).

Another issue influencing mainly rare variant detection is the chance that due to errors, two identical molecules are generated during library preparation that would likely be classified as a variant leading to false positives (J. Hong and Gresham 2017). Additionally, the PCR amplification during library preparation leads to a biased increase in the number of molecules and an accumulation of polymerase-induced errors and might even change the composition of template molecules in amplified products due to preferential amplification (Casbon et al. 2011; R. R. Singh 2020). Errors occurring in the first few PCR cycles are detrimental as they lead to a high proportion of reads containing this artifact (J. Hong and Gresham 2017). The problem of errors introduced by DNA polymerases during PCR is intensified in terms of cfDNA because of the usually very small number of template molecules present in the sample.

The LoD, as well as the sensitivity of this method, depend on the sequencing depth. The lower the coverage at a given region of interest, the lower the sensitivity at this position. Therefore, the required coverage should be determined based on the minimally required read depth at the worst covered region of interest and the DNA input amount (Barbany et al. 2019; R. R. Singh 2020). Furthermore, sensitivity and LoD depend on the DNA quality and quantity. It has been shown for a *BRAF* mutant assay in cfDNA that the minimal variant allele fraction (VAF) that can be detected is 1,1 % for 5 ng and 0.2 % for 30 ng input DNA (Willey et al. 2021). Additionally, these parameters depend on the library preparation technique and the sequencing accuracy.

Comparison of both techniques

One disadvantage of ddPCR compared to NGS is that it can only cover very few variant sites, thus providing very limited options for multiplexing. If the goal is to investigate only a few known targets with high sensitivity, ddPCR is a good choice as it allows absolute quantification of mutant and wildtype molecules (Barbany et al. 2019; Volckmar et al. 2018).

Another major disadvantage of ddPCR is that prior knowledge of the targeted variants or at least positions of interest is required, and unexpected mutations will not be detected. NGS, on the contrary, allows *de novo* identification of sequence changes of various kinds, even of structural rearrangements. Amplicon NGS easily covers a wide range of mutations in a target region.

A major disadvantage of NGS compared to ddPCR is that it is not suitable for the direct determination of the number of genome equivalents because, with NGS, it is not possible to count

DNA molecules. In terms of ddPCR, the encapsulation in droplets prior to PCR amplification qualifies it as a perfect tool for measurement of effective genome equivalents, for example, by targeting SNP variants.

NGS requires PCR amplification which leads to an **overestimation of sample size** and consequently to an underestimation of variance and a miscalculation of any statistical value that relies on the sample size. For ddPCR, this effect is weak due to the incorporation of DNA template into droplets prior to DNA amplification but can occur if more than one DNA molecule is included in a droplet. However, it can be overcome for NGS applications using enhancements, as described in the next section. In terms of subsampling errors, ddPCR is superior as well because the sample preparation for NGS requires many steps of subsampling and dilution, whereas ddPCR requires only one step of subsampling.

Very recently, Ye et al. compared both techniques in terms of sensitivity and specificity, publishing a higher sensitivity for ddPCR (0.71 compared to 0.65) and a higher specificity for NGS (0.88 compared to 0.78) detecting *KRAS* mutations in liquid biopsy samples (Ye et al. 2021). For every biomarker examination, it needs to be evaluated which technique is superior, with the main criteria being the desired level of multiplexing and prior knowledge on the mutational landscape of a disease. Careful evaluation and validation using well-characterized or artificial samples (if available) should be performed for both techniques prior to liquid biopsy examinations in research but especially in clinical routine.

1.4.2.2 Enhancing NGS accuracy

As NGS has several shortcomings, several approaches to enhance this technique in terms of sensitivity and specificity have been tried to eliminate sources of errors and striving to enable absolute quantification by NGS.

One basic enhancement that is widely used is duplex sequencing. By sequencing the forward and the reverse strand of each DNA molecule, many sequencing errors can be identified and corrected with bioinformatical methods. For example, with this approach, the error rate drops from 10^{-3} to 10^{-8} for a MiSeq sequencer (Fox et al. 2014).

In 2011 unique molecular identifiers were developed, they enhance NGS accuracy by allowing accurate correction of PCR duplicates and improve the accuracy of measurement of allelic fractions tremendously (J. Hong and Gresham 2017; Kivioja et al. 2011). Counting individual molecules is difficult due to the bias introduced by PCR, but this can be conquered by adding a random but unique label to each DNA molecule prior to PCR amplification. In general, multiple types of labels are possible, but adding a DNA label of a predefined length (base pairs) and variable sequence has prevailed (Kivioja et al. 2011). This converts a pool of identical DNA molecules into a population of distinct ones resulting in a library, where each molecule carries an identifying sequence that can be used to determine the DNA molecule it originates from. Kivioja et al. established the term unique molecular identifiers for these DNA labels, in

short UMIs (Kivioja et al. 2011). With this enhancement, NGS can even be used for absolute quantification of DNA or RNA molecules without being limited to a few different targets like ddPCR (Kivioja et al. 2011; Fu et al. 2011). UMIs help to identify and eliminate errors and increase sensitivity in amplicon sequencing, and, together with duplex sequencing, a sensitivity of 0.1 % can be achieved (Barbany et al. 2019; Volckmar et al. 2018). Unfortunately, only very few commercially available systems for library preparation provide UMIs.

Further progress in NGS enhancement via UMIs was made with the SiMSen-seq technology (simple, multiplexed, PCR-based barcoding of DNA for sensitive mutation detection using sequencing) published by Stählberg et al. in 2017. This technology incorporates UMIs and other improvements to detect rare variants in cfDNA with ultra-high sensitivity (Ståhlberg et al. 2017). The method works with minimal DNA input and allows generation of specific PCR products. The latter is not the case in many other approaches incorporating UMIs as the random sequences of such often cause nonspecific primer binding and form concatamers that may outcompete the speicific products especially in cases of high level multiplexing (Ståhlberg et al. 2017). To overcome this, SiMSen-seq uses a novel primer architecture that includes a stem-loop structure which kind of protects the UMI during the first PCR cycles. These barcode primers are attached to the DNA template molecules during a three-cycle barcoding PCR. Additionally, the technique uses ultra-low primer and enzyme concentrations, long annealing and extension times and an enzymatic termination of the first PCR to guarantee uniform amplicon yields and improve specificity. The adaptor PCR is performed right after barcoding and directly followed by bead purification resulting in a fast and simple workflow. All in all, the authors claim that this method allows the detection of variant alleles at a frequency of less than 0.1 % (Ståhlberg et al. 2017). Furthermore, a software tool for grouping the reads that carry the same barcode and thereby differentiate between true variants and artifacts that occurred in any but the first PCR cycle is supplied.

1.4.3 Bioinformatical data analysis

Several commercial software solutions are available for analysis of NGS data. However, these tools have several disadvantages, like a lack of flexibility, as only preset options can be applied to the data. Additionally, new developments in bioinformatical research are only available with a delay because they first need to be integrated into the software. Furthermore, most commercially available solutions are neither specialized for cell-free DNA nor for extremely rare variants, and only very few support error correction using UMIs. However, there are many bioinformatical tools available open source that can be used to develop software pipelines that fulfil this purpose. The following sections introduce the tools that can be used to program an analysis pipeline for NGS postprocessing and statistical evaluation of the data.

1.4.3.1 R — a general purpose programming language

The programming language GNU R is a powerful tool for data analysis, especially statistical analysis of biological data, including data visualization. R comes with a lot of packages related to bioinformatical data analysis. Besides the CRAN repository, more than 2,000 software packages are available from the software library Bioconductor (Gentleman et al. 2004; Huber et al. 2015).

NGS sequencing and variant calling results in vcf-files containing information on the called variants. The data contained in these output files need to be further investigated and interpreted in order to answer questions or review hypotheses, this can be performed via R scripts. Additionally, R can be used to identify regions of interest for sequencing, including data analysis from common databases.

1.4.3.2 Debarcer — a tool for UMI based error correction of sequencing data

At the beginning of the work presented here, the number of tools for analysis of NGS data containing UMIs was very limited, and the availability of tools additionally specialized to cfDNA was even more limited. Debarcer is a tool fulfilling these requirements that was published by Ståhlberg et al. with the accompanying workflow described in section 1.4.2.2 .

The standard workflow consists of the four steps i.) preprocessing, ii.) alignment, iii.) UMI grouping iv.) error correction and variant calling. In the preprocessing step, the reads are reheadered, identifying the reads containing the amplicons of interest. Next, the reads need to be aligned to the reference genome using the Burrows-Wheeler Alignment Tool `bwa-mem` (other alignment tools can be used as well), unaligned reads are excluded. The following step of UMI grouping and error correction is key to this workflow. The tool groups reads into families based on their UMI sequence and position in the alignment, builds a network of UMIs, and filters out reads with a not properly oriented or a mutated barcode as well as those not containing the SiMSen-seq adapter region. Debarcer generates indices for each base describing its position in the genome before calculating a consensus sequence for each family. The parameters for generation of consensus sequence can be defined by the user, the settings used for this work are described in the methods section 2.3.2 on page 75. Lastly, variant calling is performed for the specified UMI families, and vcf files are generated containing the variants detected as well as several statistics on read depth, number of reads containing the alternative allele, and so on.

1.4.3.3 Varlociraptor — an uncertainty-aware variant caller with parameter free filtration

Varlociraptor is a novel tool for variant calling because of its sophisticated statistical model that encompasses all possible sources of uncertainty as well as biases. Uncertainties may originate from mapping quality, typing or might be a result of cancer heterogeneity. Possible biases are

strand bias, read pair orientation or position bias, biases arising from homologous regions, and others. Additionally, Varlociraptor provides the opportunity to filter the resulting variants by false discovery rates (Köster et al. 2020).

The typical workflow consists of a step of preprocessing followed by the actual variant calling step. For preprocessing, an alignment is required that is used for the discovery of candidate variants. These variants are written to a vcf-file that is used as input for variant calling. In the next step, the candidate variants variant are filtered by applying thresholds for various scores prior to final variant calling (Köster et al. 2020).

1.4.3.4 Snakemake — a workflow manager for reproducible and scalable data analysis

Snakemake is a workflow management system that allows for highly reproducible and sustainable data analysis, as shown in figure 9. It gained a lot of interest (1,500 citations, source: https://badge.dimensions.ai/details/id/pub.1018944052, accessed 15.09.22) and has a huge community (users on GitHub, as from 15.09.20, accessed 15.09.22). It decomposes workflows into steps called rules, where each rule represents an operation like shell commands, invoking an external script, or many others. Each rule also defines how to obtain output files from input files which is used by Snakemake to automatically determine an execution order based on dependencies of rules on each other. Wherever possible, it parallelizes rule execution to reduce analysis runtime and to make optimal use of the system's available computation resources. Automatically inferred wildcards in input as well as output files additionally allow for parallel processing of multiple samples (Mölder et al. 2021).

Snakemake is text-based (Python and domain-specific syntax), making all parameters, scripts, and custom code fully accessible. Scripts in other languages like R can be invoked from a Snakemake rule resulting in one script for a complete workflow from raw data to visualization and statistical analysis. This leads to a high level of transparency regarding the code and its documentation and regarding the results as all parameters and settings can be traced through all steps of the analysis (Mölder et al. 2021).

Another advantage of Snakemake is tracking of code changes and automatic recomputation of changes rules. Even more important, Snakemake detects changes in rule input files and automatically performs reanalyzation executing only the rules that directly or indirectly depend on this file. Rules are not executed a second time when their output files are already present, and their input files did not change, which saves computation time. This is highly desirable in case of NGS analysis, where single analysis steps require a lot of computation time (Mölder et al. 2021).

All in all, with its reproducibility, adaptability (to extended or slightly different approaches), and transparency (as shown in figure 9), this workflow manager enables sustainable data analysis that can be technically as well as methodologically validated and thereby paves the way for implementation into clinical routines. Furthermore, Snakemake workflows developed for a

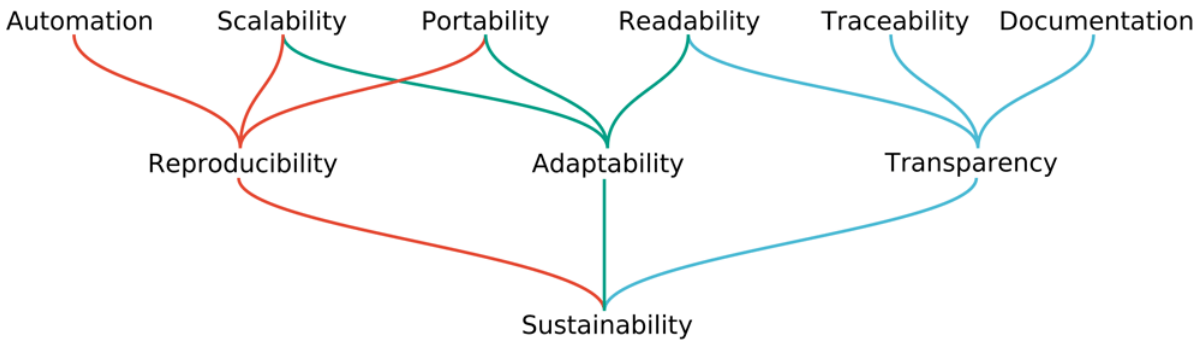

Figure 9: Snakemake concept. Graph of the aspects of sustainable data analysis covered by the workflow manager Snakemake. Taken from (Mölder et al. 2021) licensed under CC BY 4.0.

common use case in diagnostics could be exchanged between hospitals. In terms of research, workflows are already exchanged between groups as the size of the Snakemake workflow repository emphasizes (Snakemake-Workflows Contributors 2017).

1.5 Aim

1.5.1 Two biomarker tests based on similar analytical principles

The aim of the two research projects presented here was to find a biomarker for a liquid biopsy that, on the long run, can be used for risk stratification of patients in terms of routine diagnostics. The target characteristic addressed by this biomarker had to be a feature common to all patients. Loss of heterozygosity (LOH) is such a common feature of both intraocular tumors we have studied but is also a key event in the tumorigenesis of many other tumor entities. LOH can affect genomic regions ranging from a single gene locus, as in retinoblastoma, to an entire chromosome, as in uveal melanoma. In DNA from tumor tissue, LOH can be detected by clinical routine methods like microsatelite analysis however, this method is not suitable for cell-free DNA[1] due to the high background of normal DNA, low concentration, and high degree of fragmentation of this DNA species. Hence, for the development of a liquid biopsy examination using LOH as a biomarker, other measurement strategies need to be investigated.

Somatic cells, as well as tumor cells, shed DNA into the bloodstream, and therefore, both contribute to the cfDNA pool leading to a particular ctDNA ratio depending on different factors like tumor size or degree of apoptosis (for further details, see section 1.1.5). Usually, ctDNA and cfDNA are distinguished by analysis of mutations characteristic for the tumor, but if LOH is a characteristic feature of the tumor, it could be used to distinguish these two DNA species as well. DNA released by tumor cells with LOH is expected to skew the ratio of alleles in EV-DNA and cfDNA.

Single Nucleotide Polymorphisms (SNPs) are genomic variations that affect only a single base and can occur heterozygously as well as homozygously. If a SNP is heterozygous in the constitutional DNA of a patient who develops a tumor, which shows LOH in the genomic region of the SNP, then this SNP undergoes LOH as well and becomes homozygous. It is to be expected that the ctDNA derived from this tumor shows this feature as well. We hypothesize that LOH can be detected by targeting SNPs located in the region where LOH occurs or being linked to it.

Conclusively, we hypothesize that the admixture of ctDNA, carrying LOH to a cfDNA pool, leads to an allelic imbalance and that this can be detected by counting the signals from alleles of SNPs that are located in the region of LOH or linked to it. To analyze the SNP's state, we aim to detect the variant allele fraction (VAF) at the position of the SNP(s). In the somatic cells of a patient informative for a SNP of interest, the VAF is 0.5. If admixture of ctDNA has occurred, the VAF is expected to be shifted.

[1] For this subsection the terms cell-free DNA (cfDNA) and cell-free tumor DNA (ctDNA) include vesicle-derived DNA.

1.5.2 A non-invasive blood test for early detection of SPMs in Rb-survivors

Neoplasms that develop in patients with a heritable predisposition to retinoblastoma show an extensive genetic heterogeneity which makes the development of any kind of biomarker examination for early detection of SPMs challenging. There is a need for a biomarker assay that is applicable for all or at least the majority of patients. With the European cooperational project NIRBTEST (Non-invasive *RB1* cancer TEST, partner sites VUMC, Netherlands and Institut Curie, Paris) we aim to find a biomarker for non-invasive early detection of SPMs in survivors of heritable retinoblastoma. As described in chapter 1.2.3.2, there is a high need for a lifelong and very sensitive screening test that allows early detection of SPMs and improves the risk stratification for patients with heritable retinoblastoma.

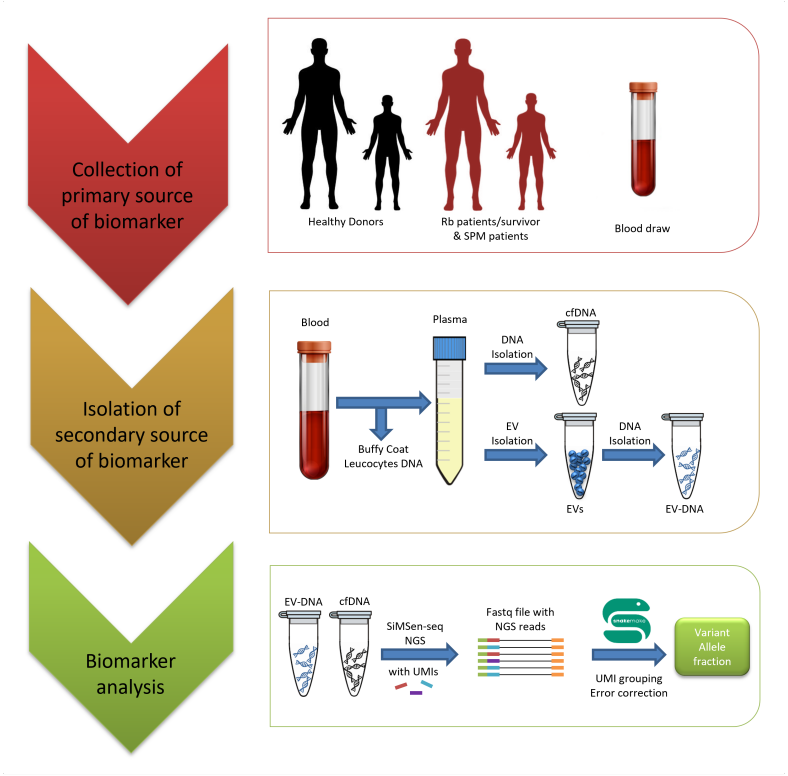

Figure 10: Scheme of the NIRBTEST workflow. EV: extracellular vesicle; EV-DNA: DNA derived from extracellular vesicles; cfDNA: cell-free DNA; SPM patient: a patient who had a second primary malignancy in any reasonable time around the blooddraw; Rb-patient: retinoblastoma patient (child); Rb-survivor: patient who survived retinoblastoma in childhood and was healthy at time of blooddraw (adult).UMI: Unique Molecular Identifier, SiMSen-seq NGS: Simple, multiplexed, PCR-based barcoding of DNA for sensitive mutation detection using sequencing method as published by Ståhlberg et al. (2017).

DNA released by tumor cells with LOH at the *RB1* locus is expected to skew the ratio of *RB1* alleles in EV-DNA and cfDNA. In individuals with SPM, allele ratios are expected to be skewed in comparison to balanced ratios expected in healthy individuals. We aim to detect these skewed allelic ratios by deep amplicon NGS of SNPs in cfDNA. To improve the analytical accuracy of our test, we choose the SiMSen-seq technology that incorporates UMIs. Subsequently, we perform a bioinformatical analysis using Debarcer, Snakemake, and Varlociraptor to receive reproducible and sustainable results. The workflow is illustrated in figure 10. Additionally, we

investigate the number of GEs in cfDNA as well as EV-DNA samples to compare these DNA specimen and find the most suitable one for our liquid biopsy approach.

1.5.3 A minimal invasive prognostic test for uveal melanoma based on cfDNA from aqueous humor and vitreous body

Prognostic testing of uveal melanoma depends on the availability of tumor tissue. Tissue sampling is a very invasive surgical procedure, and the result of prognostic testing has no influence on therapy. On the contrary, it has a very huge impact on the patient as the survival rate differs extremely between the tumor classes.

The prognosis of UM patients differs extremely based on the tumor class, which can be detected in tumor DNA. Hence, prognostic testing of uveal melanoma depends on availability of tumor tissue. Tumor tissue is readily available for large tumors, which are usually treated by enucleation, but tissue biopsy must be performed for small and medium-sized tumors. The collection of tissue samples is a very invasive surgical procedure. Since the result of the prognostic test has no influence on therapy, the benefits must be weighed carefully against the risks of the test.

Consequently, there is a high need for a less invasive method to obtain tumor DNA. A liquid biopsy could fulfill this purpose. In other tumor entities, ctDNA has already been detected in the blood of patients at the time of diagnosis, but in uveal melanoma patients, this has only been achieved in a few cases (C. H. D. Metz et al. 2013). Possible alternative sources of tumor DNA are aqueous humor (AH) or vitreous body (VB), the sampling process of these liquid biopsies is more invasive than a blood draw but less invasive than tissue sampling. Both body fluids are expected to contain higher levels of ctDNA than blood and low levels of background cfDNA due to their high proximity to the tumor.

We present a feasibility study that aims to detect ctDNA in AH and VB and evaluate the suitability of these liquid biopsies for prognostic testing of UMs. First of all, we aim to distinguish between cfDNA and ctDNA to determine the levels of ctDNA in those body fluids by sequencing *GNAQ* and *GNA11*, searching for UM characteristic mutations. The levels of ctDNA will be analyzed by deep amplicon sequencing followed by the determination of the variant allele fraction using a custom Snakemake pipeline as shown in Figure 11.

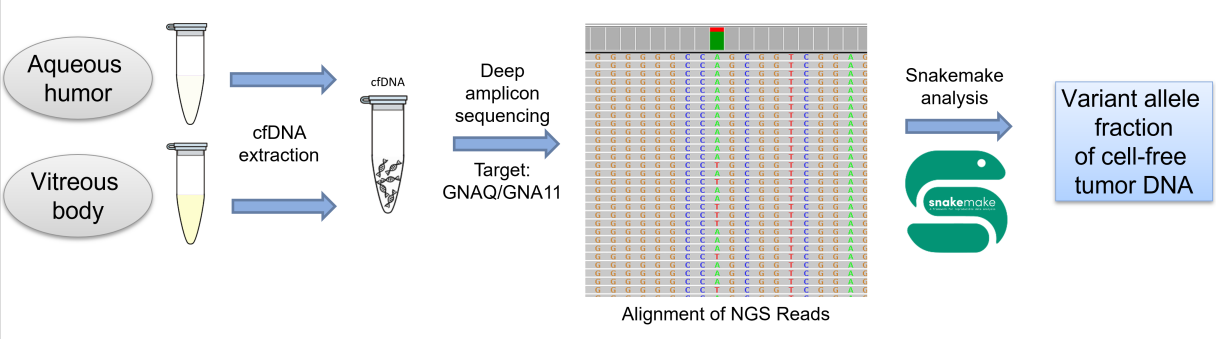

Figure 11: Scheme of the workflow for development of prognostic test for UM patients. cfDNA: cell-free DNA.

Our long-term goal is the ctDNA-based determination of UM tumor class. We aim to detect the best established biomarker monosomy 3 by determination of the allele ratio of multiple SNPs that are randomly but evenly distributed over the entire chromosome 3. DNA released by tumor cells with monosomy 3 is expected to skew the allele ratio of informative SNPs in cfDNA, which can be detected by measuring the allele ratio at each SNP locus. Our goal is to provide a proof of concept for monosomy 3 testing by NGS-based SNP sequencing in cfDNA from UM patients.

2 Material and methods

2.1 Material

In this chapter the patient cohorts from which we obtained samples are described. Also, the technical equipment, consumables, enzymes, oligonucleotides and used software are listed.

2.1.1 Patient cohorts

Samples from two different patient cohorts were used for the analysis underlying this work. Analysis associated with the development of a non-invasive blood test for early detection of SPMs in Rb-survivors were performed using blood samples taken from a retinoblastoma patients cohort. Additionally blood samples from healthy children as well as adults were collected and served as controls for this analysis. Samples of aqueous humor and vitreous body from uveal melanoma patients were used for all efforts on a minimal invasive prognostic test for uveal melanoma based on cfDNA.

2.1.1.1 Retinoblastoma patients

The european NIRBTEST study underlying this work has been carried out from Ocotber 2018 until September 2022 in three centres located in three different european countries. The participating centres were the VUMC (Vrije University Medical Center) in Amsterdam (Netherlands), the Institut Curie in Paris (France) and the Unviversity Hospital Essen (Germany).

More than 90 % of all children with retinoblastoma in Germany are treated in the university hospital Essen as it is the national reference center for retinoblastoma. The multicenter Rb-registry located at the University Hospital Essen includes children with a newly diagnosed eye tumor or a genetic predisposition for retinoblastoma since 2013. Data of the Rb-registry was used to identify, invite and include survivors of heritable retinoblastoma. Children with retinoblastoma were included in collaboration with the eye clinics department, patients with SPMs were included in collaboration with the West German Cancer Center. All patients were included after informed consent of the patients themselves or their parents. Blood was drawn and a questionaire about the current health status, treatment of past retinoblastoma and information on previous SPMs was completed. Ethical approval for patients included at the Unviersity Hospital Essen was obtained from the University of Duisburg-Essen ethics committee. Patient inclusion and sample collection were analogously performed by the cooperation partners (in the Nethderlands and France) under local ethical approvals. Samples were exchanged between countries under a material and data transfer agreement between the sites and with consent of the patients. Sample collection and preprocessing were harmonized and standardized between the centers.

2.1.1.2 Uveal melanoma patients

Uveal melanoma patients whose affected eye needed to be enucleated were included in the study. Aqueous and vitreous aspirate were taken from the enucleated eye after enucleation. This procedure resulted in no harm for the patients. Ethical approval was given by the ethics committee of the Unviersity Duisburg-Essen.

2.1.2 Technical equipment

The technical equipment used is listed below.

Device	Model	Manufacturer
Centrifuges	5804	Eppendorf
	Allegra X-22 Centrifuge	Beckman Coulter
	Avanti™ J-20 XP	Beckman Coulter
	miniSpin plus	Eppendorf
	Minizentrifuge Sprout (Plus)	Biozym Scientific
	Multifuge 3L	Heraeus
ddPCR System	QX100 Droplet Reader	Bio-Rad
Digital Printer S/W	P93D	Mitsubishi
Droplet Generator	QX100 Droplet Generator	Bio-Rad
Electronic Pipette Controler	Easypet®	Eppendorf
	Pipetus®	Hirschmann
Electrophoresis Chamber	multiSUB Choice	Cleaver Scientific
Fluorometer	Qubit 4	Invitrogen
Geldocumentation System	ChemoStar Touch 21.5	Intas
Mortar and pestle	Melamin, 125 mm	Öhmen
Nanoparticle Tracking Analysis	ZetaView	Particle Metrix
NGS Sequencer	Illumina MiSeq System	Illumina
	Illumina MiniSeq System	Illumina
Pipettes	Distriman	Gilson
	Eppendorf Research	Eppendorf
	Pipetman	Gilson

Device	Model	Manufacturer
	Pipet-Lite Multichannel	Rainin
Plate Sealer	PX1™ PCR Plate Sealer	Bio-Rad
Power Supply	Power Pro	Cleaver Scientific
Real-Time PCR System	LightCycler® 480 Instrument II	Roche Diagnostics
Sanger sequencer	Genetic Analyzer 3130XL	Applied Biosystems
Scales	analytical scale BP61	Satorius
	precision scale EW 1500-2M	Kern & Sohn
	440-35 N	Kern
Spectrophotometer	NanoDrop 2000	Thermo Scientific
Thermal Cycler	Veriti™ 96 Well thermal Cycler	Thermo Scientific
Thermomixer	Comfort 5355	Eppendorf
Tube Roller	SRT 9	Stuart
Ultracentrifuge	Optima L7-65	Beckman Coulter
Vacuum Manifold	EZ-Vac Vacuum Manifold	Zymo Research
Vortexer	7-202	neoLab
	Vortex Genie 2	Scientific Industries
Water Bath	SW-20C	Julabo

2.1.3 Consumables

The consumables used are listed below.

Consumable	Version	Manufacturer	Cat. Nr.
Amicon Ultra Centrifugal Filter	2 ml Volume, 10 kDa molecular weight cutoff	Merck	UFC201024
Blood Tubes	7.5 ml EDTA	Sarstedt	01.1605.001
Centrifugation Tubes	Cellstar® 15 ml / 50 ml	Greiner Bio-One	188271/ 227261
Chromatography Columns	Econo-Pac	Bio-Rad	7321010
ddPCR Consumables	DG8™ Cartridges	Bio-Rad	1864008

Consumable	Version	Manufacturer	Cat. Nr.
	DG8™ Gaskets	Bio-Rad	1863009
	ddPCR™ 96-Well Plates	Bio-Rad	12001925
DNA LoBind Tubes	1.5 ml	Eppendorf	9409326
Lids for PCR Reaction Tubes	8/12-Cap Strip	Applied Biosystems	N8010535/4
PCR Plate Heat Seal	foil, pierceable	Bio-Rad	1814040
PCR Reaction Tube Strips	8-Tube Strip	Applied Biosystems	N8010580
PCR Reaction Tubes	MicroAmp Reaction Tube without Cap	Applied Biosystems	N8010533
PCR / Sequencing plates	Fisher Brand 96-Well, PP, 0.3 ml semi-skirted	Fisher Scientific	14230244
Pipette Tips	diverse volumes with and without filter	Star-Lab	
	200 µl with and without filter	Rainin	
	diverse volumes with filter	Gilson	
Push Cap	neutra	Sarstedt	65.816
qEV Original Columns	70 nm, <500 µl loading	Izon	SP1
qPCR Plate	Light Cycler 480 96-well Plate, white	Roche	04729692001
qPCR Sealing Foil	Light Cycler 480 Sealing Foil	Roche	04729757001
Reagent Tubes	1.5 ml / 2 ml	Sarstedt	72.690/ .001
	Mikro-Schraubröhre 1.5 ml / 2 ml	Sarstedt	72.692/ 4.005
Sephadex Plates	MultiScreen®-HV, 96-Well Plates, 0.45 µm Hydrophilic, low Protein Binding	Merck	MAHVN4550
Serological Pipette	Cellstar, diverse volumes	Greiner Bio-One	
Sonication Tubes	microTUBE AFA Fiver pre-slit snap-cap	Covaris	520045
Tubes	14 ml, PP	Sarstedt	55.538

2.1.4 Chemicals and reagents

The chemicals and reagents used are listet below.

chemical / reagent	Manufacturer	Cat. Nr.
0.5 M EDTA, pH 8.0	AppliChem	A4892,0100
1 M Tris, pH 8.0	AppliChem	A4577,1000
1 N NaOH	AppliChem	181691.1211
2-Propanol/Isopropanol	Merck	1096342500
3 M Sodium Acetate	Serva	39572.01
5 M NaCl	AppliChem	A7006,0250
10 % SDS	ThermoFisher	24730020
Ampure XP Beads	Beckman Coulter	A63881
Chloroform : Isoamylalkohol 24 :1	AppliChem	A1935,0100
CutSmart Buffer	NEB	B7204S
dNTP Set 100 mM Solution	Thermo Fischer	R0181
Droplet Generation Oil for Probes	Bio-Rad	1863005
Droplet Reader Oil	Bio-Rad	1863004
Dulbecco's Phosphate-Buffered Solution	Gibco	12008489
Ethanol absolute	Merck	100986
Ethidiumbromid 10 mg/ml	Thermo Scientific	15585011
FastRuler Ultra Low Range DNA Ladder	ThermoScientific	SM1233
Hi-Di™ Formamid	ThermoScientific	4311320
GeneRuler 100bp Plus DNA Ladder	ThermoScientific	SM0321
illustra Sephadex G-50 DNA Grade	GE Healthcare Life Science	17057301
L Carnitin	Sigma	C0283-1G
Natronlauge 1 mol/l (1 N)	AppliChem	181691.1211
peqGold Agarose universal	VWR	35-1020
Phenol	AppliChem	A1153,0100
RNA later stabilization solution	Invitrogen	AM7020

chemical / reagent	Manufacturer	Cat. Nr.
Sepharose CL-2B (1 l)	Bio-Rad	G 17014001
TE Buffer (1x) pH 8.0	AppliChem	A0386,0500
Tris-HCl 200 mM, pH 7.0, sterile	Teknova	T2260
TriTrack Loading Dye	Thermo Fischer	R1161
water for chromatography (LC-MS Grade)	Merck	115333

2.1.5 Enzymes

The enzymes or Master Mixes containing enzymes are listet below.

Enzyme or Enzyme Containing Mix	Manufacturer	Cat. Nr.
ddPCR Supermix for Probes (no dUTP)	Bio-Rad	1863024
ddPCR Mut Assay GNAQ/GNA11	Bio-Rad	10049550
ddPCR Mut Assay SNP	Bio-Rad	100490447
ExoSAP-IT™	Applied Biosystems	12664537
HaeIII	NEB	R0108S
HotStarTaq Master Mix	Qiagen	1010023
LightCycler 480 SYBR Green I Master	Roche	04707516001
Phusion High-Fidelity DNA Polymerase	Thermo Scientific	F530S
Phusion Hot Start II DNA Polymerase	Thermo Scientific	F549S
Protease from Streptomyces griseus	Sigma-Aldrich	P5147-100MG
Proteinase K	Qiagen	19131
Q5 Polymerase MM	NEB	M0494S

2.1.6 Ready-to-use reaction systems (Kits)

Ready-to-use reaction systems (kits) used for this work are listed below. The procedure was done according to the instructions for use. Any modifications are described in the corresponding methods section of this thesis.

Kit	Manufacturer	Cat. Nr.
Agilent DNA 1000 Kit	Agilent	5067-1504
Agilent High Sensitivity DNA Kit	Agilent	5067-4626
BigDye® Terminator v1.1 Cycle Sequencing Kit	Thermo Scientific	4337451
Dynabeads™ DNA DIRECT™ Universal Kit	Invitrogen™	63006
FlexiGene DNA Kit	Qiagen	51206
NEBNext Library Quant Kit for Illumina	NEB	E7630
PME free-circulating DNA Extraction Kit	analytikjena	845-IR-0003010
Q5® Hot Start High Fidelity 2X Master Mix Kit	NEB	M0494S
QIAamp Circulating Nucleic Acid Kit	Qiagen	55114
QIAamp DNA Micro Kit	Qiagen	56304
QIAamp DNA Mini Kit	Qiagen	51304
QuantiFluor® dsDNA System	Promega	E2670
Qubit dsDNA HS Assay Kit	Invitrogen	Q32854
Qubit ssDNA Assay Kit	Invitrogen	Q10212

2.1.7 Oligonucleotides

All oligonucleotides used are listed in the appendix (8.1).

2.1.8 Software

All software used for this work is listed below.

Software	Version	Manufacturer
Atom	1.58.0	GitHub / Atom Community
Geneious Prime	2019	Dotmatics
Light Cycler 480 Software	1.2.9.11	Roche
Lyx	2.3.4.2	Lyx-Team
MiniSeq Control Software	2.0	Illumina

Software	Version	Manufacturer
Primer3web	4.1.0	Untergasser et al. 2012
QuantaSoft	1.7.4	Bio-Rad
R Studio	2021.09	RStudio, PBC
DNA Sequencing Analysis Softwar	5.1	Applied Biosystems
Sequencing Analysis Viewer	2.4.7	Illumina
Visual Studio Code	1.72.2	Microsoft

2.2 Molecular-biological methods

2.2.1 Extracting plasma from whole blood

Whole blood from patients as well as healthy donors was collected in 7.5 ml EDTA Tubes. If possible, 7.5ml of blood were drawn, however in some cases this was not possible for ethical reasons. These were immediately inverted three times and then transferred to the laboratory. A first step of centrifugation was performed at 500 g for 10 min in a swing-bucket rotor to separate the plasma from the red blood pellet. The supernatant was transferred to 15 ml centrifugation tubes without transferring the leucocytes containing buffy coat. If required, the buffy coat was transferred to a separate tube and kept at -80 °C for extraction of genomic DNA. The plasma was centrifuged again at 3000 g for 20 min for further purification. The supernatant was transferred to 1.5 ml reagent tubes and stored at -80 °C. This procedure was performed equally for all samples and conducted in the same way in every center. However, in the collaborating centers only 5 ml of blood were collected if possible due to local ethical restrictions. Samples collected in the other contries were shipped to Essen on dry ice and stored at -80°C until DNA isolation.

2.2.2 EV Isolation

EVs were isolated by sequential ultracentrifugation or by size exclusion chromatography using either self-made or commercially available columns as described below.

2.2.2.1 Ultracentrifugation

Plasma samples were centrifuged at 12,000 g for 20 min at 10 °C. If necessary, PBS was used for balancing. 200 µl of the supernatant were transferred to a new tube and kept at -80 °C. The remaining supernatant was transferred to ultracentrifugation tubes and centrifuged at 100,000 g and 10 °C for 70 min. The supernatant was removed and kept at -80 °C as a first fraction,

the pellet was resuspended in 2 ml PBS and centrifuged again with the same conditions. The supernatant was removed, the pellet resuspended in 200 µl PBS and transferred to 1.5 ml reagent tubes for storage at -80 °C.

2.2.2.2 Size Exclusion Chromatography (SEC)

SEC is a method to separate particles in solution based on their size. Larger molecules pass the columns faster than smaller molecules, because the latter are trapped in the pores of the matrix. Hence, this method can be used to enrich nanoparticles such as EVs of a specific size. Two different ways of SEC are commonly used, on the one hand SEC columns can be prepared manually, on the other hand commercially available columns can be used.

SEC with self-made columns

The sepharose was first washed by adding 500 ml of PBS followed by gentle manual shaking. After incubation at 4 °C for 4 – 24 hours to achieve separation of the two fluids, the PBS was removed. The washing procedure was repeated and afterwards fresh PBS was added. The tip of the chromatography columns was cut and sepharose solution was added. The PBS passed trough the column while the sepharose gel was forming. The column was filled with 11 ml of sepahrose solution. The filter was added on the top of the gel and slightly pushed down so that the gel level reached the 10 ml mark of the column. All columns were washed with PBS by closing them, filling them up completely and letting the PBS run through. The plasma samples were centrifuged at 14,000 g and 4 °C for 30 min and the supernatant was added to the column. Next, 1 ml PBS was added to the column and the flowthrough was discarded. Then 1 ml of PBS was added and the flowthrough was considered the first fraction. This step was repeated sequentially and only the flowthrough considered to be the 4th fraction was collected in a 1.5 ml reagent tube. For establishment processes all fractions were kept.

SEC with commercially available columns

Size exclusion chromatography of plasma samples was done using qEV original columns from Izon company with a cutoff of 70 nm according to manufacturer's guidelines. 1 ml purified plasma (extracted as described in 2.2.1) was loaded to the washed column. 2 ml PBS were added and the resulting void volume was collected. Sequentially 500 µl PBS were added and the flowthrough was collected, this was repeated eight times, collecting eight fractions in low protein bind reaction tubes.

2.2.2.3 Ultrafiltration

EVs in the solution obtained by EV isolation were further enriched by ultrafiltration using Amicon Ultra Spin Filters with a cutoff of 10 kDa and a maximum capacity of 2 ml. Approximately

500 µl of EV solution were loaded on the column. A two step centrifugation protocol was performed according to manufacturer's guidelines. The first centrifugation step was performed at 3,000 g for 10 min in a swing-bucket rotor, the second step was done at 1,000 g for 2 min. The flowthrough of the second spin was kept at -80 °C for further analysis.

2.2.3 Particle measurement

The concentration of extracellular vesicles can be determined by nanoparticle tracking analysis based on dynamic light scattering. As this measurement detects particles of all kinds the measurement precision is highly dependeing on the purity of the EV isolation. A ZetaView machine (ParticleMetrix) was used for this purpose. The calibration was performed with a 100 nm standard with a dilution of $1:1,000$ and $1:266,000$. The daily performance was checked using the internal software tool. The following paramters were set for all measurements: Positions = 11, number of cycles = 5, quality = medium, min brightness = 20, min. size = 5, max. size = 200, tracelength = 15, sensitivity = 75, shutter = 75, frame rate = 30. $80-150$ particles were used for measurement, if the number of particles detected by the software exceeded this number, the measurement was repeated. After measurement, the region of interest was defined according to the needs of the single experiment.

2.2.4 Isolation of genomic and cell-free DNA

2.2.4.1 Genomic DNA from blood

Extraction of genomic DNA from whole blood was done using the FlexiGene Kit (Qiagen) according to the manufacturer guidelines for human blood. Buffy coat from the plasma isolation process of patient samples or healthy controls was used to extract high molecular weight DNA from leucocytes with this Kit. DNA was eluted in 5 µl to 400 µl of FG3 Buffer.

2.2.4.2 DNA from tumor tissue

DNA from fresh frozen tumor tissue was isolated by Martina Fleuringer using a phenol chloroform based method described in the following. First a homogenization buffer was prepared that is composed of 75 mM NaCl, 24 mM EDTA and 10 mM Tris (pH 8.0), 250 µl of this buffer were added to the tumor tissue. In case of very large pieces of tumor tissue, a piece of approximately 20 mg was cut off on dry ice using a scalpel and used for the DNA extraction described in the following, the rest of the tissue was kept at -80° C. The tissue was dissrupted using mortar and pistil. The homogenisate was transferred to a 1.5 ml reaction tube, mortal and pistil were washed with 250 µl homogenisation buffer and the solution was transferred to the same tube. 25 µl 10 % SDS and 10 µl Proteinase K were added, the tubes were vortexed and incubated over night in a thermomixer at 56° C and 850 rpm to degradate cell membranes and proteins. 300 µl Phenol were added to the homogenisate, mixed and centrifuged at maximum speed for 4 min to

separate the nucleic acids from the proteins. The upper phase containing the hydrophilic nucleic acids was transferred to a new 1.5 ml reaction tube. After repeating the addition of phenol as well as the centrifugation, 300 µl Chloroform were added, the mixture was well mixed and centrifuged at maximum speed for 4 min to remove phenol residues. After repeating these steps as well, the upper phase containing the nucleic acids was transferred to a new screw cap tube. 50 µl 3 M sodium acetate (pH 5.2) and 900 µl ethanol absolute were added to precipitate the DNA. After careful swivelling the DNA became visible and was transferred to a new 0.5 ml tube using a glass "fishing rod" previously prepared from a glass pasteur pipette. The DNA was washed with 200 µl 70 % ethanol and dried. In case the precipated amount of DNA was not sufficient for this method, another centrifugation based method was used. Therefore the precipitate was span for 2 min at 6,700 g, the supernatant was removed and 200 µl 70 % ethanol were added. After repeating the centrifugation step, the ethanol was removed and the pellet was dried. With disregard to the method used, the pellet was resuspended in $50-400$ µl TE buffer depending on the size of the pellet. To ensure complete resuspension the samples were kept on a tube roller for two days. DNA concentration was measured via NanoDrop to check for the success of the DNA isolation.

2.2.4.3 cfDNA from plasma or aqueous humor

cfDNA from human plasma was isolated using the QIAmp Circulating Nucleic Acid Kit (Qiagen) according to the manufacturer's instructions. The vacuum protocol for $1-5$ ml plasma was used and elution was done in 30 µl AVE buffer. To isolate cfDNA from aqueous humor the same kit system, protocol and elution volume were used.

2.2.4.4 cfDNA from vitreous body aspirate

The vitreous body aspirate was transferred to a mortar, some mililiters of liquid nitrogen were added and the resulting frozen mass was mortared until the liquid nitrogen was completely evaporated. Mortaring was continued with higher pressure until a white pouder was formed. Once the pouder became liquid again the pistil and the walls of the mortar were washed with 1 ml dPBS. The PBS was kept and transferred to a 15 ml centrifugation tube. The procedure was repeated using another mililiter of dPBS. Finally all liquid was removed from the mortar and transferred to the centrifugation tube, that was used for subsequent cfDNA isolation using the protocol for 2 ml plasma.

2.2.4.5 DNA from EVs

For establishment and optimization purposes EV-DNA was isolated using different kits or using phenol and chloroform according to the method described avobe (2.2.4.2). EV enriched solutions obtained with one of the methods described above were used as starting material. The

starting volumes differed between the single experiments and are mentioned in the results section accordingly. If not stated otherwise the DNA Micro Kit (Qiagen) was used according to the manufacturer's guidelines with the modifications pointed out below. For QIAamp DNA Mini Kit the same modifications as for the QIAamp DNA Micro Kit were used. Apart from that the following Kits were tested according to manufacturer's instructions:

- PME free-circulating DNA Extraction Kit (using the SE/SBS system)
- Dynabeads™ DNA DIRECT™ Universal Kit
- QIAamp DNA Mini Kit
- QIAamp DNA Micro Kit

For DNA isolation from EVs with the QIAamp DNA Micro or Mini Kit the protocol for small blood volumes was used. If not mentioned otherwise 50 µl of EV solution were used. In deviation from the manual, no ATL buffer was added and the volume of AL buffer was decreased according to the input volume. An addtional RNAse treatment has been done if no carrier RNA was used. An additional incubation step for 10 min at room temperature (RT) was done after addition of RNAse and buffer but prior to Protease K treatment. Washing was performed with only 50 µl of ethanol. After application of distilled water in terms of elution of DNA, an additonal incubation step of 10 min at RT was added prior to centrifugation with an elongated time of 1.5 min. The flowthrough was loaded onto the column again and centriguation was perofmed according to the manual. The EV-DNA was stored at 4 °C

2.2.5 DNA concentration measurement

Concentration of genomic DNA was measured using a spectrophotometer (NanoDrop, Thermo Scientific). Concentrations of cell-free DNA and EV-DNA were analysed using fluorescence-based measurements (Qubit/ Quantifluor). All methods are described below.

2.2.5.1 Spectrophotometrical measurement of dsDNA by Nanodrop

The DNA concentration of genomic DNA was measred using a Nanodrop 1000 UV/Vis spectrophotometer (Thermo Scientific). The optical density of 1 µl sample was measured photometrically at a wavelength of 260 nm and 280 nm. A quotient of the attenuation at 260 nm and 280 nm of 1.8 is considered "pure". The DNA-concentration is calculated based on the Lambert-Beer-Law according to the following equation

$$c = \frac{A}{\varepsilon \cdot b}$$

with c describing the DNA concentration, A describing the absorbance, ε describing the molar attenuation coefficient at 260 nm and b being the optical path length. For the measurement of

dsDNA with the Nanodrop device the product of ε and b can be resolved to 50 ng-cm/µl (Michel et al. 2012).

2.2.5.2 Fluorescence based measurement by Qubit or Quantifluor

The concentration of cfDNA was always measured using the Qubit dsDNA HS Assay Kit and the Qubit System (Themor Fischer) according to manufacturer's guidelines using 1 µl of cfDNA per sample. Additionally, the Qubit dsDNA HS Assay Kit was used to for genomic DNA samples that showed low DNA concentrations (< 50 ng) measured by Nanodrop. EV-DNA concentration measurement was done using either the Qubit (same Kit as cfDNA) or the Quantifluor system according to manufacturer's guidelines. Both methods are based on fluorescent dyes which intercalate with the dsDNA.

2.2.5.3 Measurement of oligonucleotide concentrations

The concentration of barcode as well as adaptor primer dilutions used for the later described SiMSen-seq method were verified using the NanoDrop in custom mode. The analysis constant was calculated using the following equation and specifically set for each individual primer.

$$C_{analysis} = \frac{1}{\varepsilon} \cdot M \cdot 1000$$

with ε describing the molar attenuation coefficient, M describing the molecular weight and $C_{analysis}$ being the analysis constant in micrograms per OD at 260 nm wavelength.

2.2.6 Polymerase Chain Reaction (PCR)

The polymerase chain reaction (PCR) was used to ampliy specific fragments of gDNA, cfDNA or EV-DNA. The reaction consists of the three stages: Initial denaturation, primer annealing and elongation. During the first stage the DNA template is denaturated by setting temperatures to $95-98$ °C, within the second stage many cycles of primer binding, synthesis of the complementary strand and elongation lead to a duplication of PCR templates. The third stage of final elongation ensures that all PCR products are fully synthesized. Target specific primers were designed using Geneious Prime (Dotmatics) or Primer3.

The standard PCR reaction for amplification of any product consisted of 1x Phusion High Fidelity Buffer, 0.2 mM dNTPs, 0.5 µM of target specific primers, 0.4 units of Phusion High-Fidelity DNA Polymerase and $10-400$ ng DNA Template in a total volume of 20 µl. PCR Reaction was performed in a Thermal Cycler using the following cycling conditions: 30 s at 98 °C for initial denaturation, 30 cycles of 10 s at 98 °C for denaturation, 30 s at primer specific annealing temperature and 20 s at 72 °C for elongation followed by a final elongation step at 72 °C for 10 min. Primer specific annealing temperatures were calculated via the Allawi &

SantaLucia's thermodynamics method using the *Tm Calculator* by Thermo Fisher (Allawi and SantaLucia 1997; Thermo Fischer 2022, as of 09.12.22).

2.2.7 Agarose gel electrophoresis

Agarose gel electrophorersis was used to qualitatively analyse DNA fragments (PCR products, NGS libraries). Depending on the size of the pargment gels with 1 %, 2 % or 2,5 % agarose were produced by weighting the respective amount of agarose, dissolving it in 1x Tris-Acetat-EDTA buffer (TAE buffer) and heating up the solution in a microwave until it gets clear. After cooling it down 0.4 µg/ml ethidium bromide were added and the solution was casted to a gel tray. A loading dye was added to the samples prior to loading them on the gel. Aditionally, a DNA ladder was loaded to approximately determine the sizes of the fragments after electrophoresis. The gel was inserted in an horizontal gel electrophoresis chamber filled with 1x TAE buffer and for lowly abundant PCR products ethidium bromide (0.4 µg/ml) was added as well. An electric field of $100 - 130$ V (depending on the percentage of agarose in the gel) was applied. The ethidium bromide that intercalated with the DNA during the electrophoresis enabled the visual detection of the DNA bands under UV light with a wavelength of 312 nm using a gel documentation system (ChemoStar Touch 21.5, Intas).

2.2.8 Quantitative Real-Time PCR

Quantitaive Real Time PCR (qPCR) has been used to assess target primer performance in terms of the establishment of the SiMSen-seq method (Ståhlberg et al. 2017). As "qPCR mix containing SYBR Green I" (Ståhlberg et al. 2017)the LightCycler 480 SYBR Green I Master Mix (Roche) has been used. PCR reactions were prepared on a white Light Cycler 480 96-well plate (Roche), sealed with a Light Cycler 480 Sealing Foil (Roche) and processed on a LightCycler® 480 II instrument (Roche). The PCR protocol was taken from page 671 of the publication by Ståhlberg et al., the target primers tested are listet in table 13 on page 163 (Ståhlberg et al. 2017).

2.2.9 Fragment analysis using a Bioanalyzer (Agilent)

Analysis of size and concentration of DNA fragments needed for various purposes like library quality control was performed using a Bioanalyzer (Agilent). For small and lowly abundant fragments the High Sensitivity Kit was used, while for bigger and more abundant DNA fragments the DNA1000 Kit was used. Preparation and analysis of the chips was performed according to manufacturer's instructions.

2.2.10 Sanger sequencing

DNA and PCR fragments were being sequenced using the chain termination method according to Sanger (Sanger, Nicklen, and Coulson 1977). First a standard PCR was performed using target specific primers to amplify the regions of interest (cf. 2.2.6 for PCR method and 8.1 on page 162 for Primers). For Sequencing of target regions located in the genes *GNAQ* or *GNA11* the PCR reaction consisted of 1x HotStarTaq Master Mix (Qiagen) and 10 nM target specific primer mix instead. The cycling conditions were 15 min at 95 °C, 35 cycles of 30 s at 95 °C, 30 s at 60 °C and 1 min at 72 °C followed by final elongation at 72 °C for 10 min.

The BigDye ® Terminator v1.1 Cycle Sequencing Kit (Thermo Scientific) was used for preparation of the sequencing reaction. 1 µl of purifed PCR template was mixed with 1 µl primer (10 µM), 2 µl BigDye ® v1.1, 2 µl BigDye ® reaction buffer and 4 µl deionized water in order to obtain a total volume of 20 µl. The sequencing reaction was performed in a thermal cycler with the following steps. Initial denaturation at 96 °C for 1 min, 25 cycles of 96 °C for 10 s, primer hybridization at 60 °C for 5 s, 4 min at 60 °C to ensure complete elongation of the products. Primer used for this reaction were the same as for the standard PCR for any targets within the *RB1* gene, but for sequencing of regions within GNAQ or GNA11 the primers called “F-tag” and “R-tag” were used (cf. table 12 on page 162). These bind to a specific motiv of the primers used for the initial PCR.

The reaction product was purified using a sephadex plate. The wells of a 96-well MultiScreen-HV plate (Merck) were filled up with sephadex powder (GE Health Life Science). 300 µl deionized water was added and the plate was either incubated for 2 h at RT or at 4 °C for minimally one night prior to use. A sequencing plate (Fischer Brand 96-well, Fischer Scientific) was prefilled with 10 µl Hi-Di™ Formamid (Thermo Scientific). The sephadex plate was centrifuged for 5 min at 910 g to get out the water and placed on top of the prepared sequencing plate before adding the product of the sequencing reaction on top the sephadex columns. The assembly was centrifuged again with the same conditions as before.

Finally, Sanger sequencing of the purified products was performed using a Genetic Analyzer 3130XL (Applied Biosystems). The raw data was converted into fastq files using the sequencing analysis software (Thermo Scientific). Further data analysis was done using Geneious Prime (Biomatters).

2.2.11 NGS library preparation

Three different systems have been used for library preparation and will be described in the following sections. The first one is a method based on the publication by Leitão et al. (2018) that incorporates two PCR amplicfication steps and does not incorporate any commercial kits but a bead purification system. The second is the SureSelect$^{XT\ HS}$ Target Enrichment System (Agilent) and the third is the SiMSen-seq method published by Ståhlberg et al. (2017).

2.2.11.1 Library preparation for ultra deep targeted NGS

This method was used for ultra deep sequencing targeting *GNAQ* and *GNA11*. First a region around codon 209 or 183 of one of the genes was amplified by PCR using tagged target specific primer (cf. table 51 on page 183 in section 8.1 on page 162). The PCR reaction for this first PCR consisted of 1x Q5 High Fidelity Master Mix, 0.12 µM primer mix and 8 µl cfDNA template and had a total volume of 25 µl. The specificty of the products was reviewed via agarose gel electrophoresis (cf. 2.2.7) prior to a second PCR amplification step using index primer (cf. table 15) that bind to the previously introduced tags. These primers contain indices necessary for demultiplexing of samples after NGS sequencing as well as Illumina specific adapters complementary to the oligonucleotides on the Illumina flowcell. The reaction contained 1x Q5 High Fidelity HotStart Master Mix, 0.08 µM Primer Mix and 1 µl of the PCR product of the first PCR as template and had a final volume of 25 µl. The PCR product of the second PCR was also analysed via agarose gel electrophoresis (cf. 2.2.7).

Samples were pooled and purified using AMPure XP Beads (Beckmann Coulter). The bead solution was homogenized by vortexing it for 20 s, then the beads were added to the sample pool in a bead to sample ratio of 1.2. The solution was mixed via pipetting, kept at RT for 10 min to ensure DNA binding to the beads and then attached to a magnetic stand for 5 min to seperate beads and DNA from the fluid. The supernant was discarded and 200 µl of fresh 70 % ethanol were added, the tubes were attached to the magnet for 1 min and the supernatant was discarded. After repeating this washing step the beads were dried by incubating the open tubes at RT for 10 min or until all ethanol residues were evaporated. To elute the DNA from the beads 10 µl of TE buffer were added, beads were resuspended by pipetting, attached to the magnet for 1 min and the supernatant containg the DNA was transferred to a new 1.5 ml screw cap tube.

2.2.11.2 SureSelect$^{\text{XT HS}}$ Target Enrichment System (Agilent)

For enrichment and sequencing of SNPs on chromosome 3 we used the SureSelect$^{\text{XT HS}}$ Target Enrichment System (Agilent). The library preparation was performed according to manufacturer's guidelines but DNA fragmentation was skipped for cfDNA samples due to the natural fragmentation of this DNA species. The SureSelect$^{\text{XT HS}}$target enrichment workflow was started with the step of molecular barcoding of DNA libraries prior to PCR amplification using index primers contained in the library preparation kit. The correct size and appropriate concentration of the libraries were checked on a Bioanalyzer (Agilent) using the DNA1000 Kit and Chip (Agilent) as described in 2.2.9. The prepared libraries were then hybridized and captured using streptavidin beads and a custom hybridization probe. Captured libraries were again amplified via PCR and size as well as concentration were checked on a Bioanalyzer using the High Sensitivity Kit and Chip (Agilent) (cf. 2.2.9).

2.2.11.3 SiMSen-seq

For targeted sequencing of SNPs on chromosome 13 the SiMSen-seq (Simple, multiplexed, PCR-based barcoding of DNA for sensitive mutation detection using sequencing) method published by Ståhlberg et al. 2017 was used. This methods uses primers with molecular barcodes that are introduced during a three-cycle barcoding PCR. A key innovation of the method is that the barcodes are hidden behind built-in stem loop structures. This avoids two common problems caused by the random sequences of the molecular barcodes, nonspecific primer binding and the formation of primer concatamers.

All steps of the library preparation workflow were performed according to manufacturer's guidelines unless stated otherwise in chapter 3.1.1.2. Briefly described, a barcoding PCR is performed using target specific barcode primer as listed in table 14 on page 164. After these three cycles the PCR gets inactivated by dilution and protease treatment, which allows to directly continue performing the adaptor PCR without the need for a purification. Adapter primer can be found in the supplementary table S1 of Ståhlberg et al. 2017. PCR product purification using AmPureXP Beads (Beckmann Coulter) is performed after the adapter PCR as described in the publication.

2.2.12 Quantification of NGS libraries

NGS libraries were quantified using the NEBNext Library Quant Kit for Illumina (NEB) via quantitative PCR according to manufacturer's protocol. Six standards of known molarity were used to calculate a calibration curve. Each library was measured in triplicates and in two different dilutions of $1:10,000$ and $1:100,000$. Molarities were calculated using the NEBioCalculator supplied by the manufacturer which is accessible online (New England Bioland GmbH 2022 as of 09.12.22).

2.2.13 NGS Sequencing

After library preparation, library quality control (fragment size and concentration) using a bioanalyzer and library quantification the libraries were denatured and diluted according to the guidelines for sequencing on an Illumina device. Briefly, libraries were normalized to 10 nM, pooled and diluted to 1 nM. The library pool was denatured using 0.1 N NaOH, hybridized and diluted to loading concentration. SiMSen-seq libraries from genomic DNA, libraries prepared with the SureSelect$^{\text{XT HS}}$ Target Enrichment System and libaries prepared according to Leitão et al. 2018 were diluted to a loading concentration of 1.4 pM. SiMSen-seq libraries from cfDNA on the contrary were diluted to 1.6 pM. Either the Illumina MiSeq oder the Illumina MiniSeq System were used for NGS sequencing, both devices perform sequencing according to the sequencing by synthesis method.

Briefly explained the DNA templates hybridize to the flowcells surface by specific oligo adapters added during library preparation that are complementary to the oligos on the flowcell. During

cluster generation the DNA templates are clonaly amplified by bridge amplification describing a process where the original DNA molecule undergoes multiple cycles of complementary strand formation, bridge formation and hybridization to flowcell oligos. Within the following process of sequencing by synthesis fluorescently labeled nucleotides compete for being integrated during the synthesis of the complementary strand, if inserted emitting a fluorescence signal whose wavelength as well as intensity are detected. Together with an image of the flowcell taken at time of nucleotide insertion these measurements determine the base call. After the first read is fully sequenced and a process of washing, hybridization, index read sequencing, linearization and cleavage of the forward strand has been completed the sequencing of the reverse strand starts and is performed in the same manner as the forward strand.

2.2.14 Droplet Digital PCR

The Droplet Digital PCR workflow consists of the four steps sample preparation, droplet generation, PCR and droplet analysis. For sample preparation first a master mix has been prepared that consisted of 10 µl ddPCR Supermix for Probes (no dUTP, Bio-Rad), 3 µl ddH_2O, 1 µl restriction enzyme HaeIII mix (NEB) and 1 µl primer/probe Assay Mix (Bio-Rad) per sample. The restriction enzyme mix was prepared by adding 20 µl enzyme to 40 µl 1x CutSmart Buffer (NEB). For each sample 15 µl master mix were added to three wells of a 96-well plate in order to perform triplicate analysis, 5 µl DNA template were added to each well. For genomic DNA samples 1 µl of DNA template was used and additional ddH_2O was added to reach a volume of 20 µl.

For the next step of droplet generation 20 µl PCR reaction were loaded into the sample wells of a DG8™ Cartridge (Bio-Rad) and 70 µl of Droplet Generation Oil (Bio-Rad) were loaded into the bottom wells of the same cartridge. The cartrdige was sealed with a DG8™ Gasket (Bio-Rad) and placed into the Droplet Generator (Bio-Rad). After droplet generation 45 µl of the droplet containing emulsion were transferred to a semiskirted 96-well plate (Bio-Rad). The PCR plate was heat sealed using the PX1™ PCR Plate Sealer (Bio-Rad) and pierceable foil heat seal.

PCR was performed in a standard thermal cycler with one cycle of enzyme activation at 95 °C for 10 min, 40 cycles of denaturation at 94 °C for 30 s and primer/probe annealing and extension at 52 °C for 1 min followed by enzyme deactivation at 98 °C for 10 min. After PCR reaction the plate was placed in the Droplet Reader (Bio-Rad) where the fluoresence signals of each single droplet were detected. These raw signals were analysed using the QuantaSoft Software (Bio-Rad) and the number of genome quivalents was calculated using Poisson statistics. Results have been analysed and visualized using the R programming language.

2.3 Bioinformatical methods

Various bioinformatical methods have been used for data generation and analysis. Pipelines newly developed for this work are explained in the results section. In the following, the methods used here as well as their use cases are listed.

2.3.1 Snakemake

All bioinformatic pipelines presented in this work were made with the workflow manager Snakemake. Data visualisation was either included by adding rules calling R scripts or were performed subsequently using R and RStudio. The build-in rulegraph option was used to generate the directed acyclig graphs shown in the results section of this work. The source code of the most important Snakemake workflows is shown in chapter 8.3. Snakemake was also used to handle package dependencies via its integration of the python package manager conda.

2.3.2 Debarcer

The software tool debarcer provided by Ståhlberg et al. (2017) was used for UMI gouping and error correction for the part of this work related to retinoblastoma. The debarcer workflow was conducted as indicated in the GitHub repository's documentation and wiki (https://github.com/oicr-gsi/debarcer as of 09.12.22) but executed via snakemake. The most recent version available in the bioconda channel was used via the conda integration of snakemake. All software dependencies were also handled using snakemakes `--use-conda` option. The following setings werde used for configration:

`min_family_sizes`= 3,

`percent_consensus_threshold`= 30,

`count_consensus_threshold`= 10,

`umi_edit_distance_threshold`= 1,

`umi_family_pos_threshold`= 10.

All other settings can be taken from the workflow, shown in section 8.3 on page 170.

2.3.3 Varlociraptor

The bioinformatic tool Varlociraptor was used for uncertainty-aware variant calling and calculation of probabilites for LOH in the version 5.3.3 (Köster et al. 2020). It was included in the respective snakemake workflow.

2.3.4 Python scripts

Python scripts were used for manipulation of VCF files in order to add the event tag needed by varlociraptor. Additionally, vcf files were modified using Python in order to allow their import into vcfR package for conversion into a dataframe.

2.3.5 Bash scripts

Bash scripts were used for file renaming and during establishment of processes.

2.3.6 R packages used

R markdown was used for reproducible execution of R code. Vcf files were imported and converted to dataframes using the vcfR library by Knaus and Grünwald (2017). Data transformation was performed using functions included in the tidyverse colection of packages (Wickham et al. 2019). The bioconductor package gpart was used for haplotype and LD analysis (S. A. Kim and Yoo 2021). Additionally, the LDlinkR package was used for queries of the LDproxy API (Machiela and Chanock 2015). Data visualisation was done using ggplot2 for plotting and the patchwork package for layouting multiple plots (Wickham 2016; Pedersen 2022).

In terms of bioinformatical analysis a SNP with a VAF between 0.4 and 0.6 was classified as informative or heterozygous. If a SNPs showed a VAF > 0.9 or < 0.1 or if the VAF could not be determined, but the read depth of the reference allele was higher than 100 reads it was classified as non-informative. If the VAF was outside the defined regions or if no variant alleles and less than 100 reference alleles were detected, the SNP was classified as undefined or the analysis was considered to be failed respectively.

3 Results

In this section, the results of the two aims described in the introduction will be presented. Although the common aim is to develop a liquid biopsy examination, the approaches are fundamentally different and will therefore be kept separate. First, the development of a non-invasive blood test for early detection of SPMs in Rb-survivors, its validation, and application to a european Rb-cohort will be described. Second, the results of a feasibility study aiming to develop a minimal invasive prognostic test for uveal melanoma will be presented.

3.1 A non-invasive blood test for early detection of SPMs in Rb-survivors

The survival rate of retinoblastoma exceeds 95 % in developed countries (Temming, Arendt, Viehmann, Eisele, Le Guin, Schündeln, Biewald, Mäusert, et al. 2016), but nevertheless, many patients with heritable retinoblastoma die later in life. The main cause is the development of SPMs, a diverse spectrum of malignancies with highly variable mutational landscapes. LOH is a very common feature of these tumors occurring only in carriers of heterozygous *RB1* variants. Thus, we aim to develop a blood-based test for the early detection of SPMs in order to improve risk stratification and provide a lifelong and very sensitive screening method for Rb-survivors that improves their quality of life. Technically we aim to detect allelic imbalance as a result of LOH in cfDNA and EV-DNA by targeting SNPs that indicate the allele status at the *RB1* locus. We aim to use blood asprimary sample as it contains cfDNA and EV-DNA, two biomolecules that can potentially be used to detect allelic imbalance.

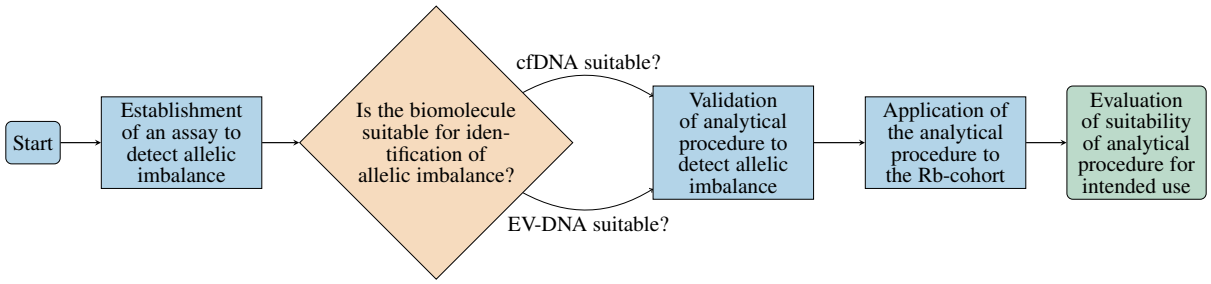

Figure 12: Workflow scheme. The Flowchart describes the steps from the establishment of the assay to application to a testing cohort with the goal of evaluating the suitability of the analytical procedure for the intended use. EV-DNA: DNA derived from extracellular vesicles, cfDNA: cell-free DNA, Rb-cohort: patient cohort consisting of Rb-patients, adult survivors of retinoblastoma and patients who had an SPM in a reasonable time around the blooddraw.

As shown in Figure 12, the first step is establishing an assay to detect allelic imbalance. Next, the suitability of the biomolecule for the intended use needs to be verified. The main criterion for suitability is the number of genome equivalents that can be obtained, as this is critical for allele counting required to determine the VAF and thus detect allelic imbalance. If the biomolecules are suitable, validation of the analytical procedure needs to be performed for each biomolecule separately. If the validation is successful, then the analytical procedure can be tested on samples from an Rb-cohort. The results of this test can be used to evaluate the suitability of the analytical procedure for the intended use, namely to detect second primary malignancies in Rb-survivors.

3.1.1 Establishment of an assay to detect allelic imbalance

The establishment process can be divided into three main parts. First, a database search needs to be performed to identify SNPs suitable for detection of LOH at the *RB1* gene locus. The amplifiability and sequencability of these SNPs need to be reviewed. The second step is the establishment of the SimSen-seq method in order to obtain sequencing data for the selected SNPs. The method has been chosen due to the incorporation of UMIs and the resulting high level of analytical accuracy. In a third step, the results of the mplicon sequencing are subjected to a bioinformatical analysis calculating the variant allele fraction at the given SNP positions.

3.1.1.1 Selecting SNPs for allelic imbalance detection

The dbSNP database provided by the National Center for Biotechnology Information (NCBI) was queried for SNPs with a minor allele frequency in the European population of more than 0.25 and an R^2 value with SNP rs2252544 of more than 0.925. The whole process of SNP selection is illustrated in figure 13. The R^2 value is a measure of the linkage disequilibrium (LD) between two genomic loci. It describes the square of the correlation coefficient between two variables, in this case, the first variable indicates the presence of a specific allele at SNP rs2252544, and the second indicates the presence of the same allele at the currently inspected SNP from the database (VanLiere and Rosenberg 2008). SNP rs2252544 has been chosen because it is frequently heterozygous in carriers of constitutional *RB1* variants (finding based on a large patient cohort from our institute, data not published). Hence we assume that SNPs which are in LD with this SNP are frequently heterozygous in these patients as well. The pursued assay can only be applied to patients who are constitutionally heterozygous for the targeted SNPs, so SNPs with a high frequency of heterozygosity are highly beneficial. The database query has been performed by Prof. Dr. Dietmar Lohmann and resulted in 15 SNPs listed in table 9 that fulfill the criteria.

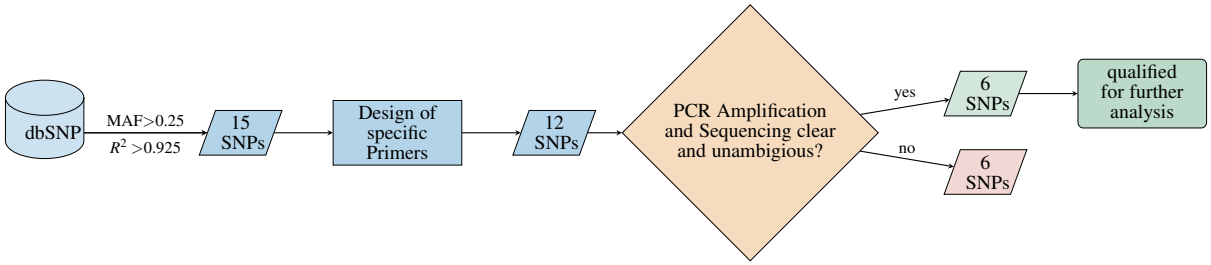

Figure 13: SNP selection process Scheme of the process of SNP Selection, filtering, and testing with the aim to find SNPs that are qualified for further (NGS) analysis. SNP rs2252544 is known to be frequently heterozygous in Rb-patients used as bait SNP for SNPs in linkage disequilibrium. MAF: Minor allele frequency (in this case in the European population), R²: Measure of linkage disequilibrium, SNP: Single Nucleotide Polymorphism.

As shown in figure 13, the attempt to design specific primers was successful for 12 of 15 SNPs. In general, primer design was challenging as the genomic location of the SNPs was intronic and recurrently highly repetitive and GC rich. Accordingly, PCR amplification led to high levels of unspecific products, and sequencing resulted in highly overlayed and ambiguous sequences in

Table 9: Selection of SNPs obtained from dbSNP query. The following filter settings were used: 1) minor allele frequency in the european population > 0.25 and 2) Linkage Disequilibrium with rs2252544: $R^2 > 0.925$. The boldly printed row marks the best suitable SNP for the given assay. MAF: Minor allele frequency (in this case, in the European population); SNP: Single Nucleotide Polymorphism.

	RefSeq ID	Variant	Ancestral	MAF	Position	Allele Frequency	
SNP#1	rs9535007	C/A	A	0.44	48282894	C: 0.725 (729)	A: 0.275 (277)
SNP#2	rs2254423	A/G	G	0.44	48276961	A: 0.724 (728)	G: 0.276 (278)
SNP#3	rs9535002	A/C	C	0.48	48272478	A: 0.722 (726)	C: 0.278 (280)
SNP#4	rs9568029	T/C	T	0.47	48294399	T: 0.275 (277)	C: 0.725 (729)
SNP#5	rs113609690	-/AGTT	Insertion	0.47	48272330	-:0.722 (726)	AGTT: 0.278 (280)
SNP#6	rs55901083	T/A/G	G	0.44	48282200	T: 0.724 (728)	G: 0.276 (278)
SNP#7	rs112402962	-/AC	Insertion	0.44	48282197	-: 0.724 (728)	AC: 0.276 (278)
SNP#8	rs1981434	G/A/C	G	0.49	48307018	G: 0.279 (281)	C: 0.721 (725)
SNP#9	rs4600372	G/A	G	0.44	48300273	G: 0.275 (277)	A: 0.725 (729)
SNP#10	rs4594153	T/A/C	T	0.44	48300280	T: 0.275 (277)	A: 0.725 (729)
SNP#11	rs9535016	A/G	A	0.47	48331081	A: 0.282 (284)	G: 0.718 (722)
SNP#12	rs4151450	C/G	C	0.48	48344038	C: 0.282 (284)	G: 0.718 (722)
SNP#13	rs9535015	C/A/T	C	0.48	48330373	C: 0.283 (285)	A: 0.717 (721)
SNP#14	**rs198619**	**A/G/T**	**A**	**0.47**	**48360439**	**A: 0.282 (284)**	**T: 0.718 (722)**
SNP#15	rs2252544	G/A	G	0.49	48304156	G: 0.287 (289)	A: 0.713 (717)

the case of four more SNPs. Additionally, two SNPs were only 3 bp distant from each other and excluded as this would cause problems in the analysis of the NGS data. Ultimately, six SNPs highlighted green in table 9 passed the qualification test and were used for the establishment of the SimSen-seq method for NGS sequencing.

The best performing SNP in terms of amplifiability, PCR specificity, and sequencability was rs198619, printed boldly in the table. Hereafter all SNPs are referred to by their tag according to the first column of table 9, e.g., SNP 14 for SNP rs198619 to improve readibility. SNP 14 was chosen for the development of a ddPCR assay to determine the number of GEs as shown in figure 12. Furthermore, Sanger sequencing targeting this SNP was performed for ten genomic DNA samples that were known to be heterozygous for the SNP rs2252544 in order to check the linkage disequilibrium. Nine of the ten samples tested were heterozygous.

3.1.1.2 Establishment of the SiMSen-seq Method

The establishment of the SiMSen-seq method was performed according to the guidelines from Ståhlberg et al. 2017 as far as possible. First, new target primers had to be designed according to the requirements of the method for the six SNPs that passed the previous analysis. The same challenges in primer design as described before had to be overcome, and due to knowledge of previous difficulties, two primer pairs were designed per SNP to find the one with the highest possible specificity and maximize PCR efficiency. Standard PCRs using the newly designed Primers were performed and optimized in terms of annealing temperature and level of unspecific PCR products (see also supplementary figure 50). Three criteria had to be fulfilled by the SNP PCRs to qualify the SNPs for further establishment steps. First, the PCR reaction needs to be

Table 10: Results of target primer testing. PCR efficiency calculated using the formula $10^{-\frac{1}{slope}}$ with the slope being derived from the linear correlation of the cycle of quantification and the (decadic) logarithm of the DNA input, "good" specificity describes that only one specific PCR product is produced. SNP: Single Nucleotide Polymorphism, TP7: Control Assay according to Ståhlberg et al. (2017).

SNP	4	5	8	11	12	14	TP7 (control)
PCR efficiency [%]	100	82.5	97	83	81.7	82.5	86.2 / 91
Specificity	good	poor	good	good	good	good	good
negative control	signal	no signal	no signal	no signal	no signal	no signal	no signal

highly specific, amplifying only the desired target region. Second, no template controls must not contain any PCR products, and third, the PCR efficiency had to be minimally 90 %.

Accordingly, PCR reactions showing unspecific products in no template controls or unspecific products in reactions with template that are in the same size range as the desired product were excluded. However, primer pairs leading to huge unspecific products were kept, as it is to be expected that those can be easily removed by size-based bead purification at the end of library preparation. As a last checkpoint, the PCR efficiency was investigated by performing quantitative PCR using SYBR green according to the protocol. For this, a dilution series of genomic DNA ranging from 0.1 ng/µl to 5 ng/µl was generated. This range covers the expected range of cfDNA concentrations obtainable from Rb-patients. PCR efficiency was calculated using the formula $efficiency_{PCR} = 10^{-\frac{1}{slope}}$ with the slope being derived from the linear correlation of the cycle of quantification and the decadic logarithm of the DNA input. Additionally, a melting curve analysis was performed to further investigate the specificity of the primer. The results of the three tests are summarized in table 10.

The TP7 assay is a control assay provided by the authors that helps to normalize laboratory, device, and laboratorian-induced bias. We performed two runs of qPCR and found PCR efficiencies to be generally shifted between the runs by around 5 %. Additionally, in our hands, the efficiency of the control assay was lower than indicated in the protocol. Consequently, the limit of required PCR efficiency was lowered from 90 % to 80 %. As pointed out in the table, all assays reached at least 80 % PCR efficiency and showed no product in the negative control except for SNP 4 assay. This assay showed a signal in a very late PCR cycle, which was ignored due to the high cycle number. The specificity was determined by agarose gel electrophoresis but was further analyzed by fragment analysis using a bioanalyzer (cf. supplementary figure 51). All assays were highly specific except for SNP 5 assay, which showed contradictory results in agarose gel and fragment analysis. As the origin of this inconsistency could not be found, the establishment process of this assay was continued to check if unspecific products can be observed after library preparation as well. Ultimately all six SNPs were considered to be appropriate for further analysis, so barcode primers were designed for all of them.

Barcoding PCR was performed according to the guidelines. Due to its very low amount, the PCR product generated during this three-cycle PCR can not be analyzed. Hence the adaptor PCR was performed right after, and the correct formation of the final construct was analyzed. Instead of the Real-Time PCR Assay suggested by Ståhlberg et al. (2017), a conventional PCR

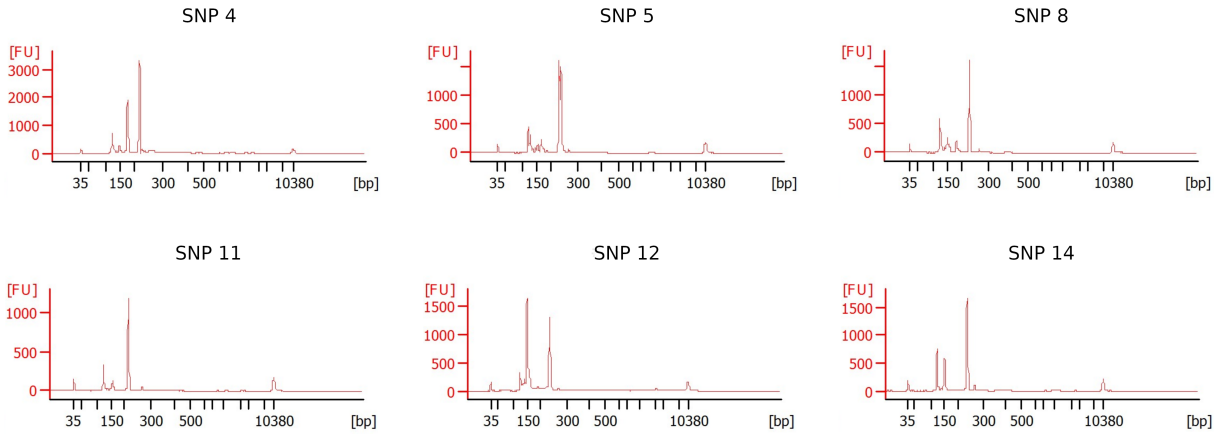

Figure 14: Bionalyzer results for adaptor primer testing. PCR products were analysed using an Bioanalyzer (Agilent) and the High Sensitivity Assay Kit and Chip (Agilent). SNP Numbering is according to table 9; SNP: Single Nucleotide Polymorphism, FU: fluorescence units.

followed by agarose gel electrophoresis (cf. supplementary figure 52) and fragment analysis (displayed in figure 14) was performed, because the available Real-Time PCR device did not fulfil the requirements for the assay described in the publication.

The product sizes of all assays were approximately as expected, but all, including the TP7 control assay, showed additional unspecific products smaller than the expected ones. In case of some assays, like the SNP 12 assay, the results were not consistent between the fragment analysis and the agarose gel. According to the bioanalyzer results, levels of unspecific products were even higher than the specific ones for SNP 12, while on agarose gel, specific products seemed to be more abundant than the unspecific ones. More importantly, the control reactions without DNA template did not show any specific but the same unspecific products, which proves that they are unspecific and presumably result from primer cross-reactions. Those fragments that differed greatly in size from the specific products will be removed by bead purification. Some efforts have been made to optimize the number of cycles of adaptor PCR in order to reduce the level of unspecific products (see supplementary figure 53). An increase in the cycle number resulted in an increase of specific but also unspecific products, while fewer cycles did not result in less unspecific products, so no optimization could be achieved.

As a last step, the PCR products of Barcode PCR and Adaptor PCR were purified using magnetic beads that removed fragments of sizes bigger than a certain cutoff. The cutoff results from the ratio of beads to PCR products which has been set to 1.0 by Ståhlberg et al. We attempted to optimize this ratio and found that for our assay a bead ratio of 0.9 leads to fewer unspecific products without losing the specific ones (shown in supplementary figure 54). A further decrease (ratio 0.8) led to slightly reduced amounts of unspecific products but also to a significant loss of specific product. Therefore a bead ratio of 0.9 was chosen for library purification. After purification, libraries were again checked on a bioanalyzer, quantified by qPCR, denatured, and dilutedand then loaded on an Illumina sequencer.

In summary, the wet lab part of the SimSenSeq method published by Ståhlberg et al. has been successfully established for 6 SNPs within the *RB1* gene that are in LD to each other and a

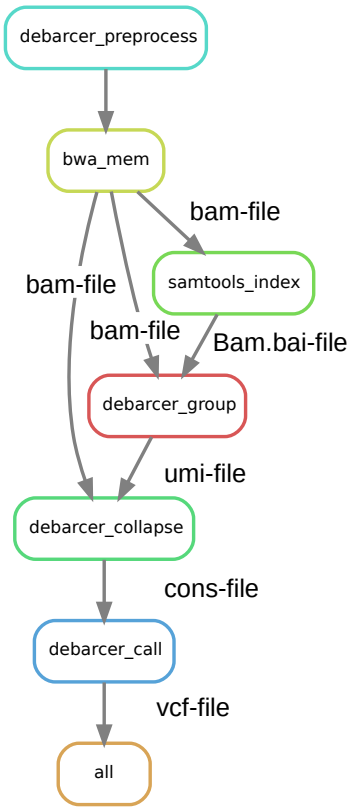

Figure 15: DAG of rules of Snakemake pipeline to analyze SiMSen-seq data. Each box represents a rule that is part of the Snakemake workflow applied to obtain the variant allele fraction from the fastq files, including error correction by unique molecular identifier (UMI) grouping. The graph obtained from Snakemake was annotated with the file types that are the output of the rule above and the input of the rule below.

commonly heterozygous SNP in intron 1. Sequencing of these SNPs resulted in fastq files that can be subjected to the bioinformatical pipeline described in the next section to determine the variant allele fraction at the targeted SNP locus and ultimately identify allelic imbalance.

3.1.1.3 Establishment of a bioinformatic pipeline

The previously described bioinformatic tool debarcer provided by Ståhlberg et al. was used to calculate UMI corrected variant allele fractions. It consists of a workflow of bash commands that are executed one after another. The execution of the workflow steps is very arbitrary for huge sample sets, and the computation time is high as no parallelization is possible. To overcome these weaknesses, we developed a Snakemake workflow. Figure 15 shows the directed acyclic graph (DAG) of rules giving an overview of the implemented Snakemake workflow.

The rules shown in colored circles describe the different steps of the workflow and are handled automatically based on their input and output files. The final output is a vcf-file (variant call format file) that contains the allele ratios of the variant as well as the reference allele and additional statistical values. The annotation next to the arrows indicates the files being the output of the preceding rule and the input of the subsequent rule. The designed Snakemake workflow allows parallel analysis of all samples sequenced, automatically handles replicate analysis and

allows parallelization of analysis of different target regions, and has a good scaling behavior in regard to the number of processed samples. Furthermore, it allows to generate a joint report on all replicates as well as regions (SNPs) a sample consists of.

3.1.2 Evaluating the suitability of EV-DNA and cfDNA for identification of allelic imbalance

The primary sample used for liquid biopsy examination is blood, a body fluid that contains a huge variety of biomolecules. Two of them are cfDNA and EV-DNA, both being part of the cell-free components. Prior to validation of the investigation procedure, it needs to be evaluated if the biomolecules (EV-DNA and cfDNA) obtained from the liquid biopsy are suitable for the intended use, namely the identification of allelic imbalance. It needs to be examined if sufficient numbers of DNA fragments covering the target regions can be obtained from these DNA species. The exact number of DNA fragments that is sufficient depends on the level of allelic imbalance and is therefore dependent on the disease state. Based on previous studies, it is to be expected that at least 5 % ctDNA needs to be detectable to allow early diagnosis of SPMs, however, this is difficult to determine due to the different tumor entities of SPMs (Butler, Spellman, and Gray 2017; Shulman et al. 2018; Andersson et al. 2020).

3.1.2.1 Criterion for validation: The number of effective GEs

To answer the question if the number of DNA fragments containing the target SNPs is sufficient to detect allelic imbalance, it is necessary to develop an assay to count the number of GEs. Conventional (fluorescence-based) DNA measurement methods are insufficient for the detection of EV-DNA and cfDNA levels as they are usually lowly abundant and highly fragmented. Additionally, these methods do not reflect the number of effective genome equivalents but only the general amount of DNA. Moreover, carrier RNA used for cfDNA extraction and partly for EV-DNA isolation interferes with fluorescence measurements and leads to a bias in the measurement outcome. Consequently, a more specific and more sensitive assay measuring not only DNA content in general but availability of the target regions in specific needs to be developed. As ddPCR is the best suitable method for this purpose (cf. 1.4.2.1) we established it for SNP14 in order to count the number of GEs in our samples. We first ordered specific primers and probes that did not contain locked nucleic acids, but these probes did not work for our assay. With a new probe containing this patented feature and after optimizing the level of rain (cf. 1.4.2.1 for details) and the stringency of the baseline, the performance of the assay was good. The established assay is shown in figure 16. Graph A negative control containing no DNA, graph B shows a positive control containing approximately 10 ng genomic DNA from a healthy individual.

From the figure, it can be concluded that the signal in the positive control is strong and that the negative control contains no positive droplets. Figure 16 C shows a commercially available,

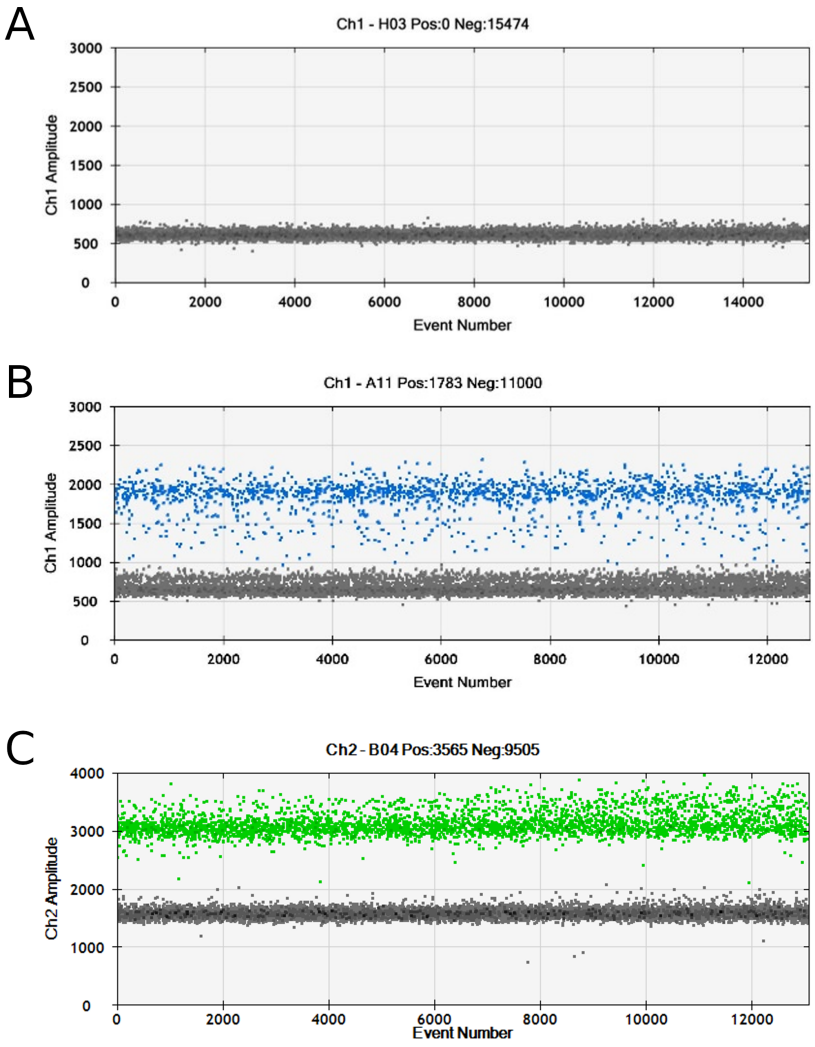

Figure 16: ddPCR assay compared to reference assay. Fluoresencence amplitude of ddPCR measurement, blue dots indicate positive (template containing) droplets in the FAM channel, green dots indicate positive droplets in the HEX channel, grey dots indicate negative (empty) droplets. A) No Template control B) Positive control containing ~10 ng gDNA, SNP14 assay C) Positive control containing ~10 ng gDNA, reference assay targeting *BRAF*, wet lab validated by supplier (Bio-Rad). Ch1: channel 1; ch2: channel 2.

wet lab validated assay targeting *BRAF* that is widely used for diagnostic purposes. We use it as a reference for the performance of our own assay targeting SNP 14. We had to compare the FAM channel of our assay with the HEX channel of the reference assay because, in case of the reference assay, the FAM channel detects the mutated *BRAF* while the HEX channel detects the wildtype *BRAF* and samples from patients with mutations in *BRAF* were not available to us. In comparison, our assay shows good performance but higher levels of rain than the reference assay. The amplitude of the negative droplets, also called baseline, was lower and thereby superior in our assay, while the difference between the positive and negative droplets is similar in both assays with a magnitude of around 1,500. This means that a good separation between droplets containing DNA and empty droplets has been achieved.

3.1.2.2 Measuring the amount of GEs in EV-DNA obtained from blood samples and efforts to increase it

Once we had established the ddPCR as an auxiliary assay, we were able to precisely measure the number of GEs present in EV-DNA and cfDNA obtained from blood samples. First, we aimed to check if the number of GEs in EV-DNA meets the criterion of being sufficient for the detection of allelic imbalance, as explained above. When applying the assay that was established on genomic DNA to EV-DNA from healthy donors, we were not able to detect any genome equivalents. However, the positive control containing genomic DNA, as well as the no template control, showed the expected results. For this analysis, EVs were isolated by size exclusion chromatography (SEC) using self-made columns, and EV-DNA was isolated using the DNA Micro Kit from Qiagen. Assuming that the EV-isolation, as well as the EV-DNA isolation technique, might be the reason for the unmeasurably low amount of GEs, we attempted to improve both procedures. As explained in the chapters 1.1.4.3 and 1.1.4.6, the EV-DNA content is thought to differ between the different EV subtypes, and the EV isolation strategy has a high impact on the composition of EV subtypes and thereby on the amount of DNA that can be obtained.

Optimization of EV isolation method

First, we aimed to improve the EV isolation strategy as a higher EV yield, further enrichment of EVs, or an EV composition that is optimized for our needs might help to increase levels of EV-DNA. In the beginning, we compared ultracentrifugation (UC) with the previously used SEC to see if EV isolation by UC might yield more EVs. As we were only interested in the EV-DNA, we compared these methods based on the EV-DNA concentration as well as the total amount of DNA we can obtain from EVs received from healthy donors' blood. Figure 17 shows the results of this comparison, the DNA concentration shown in the left plot was higher in EVs isolated with UC, but the total amount of DNA was higher in the EV fraction extracted by SEC in two of three samples.

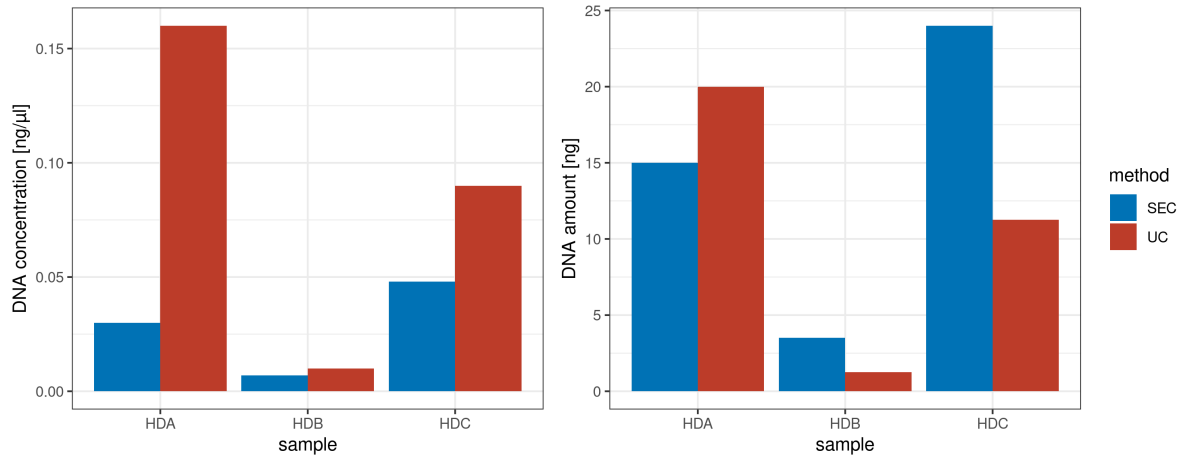

Figure 17: Comparison of EV-DNA amount in EVs isolated from healthy donor's plasma by SEC or UC. DNA concentration was measured by fluorescence based methods (Quantifluor) and DNA amount was calculated by multiplying DNA concentration with DNA volume. SEC was performed using self-made columns. DNA isolation was done using the Qiagen Micro Kit (Qiagen). SEC: Size exclusion chromatography, UC: Ultracentrifugation, HD: Healthy donor

Consequently, we continued with SEC as EV-isolation method. As the volume of EV-containing sample that can be inserted in subsequent DNA isolation is very limited, only a small part of the EV sample could be used so far. To reach the putative DNA amounts shown in figure 17, the whole EV sample needs to be taken for DNA isolation. To achieve this, the EV sample needs to be concentrated. We performed ultrafiltration after SEC using Amicon spin filters and compared the resulting DNA concentration to the DNA concentration found in non-concentrated EVs, as displayed in figure 18.

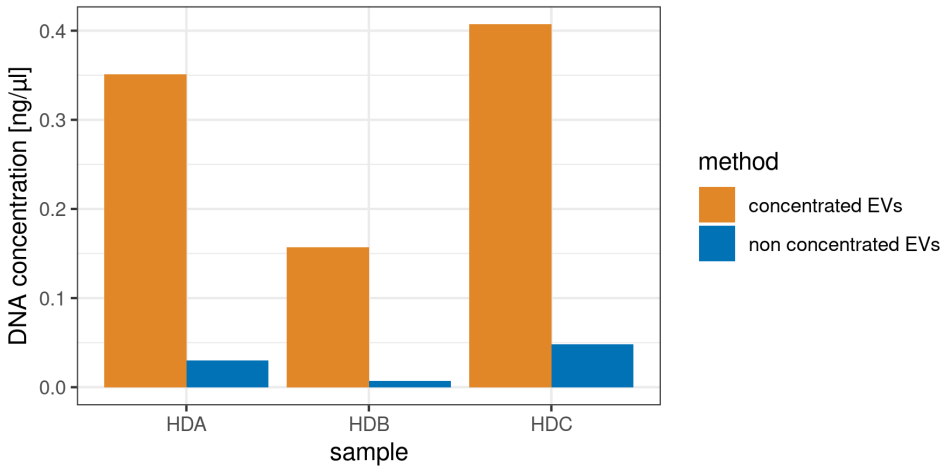

Figure 18: Concentration of DNA obtained from concentrated and non-concentrated EVs. Extracellular vesicles (EVs) were isolated with SEC (self-made columns). Concentration was performed by ultrafiltration using Amicon Spin Filters (10 kDa molecular weight cutoff, 2 ml capacity). DNA isolation was done using the Qiagen Micro Kit (Qiagen). HD: Healthy Donor

We observed a high increase in DNA levels from concentrated samples compared to non-concentrated samples from the same healthy donor. For budget reasons and as no carrier RNA has been used, DNA concentrations were measured by Quantifluor (fluorescence-based method, cf. 2.2.5.2 for details). Despite the tremendous increase in DNA levels, the concentration was

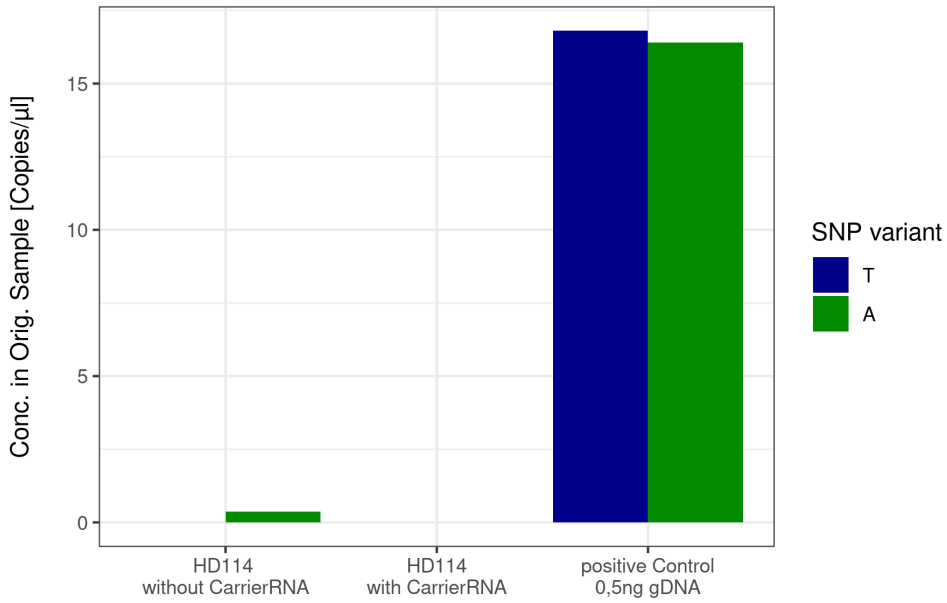

Figure 19: Number of GEs in EV-DNA from EVs isolated with SEC using qEV columns. EVs were isolated by SEC using qEV columns (Izon) from plasma of a healthy donor. DNA was isolated using the Qiagen Micro Kit with or without CarrierRNA as indicated. As a positive control 0.5ng genomic DNA (obtained from leucocytes) was used. DdPCR was performed measuring the DNA concentration in the original sample in copies/µl. The variant of SNP 14 (rs198619) being Thymin (T) is measured in the FAM channel and shown in blue, the variant of Adenin (A) is measured in the HEX channel and displayed in green. HD: healthy donor; SNP: Single Nucleotide Polymorphism; gDNA: genomic DNA.

still very low, with a maximum of 0.4 ng/µl. We hypothesized that SEC columns with different specified cutoffs, as the qEV columns recently developed by the Izon company, might allow us to further optimize the DNA yield.We chose qEV columns with a cutoff of 70 nm, aiming to extract large EVs, that are thought to posess higher amounts of DNA, and analysed the number of GEs that can be obtained with this method from a plasma sample of a healthy donor. From one part of the sample, we isolated DNA as done before, and from the other part, we isolated DNA with the same kit but added carrier RNA. Due to the use of carrier RNA, we performed ddPCR and investigated the number of GEs as displayed in figure 19.

A positive control containing 0.5 ng genomic DNA was included in the experiment to serve as a reference and ensure that the ddPCR assay was done correctly. The control shows the expected number of GEs, but no GEs could be detected in the EV-DNA samples. In summary, ultrafiltration of the EV sample and DNA isolation from the complete filtrate led to a large increase in DNA amount measured by Quantifluor. All other attempts to optimize the EV isolation strategy in terms of obtainable DNA amount failed. Another point of optimization within the procedure of extracting DNA from EVs is the DNA isolation method used.

Optimization of EV-DNA isolation strategy

We conducted a systematic comparison of different DNA isolation strategies to maximize the number of effective GEs that can be obtained from a plasma sample. Figure 20 depicts that no effective GEs could be found no matter the strategy used to extract DNA. As in previous ddPCR

experiments, a positive control was included, and it showed the expected results. Thereupon the DNA yield from EVs can not be increased by changing the DNA isolation strategy.

Number of GEs higher in patients?

It is known that the amount of EVs is increased in cancer patients compared to healthy controls (cf. chapter 1.1.4.5), hence as a next step, we isolated EVs from Rb-patients and Rb-survivors to see if the numbers of EVs might be increased. Any biomarker assay needs to be applicable to healthy controls as well, but if we are able to detect EV-DNA in any sample, we gain knowledge on the success and limit of detection of our process, which in turn helps us to decide if any further optimization is reasonable. Prior to DNA isolation, we wanted to ensure that EV isolation by SEC was successful and, for that purpose, strived to investigate the number of EVs obtained from our samples. With the methods available at the time these experiments were performed, it was barely possible to precisely measure the number of EVs. The best approximation available was nanoparticle tracking analysis by dynamic light scattering using a ZetaView. This can only be considered an approximation as it detects not only EVs but any kind of particles in a specified size range and, as the precision of the measurement is poor. The results of this analysis are shown in figure 21.

EVs were found in healthy donors as well as Rb-patients and Rb-survivors, so the EV isolation can be considered successful. Numbers differed between the individual samples, but contrary to the findings from the literature on cancer patients in general, no significant difference between Rb-patients and healthy controls was detectable. However, to our knowledge, it has not yet been shown if retinoblastomas shed EVs into the bloodstream. Next, we measured the number of GEs in these patient samples as displayed in figure 22.

Also, at the DNA level, there was no significant difference between the groups. In this experiment, some, but very few, droplets containing DNA were detected. The concentration in the original EV-DNA sample is below one GE per µl in all samples tested. It can not be excluded that these very few positive droplets result from errors or contamination during EV-isolation or EV-DNA isolation. Errors during ddPCR processing are also possible but very unlikely because the negative control included in the experiment did not show any positive droplets.

For cancers like osteosarcoma it is known that they shed EVs into the bloodstream, so we expected that samples from SPM patients, which are most often osteosarcomas, might show increased numbers of EVs and thereby higher amounts of EV-DNA than retinoblastoma patients or healthy controls Yang et al. (2022). To save our lowly abundant SPM samples, we isolated EVs and, subsequently, EV-DNA from patients with metastatic head and neck cancer instead, because these samples were available to us and these tumors are known to shed EVs into the bloodstream as well Qu et al. (2020). For this analysis, we performed EV isolation by SEC, using qEV columns (Izon). The result of the ddPCR experiment on these samples is shown in figure 23. DNA levels were several magnitudes higher than in all previous experiments, but with a maximum of eight GEs per µl, the DNA content remains to be minimal.

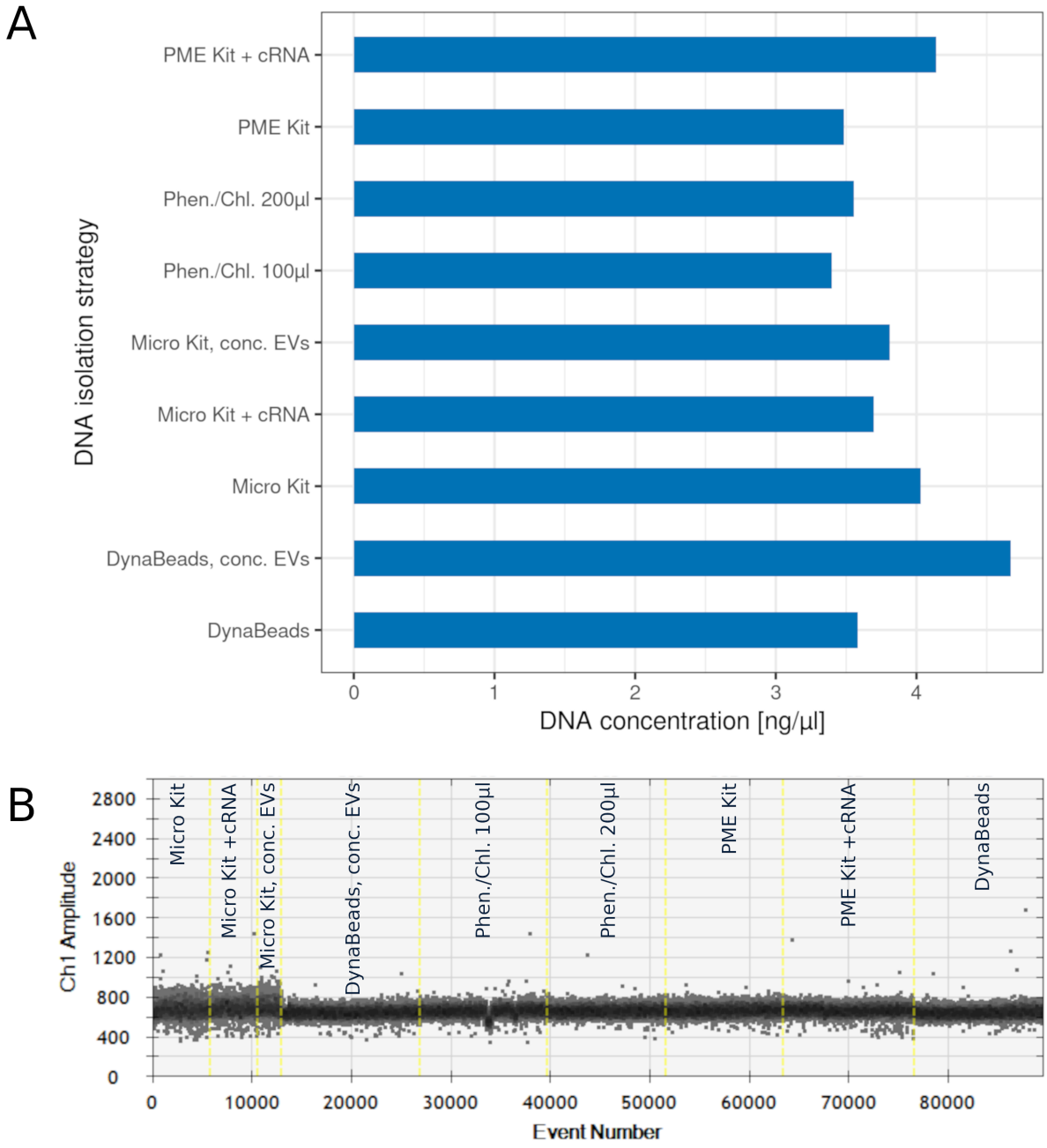

Figure 20: Comparison of different EV-DNA isolation methods. EV-DNA was extracted from EVs (isolated by SEC from healthy donors' plasma) using different DNA isolation strategies. A) Concentration of EV-DNA measured by fluorescence based measurement. B) Fluoresence amplitude of FAM fluoresencence measured by ddPCR. Phen./Chl.: DNA extraction via phenol chloroform based method, Micro Kit: EV-DNA extracted using the QIAmp DNA Micro Kit , PME Kit: EV-DNA extracted using the PME free-circulating DNA Extraction Kit, DynaBeads: EV-DNA extracted using the Dynabeads DNA DIRECT Universal Kit, cRNA: Carrier RNA.

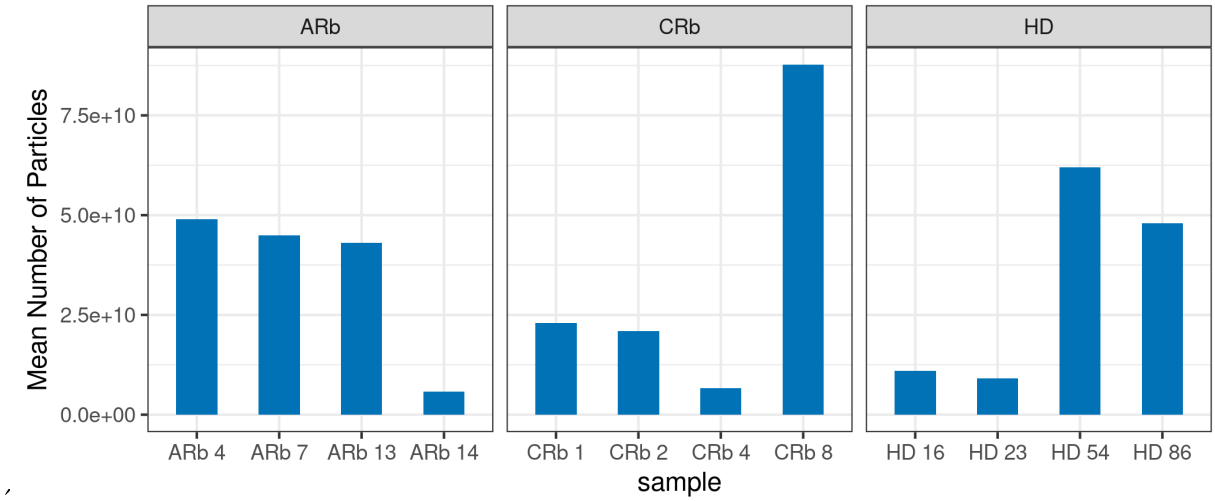

Figure 21: Numbers of EV-like particles in different patient and control samples measured by nanoparticle tracking analysis. The analysis was performed using a ZetaView (ParticleMetrix). ARb: Adult Rb-survivor, CRb: Rb-patient (child), HD: Healthy Donor.

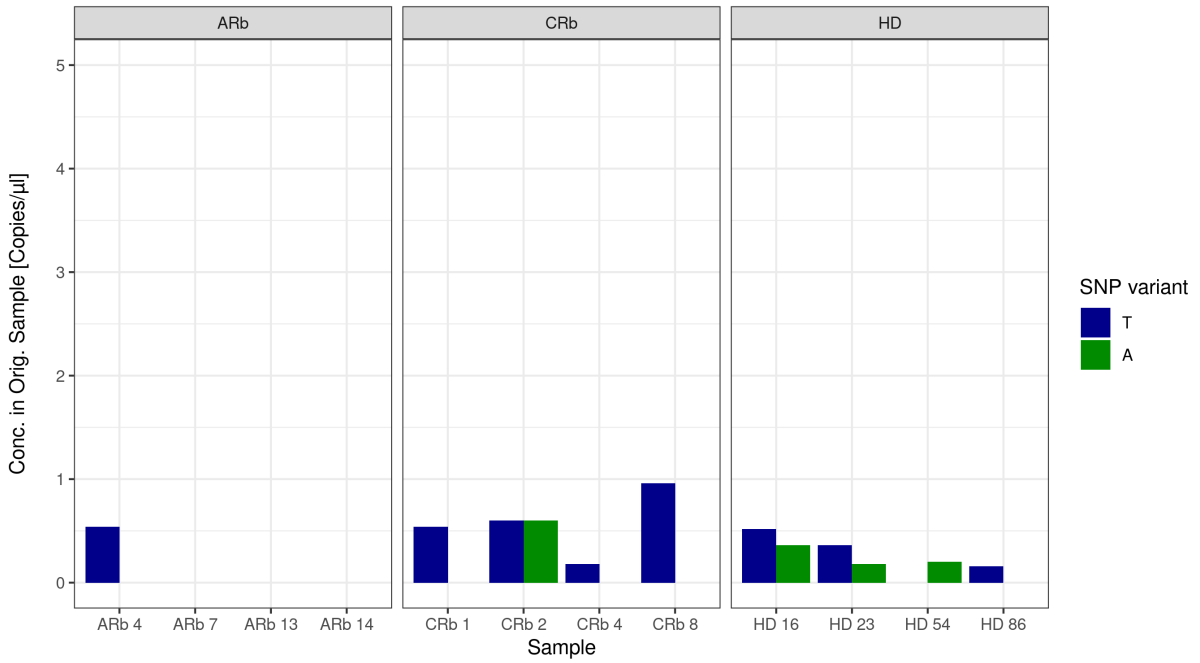

Figure 22: Number of GEs in EV-DNA derived from plasma from Rb-patients, Rb-survivors and healthy donors. EVs were isolated by SEC (self-made columns) from plasma of different patients and healthy controls. DNA was isolated using the DNA Micro Kit (Qiagen). DdPCR was performed measuring the DNA concentration in the original sample in copies/µl. The variant of SNP 14 (rs198619) being Thymin (T) is measured in the FAM channel and shown in blue, the variant of Adenin (A) is measured in the HEX channel and displayed in green. ARb: Adult Rb-survivor, CRb: Rb-patient (child), HD: Healthy donor; SNP: Single Nucleotide Polymorphism..

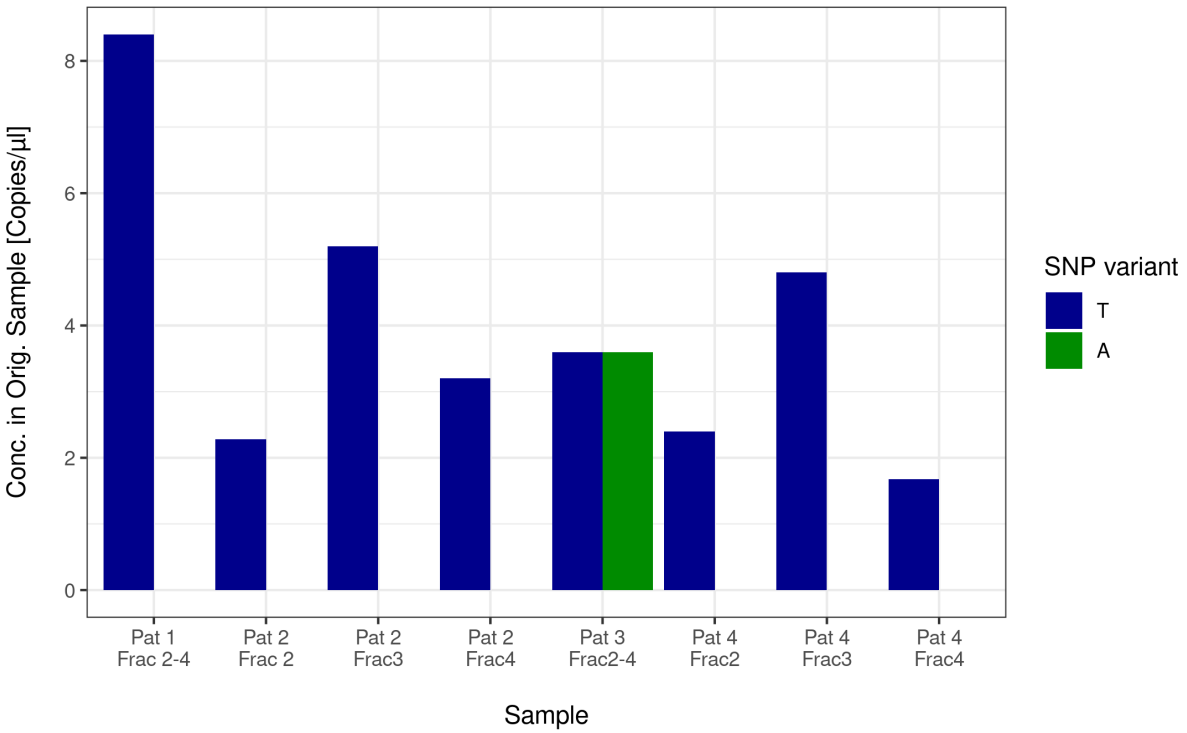

Figure 23: Number of GEs in EV-DNA from plasma of patients with metastatic head and neck cancer. EVs were isolated by SEC (qEV columns, cutoff 70 nm (Izon)) from plasma of patients with metastatic head and neck cancer followed by concentration of EVs via ultrafiltration (Amicon Ultra spin filters, 10 kDa cutoff). DNA was isolated using the Qiagen Micro Kit. ddPCR was performed measuring the DNA concentration in the original sample in copies/µl. The variant of SNP 14 (rs198619) being Thymin (T) is measured in the FAM channel and shown in blue, the variant of Adenin (A) is measured in the HEX channel and displayed in green. Pat: Patient, Frac: Fraction(s) of SEC, SNP: Single Nucleotide Polymorphism.

Conclusively, the amount of GEs in EV-DNA found in healthy donors, Rb-patients, patients of metastatic head and neck cancer, and expected in SPM-patients is not sufficient for the detection of allelic imbalance. All efforts taken to increase the DNA yield did not lead to a sufficient increase. Ultimately EV-DNA is no suitable biomolecule for our liquid biopsy examination, as it does not meet the criterion of sufficient numbers of GEs, which is mandatory for allele counting and the detection of LOH.

3.1.2.3 Measuring the amount of GEs in cfDNA obtained from blood samples

In contrast to EV-DNA, cfDNA has been widely used as a biomarker, is already used in clinical routine, and is part of external quality assurance and harmonization initiatives like the European Molecular Genetics Quality Network (EMQN). Hence the isolation of cfDNA is more standardized than the isolation of EV-DNA, and the kit system used to isolate DNA in this work has been applied in many publications. Fluoresence-based methods are commonly used for cfDNA quantification, despite the bias introduced by the carrier RNA added to the sample during isolation. To overcome this and to measure the effective GEs required to evaluate if cfDNA is suitable for the detection of allelic imbalance, we tested the number of GEs by ddPCR as shown in figure 24. In case of cfDNA, our first ddPCR approach on healthy donors' DNA was successful, so we directly continued to investigate patient samples.

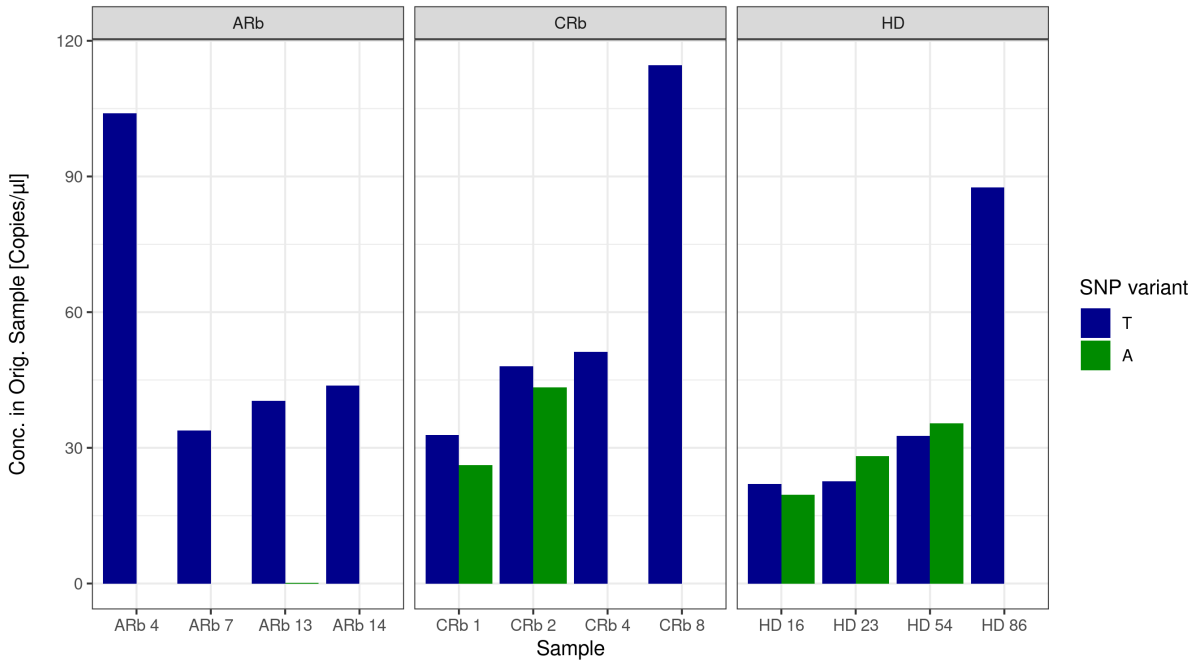

Figure 24: Number of GEs in cf-DNA derived from plasma from Rb-patients, Rb-survivors and healthy donors. cfDNA was isolated from plasma of different patients and healthy controls using the QiAmp Circulating Nucleic Acit Kit (Qiagen). ddPCR was performed measuring the DNA concentration in the original sample in copies/µl. The variant of SNP 14 (rs198619) being Thymin (T) is measured in the FAM channel and shown in blue, the variant of Adenin (A) is measured in the HEX channel and plotted in green. ARb: Adult Rb-survivor, CRb: Rb-patient (child), HD: Healthy Donor, SNP: Single Nucleotide Polymorphism.

It becomes obvious that the numbers of GEs in cfDNA are much higher than the numbers of GEs in EV-DNA in all samples tested. Some individuals (ARb 4, CRb 8, and HD 86) show highly elevated levels of cfDNA compared to other individuals, independent of their group. Hence, these observations can not be correlated to the disease state. For cf-DNA that is directly obtained from blood, there are no other optimization methods than the kit system used for cfDNA isolation. We compared two kits and found no differences, so no further efforts to optimize the DNA yield were made (data not shown).

In conclusion, cfDNA is more suitable than EV-DNA to detect allelic imbalance because of the higher number of GEs. Nevertheless, the question of whether the number of effective GEs obtainable from cfDNA is sufficient to detect allelic imbalance remains. To answer this question, we investigated the number of GEs that can be obtained from cfDNA based on the results from the previous ddPCR experiment as shown in figure 25A and modeled the correlation of the number of GEs and the fraction of cell-free tumor DNA (figure 25B, kindly provided by Dr. Christopher Schröder) using a false positive or negative rate of less than 5 % (modeling was performed by Dr. Christopher Schröder) .

The median amount of GEs in cfDNA displayed in part A equals 1,263 GEs. Based on part B of the figure, it can be concluded that this number of GEs is sufficient to detect approximately 10 % cell-free tumor DNA. In order to detect the intended amount of at least 5 % ctDNA, more than 4,000 GEs would be needed. Anyhow, this is calculated based on a very small sample set and does not reflect the numbers of GEs in SPMs, which are expected to be elevated due

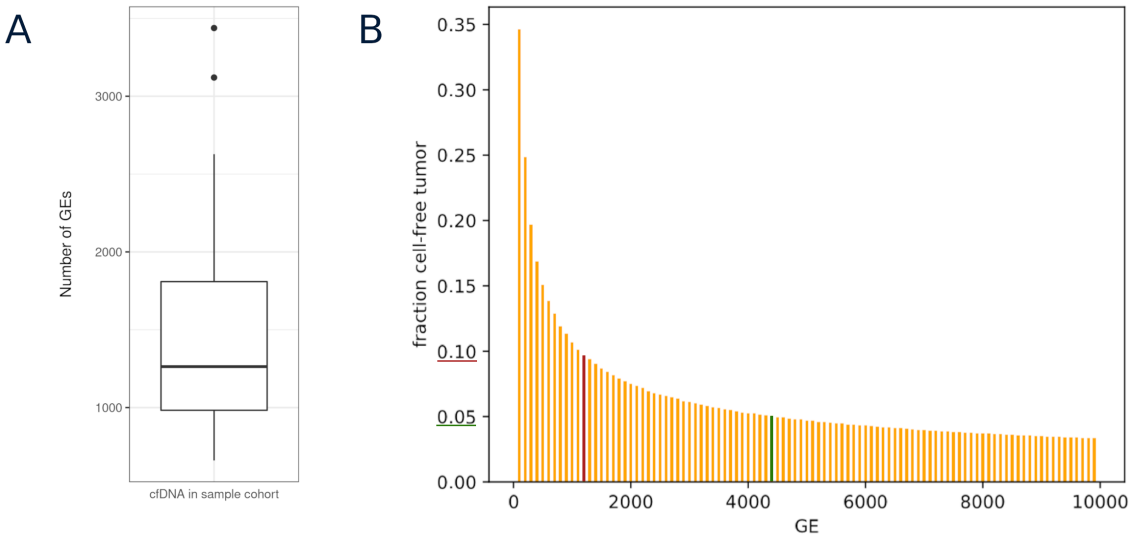

Figure 25: Correlation of number of GEs and fraction of cell-free tumor DNA A) Boxplot of number of genome equivalents (GEs) detected in cell-free DNA (cfDNA) samples from 4 Rb-patients, 4 Rb-survivors and 4 healthy controls. B) Prediction of limit of detection (LoD) of the fraction of cell-free tumor DNA depending on the number of genome equivalents (GEs). The green bar/score indicates the targeted LoD, red bar/score indicates the LoD that can be reached given the number of GEs detected in cfDNA (A). Figure B was kindly provided by Dr. Christopher Schröder.

to findings from the literature as explained in chapter 1.1.5. Additionally, there are no other biomarker screening tests available for SPMs in Rb-survivors, so a method that can detect 10 % of ctDNA may still be clinically relevant and, therefore, we proceeded, aiming to validate the established method based on cfDNA.

3.1.3 Validation of the established procedure to detect allelic imbalance

Prior to the application of the established procedure, it needs to be validated by providing objective evidence that it fulfills the intended use. As described in chapter 1.4, analytical accuracy is very important when aiming to develop a liquid biopsy examination. High levels of sensitivity and specificity and a low error rate lead to high analytical accuracy. The LoD is also key for all biomarker assays that deal with the detection of rare variants. It is primarily set by the number of detection units for any kind of counting process, like the determination of allele ratios. The detection units are the effective GEs in this case, hence the LoD is expected to be approximately 10 %, as explained above. Apart from that, the actual LoD of the established method depends on various factors, as illustrated in figure 8 in chapter 1.4. To investigate the actual LoD, we conducted the assay on genomic reference samples with artificial admixtures of known proportions of tumor DNA. The results of these investigations are outlined in the next chapter. As we established a set of tests, each for a specific target (SNP), we had different testing strategies available that we could choose from. To identify the optimal testing strategy, we evaluated the performance of each SNP assay as well as different degrees of multiplexing, with the criterion for optimization being the information on the allelic imbalance as described in chapter 3.1.3.2.

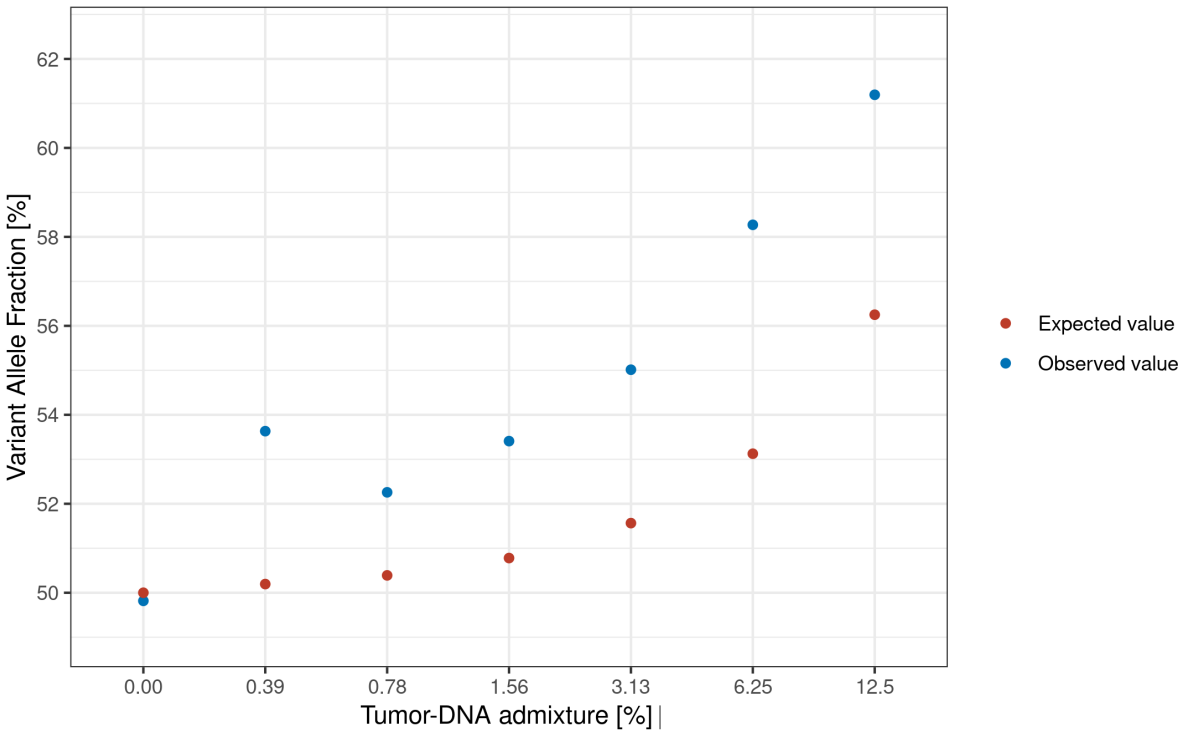

Figure 26: Observed and expected VAF in samples with artifical tumor DNA admixture. Samples with different proportions of tumor DNA admixture were generated and analyzed with the established assay targeting SNP 14 (rs198619). The expected VAF was calculated using the formula $0.5 \cdot (1+\beta)$, with β being the proportion of tumor DNA admixture. Measurements with a raw depth ≤ 100 were excluded.

3.1.3.1 Genomic reference samples to investigate sensitivity and LoD

To investigate the sensitivity and the LoD of our previously established assay, we generated samples with different proportions of tumor DNA admixture. In detail, we chose one Rb-patient from which constitutional DNA (from blood), as well as tumor DNA, were available. We diluted both DNA samples to equal concentrations (2 ng/µl) and created mixtures of both samples by adding different volumes of tumor DNA to the constitutional DNA. The resulting seven samples possessed tumor DNA admixtures of $0-12.5\,\%$. 10 ng DNA of these artificial samples were used for NGS library preparation targeting SNP 14 and sequenced performing single measurements. Figure 26 shows the VAF detected in these admixture samples compared to the expected VAF.

The expected VAF was calculated based on the true allele ratio expected in a patient, not considering the sampling error due to the drawing process. As this analysis was performed using 10 ng genomic DNA, the statistical errors would not reflect the challenges that have to be overcome by the final assay based on cfDNA and hence will not be considered in this case. Given that β is the proportion of tumor cells the tumor DNA in the admixture sample is derived from, and α is the proportion of constitutional DNA derived from healthy cells with $0 \leq \alpha, \beta \leq 1$, then it is given that $\alpha + \beta = 1$. Further, given that the number of cells in our sample is m and the number of alleles in these cells is d, it results that $d = 2m$. Analogously, with the allele ratios for the normal allele being a, the allele ratio for the variant allele (VAF) being b, and $0 \leq a, b \leq 1$, it is given that $a + b = 1$. Setting the allele ratio in relation to the genotype or the cells of origin

respectively, we get that the alleles derived from healthy cells are $d_A = \alpha$ and the alleles derived from tumor cells are $d_B = \alpha + 2\beta$. Under the simplifying assumption that $m = 1$ and $m \in \mathbb{R}^+$, it is given that $m = \alpha + \beta = 1$ and $d = 2(\alpha + \beta) = 2$. All this is taken together to obtain the following equations, which can be applied to calculate the expected allele ratio of the normal allele a, and the expected allele ratio of the variant allele b given the proportion of tumor DNA admixture β:

$$a = \frac{d_A}{d} = \frac{\alpha}{2} = \frac{1-\beta}{2}$$

$$b = \frac{d_B}{d} = \frac{\alpha + 2\beta}{2} = \frac{(1-\beta)+2\beta}{2} = \frac{1+\beta}{2}.$$

Comparing the expected VAF with the observed VAF shown in figure 26, it becomes obvious that there is a shift between the two values except for the VAF at 0.39 % tumor DNA admixture, which needs to be considered an outlier. A possible reason for this shift is the very limited accuracy of DNA concentration measurement at such low concentrations and the resultingly unequal concentrations of the two DNA specimens in the mixture. Additionally the pipetting error could be a reason for the discrepancies as the sample that deviates has been the last sample of the dilution series, so the propagation of the pipetting error has the highest impact.

The LoD as determined by this analysis is about 0.78 %, but it needs to be taken into account that 10 ng of genomic DNA has been used for this experiment, a DNA amount that can not be expected in cfDNA from low plasma volumes, as collected from the Rb-cohort. The amounts of GEs evaluated in this analysis are much higher than the GEs shown to be present in cfDNA by ddPCR. Consequently, the error rates are much lower, as pointed out in chapter 1.4. In order to gain reference samples that are more suitable for validation of the assay, we aimed to establish our assay for SNPs on chromosome 3 as we had samples from uveal melanoma patients at hand, whose proportion of ctDNA was already characterized by other validated NGS methods. The approach failed due to high levels of intra-assay as well as inter-assay variability that did not allow precise measurements of the VAF in healthy donors (data not shown).

Instead, we aimed to analyze not only SNP 14, but all SNPs because we hypothesized that multiple independent measurements on different SNPs increase the sensitivity and specificity of our assay. Again we used samples with artificially introduced tumor DNA admixture but a reduced DNA amount of only 5 ng, and we investigated only three different proportions of tumor DNA (0 %, 1 %, 5 %). Additionally, we performed a triplicate analysis and calculated the mean of the three measurements to overcome errors introduced during the procedure of library preparation and sequencing. The VAFs measured by each assay are plotted in figure 27 and compared to the expected VAF given the level of tumor DNA admixture, calculated as explained above.

From the figure, it can be taken that SNP 5 and SNP 8 highly deviate from the expected VAF, especially at 5 % tumor DNA. All other SNPs cluster quite close to the expected VAF. Again it

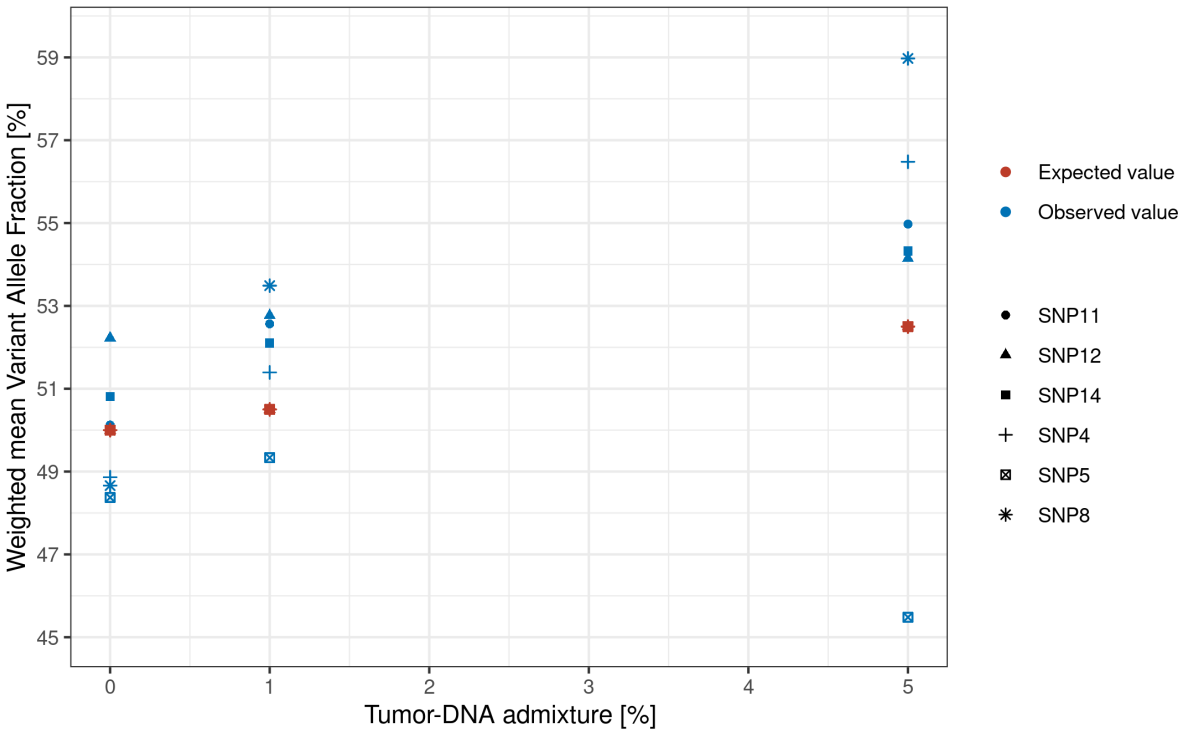

Figure 27: Observed and expected VAF of multiple SPNs and replicates in samples with artificial tumor DNA admixture Samples with different proportions of tumor DNA admixture were generated and analyzed with the established assay targeting different SNPs as indicated by the shapes. The expected VAF was calculated using the formula $0.5 \cdot (1 + \beta)$, with β being the proportion of tumor DNA admixture. All analyses were performed in triplicates. Measurements with a raw depth ≤ 200 were excluded. SNP: Single Nucleotide Polymorphism.

needs to be taken into account that the actual proportion of tumor DNA present in the admixture sample might be slightly shifted from the putative proportion. This is due to the limited precision of DNA concentration, and errors during the generation of admixture samples that are not eliminated by replicate analysis. A shift in the VAF between the measurements can clearly be detected for all SNPs but SNP 5, with even the separation between 0 % and 1 % tumor DNA admixture being very clear. Performing linear regression analysis, the slope of the linear regression line is highly comparable between the observed and expected VAFs (data not shown).

In summary, the established assay is valid to distinguish between different proportions of tumor DNA contained in DNA from blood and to detect 1 % Tumor-DNA admixture in genomic DNA samples. It could not be evaluated if this is true for cfDNA as well as the approach to investigate cfDNA samples with known proportions of ctDNA failed. We found the accuracy of the assay to be highly variable based on the targeted SNP, but this needs further investigation. Additionally, from these experiments, it can not be concluded if the analysis of multiple different SNPs increases the analytical accuracy.

3.1.3.2 Evaluation of assay performance and degree of multiplexing

To further investigate the performance of the assay on each SNP and to evaluate different degrees of multiplexing, we performed a series of different experiments investigating differences

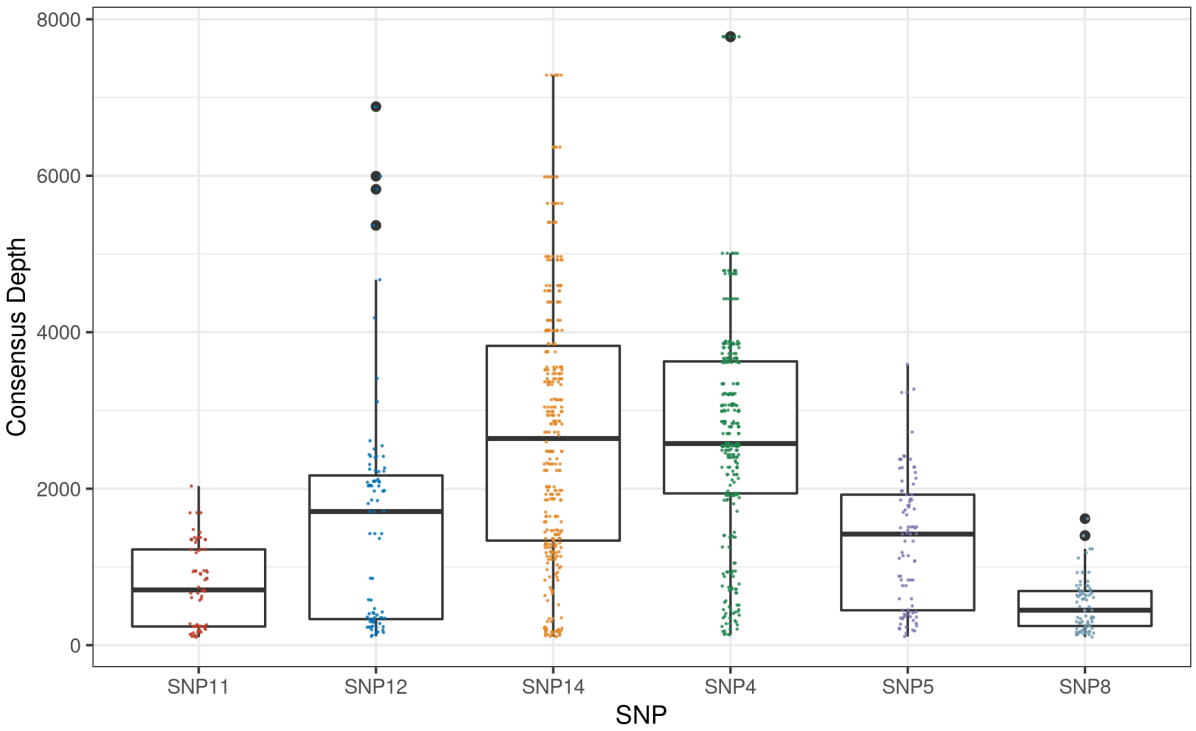

Figure 28: Comparison of the consensus depth of the individual SNP assays. Consensus depth after UMI correction achieved with the different SNP assays in cell-free DNA (cfDNA) and genomic DNA from patients and healthy controls. Measurements with a consensus depth ≤ 100 were excluded. SNP: Single Nucleotide Polymorphism, UMI : Unique Molecular Identifier.

in the consensus depth depending on the targeted SNP as well as several SNP combinations in multiplex approaches. Additionally, we evaluated the analytical accuracy of measuring the VAF in healthy individuals who are thought to have a VAF of 50 % for the different SNPs and multiplexes thereof.

Evaluation of the performance of each SNP assay

First, we compared the six SNP assays we established in terms of consensus depth after UMI correction, as presented in figure 28.

The analysis provides evidence that amplification and analysis of SNP 8 is very inefficient as only a small proportion of NGS reads contained the respective amplicon. Also, assays targeting SNP 11 show a relatively low consensus depth, while assays targeting SNP 12 and SNP 5 show a median consensus depth, and SNP 14 and SNP 4 assays show a highly variable, but in median, the highest consensus depth. The spectrum in consensus depth probably originates from the huge variety of samples and DNA amounts used in the experiments underlying this plot. Additionally, different degrees of sample multiplexing and SNP multiplexing, deviations in cluster densities in the different NGS runs, and inconsistent NGS library qualities are causative for the high variance observed here. Nevertheless, the consensus depth of the different amplicons is comparable, and the analysis unravels significant differences in the sequencing efficiency of these SNPs. This is an important finding for the validation of the assay, as the accuracy of the VAF measurement primarily depends on the consensus depth, which is a measure of the number

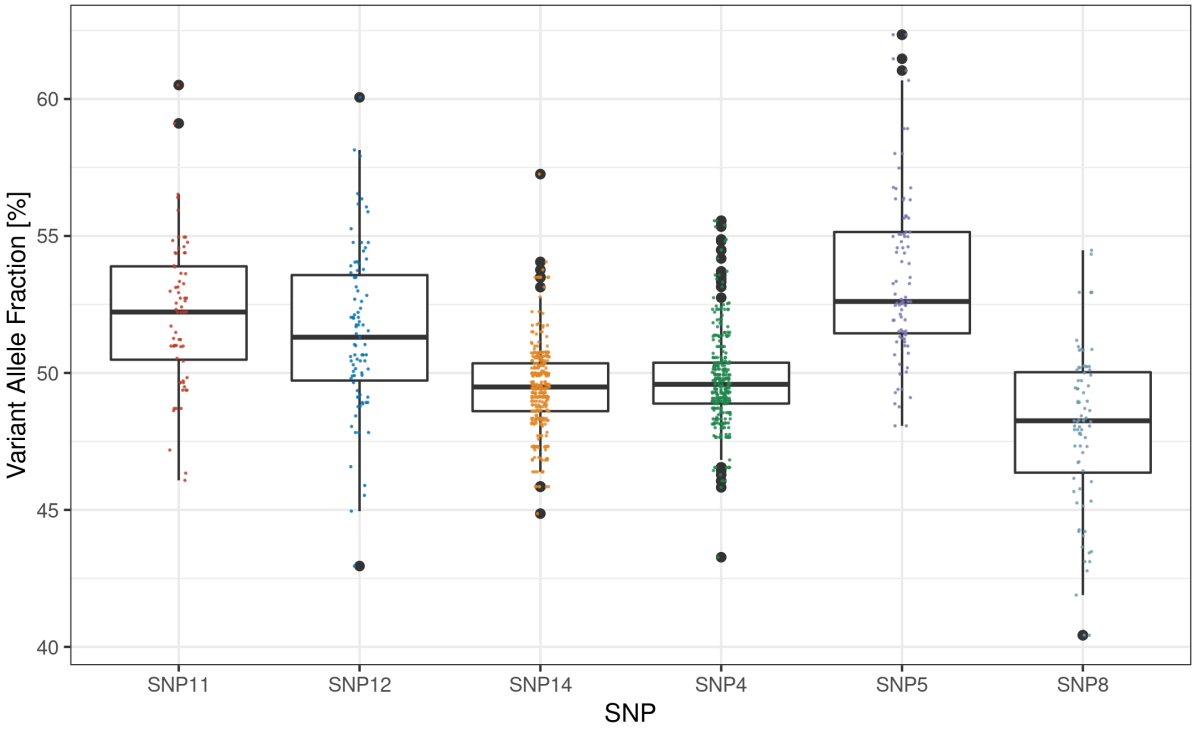

Figure 29: Comparison of the VAF measured with the different SNP assays. UMI corrected variant allele fraction (VAF) achieved with the different single nucleotide polymorphism (SNP) assays in cell-free DNA (cfDNA) and genomic DNA from patients and healthy controls. Measurements with a consensus depth ≤ 100 were excluded. UMI : Unique Molecular Identifier.

of GEs that were considered. If the amount of cfDNA molecules obtained is comparably low, then the proportion of variant reads obtained does not accurately reflect the proportion in the bloodstream.

Next, we investigated the analytical accuracy of measurements in healthy controls which are expected to show a VAF of 50 %. As shown in figure 29, SNP 5 and SNP 8 showed the highest shift between the observed and the expected VAF. That proves the importance of the consensus depth for the accuracy of the VAF measurement as the SNPs that showed low consensus depth (see figure 28) also show the highest levels of deviation in VAF as already observed in figure 27. Accordingly, SNPs 14 and 4, which showed a high consensus depth, show a relatively low shift from the expected VAF, with SNP14 having the highest analytical accuracy but high levels of variance. Additionally, in case of these two SNPs the measurements are almost equally distributed around 50 % VAF, with a deviation of not more than 5 % VAF in all cases except very few outliers. The third best results were accomplished for SNP12, which shows a median shift of the VAF from the expected value of only approximately 1.5 %, VAF but higher levels of variance as indicated by the boxplot. Conclusively, SNPs 14, 4, and 12 are the best targets to detect allelic imbalance.

Evaluation of different multiplexing approaches

The best way would be to investigate all six SNPs (or at least the four ones performing well) in individual assays and in triplicate analysis, but this is not feasible due to the limited amount of

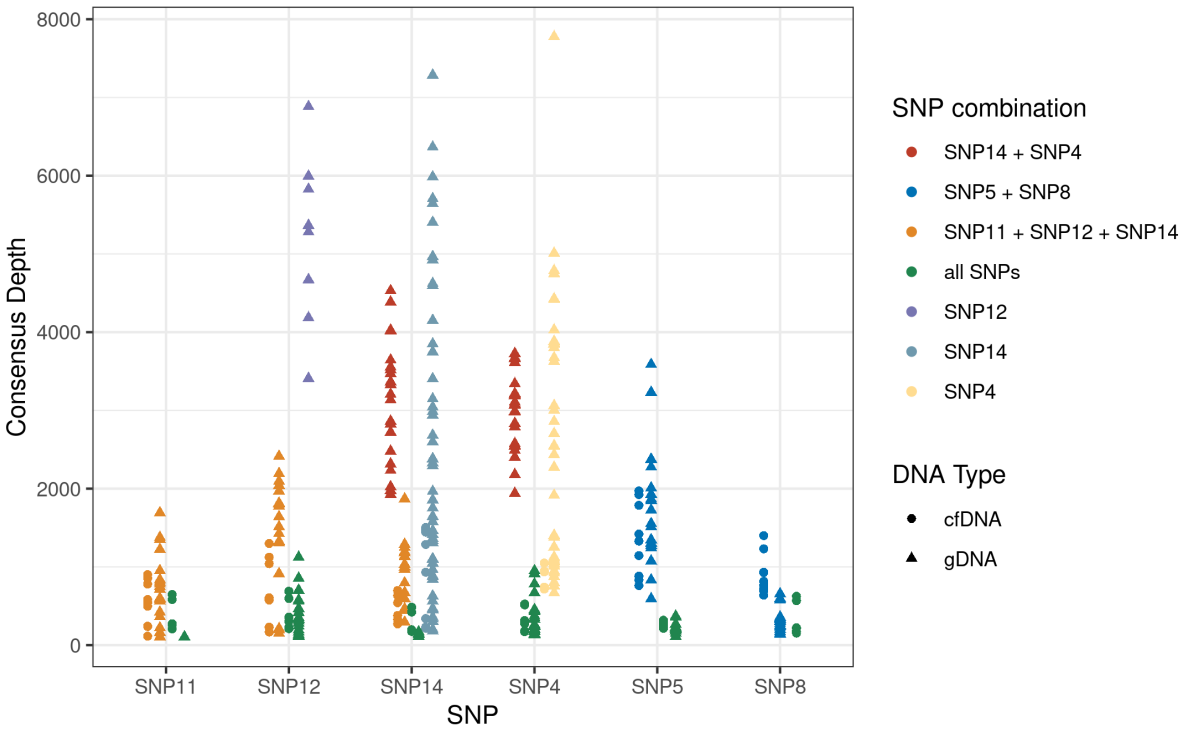

Figure 30: Comparison of consensus depth of the SNP assays and different multiplex approaches. Consensus depth after UMI correction achieved with the different SNP assays in cfDNA and gDNA (as indicated) from patients and healthy controls. Measurements with a consensus depth ≤ 100 were excluded. SNP: Single Nucleotide Polymorphism, cfDNA: cell-free DNA, gDNA: genomic DNA, UMI : Unique Molecular Identifier.

´ available per sample. As a consequence, there is always a trade-off between the number of targeted SNPs, biological replicates, and the DNA amount per assay. Conclusively, multiplexing is highly desirable and favorable, which is why the SimSen-seq method was chosen, as the authors claim that multiplexing is possible and can be easily implemented. That is why we investigated different degrees of multiplexing by combining barcode primers for different SNPs and amplifying all amplicons in a single PCR reaction.

Figure 30 gives an overview of the different multiplex approaches and shows the consensus depth for each multiplex approach in comparison to the respective singleplex approaches where applicable. Some approaches were tested not only on genomic DNA but also on cfDNA, as indicated by the shape of the data points.

The full multiplex approach incorporating all six SNPs shows a consensus depth of rarely 1,000 reads and is consequently not suitable for the analysis of allelic imbalance. The multiplex approach targeting the three SNPs 11, 12, and 14 shows a higher but still marginal consensus depth. The multiplex consisting of SNPs 5 and 8 performs poorly, but this is likely due to the low consensus depth of these SNPs in general. The only multiplex approach showing a comparably high consensus depth is the one consisting of SNPs 4 and 14. However, the single analysis approaches targeting SNP14 and SNP4, respectively, perform at least as well as the multiplex, and in some cases, they even show higher consensus depth levels. We observed higher levels of unspecific products on agarose gels after electrohoresis when performing multiplex assays, even if they consist of only two assays, than when targeting only one SNP. In summary, the

singleplex assays outperformed the multiplex assays so that no multiplexing will be performed despite the limited amount of cfDNA. Single analysis of the three best-performing SNPs 14, 4, and 12 will be carried out instead with replicate analysis wherever possible, given the amount of cfDNA available.

Data obtained from genomic DNA for SNPs 14, 4, and 12 during previous experiments was jointly plotted to evaluate the expected measurement accuracy of the designed assay, as shown in figure 31. We combined the results of all analyses of the chosen SNPs and plotted the data with respect to the number of observations (only from singleplex analysis) included in each measured VAF as indicated by the size of the dots. All analyses underlying these plots were done on gDNA samples from Rb-patients and Rb-survivors, thereby this analysis can serve only to a limited extent as a real example for the liquid biopsy we aim to develop, but the number of measurements per sample required for this comparison could not be executed using cfDNA without processing higher amounts of blood than available.

We calculated the mean variant allele fraction per sample over all SNPs tested. As the results of the different SNP assays varied in consensus depth, we calculated a weighted arithmetic mean using:

$$\bar{x} = \frac{\sum_{i=1}^{n} w_i \cdot x_i}{\sum_{i=1}^{n} w_i}.$$

Here, $\bar{x}$ is the weighted arithmetic mean of the variant allele fraction of a given sample, and n is the total number of measurements done for this sample. w is the weight that is, in this case, the quotient of the consensus depth of the given measurement (i) and the sum of the consensus depth of all measurements done for a given sample. x is the variant allele fraction resulting from the measurement i.

The VAF is variable between samples as well as between individual measurements per sample, but the scale of this variation ranges only from 48 % to 51 % VAF. All in all, the assay is suitable for the investigation procedure of detecting allelic imbalance in patients of heritable retinoblastoma by targeting three different SNPs on chromosome 13 (rs9568029, rs4151450, and rs198619). Applying this method to cfDNA from plasma samples of an Rb-cohort consisting of Rb-patients, Rb-survivors, SPM-patients and healthy controls will allow a final review on the suitability of this method for early detection of SPMs in patients of heritable retinoblastoma.

3.1.4 Application of the assay to a cohort of Rb- and SPM-patients and survivors

Within a European cooperational project with partners from Amsterdam (Netherlands) and Paris (France), we collected patient samples from patients with retinoblastoma, adult Rb-survivor, SPM-patients, and healthy controls (adults and children) (cf. 2.1.1 for more details and inclusion criteria). The characteristics of this cohort and the received treatments will be described in the following. We tested all patients included in the study and several healthy donors for constitutional heterozygosity by performing our assay in a full multiplex approach targeting all

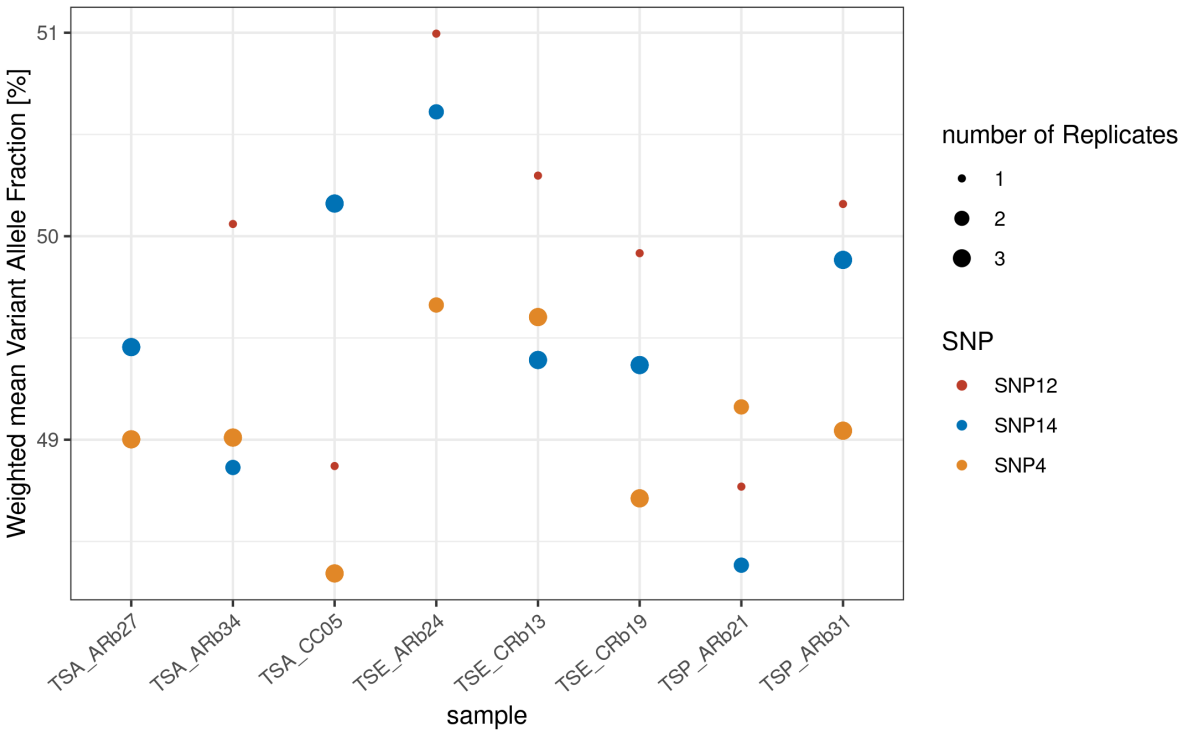

Figure 31: Measurements of VAF with selected SNP assays. Weighted arithmetic mean of VAF replicate measurements in different patient samples. The weights were calculated based on the proportion of consensus reads per measurement of total consensus depth over all measurements. Selection of SNPs according to choice for further sequencing (best three). Measurements with a consensus depth ≤ 100 were excluded. SNP: Single Nucleotide Polymorphism, TSA/TSE/TSP: site of sample collection (A: Amsterdam, E: Essen, P: Paris), ARb: adult Rb-survivor, CRb: Rb-patient (child), CC: healthy control child.

six SNPs. Afterward, we adapted our assay to cfDNA and the restricted amounts available from the Rb-cohort and analyzed all samples from patients being heterozygous for these SNPs. We analyzed the VAF and the consensus depth in each group as described in the following. Finally, we studied the variability of our data aiming to distinguish between measurement uncertainties and skewed allelic ratios caused by the presence of an SPM tumor. Lastly, we aimed to overcome these uncertainties and calculate the probability of LOH using Varlociraptor.

3.1.4.1 Characterization of cohort

First, we characterized our multi-center cohort in terms of general properties, the laterality of retinoblastoma they suffer or suffered in childhood, genetic predisposition, and known SPM tumors. We classified the patients into four groups. The first group, Rb-patients consists of children diagnosed with retinoblastoma that were included in the study at the time of diagnosis. This group includes patients with non-heritable retinoblastoma. Blood sampling from these patients was performed prior to treatment. The second group, Rb-survivors, includes individuals, that are considered healthy at the time of blood draw and survived heritable retinoblastoma in childhood. These patients are considered to be carriers of a constitutional *RB1* variant due to pathogenic RB1 mutation found in blood, bilateral disease, or positive family history. The mutation in the *RB1* gene has not been found or not been detected in very few patients, but these

Table 11: Characterization of the Rb-Cohort. Rb-patients: Patients having untreated retinoblastoma at the time of blood draw; Rb-survivor: Individuals, that are considered healthy at the time of blood draw, survived retinoblastoma in childhood, and are carriers of a constitutional *RB1*-variant; Healthy Control: Patients who do not have any relevant known diseases at the time of blood draw; SPM-patient: Patients who had a second primary malignancy (SPM) at any resonable time around the blood draw.

Characteristic	Rb-patient	Rb-survivor	Healthy Control	SPM-patients	Total
Gender					
Male	18	57	91	16	182
Female	22	64	86	31	203
Age					
child	41	0	25	6	72
adult	0	121	153	41	315
laterality					
bilateral	19	97	N/A	42	158
unilateral	20	23	N/A	5	48
genetic predisposition					
yes	24	120	N/A	47	191
no	11	1	N/A	0	12
SPM					
active	0	0	N/A	15	15
previous	0	0	N/A	21	21
future	0	0	N/A	11	11
Sample size (Total)	41	121	178	47	387

patients had a positive family history and or have been bilaterally affected (see also 1.2.1). In this group, only individuals older than 18 years were included. For control purposes, we also collected blood from Individuals that did not have any relevant known diseases at the time of the blood draw (Healthy Control group). These samples make up the third group. The fourth group consists of patients who had an SPM at the time of the blood draw (active SPM), before the blood draw (previous SPM), or during one year of follow-up (future SPM). Characteristics of the different groups of our patient cohort are described in table 11.

The mean age of the children was 2.75 years, while the mean age of the adults included was 30.99 years, excluding the healthy control patients. In terms of retinoblastoma, more patients were affected bilaterally than unilaterally, which correlates with the increased number of patients with a genetic predisposition. This is because heritability was an inclusion criterion for Rb-survivors, as only these are likely to develop SPMs. Of the patients, who had an SPM at the time of blood draw (active SPM), six were children, and nine were adults, but it needs to be taken into account that access to children with an SPM was easier than to adults. Rb-patients are usually followed up performing routine controls in regular time intervals and are seen in the departments performing this study, whereas in their adulthood, patients are no longer followed. Usually, patients contact local hospitals and oncologists in case of SPM development, so they are not recognized by the centers and, consequently, can not be included in the study. Of the patients who had an active SPM, 10 received EBRT as a treatment for retinoblastoma in childhood. Additionally, 21 patients reported that they already had an SPM in the past (previous

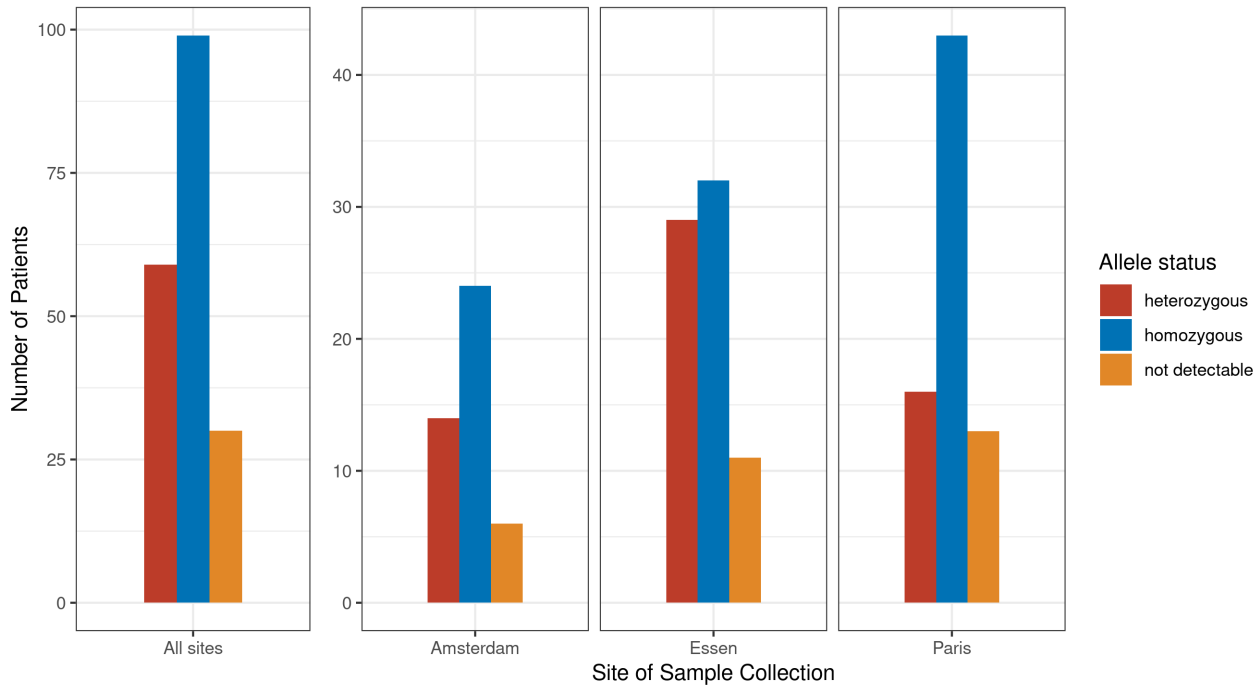

Figure 32: Number of patients per allele status. Allelic state was detected in genomic DNA from leucocytes by sequencing six Single Nucleotide Polymorphisms (SNPs).

SPM), and the time interval between the diagnosis of the SPM and the blood draw varied. From eleven patients we came to know that they were diagnosed with an SPM after the blood draw for our study, so these patients might already have had an SPM at the time of blood draw (future SPM).

After collecting the samples, we started to analyze the allele status of each patient at the positions of our six SNPs based on leucocytes' DNA using our established assay. This is necessary as our assay can only be applied to patients being heterozygous for the targeted SNPs (informative patients). We were not able to detect the allele status at each SNP position in each patient. Consequently, we considered a patients allele status to be heterozygous if at least three SNP positions could be evaluated and the VAF at these positions was between 40 % and 60 %. Accordingly, a patient's allele status was considered homozygous if a VAF of more than 90 % could be measured at minimally 3 SNP positions. If none of these conditions was met the allele status of the patient was not detectable, the main reason for that was a low consensus depth.

Figure 32 displays the total number of patients with a given allele status relative to the site of sample collection. The allele status of 30 patients could not be determined, but 59 patients were considered to be heterozygous and, thereby, informative. Comparing the numbers of patients per site of sample collection, it can be seen that not only the numbers of patients included but also the ratio of patients with a heterozygous and homozygous allele status differed hugely between the countries. In our own patient cohort, we observed the ratio expected due to the parameters of the database query we performed to select the SNPs, where we filtered for SNPs with the highest possible MAF in the European population and linkage disequilibrium with a SNP known to be frequently heterozygous in retinoblastoma patients treated at our center. In

the cohort from Paris, on the contrary, we found approximately three times more patients having a homozygous than a heterozygous allele status. Overall, roughly one-third of all patients (59 patients) included in the study possessed a heterozygous allele status and were thus selected for cfDNA sequencing, investigating the VAF and aiming to detect allelic imbalance.

3.1.4.2 Adaption of the assay to the restricted availability of cfDNA

Aiming to validate our assay and to answer the question if we can detect allelic imbalance, we applied our assay to the cohort described in 3.1.4.1. Volumes of plasma used for cfDNA isolation ranged from 1-4 ml due to limited sample availability. The amount of plasma in the samples from the collaboration partners was lower than in the samples collected in Essen. This was because in France and the Netherlands, only 10 ml of blood could be drawn due to ethical restrictions. Additionally, we aimed to keep sample volumes equal for all patients, including young Rb-children. From the 10 ml of blood drawn, 5 ml was available for the analysis presented here. The other 5 ml of blood was used for the development of another biomarker assay for early detection of SPMs performed in Amsterdam that is not presented here. As pointed out before, we conducted the assay on the three best-performing SNPs (SNP12, SNP14, and SNP4), using 7 µl cfDNA each. Additionally, we repeated the assay on SNP 12 if enough material was available. In cases with very limited cfDNA, we did not limit the amount of cfDNA per assay but performed fewer assays on only one or two SNPs.

Figure 33 shows the weighted arithmetic mean of the VAF for the different groups of the Rb-cohort. Additionally, the consensus depth is indicated by the size of the data points. In general, outliers possess a very low consensus depth. Allele countings equal a statistical drawing process comparable to an urn model, with the urn being the patient sample, the balls being the alleles and the drawing process being our assay. This is strongly simplified, as the process of library preparation and sequencing includes not only one but multiple drawing processes that are additionally biased by sampling errors, pipetting errors, base call, mapping qualities, etc., as shown in the graph of the process (Figure 8).

Nevertheless, our measurement can be described as a Bernoulli process, and, therefore, it applies that the higher the number of drawings, the lower the deviation of the observed value from the actual value. For our assay, this means that the higher the consensus depth, the lower the uncertainty of the measured VAF. This is based on the assumption that the consensus depth is equal to the number of GEs tested, which is reasonable because of the UMI error correction performed. The actual value is, in this case, the VAF present in the sample, which in turn mirrors the VAF of all cfDNA in the bloodstream with disregard to any bias introduced by sampling errors and alike. In summary, consensus depth is key for a precise measurement of the VAF.

Having a closer look at the individual samples tested and taking the weighted standard deviation into account figure 34 shows that measurement accuracy differs not only between samples but also between the groups. The standard deviation is directly dependent on the consensus depth that is indicated by a color gradient.

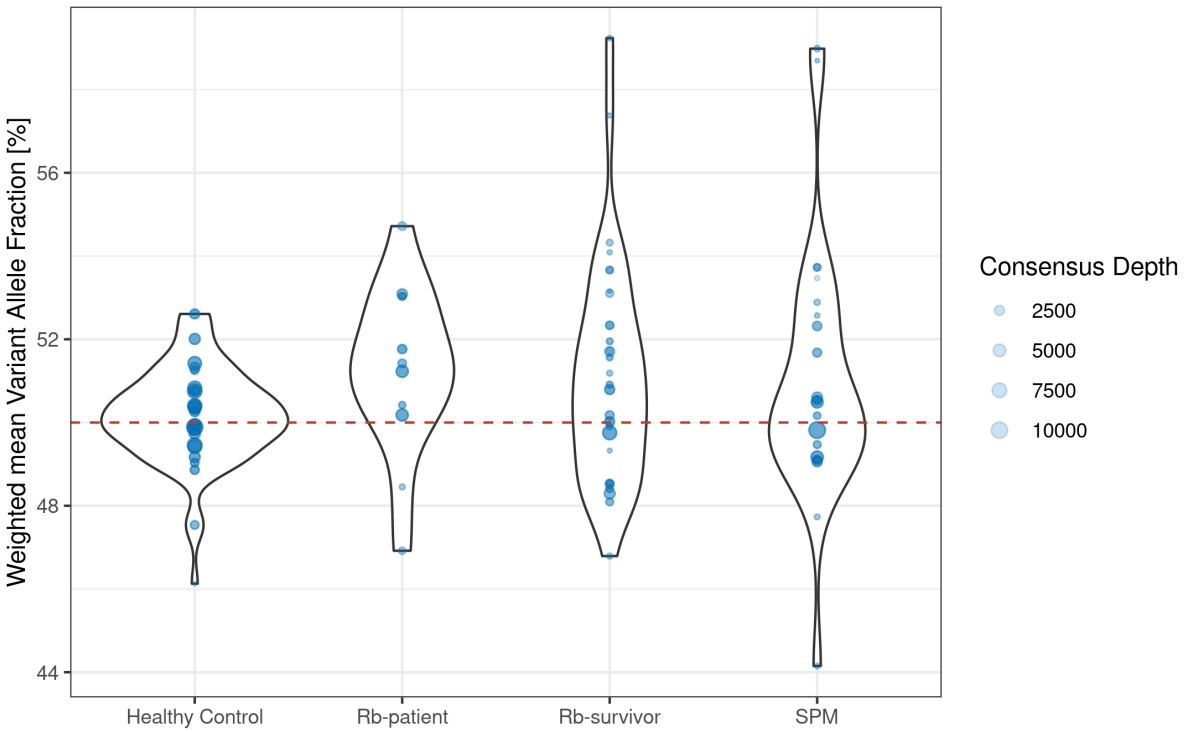

Figure 33: Violin plot of the weighted arithmetic mean VAF per group. Mean of four measurements at three different SNP positions if the availability of material was sufficient. Weights were calculated based on the proportion of consensus reads per measurement on total consensus depth overall measurements. Measurements with a consensus depth < 100 and measurements with $VAF \geq 95\,\%$ or $VAF \leq 5\,\%$ were excluded. Rb-patient: Patients having untreated retinoblastoma at the time of blood draw; Rb-survivor: Individuals, that are considered healthy at the time of blood draw, survived retinoblastoma in childhood, and are carriers of a constitutional *RB1*-variant; Healthy Control: Patients who do not have any relevant known diseases at the time of blood draw; SPM: Patients who had a second primary malignancy (SPM) at any resonable time around the blood draw, SNP: Single Nucleotide Polymorphism, VAF: Variant Allele Fraction.

3.1.4.3 Descriptive statistical analysis results per group

In the following the results of the analysis of cfDNA from the Rb-cohort shown in figures 33 and 34 will be described for each group of patients. Furthermore, the results of the measurement of allelic imbalance will be compared to the results expected for each group.

Healthy Controls: no positive signal of alleleic imbalance expected

This group of individuals did not have any relevant disease at the time of the blood draw. Hence none of these samples is expected to show a shift in the VAF and, thereby, allelic imbalance. These samples were included in the study to serve as negative controls. From figure 33 it can be taken that the healthy controls show the expected VAF of approximately 50 % with a maximum of data density at exactly 50 %.

All samples from adult healthy controls were collected in Essen, and the blood volume of all samples was approximately 7.5 ml. Hence the amount of plasma was higher in this group than in the other three groups. Therefore the consensus depth is comparably high, and the standard deviation is much smaller than in all other groups. The measure of dispersion given by the standard deviation equals approximately 5 % for several healthy control samples (cf. figure 34).

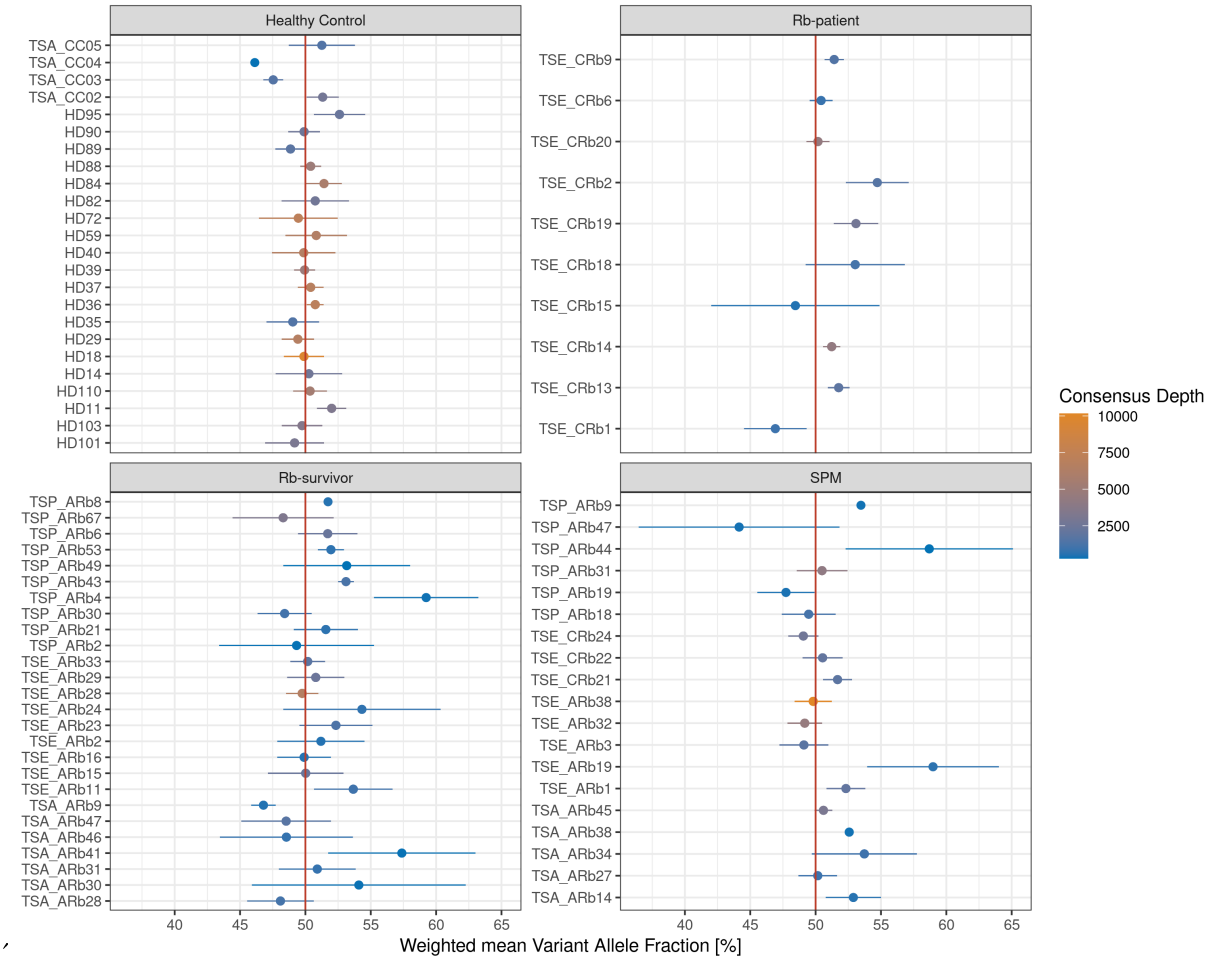

Figure 34: Weighted arithmetic mean VAF and weighted standard deviation per group and sample. Mean of four measurements at three different SNP positions if the availability of material was sufficient. Weights were calculated based on the proportion of consensus reads per measurement on total consensus depth overall measurements. Consensus depth is UMI-corrected Raw Depth. Measurements with a consensus depth < 100 and measurements with $VAF \geq 95\,\%$ or $VAF \leq 5\,\%$ were excluded. ARb: Adult Rb-survivor, CRb: Rb-patient (child), HD: Healthy Donor, CC: healthy control child, Rb-patient: Patients having untreated retinoblastoma at the time of blood draw; Rb-survivor: Individuals, that are considered healthy at the time of blood draw, survived retinoblastoma in childhood, and are carriers of a constitutional *RB1*-variant; Healthy Control: Patients who do not have any relevant known diseases at the time of blood draw; SPM: Patients who had a second primary malignancy (SPM) at any resonable time around the blood draw, SNP: Single Nucleotide Polymorphism, TSA/TSE/TSP: site of sample collection (A: Amsterdam, E: Essen, P: Paris), VAF: Variant Allele Fraction, UMI: Unique Molecular Identifier.

The two samples showing the highest deviation (CC04 and CC03) were derived from small children from which only around 1.3 ml of plasma was available. As a result, the consensus depth of these measurements was below 300, and additionally, for CC04, only two SNPs could be successfully analyzed.

Taken together, this shows that the targeted limit of detection of 5 % ctDNA could not be achieved with this assay. However, none of the measurements or calculated standard errors were below 45 % VAF or above 55 % VAF. These values would be expected in the case of 10 % ctDNA, as described in 3.1.3.1. Hence, the expected limit of detection of 10 % ctDNA, which was predicted based on the median number of GEs measured by ddPCR, could be reached based on the findings in the healthy control group.

Rb-patients: retinoblastoma present at time of sampling

Patients in the group of Rb-patients had retinoblastoma at the time of sampling and, thus, in principle, have ctDNA in their blood. However, the proportion of ctDNA is expected to be well below 5 % Jiménez et al. (2021) and Francis et al. (2021). The measurements of cfDNA from Rb-patients are not expected to show any positive signal, however, this can not be excluded, as discussed in 4.1. The VAFs of the samples from this group are a bit more scattered but show a distribution similar to the healthy donors (cf. figure 33). None of the measured VAFs is shifted from 50 % by more than 5 %, so none of the samples shows a signal above the limit of detection, as shown in figure 34.

Rb-survivors: no positive signal expected

The patients in the group of Rb-survivors have a genetic predisposition as described above but did not have a second tumor at the time of the blood draw. Additionally, they neither had an SPM prior to the blood draw nor during follow-up, which was until approximately one year after the blood draw. Hence no positive signals are expected from this group. Consequently, the two samples that show a VAF of more than 55 % need to be considered false positives.

When compared to the group of healthy controls, this group has a higher proportion of samples with low plasma volumes because less blood was available from these patients, as described previously. Accordingly, the consensus depth of these measurements is lower, and the degree of scattering is higher (cf. figure 34). In the violin plot, a slightly upward-shifted distribution is observed, but most data points escaping the range of the healthy donor group have a low consensus depth and are, therefore, less reliable. The intersample variability present in the Rb-survivor group additionally indicates a low precision of the measurement. Accordingly, the measurements with high consensus depth are close to the expected VAF of 50 %.

SPM patients: expected to be enriched with positive signals

It is to be expected that some of this group's samples show a positive signal due to an SPM present at the time of the blood draw. Figure 33 shows a bivariate distribution with a higher

density at 50 % VAF and a lower density at approximately 53 % VAF. However, the measurements of higher VAFs have a low consensus depth, while measurements with high consensus depth are close to the VAF of 50 % expected if no tumor is present. As shown in figure 34, three samples show a shift of the VAF of more than 5 % and are thereby considered positive.

Conclusion

In conclusion, some questions remain unresolved. The proportion of expected positive measurements differs between the subgroups of patients with previous, active, and future SPMs. Hence a more detailed analysis of this group needs to be performed to answer the question of which of the samples showing a shifted VAF are expected to be positive.

Furthermore, the statistical analysis showed a high correlation between the analytical accuracy and the consensus depth, which is considered to reflect the number of GEs analyzed. This is to be expected due to the Bernoulli process underlying these measurements, as described previously. But which degree of deviation from 50 % VAF would be expected due to the statistical drawing process and can hence be explained by statistical uncertainty due to insufficient numbers of GEs analyzed only?

3.1.4.4 Advanced statistical analyis of data

To answer these questions, we aimed to investigate the deviation of the measured value from the actual value that would be expected due to the statistical drawing process. As the binomial distribution describes the results of a Bernoulli process, we can assume that given the number of GEs tested, the probability for a specific number of variant alleles follows a binomial distribution. Thus we can use the standard deviation given for a binomial distribution to quantify the effect of the number of GEs analyzed on the certainty of the measurement.

The formula for the standard deviation of the binomial distribution is:

$$\sigma = \sqrt{n \cdot p \cdot (1-p)}$$

with the probability of "drawing" a variant allele assuming that the individual is healthy being $p = 0.5$, the standard deviation only depends on the number of drawings n. In this case, the number of drawings is the number of GEs tested, and due to the UMI correction, the consensus depth can be considered equal to the number of GEs.

Figure 35 shows the resulting expected measurement range, the direct dependency on the number of GEs can also be observed by comparing the spread of the expected values with the color indicating the consensus depth. It can be taken from the plots that the measured value is outside the expected range for some samples. If there were no other errors than the one caused by the statistic drawing process underlying this analysis, we would assume that those measurements that are outside the range plotted here can be considered actual shifts of the VAF caused by allelic imbalance due to SPM presence.

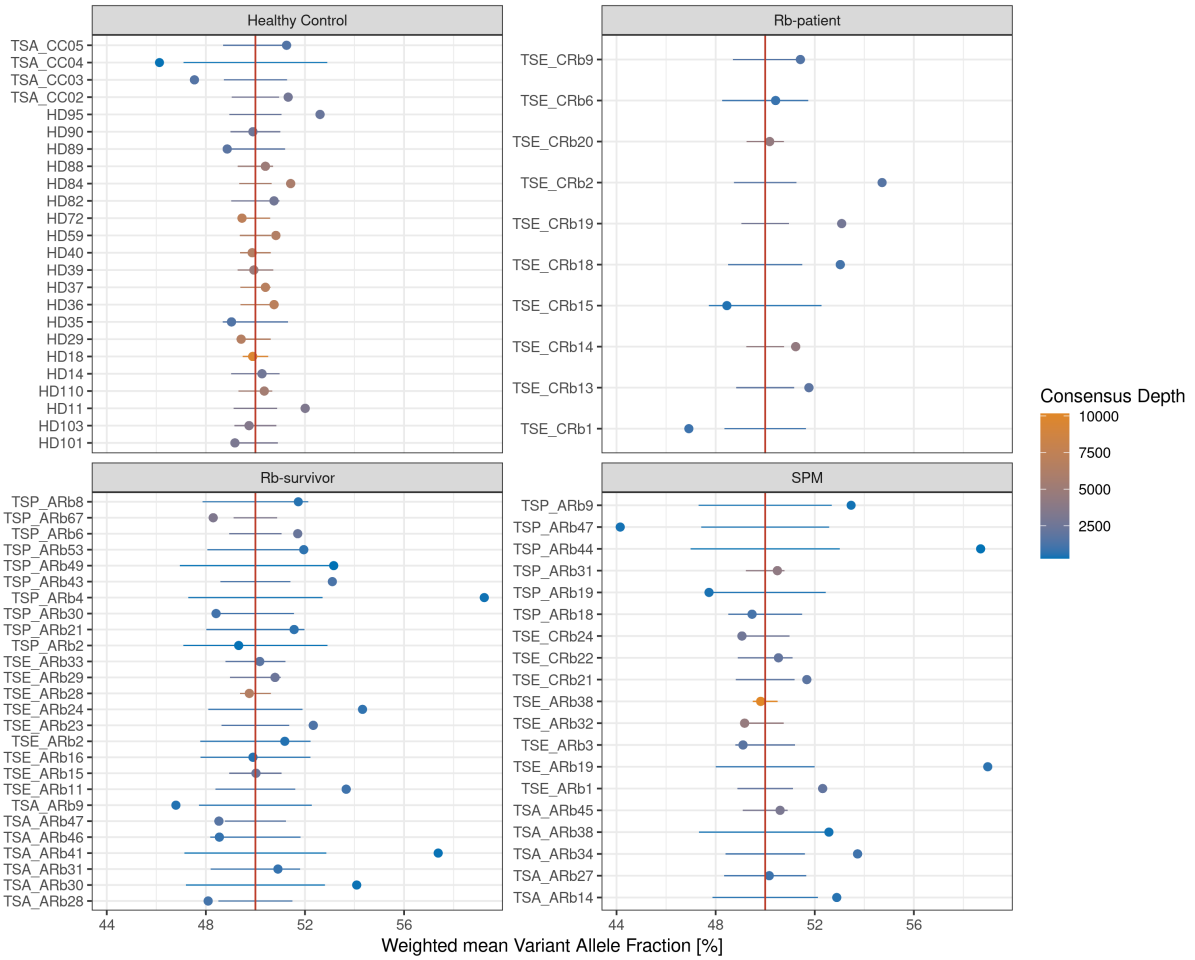

Figure 35: Expected range of VAF based on bionomal standard deviation. Mean of four measurements at three different SNP positions if the availability of material was sufficient. Weights were calculated based on the proportion of consensus reads per measurement on total consensus depth over all measurements. Consensus depth is the UMI-corrected raw depth. Measurements with a consensus depth < 100 and measurements with $VAF \geq 95\,\%$ or $VAF \leq 5\,\%$ were excluded. ARb: Adult Rb-survivor, CRb: Rb-patient (child), HD: Healthy Donor, CC: Healthy control child, Rb-patient: Patients having untreated retinoblastoma at the time of blood draw; Rb-survivor: Individuals, that are considered healthy at the time of blood draw, survived retinoblastoma in childhood, and are carriers of a constitutional *RB1*-variant; Healthy Control: Patients who do not have any relevant known diseases at the time of blood draw; SPM: Patients who had a second primary malignancy (SPM) at any resonable time around the blood draw, SNP: Single Nucleotide Polymorphism, TSA/TSE/TSP: site of sample collection (A: Amsterdam, E: Essen, P: Paris), VAF: Variant Allele Fraction, UMI: Unique Molecular Identifier.

In the group of **healthy controls,** four measurements can be observed that are outside the range of the statistical error. However, two of them are samples from children that were already discussed previously. The low consensus depth of CC04 becomes more obvious in this visualization because of the large error bar. None of these four samples shows a high consensus depth, but some show intermediate consensus depths. All four samples are false positive as these patients did not have a tumor at the time of the blood draw.

Within the group of **Rb-survivors** the consensus depth of the measurements is lower than in the group of healthy controls, as pointed out before. This can be observed by the light blue color as well as the large error bars in the majority of samples. Measurements with a high consensus depth show a VAF very close to 50 % as TSE-ARb28 or TSE-ARb15, for example. Two samples show a VAF that is shifted by more than 5 % and is hence above the limit of detection of 10 % ctDNA. At follow-up, these patients reported that they did not have an SPM after the blood draw, and therefore these results are false positives.

In the group of **Rb-patients** more than half of the measurements show a VAF that is outside the range of the statistical error. However, none of these values are shifted by more than 5 %, and therefore all measurements are considered negative.

From the group of **SPM patients**, nearly half of the samples show a VAF that is outside the range of the statistical error. However, the same is true for the Rb-survivors, those measurements that show such a shift have a low consensus depth, whereas those measurements showing a high consensus depth are close to 50 % VAF.

To answer the question of which type of SPM (active, future, or previous) the samples showing a shifted VAF are, we had a closer look at the results from the group of SPM patients. These samples were thought to serve as positive controls as they have been diagnosed with an SPM by clinical routine methods. As already pointed out in the previous section, we further classified these patients into active SPM, future SPM, and previous SPM, as shown in figure 36. The type of presentation is the same as in figure 34 with error bars representing the weighted standard deviation.

The group of patients with **active SPMs** consists of only four patient samples, which results from the fact that these were most difficult to obtain, and despite international collaboration, only very few samples could be collected. Additionally, our assay is only applicable to patients who are constitutively heterozygous for the SNPs tested here, which has further narrowed the selection of patients presented in this plot. Active SPMs are the only patients where we would expect allelic imbalance and hence a shift in the variant allele fraction found in cfDNA. However, the extent of this shift is unknown because the amount of ctDNA present in these samples is not known. As shown in figure 36, none of these samples showed a positive result. Moreover, all samples show a VAF that is very close to 50 % with a maximum shift of less than 2.5 %. Therefore all results from this group are negative. Possible reasons for this will be discussed in the next chapter (4.1).

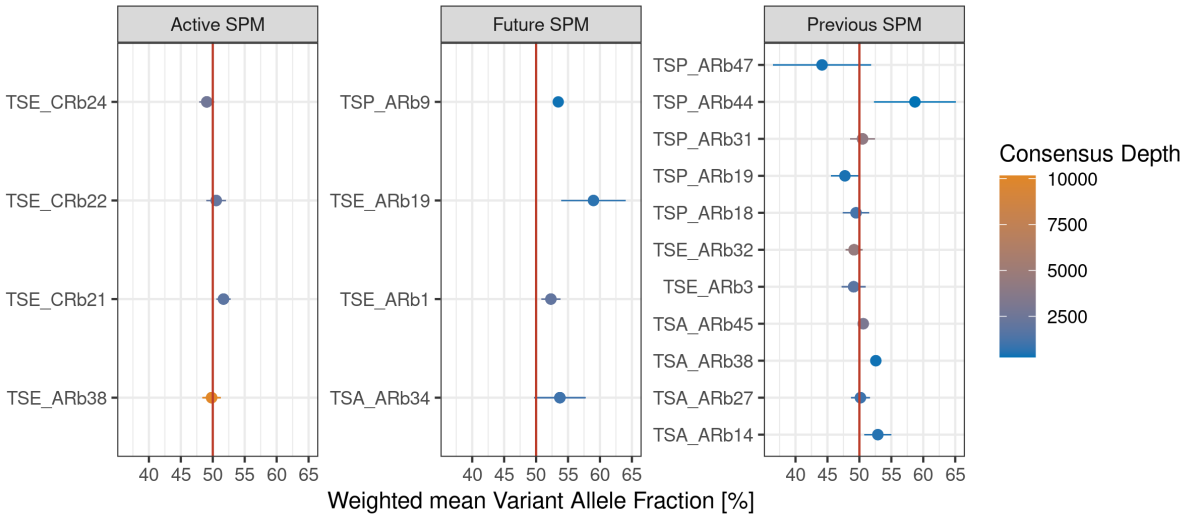

Figure 36: Weighted arithmetic mean VAF per type of SPM. Mean of four measurements at three different single nucleotide polymorphism (SNP) positions if the availability of material was sufficient. Weights were calculated based on the proportion of consensus reads per measurement on total consensus depth overall measurements. Consensus depth is UMI-corrected Raw Depth. Measurements with a consensus depth < 100 and measurements with $VAF \geq 95\,\%$ or $VAF \leq 5\,\%$ were excluded. ARb: Adult Rb-survivor, CRb: Rb-patient (child), TSA/TSE/TSP: site of sample collection (A: Amsterdam, E: Essen, P: Paris), VAF: variant allele fraction, UMI: Unique Molecular Identifier.

Samples from **future SPM** patients who developed an SPM after the blood draw are highly likely to show allelic imbalance as well, but the degree of the expected shift differs based on the amount of time between the blood draw and the SPM development. These samples were intended to serve as an indicator of how early we can detect an SPM and if this biomarker can be used as a diagnostic biomarker. Also, in this group, only four suitable samples could be collected, and from these samples, one (TSE_ARb19) showed a VAF of more than 55 % and is thereby considered positive. The reliability of this will be discussed in chapter 4.1 by taking clinical data into account.

In the group of **previous SPM** patients, two samples showed a shift in the VAF of more than 5 % (TSP ARb47 and TSP ARb44). These measurements show a high level of statistical error resulting from a low consensus depth. Also, the reliability of these results will be discussed in chapter 4.1 by comparing the results with the time interval between the diagnosis of SPM and the blood draw in terms of this study.

No positive results were detected in the samples from patients with an active SPM which were expected to be enriched with positive signals. This might be because the limit of detection is insufficient to detect the levels of ctDNA released by these tumors. Even if the wet-lab part of the analysis could be improved, no ctDNA is left from these patients to repeat the analysis. Hence the only option to lower the limit of detection is to improve the data analysis.

In summary, the assay used for the analysis of cfDNA from the cohort of the NIRBTEST study is not suitable for the intended use, which was to detect positive signals from SPMs, because it showed false positive results in the group of healthy controls as well as Rb-survivors which did not develop an SPM at least one year after blood draw. So far, we supposed that the consensus

depth equals the number of genome equivalents due to UMI correction. Consequently, we assumed that shifts of the VAF result from skewed allelic ratios only. However, there might be other factors influencing the VAF, like additional measurement uncertainties that could not be eliminated by UMI correction.

To overcome these suspected uncertainties and improve the limit of detection, we decided to repeat the analysis of the sequencing data using Varlociraptor, which is an uncertainty-aware variant caller as described in 1.4.3.3 (Köster et al. 2020).

3.1.4.5 Varlociraptor approach to calculate probability of LOH

Aiming to achieve a higher level of error correction and calculate the probability of LOH with high certainty, we decided to analyze our data with Varlociraptor (Köster et al. 2020). The statistical model behind this bioinformatic tool takes all possible sources of uncertainty and almost all possible biases into account. For example, it considers mapping uncertainty and biases by read position, read pair orientation, or sampling. In order to combine UMI grouping and error correction with Varlociraptor, we had to replace debarcer with another tool because debarcer does not generate UMI-corrected bam files, which are required by Varlociraptor. A new pipeline for UMI consensus calling was developed by Felix Mölder and Johannes Köster. It has not yet been published, but the wrappers building up this pipeline are already available in the Snakemake wrappers repository (https://snakemake-wrappers.readthedocs.io/en/stable/). Its functionality will be shortly described in the following, the DAG of rules of the full pipeline is shown in figure 37.

First, an alignment is generated, then UMIs are annotated, and duplicates are marked. Next, the alignment is used to assign the reads to one of the three classes, “paired-end”, “single-end”, and “skipped”. fastq files are generated for each class. “Paired-end” reads have non-overlapping forward and reverse reads, while “single-end” reads have either overlapping forward and reverse reads or do not have a complementary read. The “skipped” class consists of reads that were skipped due to soft-clipping or inappropriate mapping. Two new alignments are created based on all reads that were not skipped, one for the correctly “paired-end” reads and one for the “single-end” or overlapping “paired-end” reads. The skipped reads are sorted, duplicates are marked, and a separate alignment is created. Lastly, all three alignments are merged to generate a single consensus alignment (`merge_consensus_reads` in the DAG) that contains UMI-corrected reads and can be used for further analysis.

As indicated in the DAG, the next step was to perform variant calling via `freebayes` (Garrison and Marth 2012) to obtain candidate variants for each sample. The candidate variants and the consensus alignment were then given to Varlociraptor to analyze the probability of LOH. The scenario used to distinguish between presence and absence of LOH and to determine the allele that is affected by the loss is the following:

```
events:
```

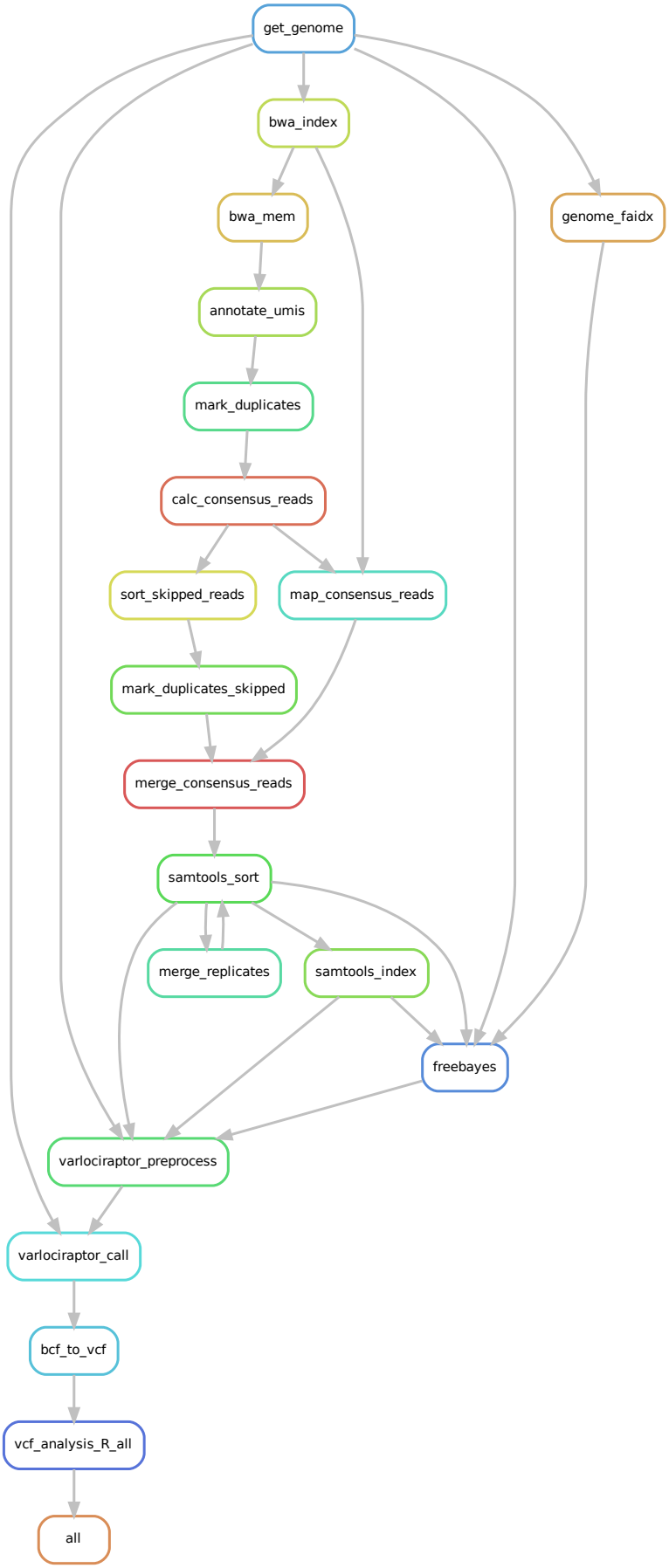

Figure 37: DAG of rules of snakemake pipeline to determine probability of LOH. Each box represents a rule that is part of the Snakemake (Mölder et al. 2021) workflow applied to analyze the probability of loss of heterozygosity (LOH) using Varlociraptor (Köster et al. 2020) and unique molecular identifier (UMI) consensus calling (Mölder and Köster, unpublished).

```
loh_variant:  "blood:]0.0,0.5["
loh_reference:  "blood:]0.5,1.0]"
no_loh:  "blood:0.5"
```

Due to the linkage disequilibrium of the SNPs, we first assigned all variants called by `freebayes` to the same haplotype by defining them to be part of the same event. This we managed by adding `EVENT=haplotype1` to the vcf file after variant calling. Varlociraptor then calculated a joint posterior probability over all SNPs for each of the three events. Varlociraptor calculated the a posteriori distribution of the allele frequencies as a density function for all three events defined in the scenario. However, this resulted in high numbers of false positive results in the group of healthy donors.

So we decided to calculate the probabilities for LOH individually for each SNP for several reasons. First, the haplotype function of Varlociraptor has not yet been tested on data derived from biological samples. Second, in terms of evaluation of the assay performance, independent testing is superior, as it allows a deeper insight into the analysis performed. We used the mode of the maximum likelihood distribution, which is part of the output of Varlociraptor to calculate a joint posterior probability for LOH with disregard to the allele (reference or variant) where the LOH was detected. For the calculation of the probability of LOH $P_x(LOH)$, we used the following equation

$$
\begin{aligned}
P(LOH_{\text{var}}) &= P_{12}(LOH_{\text{var}}) \cdot P_{14}(LOH_{\text{var}}) \cdot P_4(LOH_{\text{var}}) \\
P(LOH_{\text{ref}}) &= P_{12}(LOH_{\text{ref}}) \cdot P_{14}(LOH_{\text{ref}}) \cdot P_4(LOH_{\text{ref}}) \\
P(LOH) &= P(LOH_{\text{var}}) + P(LOH_{\text{ref}})
\end{aligned}
$$

where x is the number of the SNP used to calculate the probability, LOH_{var} being the loss of heterozygosity of the variant allele LOH_{ref}being the loss of heterozygosity of the reference allele. The results for each sample are shown in figure 38.

All patients could be classified as having either a high or a low probability for LOH; none of the patients had a medium probability of LOH. This analysis resulted in much fewer false-positive results than the analysis using debarcer and UMI correction only. Only one healthy control (HD 103) shows a high probability for LOH, which is considered a false positive. The same is true for the group of Rb-survivors and Rb-patients, where TSA-ARb13 or TSE-CRb14 showed a positive result, respectively. These are considered to be false positives as well. In the group of SPM patients, none of the measurements resulted in a high probability for LOH, although this group was expected to be enriched with positive measurements.

We investigated the number of reads supporting these outcomes using the posterior odds calculation that is part of the Varlociraptor output. Figure 39 presents the number of reads for each Kass Raftery Score. The number of reads was highest for the healthy donors, which is probably because of the higher blood volumes available from these patients compared to the mean

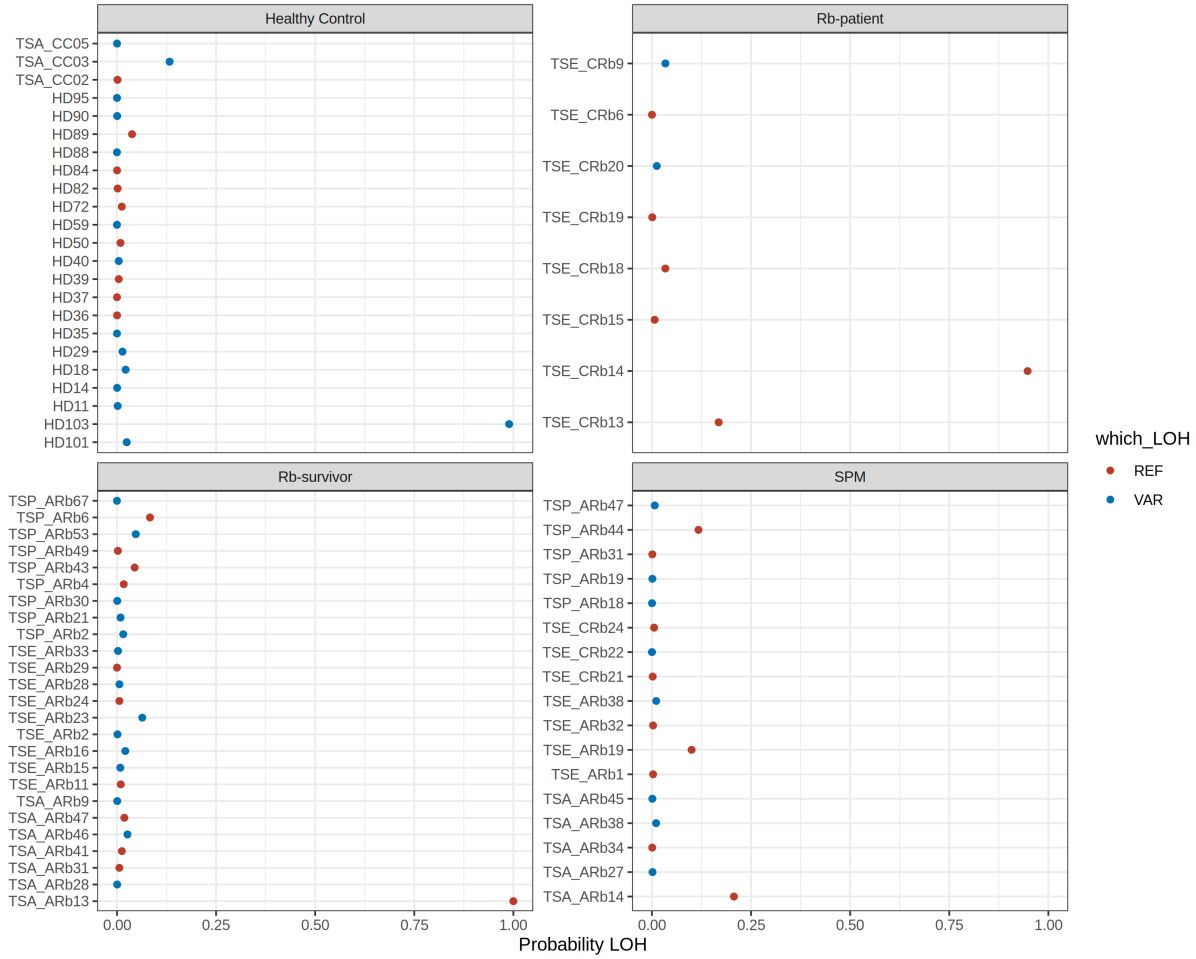

Figure 38: Posterior probability of loss of heterozygosity (LOH). Calculation was done using Varlociraptor, and the events were defined as such: loh_variant: "blood:]0.0,0.5["; loh_reference: "blood:]0.5,1.0]"; no_loh: "blood:0.5". All single nucleotide polymorphisms were classified as the same event “haplotype1” due to their linkage disequilibrium. ARb: Adult Rb-survivor, CRb: Rb-patient (child), HD: Healthy Donor, CC: healthy control child, TSA/TSE/TSP: site of sample collection (A: Amsterdam, E: Essen, P: Paris), REF: reference allele, VAR: variant allele.

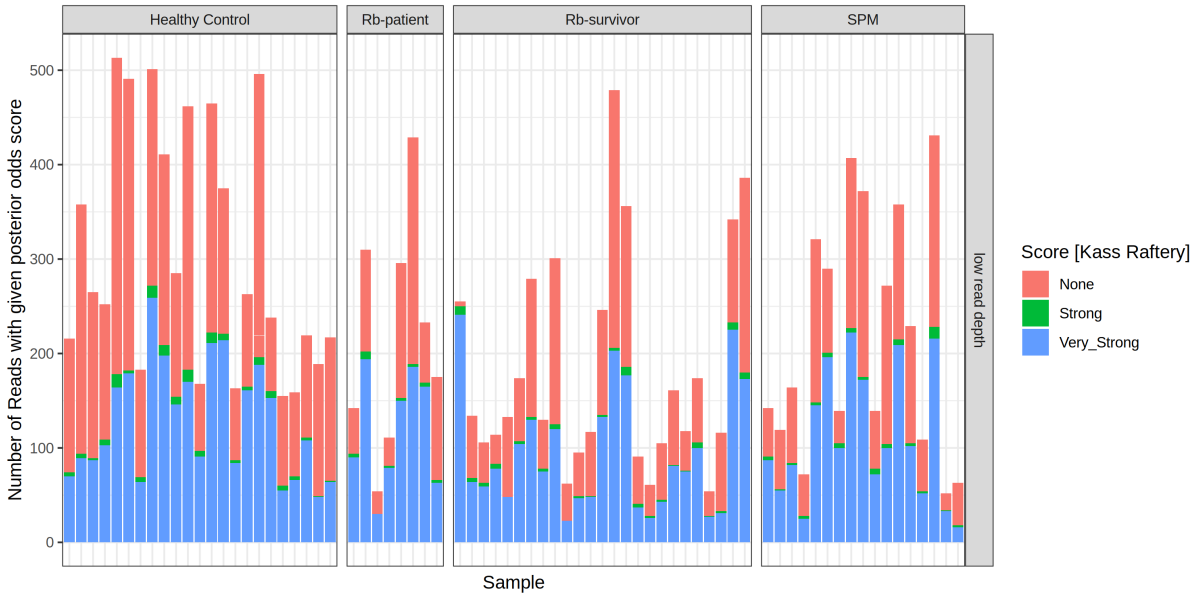

Figure 39: Number of reads with given posterior odds score. Kass Raftery scores for posterior odds as calculated by Varlociraptor after UMI-corrected consensus calling. UMI: Unique Molecular Identifier, Rb-patient: retinoblastoma patient (child), SPM: patients who had a second primary malignancy in any reasonable time around the bloddraw.

blood volume in the other groups. For most of the samples, less than 400 consensus reads could be achieved. This number is about 10-fold lower than the consensus depth after UMI correction using debarcer and critical for counting allele ratios in mixtures of cfDNA and ctDNA, as pointed out before. Given a consensus depth of 400 and assuming that this reflects the number of GEs analyzed, the standard deviation of the binomial distribution is 10. Hence deviations of the VAF of 2.5 % would be expected due to the statistical drawing process only. Consequently, the limit of detection of this assay is not sufficient to detect 5 % ctDNA or less but sufficient to detect more than 5 % ctDNA, given the number of GEs in the samples tested.

In summary, we presented a very promising pipeline for UMI consensus calling and estimation of posterior probabilities for LOH that can be easily applied to other approaches. We found some false positive results also with this analysis method, and further analysis is needed to identify the origin of these. It needs to be concluded that the samples collected within the European NIRBTEST study are not sufficient to detect allelic imbalance and validate this assay because of low numbers of GEs resulting in low consensus depths and due to missing knowledge about the presence of a tumor at the time of blood draw as well as ctDNA levels.

3.2 A prognostic test for uveal melanoma

The prognosis for UM patients differs tremendously based on the tumor class (cf. figure 7), so it can serve as a prognostic biomarker. The best established prognostic biomarker that is used to distinguish between the two classes of UM is the chromosome 3 status. Patients with monosomy 3 tumors have a worse prognosis as these tumors metastasize more frequently than disomy 3 tumors. For patients receiving eye preserving therapy, the tumor tissue needed for testing is currently obtained by *in situ* tissue biopsies, which is associated with risks of microseeding of tumor cells or hemorrhage into the VB. Additionally, if a tissue biopsy cannot be performed for any reason, the patients cannot receive a prognosis. Hence, there is a high need for a non- or less-invasive procedure. The least invasive procedure to obtain tumor DNA is a blood draw, but it has been shown in previous studies (Le Guin, Bornfeld, et al. 2021) that no ctDNA is detectable in blood at the time of diagnosis. Other sources of ctDNA that can be obtained less invasively might be aqueous humor (AH) or vitreous body aspirate (VB), so we performed a feasibility study to investigate if these samples contain enough ctDNA to analyze prognostic genetic biomarkers. We used deep amplicon sequencing targeting UM-specific mutations in *GNAQ* and *GNA11* to detect and determine the proportion of ctDNA in AH and VB. In order to develop a strategy to analyze the chromosome 3 status of the ctDNA in these samples, we selected a set of SNPs distributed over the whole chromosome 3 and used the Agilent SureSelect XT HS Target enrichment system to perform NGS sequencing of the enriched SNPs containing fragments. An allele ratio of constitutionally heterozygous SNPs that deviates from 0.5 in cfDNA would indicate monosomy 3.

3.2.1 ctDNA can be detected in cfDNA from AH and VB

We performed a feasibility study investigating if ctDNA can be detected in AH and VB. Samples were collected from 18 UM patients having large tumors that needed to be enucleated. The study was conducted on enucleated eyes as adverse effects for the patient are excluded in this setting. We extracted cfDNA from both types of samples, from AH samples it could be extracted directly, while VB samples needed physical disruption (more details in 2.2.4.4). Additionally, we isolated tumor DNA and performed Sanger sequencing of codons 209 and 183 of *GNAQ* and *GNA11*, we identified the oncogenic mutation in all 18 tumor tissue samples. This step was performed to gain additional information for assay development, but it is not required for the analysis of ctDNA.

As a first step towards the detection of ctDNA in the liquid biopsy samples, we performed Sanger sequencing on cfDNA from five VB samples and seven AH samples to determine whether the mutations identified in *GNAQ/11* in the respective tumor samples can be found in these samples as well. We were able to detect ctDNA in two of the VB samples, and in three of the AH samples, we found a weak signal of the mutated allele present in either the forward or the reverse read but never in both. Conclusively, the results of Sanger sequencing on AH

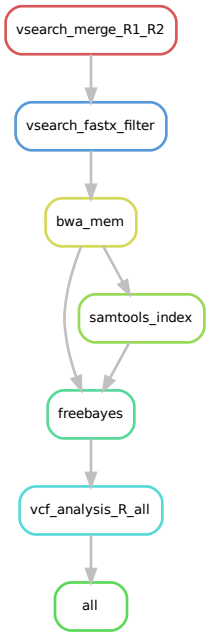

Figure 40: Directed acyclic graph of rules of the Snakemake pipeline for detection of ctDNA in cfDNA. Each box represents a rule that is part of the Snakemake workflow applied to analyze the fastq files to determine the ratio of ctDNA. The graph was obtained from Snakemake using the built-in function. cfDNA: cell-free DNA, ctDNA: cell-free tumor-DNA

samples might lack sensitivity, so we continued the analyses using Deep Amplicon Sequencing, a method that has already been approved for the analysis of cfDNA from blood and has been shown to be highly sensitive (Le Guin, K. A. Metz, et al. 2019). The published method also incorporates a basic bioinformatic pipeline for variant calling and assessment of the allele fraction. However, this pipeline does not incorporate an alignment and does not allow any paralellization, so we established a new Snakemake pipeline for analysis of the fastq files, as shown in figure 40.

Within this pipeline, the first step is to merge the paired-end sequencing reads and discard reads that could not be merged with the given parameters. After adapter trimming, an alignment is performed using the "mem" variant of the Burrows-Wheeler Alignment Tool (H. Li and Durbin 2009). The resulting bam file was indexed, and variant calling was performed using freebayes (Garrison and Marth 2012). Lastly, the vcf files generated were aggregated into a dataframe by executing an R-script using the vcfR package (Knaus and Grünwald 2017) and transformed using packages from the tidyverse package. We compared the results of our pipeline with the results from the previously published pipeline by Le Guin, K. A. Metz, et al., ctDNA levels were consistent or differed just slightly between the pipelines, especially for the samples containing high levels of ctDNA.

Using deep amplicon sequencing, we analyzed VB samples from nine patients and AH samples from 14 patients. Additionally, we investigated cfDNA from plasma samples of four healthy donors as a control. VB or AH samples from healthy donors or non-cancer patients were not available to us as this would require an invasive surgery which is ethically unacceptable solely for research purposes. We performed targeted sequencing of the region containing the mutation

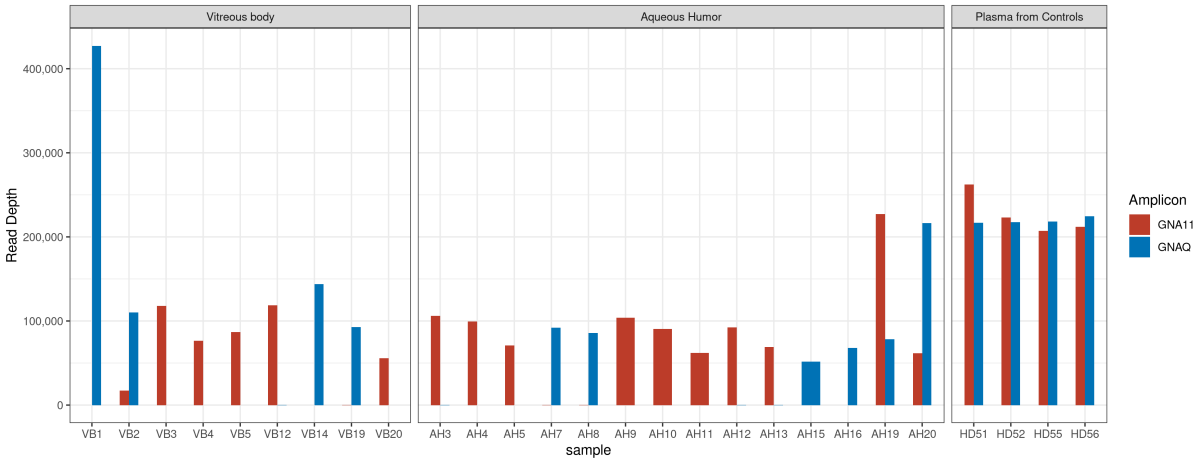

Figure 41: Read depth of deep amplicon sequencing. *GNAQ* and *GNA11* target regions were sequenced in cell-free DNA (cfDNA) obtained from vitreous body and aqueous humor samples from uveal melanoma patients and from healthy donors' plasma. VB: Vitreous Body, AH: Aqueous Humor, HD: Healthy Donor.

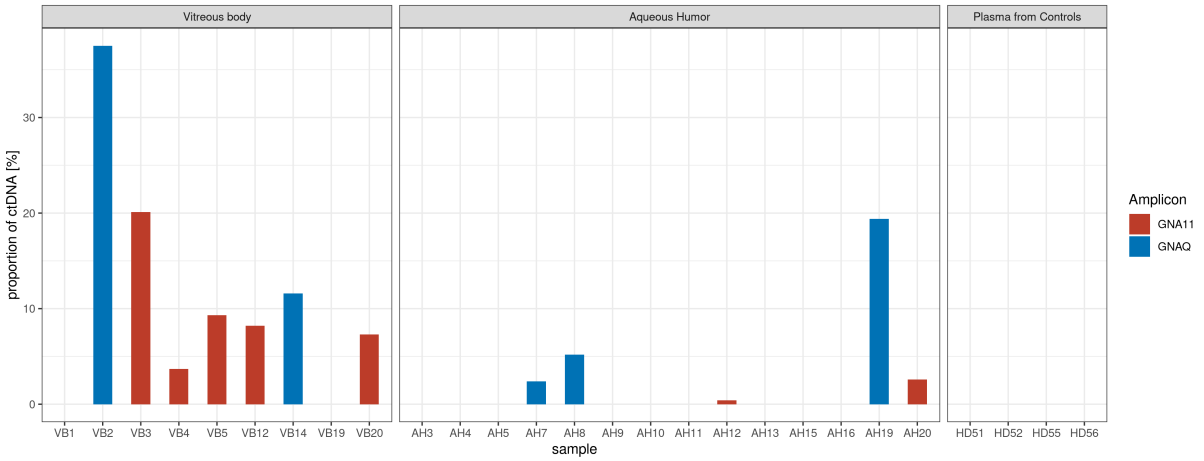

Figure 42: Proportion of ctDNA detected in VB and AH samples. Cell-free DNA (cfDNA) obtained from vitreous body and aqueous humor samples from uveal melanoma (UM) patients and from healthy donors plasma was sequenced targeting regions within *GNAQ* and *GNA11* containing UM-specific mutation sites. The proportion of cell-free tumor-DNA (ctDNA) is equivalent to the percentage of reads containing the expected mutation (based on tumor DNA profiling). VB: Vitreous Body, AH: Aqueous Humor.

that was previously identified in the tumor DNA. As a negative control, we also sequenced the site where no mutation was found in three of our samples (VB2, AH19, and AH20). Figures 41 and 42 show the results of this approach.

Analysis of the results showed that sequencing was successful for all samples with a read depth above 50.000 reads (figure 41). The figure also shows that the read depth differed between the samples. The proportion of ctDNA in each sample varies from 3.7 % to 37.5 % in VB samples and 0.4 % to 19.4 % in AH samples. Neither the control samples from healthy donors nor the non-mutated region in patient-derived cfDNA show any mutant reads. Taken together, this indicates that the assay is specific. However, sensitivity, specificity and, LoD need to be further investigated in a larger cohort for validation of the assay.

We found that ctDNA was detectable in 78 % of the VB samples (seven of nine) and 36 % of the AH samples (five of 14). Consequently, due to the detection rate of 78%, VB seems to be a

more usable source of ctDNA than AH. Furthermore, the level of ctDNA is higher, with a mean value of 14 %.

In summary, with the established method of deep amplicon sequencing and the newly developed Snakemake pipeline, ctDNA could be detected in most of the VB samples and more than one-third of the AH samples. These results qualify AH and VB as suitable sources of tumor-specific biomarkers. So far, only the presence of ctDNA has been analyzed, which can serve as a diagnostic but not as a prognostic biomarker. Thus, we tried to develop an assay based on cfDNA from AH and VB that detects the chromosome 3 status, which can be utilized as a prognostic biomarker for UM.

3.2.2 Detection of monosomy 3 in cfDNA by NGS sequencing

Classification of UM by chromosome 3 status is widely used as a prognostic biomarker for UM. A long-established and very well-validated method to determine the chromosome 3 status in samples of UM tissue is microsatellite analysis. Currently, analysis of chromosome 3 status requires the availability of tumor cells obtained by enucleation or tissue biopsy. Detecting the chromosome 3 status based on AH or VB samples would be less invasive, reduce risks and be available to all patients.

Here we develop a method to detect chromosome 3 dosage alterations in cfDNA. The assay is based on a sequence enrichment strategy targeting a set of SNPs that is deviated from the exon enrichment known from gene panel sequencing(Tewhey et al. 2009; Gnirke et al. 2009). We selected SNPs distributed over the whole chromosome 3. We expect the VAF of those heterozygous SNPs to be 0.5 in the cfDNA of healthy individuals or UM patients who have a tumor with disomy 3. In case of the presence of a tumor DNA with monosomy 3 a VAF unequal to 0.5 is expected for chromosome 3 SNPs. Consequently, we hypothesize that the VAF of informative SNPs on chromosome 3 can be used as an indicator for chromosome 3 status and hence as a prognostic biomarker for UM patients.

To select SNPs that are suitable for our assay, we developed a bioinformatic pipeline using the programming language R. Figure 43 shows the scheme of this process. As a first step, we queried the database of the 1000 genomes project via Ensembl, searching for SNPs that have a minor allele frequency (MAF) in the European population that is as close to 0.5 as possible so that a sufficient number of SNPs remains after filtering.

Next, we divided chromosome 3 into ten regions of 2 MBp and an additional region around *BAP1* in order to achieve an equal distribution of SNPs over the whole chromosome. We wanted

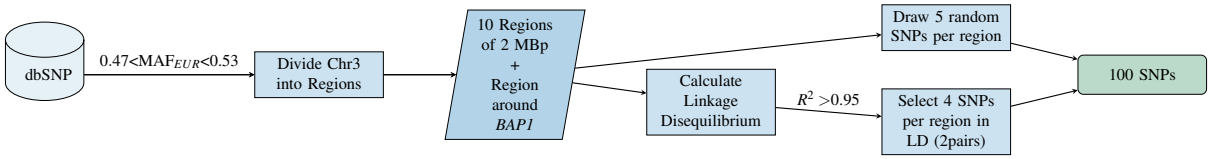

Figure 43: Process of selection of single nucleotide polymorphisms (SNPs).

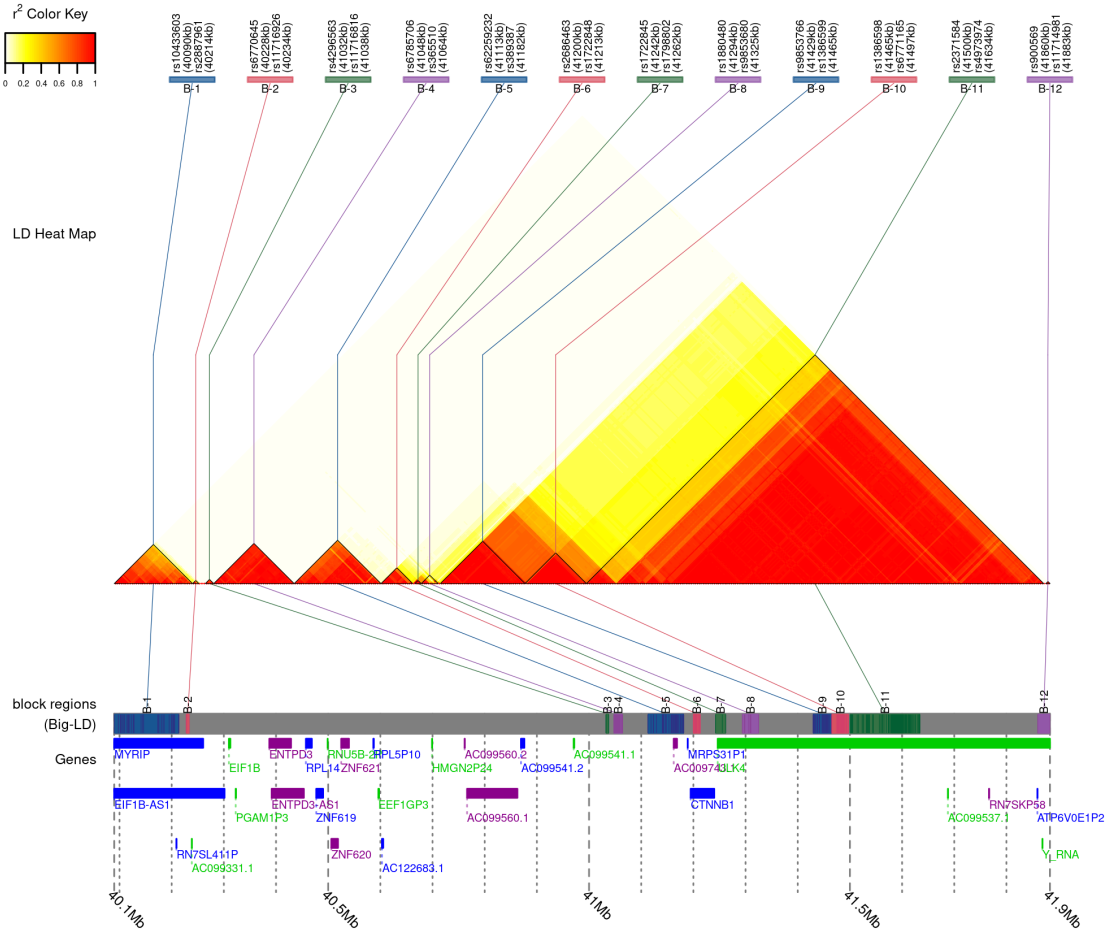

Figure 44: Heatmap of chr3:40-42Mb. Heatmap generated using the LDblockHeatmap function of the gpart package, which is part of the Bioconductor repository. Minor allele frequency of the single nucleotide polymorphisms shown here: 0.49-0.51.

not only to draw random SNPs per region but also to choose SNPs for each region that are in LD (linkage disequilibrium) with each other. Therefore we included several steps in our pipeline to calculate LD and find two pairs of linked SNPs per region.

We calculated the LD per region using the `BigLD` function from the Bioconductor package "gpart" (S. A. Kim and Yoo 2021). The Big-LD algorithm underlying this function was published in S. A. Kim, Brossard, et al. 2019. For visualization of the LD blocks, we generated a heatmap for each region with the `LDblockheatmap` function of the same package. An exemplary heatmap is displayed in figure 44.

In the heatmap, one huge, one medium-sized, and several small LD blocks can be found. However, this pattern differed between the regions, some showed a few huge blocks, and some showed plenty of small blocks. For each region, we selected one pair of SNPs in LD from the biggest LD block and one pair of SNPs from the second biggest block. As the start and stop SNP were directly given from the function, we selected the starting SNP of each of the two blocks. Then we searched for a partner SNP in the same block so that the two partners have the highest possible LD score with each other, but minimally $R^2 > 0.95$. To do so, we used

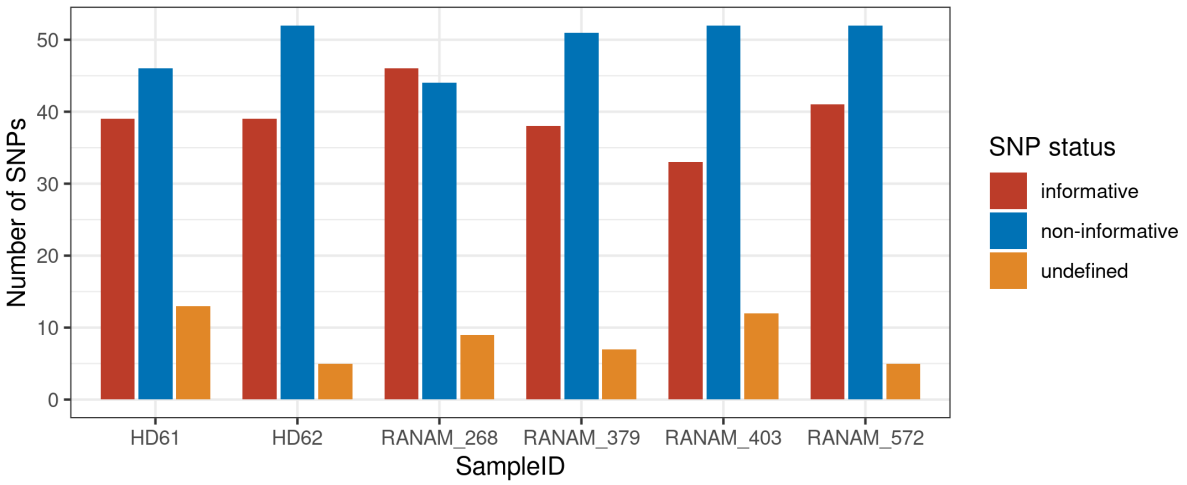

Figure 45: SNP state in plasma cfDNA samples from uveal melanoma (UM) patients as detected by NGS sequencing. Non informative: VAF > 0.9 or VAF <0.1; informative: 0.4 < VAF < 0.6; undefined: VAF could not be assigned to any of the two states. SNP: Single Nulceotide Polymorphism, cfDNA: cell-free DNA, HD: Healthy Donor, RANAM: UM patient who participated in a study named RANAM, VAF: Variant Allele Fraction.

the `LDproxy` function of the "LDlinkR" package, which accesses the LDlink webtool API and queries the LDproxy API (Machiela and Chanock 2015). Of the remaining filtered SNPs, we drew five random SNPs from each region. We ended up with 100 SNPs that are randomly but equally distributed over the whole chromosome 3 with an additional focus on the *BAP1* region.

In order to enrich the DNA fragments flanking these SNPs, we used the SureSelect$^{\text{XT HS}}$ Target Enrichment System (Agilent). This system incorporates a Software called SureDesign that helps to design hybridization probes specific for the regions of interest. This software also rejects positions in the genome that can not be targeted with this system for any reason. When we inserted our set of SNPs in SureDesign, several SNPs were rejected, so we had to repeat the bioinformatical analysis searching for alternative SNPs. We repeated this procedure by trial and error until we found approximately 100 SNPs that were accepted. We ordered the DNA enrichment Kit containing probes flanking 100 bp around each SNP.

As a proof of concept and for establishment, we performed SNP enrichment of six plasma cfDNA samples with a known ctDNA content using the SureSelect$^{\text{XT HS}}$ Target Enrichment System (Agilent) for library preparation. Two samples were derived from healthy donors, and four samples were obtained from UM patients during a previous study. The ctDNA levels in these samples, as detected by deep amplicon sequencing (Le Guin, K. A. Metz, et al. 2019), were 1 % ctDNA or less. After NGS analysis of the SNP enriched samples, we determined the SNP ratio of each locus using the previously described Snakemake pipeline as presented in figure 40. 96-98 of the 99 SNPs were detected in the six samples. For further analysis, we excluded non-informative SNPs and SNPs that were undefined (5-13 %). Approximately 35-45 % of the SNPs were informative, as shown in figure 45.

Next, we had a closer look at the individual VAF measurements per SNP and compared them to the read depth. We expected a VAF of 50 %, but as presented in figure 46 (page 123), we found the VAF to be shifted from 50 % for most SNPs. The allele ratio was mainly shifted towards

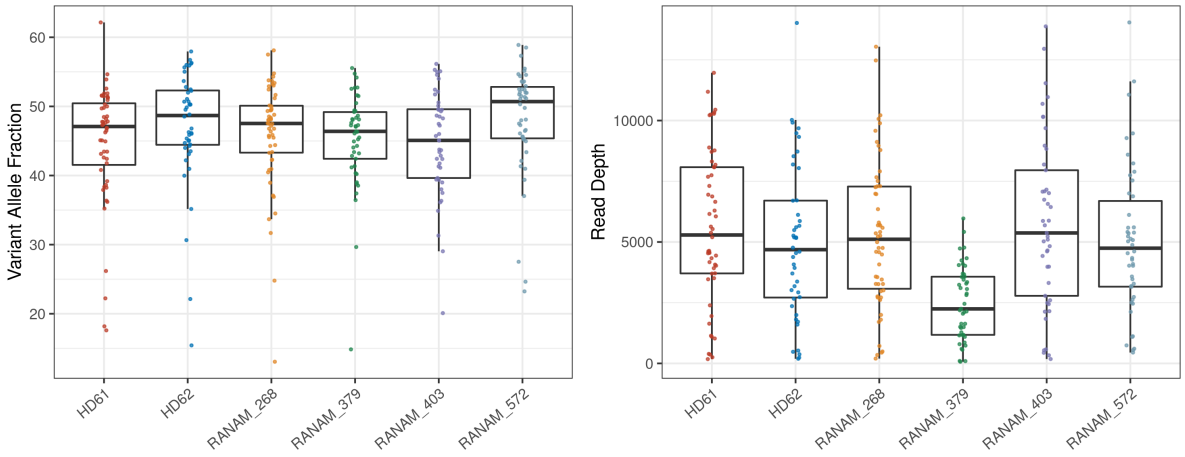

Figure 46: VAF and read repth observed in the analysis of plasma cfDNA samples. Sample IDs starting with HD indicate healthy donors, SampleIDs starting with RANAM indicate uveal melanoma patients. Samples were sequenced by NGS Sequencing using the SureSelect$^{XT\ HS}$ Target Enrichment System (Agilent) with a custom SNP library. Fastq files were analyzed using a Snakemake pipeline for alignment and variant calling. SNP: Single Nulceotide Polymorphism, VAF: Variant Allele Fraction

the reference allele. The scattering of VAF is smallest for sample RANAM 379, this sample showed a very low read depth. The sample RANAM 403 showed a high degree of scattering in VAF measurements and was sequenced with a comparably high but highly variable read depth. This data shows that the deviation of the VAF from the expected value is not correlated with the read depth. No difference could be detected between the healthy donors and the UM patients who are thought to have a proportion of ctDNA of 1 % or less.

To improve the quality of the measurement, we reanalyzed these samples using UMIs that are incorporated in the SureSelect$^{XT\ HS}$ Target Enrichment System (Agilent). Additionally, we applied a filtering step eliminating all measurements that have a UMI corrected Consensus Depth of fewer than 1.000 reads. Results are shown in figure 47, compared to figure 46, the range of the VAFs is much smaller, and many outliers were removed by UMI correction or filtering. In the left part of the figure, also the weighted arithmetic mean is shown as a black dot, this value ranges only between 47 % and 50 % VAF and was calculated as described in chapter 3.1.3.2. As our aim is to detect monosomy 3 and as we expect all informative SNPs to have the same VAF, we can use this value as a biomarker. The mean UMI corrected consensus depth shown in the right plot is much lower than the read depth presented in the previous figure, with its mean over all samples being around 2.000 reads.

Furthermore, we aimed to analyze the baseline of VAF for each SNP in the constitutional DNA of each patient. Thus, we sequenced genomic DNA from the patients RANAM 268 and RANAM 379 using 7 ng, 15 ng and 30 ng DNA (30 ng only for RANAM 268). Data from these experiments is not shown because the coverage was very low.

In summary, we conducted a feasibility study with the goal to examine whether ctDNA can be found in VB and AH of UM patients. We detected ctDNA in both sample types using deep amplicon NGS and a newly developed Snakemake pipeline. The ctDNA content, as well as the

proportion of samples in which it could be detected, was higher in VB than in AH samples, with a ctDNA content of up to 37 %.

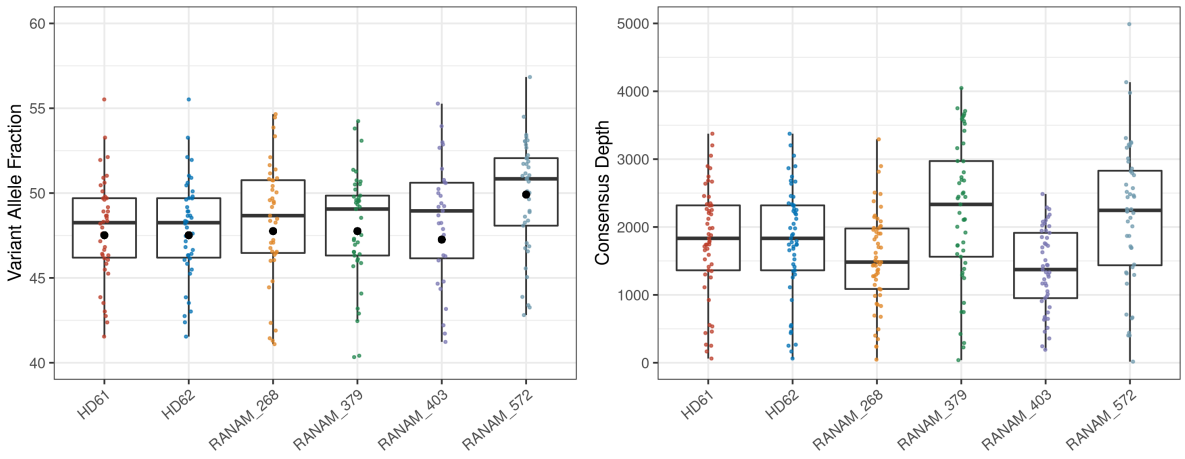

Figure 47: VAF and read depth observed in the analysis of plasma cfDNA samples after UMI correction. Sample IDs starting with HD indicate healthy donors, SampleIDs starting with RANAM indicate uveal melanoma patients. Samples were sequenced by NGS Sequencing using the SureSelect$^{XT\ HS}$ Target Enrichment System (Agilent) with a custom SNP library. Fastq files were analyzed using a Snakemake pipeline for alignment and variant calling. VAF: Variant Allele Fraction.

Furthermore, we aimed to detect UM tumor class which can serve as a prognostic biomarker in cfDNA from AH and VB by analyzing the chromosome 3 allele ratio. The allele ratio could be detected for around 90 % of the SNPs, and a mean read depth of around 5000 reads could be achieved.

4 Discussion

In the following, the results of the two projects presented in this work will be summarized and interpreted. Strengths and limitations, as well as the potential for optimization of the two approaches, will be discussed. In addition, strategies for the optimization of biomarker assays based on liquid biopsies, in general, will be presented. Furthermore, the impact of the use of UMIs and uncertainty-aware variant calling on the number of reliable sequencing reads and measurement accuracy will be analyzed.

4.1 A non-invasive blood test for early detection of SPMs

The aim of this project was to develop a non-invasive blood test for the early detection of SPMs in Rb-survivors. An assay based on genomic DNA was established, validated and the suitability of the analysis of EV-DNA and cfDNA for the intended use was reviewed. We applied our assay to cfDNA from an Rb-cohort included in a European cooperational study. In the following, the results of the establishment and validation of the assay will be reviewed, and its clinical relevance will be discussed. Furthermore, the results obtained by application of this assay will be interpreted and compared to clinical data, especially the likeliness of the presence of a tumor at the time of blood draw will be evaluated. Finally, perspectives and the potential of this assay for future projects will be discussed.

4.1.1 Establishing an assay to detect SPMs in Rb-survivors

We intended to use allelic imbalance caused by loss of heterozygosity as a prognostic biomarker to detect the presence of SPMs. Allelic imbalance we detected by measuring the allele ratios of SNPs located on the RB1 gene in EV-DNA and cfDNA. Analysis was based on data obtained by the SiMSen-seq method for six SNPs. Data were processed via a bioinformatical pipeline for the determination of VAFs.

The criterion for suitability of the biomolecules cfDNA and EV-DNA for our liquid biopsy examination was the number of effective genome equivalents (GEs) needed for the detection of at least 5 % of ctDNA in cfDNA. Despite testing various approaches to increase the number of GEs obtained from EV-DNA, the minimum number of effective GES was not reached, and thus we did not further investigate EV-DNA. Although cfDNA also did not reach this minimum level, with a mean of $1,200$ GEs, cfDNA detection of around 10 % of ctDNA appears to be feasible. As there are no other biomarker screening tests available for SPMs in Rb-survivors, a method that can detect 10 % of ctDNA could still be clinically relevant, and, therefore, we continued with cfDNA analysis.

4.1.2 Validation of the assay was successful on gDNA but not on cfDNA

Next, we validated our assay using reference samples (artificial tumor DNA admixtures). We obtained a median consensus depth of 1,800-2,700 GEs and detected the presence of tumor DNA in admixtures with 1 % tumor DNA. This showed that this method is valid for the detection of tumor DNA at a level of detection of 1%. Furthermore, we tested a multiplex assay approach but found that the singleplex assays showed a superior consensus depth and a lower deviation of the measured VAF from the expected value. Therefore we did not further follow multiplex assay designs.

After validation of the LoD, we applied the method to cfDNA extracts obtained from our cohort to explore if the analytical procedure is suitable for the intended use. Genotyping the patients of the cohort showed that the proportion of informative patients (i.e., those with heterozygous genotype) was lower than expected from the population data available to us. The proportion of homozygous patients was higher than expected in the cohort from Paris. Filter criteria used for SNP selection included a high MAF in the European population, and all sites that contributed patients (Paris, Amsterdam, Essen) are located in western Europe. Because of data protection laws, we cannot determine if the ethnical backgrounds of patients in the cohort from Paris were enriched for non-European origin, which could be a reason for that. Lower than-expected informativity lowered the number of patients our assay was successfully applied to, and this also decreased the number of patients with an active SPM within the study group that may serve as positive controls and thus is valuable for the evaluation of our assay.

Aiming to validate our assay and to answer the question of whether we can detect allelic imbalance, we applied our assay to the cohort described in 3.1.4.1. Therefore the amount of input DNA had to be adapted because the availability of cfDNA from this cohort was very limited. This was on the one hand because sample volumes were kept equal for all patients, including young Rb-children, and on the other hand, due to ethical restrictions in the collaborating countries. Hence plasma volumes ranged from $1-4$ ml, with amounts of samples from Paris and Amsterdam being generally lower.

For rare diseases like SPMs in survivors of retinoblastoma, recruitment of large patient cohorts is very challenging. At the same time, sufficient sample sizes are key for high levels of sensitivity and specificity and statistically meaningful results. Because of this, many researchers had to collaborate to form large transnational groups such as, in our case, the European retinoblastoma group (EURbG). However, transnational collaborational projects face many challenges concerning ethical approvals or agreements for material and data transfer, and these cause restrictions on the availability of material and data.

4.1.3 Statistical analysis showed the presence of false positive signals

We analyzed the VAF of each patient and calculated a weighted arithmetic mean. The samples from the group of healthy donors, which served as negative controls, showed a VAF of

approximately 50%, as expected. But we found the measure of dispersion given by the standard deviation to be approximately 2.5 % VAF for several samples. Consequently, an LoD of 5 % ctDNA could not be reached. Based on the number of expected GEs, we estimated an LoD of 10 % ctDNA, which corresponds to a VAF lower or equal to 45 % and higher or equal to 55 %. As none of the measurements exceeded this range in the healthy control group, an LoD of 10% ctDNA could be reached in this group.

In the group of Rb-patients we expected no positive results either. These patients had retinoblastoma at the time of blood draw and, therefore, probably had some ctDNA in their blood, but it is expected that the proportion is well below 5 % for the majority of patients and below 10% for almost all patients (Jiménez et al. 2021; Francis et al. 2021). In fact, none of the measurements we obtained was above the limit of detection, and thus, we consider the results from this group to be true negatives. From the group of Rb-survivors we also did not expect signals of ctDNA as these patients were without known active tumor at time of blood draw and also did not develop an SPM at least within one year of follow-up. In this group, the proportion of samples with low plasma volumes was higher than in healthy controls due to the difficulties described before. Contrary to our expectation, we found two samples (TSP ARb4 and TSA ARb41) with a VAF higher than 55 %, which are hence false positives.

From the group of SPM patients and especially from the active SPMs, we expected at least some patients to show positive results. The active SPMs were osteosarcoma, rhabdomyosarcoma, or leiomyosarcoma, all typical SPM tumor types, and one spindle-cell carcinoma. All samples were measured with a high consensus depth resulting in a small standard deviation, but all measurements were clearly negative, with VAFs being very close to 50 % VAF. In the groups of previous and future SPMs, three patient samples TSP ARb47, TSP ARb 44, and TSE ARb19, showed VAFs above the LoD. The first two had an SPM in the past, while TSE ARb19 had an SPM after blood draw.

To evaluate and validate our assay, sensitivity and specificity need to be determined. From the groups of healthy controls and Rb-survivors, we can identify the numbers of true negatives and false positives. But the numbers of true positives and false negatives can not be determined due to missing data. Especially for future but also for previous SPM patients, it is not known with absolute certainty if any of the patients had a tumor at time of blood draw. The active SPM-patients had a tumor at the time of blood draw, but it is not confirmed that the tumor entities showed LOH. Furthermore, it is not known if the ctDNA content in these samples was above the LoD of this assay.

This could be overcome by testing the presence of a tumor-specific genetic alteration in the cfDNA from the blood of the patients who were considered false positive or false negative, but tumor material would be needed. An example of such an approach is the strategy we have performed for uveal melanoma within this work. A candidate gene for a search for a specific genetic alteration is the *TP53*, as alterations in this gene are frequent in osteosarcomas which are the most abundant SPM tumors. This additional analysis would allow the precise identification of true positive and true negative results. This, in turn, would permit the evaluation of sensitivity

and specificity and, thereby, validation of the assay. Furthermore, it would allow a more accurate determination of the limit of detection. In spite of that additional data or material was not available from this cohort due to data protection laws and regulations regarding the exchange of patient-specific data between the countries. Consequently, the sensitivity and specificity of this assay could not be determined.

4.1.4 Probability of the presence of tumor at the time of blood draw in SPM patients

Within the group of active SPM patients, no positive signals were detected. The low amounts of cfDNA, which resulted from the restrictions mentioned above, increased the LoD to a level higher than that obtained in the assays on genomic DNA with tumor DNA admixtures. Considering the results from other studies (Butler, Spellman, and Gray 2017; Shulman et al. 2018; Andersson et al. 2020), the proportion of ctDNA present in blood might be below 5 %, this is well below the LoD of 10% we could reach. Therefore, if ctDNA was present in these samples, we likely have missed it below the limit of detection of our assay.

The probability that a tumor was already present at the time of blood draw is influenced by many aspects. The amount of time between the SPM diagnosis and the blood draw has the highest impact. The probability for the presence of tumor DNA in the bloodstream decreases with increasing time distance between blood draw and diagnosis. The patient with the highest likelihood of the presence of a ctDNA signal was **TSE ARb1,** as this patient had a pleomorphic sarcoma of the right orbita only three months after blood draw, but the measurement was negative.

An additional aspect is the probability that a tumor was present but not diagnosed for a given amount of time. This is more likely in the group of adult Rb-survivors than for a child because children undergo periodic routine controls. Adults, on the contrary, often dismiss symptoms or rate them as marginal. Parameters like the size of the tumor at the time of diagnosis or the point in time the patient started to have symptoms could be taken into account to estimate the likelihood of a positive result. However, this data was not acquired within this study and hence is not available to us except for TSE ARb19.

Instead of the group of active SPMs, we found positive signals in the groups of previous and future SPM patients. Patient **TSP ARb44** had a leiomyosarcoma more than four years before the blood draw, and this tumor was successfully treated at that time. Therefore the positive signal found in this patient has to be considered a false positive. **TSP ARb47**, another of the three SPM patients showing VAFs above the threshold, was diagnosed with a high-grade urothelial carcinoma about two years before inclusion into the study. This cancer was resected around one year and six months prior to blood draw. The patient was affected bilaterally, and hence heritable retinoblastoma is plausible (cf. 1.2.1), but no *RB1* mutation was detected in the blood. Therefore it is not certain if the tumor was an SPM on the background of heritable predisposition. If it is not an SPM, the probability that the tumor shows LOH at the RB1 locus and can hence be detected with our assay is lower. Additionally, the measurement quality was

poor, and the standard deviation was high because the low amount of only 1 ml of plasma that was available from this patient resulted in a very low read count. Consequently, after medical validation, this measurement needs to be considered a false positive.

In the other patient **TSE ARb19,** a pleomorphic sarcoma was diagnosed in the main nasal cavity 15 months after the blood draw. This grade three pleomorphic sarcoma was $8.1 \times 4.2 \times 3$ cm in size and had already infiltrated adjacent tissue leading to impaired nasal breathing and vision. Hence, it is to be assumed that the tumor remained undetected for some time. It is still unknown when it started growing, but the clinical parameters increase the probability that this tumor has already been present at the time of blood draw. So the positive result for this patient could be a true positive if the tumor was already present at the time of blood draw.

4.1.5 Future Perspectives

Using allelic imbalance as a biomarker for early detection of SPMs is still a promising concept if certain limitations that we encountered in this pilot stud, are overcome and if the study design is improved. Concerning study design, it would be better not to include Rb-Children in the study because the probability of the presence of an SPM is relatively low. Additionally, the blood volumes available from small children are not suitable for this type of analysis as the amount of cfDNA that can be obtained is not sufficient. With only adults included in the study, blood volumes could be increased to 30 ml. Together with the use of cfDNA preservative tubes (e.g., Cell-Free DNA BCT Tubes (Streck)), this would presumably increase the number of effective GEs and allow the detection of 5 % ctDNA or even less. Key to the success of future studies would also be to include more SPM patients, which is very challenging but highly desirable to have positive controls for the biomarker assay. Collaborations with multiple oncologists or cancer centers might help to reach this goal. Genetic features of SPM tumors are not yet fully understood, but performing WES or WGS of Blood-DNA and tumor DNA of such patients would allow for gaining more insight into the mutational landscape. This analysis might reveal other potential DNA-based biomarkers for SPMs that can be used for the early detection of such tumors described in 1.2.3.2. *TP53* might be a good candidate for a biomarker because it is a main driver gene for the most common SPM entity osteosarcoma, and mutations in *TP53* were found in 75–90 % of osteosarcomas (Wu and Livingston 2020). WGS of osteosarcomas also revealed that somatic copy number alterations are frequent, and hence these might also be used as a biomarker (Negri et al. 2019; Friend et al. 1986; Wu and Livingston 2020; Kovac et al. 2015). However, only if mutations in *TP53* or copy number alterations are also frequent in other SPM tumor types these can be used as a biomarker for early detection of a broader spectrum of SPMs, and this needs to be further investigated. Although a biomarker that can be applied to detect only one SPM type or a subset of SPMs would already be valuable, given that currently, there is no screening available for survivors of heritable retinoblastoma.

4.2 A minimally invasive prognostic test for UM based on cfDNA

We aimed to develop a prognostic test for uveal melanoma based on cfDNA that is as less invasive as possible. Previous studies have shown that ctDNA is not detectable in blood at the time of diagnosis (Le Guin, Bornfeld, et al. 2021). Hence, we decided to investigate aqueous humor and vitreous body aspirate as possible sources of ctDNA. The sampling of both liquid biopsy specimens is associated with significantly fewer side effects and is less invasive than the collection of tumor tissue.

4.2.1 Suitability of AH and VB for analysis of cfDNA-derived biomarkers

We found that cfDNA from AH or VB of UM patients contains ctDNA at the time of diagnosis and can therefore be used for prognostic biomarker testing. Previous studies identified cfDNA from AH or VB as a suitable source for biomarkers as well, but little is known about these specimens in UM patients (Xu et al. 2020; X. Wang et al. 2022; Berry et al. 2017). A Pubmed search using the keywords aqueous humor, uveal melanoma, and cfDNA (date of accession: 29.11.2022) resulted in only one publication.

Im et al. examined if the concentration of ctDNA in AH from UM patients is sufficient for genetic analysis, such as shallow Whole Genome Sequencing (WGS) and analysis of somatic copy number alterations (SCNAs). They proved that SCNAs and mutations can be detected in ctDNA from AH in post-radiation samples of ciliar body UMs (Im et al. 2022). But in contrast to our findings, they did not find ctDNA in any of the pre-radiation samples.

CfDNA from Vitreous body samples has to our knowledge, not yet been investigated in UMs, but it has been shown in other diseases like vitreoretinal lymphoma that mutational analysis of vitreous fluids is feasible (Bonzheim et al. 2022; Velez et al. 2021).

Conclusively, the detection of chromosome 3 status in cfDNA from AH or VB of UM patients is a novel approach. Both body fluids have a high potential to serve as a liquid biopsy for prognostic biomarker testing.

4.2.2 ctDNA was detected in the majority of samples

In VB and AH samples from UM patients, unlike in blood, we found high proportions of ct DNA (up to 37.5 %) at the time of diagnosis. CtDNA was detectable in 78 % of VB samples and in 36 % of AH samples. The proportion of ctDNA was below the limit of detection in nine AH samples and two VB sample.

One reason for the lack of detection of tumor DNA in VB or AH in some patients besides technical reasons could be that tumors release different amounts of DNA. In some cases, the DNA quantity might be below the detection limit of our methods. Whether this is related to the size of the tumor or other clinical parameters would have to be investigated in a study with significantly larger numbers of patients.

An approach to increase the proportion of ctDNA would be to treat the tumor cells before sampling. It is plausible to assume that by treating the tumor, the tumor cells die and release DNA into neighboring fluids. The way in which the tumor cells are treated seems to be irrelevant. However, radiation therapy using ruthenium applicators is currently the most widely used therapy (Reichstein and Brock 2021).

4.2.3 Feasibility study was successful, but the sampling procedures must be changed

The study performed here was a feasibility study containing a low number of samples, and results are subject to further limitations. The samples analyzed are not representative of the majority of tumors, as liquid biopsies for this study were obtained from large tumors subjected to enucleation. These large tumors might shed more DNA into the aqueous humor and vitreous body compared to smaller tumors. On the other hand, it cannot be excluded that these samples contain tumor cells due to the surgical procedure these eyes underwent prior to sample collection. For histopathological evaluation of the tumor, the eyes are cut in two halves after enucleation in the operating room, with the cutting plane passing through the tumor. As this is performed prior to sampling of AH and VB, it cannot be excluded that tumor cells are carried into both compartments.

Our feasibility study showed that ctDNA could be detected in most, but not all patients at time of diagnosis, and proportions of ctDNA were high, especially in VB samples. Hence, characteristics of cfDNA from AH or VB are promising biomarkers for diagnostic and prognostic testing. However, the shortcomings discussed above require new extended studies with optimized study designs to evaluate the suitability of this biomarker examination for routine prognostic testing

4.2.4 Chromosome 3 analysis of cfDNA by deep SNP sequencing assay

Here we developed an assay to detect somatic loss of chromosome 3 (monosomy 3) in cfDNA based on SNP enrichment followed by deep sequencing of enriched fragments and analysis of allelic ratios. We tested it on cfDNA from the plasma of healthy donors and UM patients. In disomy 3 tumors and healthy individuals, we expected the allele ratio over all informative markers to be balanced, while in tumors with monosomy 3 we expected skewed allele ratios. Contrary to our expectation, we found the mean allele ratio over all SNPs to be altered by around 5 % for all but one sample with disomy 3. Because of these alterations, the targeted LoD of 5 % ctDNA could not be reached.

The reasons for these skewed allele ratios are unknown, but possible causes could be identified by performing the deep SNP sequencing assay on cfDNA reference material of known tumor proportion. Additionally, a comparative analysis of the allele ratios of each SNP in cfDNA and the allele ratios detected for the same SNP in matched genomic DNA samples might help to identify the causes for these deviations.

One possible cause might be that the SNPs showing highly deviated allele ratios in healthy control samples have features that are unfavorable for the analysis, e.g., for the enrichment method used here. To identify these features, the SNPs showing highly deviated allele ratios in healthy control samples could be compared to each other as well as to the better-performing SNPs. Features that are common within the group of SNPs showing deviated allele ratios but uncommon in the group of SNPs showing allele ratios close to 50 % are likely to be unfavorable for the analysis.

Examples of such features could be other SNPs affecting the probe binding site, a location within a highly repetitive region in general, or an STR in particular, with the former leading to unspecific binding and the latter causing an unbalanced capture of the alleles. A resulting possible improvement of the assay would be to add filter criteria to the SNP selection process that exclude SNPs with unfavorable features. Also, quality control filter criteria could be added (e.g., mapping quality filter). Additionally, more informative SNPs could be added to the analysis.

A possible pursuing project would be to detect the ctDNA content per sample by sequencing *GNAQ* and *GNA11* and analyze the VAF of each SNP using Varlociraptor using the ctDNA proportion as a prior. Configuration of the scenario using this prior would improve VAF measurements due to the uncertainty aware variant calling of Varlociraptor (cf. 50) and might help to lower the limit of detection of this method (Köster et al. 2020).

4.2.5 Perspective: Possible alternative biomarkers and assays for prognostic testing of UM

Instead of optimizing the SNP-based approach, future studies could also focus on the development of other strategies to detect chromosome 3 status or use other tumor class discriminating features as prognostic biomarkers (cf. 7 on page 41). One feature that can be analyzed based on cfDNA by panel sequencing is the mutation pattern of UM-specific genes. In contrast to chromosome 3 status, it has, to our knowledge, not been used for prognostic testing so far. However, a strong correlation between inactivating somatic BAP1 mutations and poor prognosis was found (Koopmans et al. 2014). A disadvantage of this marker is that it will misclassify about 10-20 % of patients whose class two tumor does not carry a detectable BAP1 mutation. (Decatur et al. 2016; Martin et al. 2013).

Another prognostic marker used in clinical routine is the gene expression pattern (Onken, Worley, Char, et al. 2012). It can not be analyzed using cfDNA but could be investigated using cell-free RNA. To our knowledge, there have been no studies on cell-free RNA from UM patients so far. There is a proprietary test available for prognostic testing of gene expression patterns in uveal melanomas that hampers the use of this marker in research due to increased costs.

For future studies, we would suggest shallow WGS of cfDNA fur the identification of chromosomal losses in ctDNA. In addition to the chromosome 3 status, this technique allows the

investigation of tumor-specific mutations. It could replace the SNP enrichment analysis and be used for prognostic testing of UM based on cfDNA from AH or VB. If low coverage is sufficient, the test would even be suitable for routine diagnostics. The NIPT test is a similar test, as it is also based on WGS of cfDNA and has been widely used for diagnostic purposes (Brady et al. 2016; Alberry et al. 2021; Hartwig et al. 2017).

4.3 Optimization of biomarker assays based on liquid biopsies

There are several aspects that have to be addressed when optimizing future biomarker studies based on cfDNA from liquid biopsies. One parameter is the number of GEs, which is important, especially for statistical counting processes such as the determination of allele ratios. This parameter is key for the precise estimation of VAF and also determines the limit of detection. In both studies presented here, the number of GEs was too low to reach the targeted limit of detection. Hence the amount of cfDNA available for the analysis must be increased.

The cfDNA amount obtained is influenced by one major and two minor factors. The first and most important is the volume of liquid biopsy sample the cfDNA is derived from. Sample volume is often limited due to ethical or technical reasons but nevertheless needs to be sufficient to obtain the numbers of GEs required for the assay at the sensitivity of choice.

In addition, the two minor factors further influence the cfDNA yield: i)choice of the blood collection tube and ii) the tubes used to elute cfDNA in terms of isolation. It is important to use blood collection tubes that contain cfDNA stabilizing reagents, for example, the commercially available Cell-Free DNA BCT tubes (Streck). This ensures cfDNA stability in the samples at ambient temperatures for 14 days and eliminates the need for immediate plasma preparation, which is of great advantage, especially for samples that are obtained alongside routine clinical procedures and or are received from afar. In addition, using DNA LoBind tubes for cfDNA extraction is expected to improve cfDNA recovery by reducing sample-to-surface binding.

Another aspect of optimization is cf DNA quantification. This should be performed by ddPCR or quantitative Real-Time PCR instead of measurements based on fluorescently labeled DNA intercalating dyes. An accurate determination of the number of effective GEs is important for all downstream analytical steps, including bioinformatical analysis.

Another parameter related to the number of GEs is the number of (consensus) reads. We observed the read or consensus depth to be different between healthy donor samples and samples from Rb-survivors. The former show comparably high read depths, while the latter show a rather low read depth. One reason for that might be the time interval between cfDNA isolation and downstream analysis. The healthy donor samples were analyzed within a very short time after cfDNA isolation, while the RB survivor samples were processed months after cfDNA extraction. The cause for this might be related to cfDNA degradation after cfDNA isolation, which can be avoided if the analysis is performed as shortly after cfDNA isolation as possible.

A further aspect that is relevant for SNP sequencing is an improvement of the SNP selection process. Most of the SNPs investigated in this work are located in deep intronic regions. These regions frequently contain repetitive sequences and are often GC-rich, both characteristics that make it difficult to select specific primers or probes, and this may cause problems during sequencing. Applying additional filter criteria to the search criteria for appropriate SNPs might help to reduce this problem.

It is important to note that the establishment and validation of assays used to assess cfDNA biomarkers are essential, in particular, if they are used in clinical routine diagnostics. To validate a biomarker for the intended use, the sensitivity and LoD of the assay can be tested on traceable reference materials (Dong et al. 2018). Within this work, it has been shown that the sensitivity and LoD of an established assay can vary greatly between cfDNA and genomic DNA samples. This issue needs to be specifically addressed when using reference material for validation. These should be as little artificial as possible and mirror the actual analytical process in the best possible way (Dong et al. 2018). Therefore not only genomic DNA but also cfDNA-based reference material has to be used. This requirement is addressed by a growing repertoire of commercially available reference material, which is artificially produced cfDNA of known genetic alterations with specified VAFs. Ideally, it would be cfDNA from patients who has been well characterized using other validated methods. Additionally, the fact that the level of unspecific products was highly increased in cfDNA compared to gDNA when using multiplex approaches showed that also the performance of a given assay might differ between the DNA species.

Another strategy that helps to improve both sensitivity and LoD and allows to precisely estimate the variance is the incorporation of UMIs in the sequencing library. These barcodes help to overcome statistical inflation when counting PCR products, which would lead to an overestimation of sample size and hence to an underestimation of variance, especially when counts are obtained by cfDNA sequencing. Additionally, they enable the elimination of sequencing errors. The impact of UMIs on cfDNA sequencing is discussed in more detail in the next chapter.

4.4 Impact of UMIs and uncertainty-aware variant calling

Determinating SNP allele ratios in cfDNA by deep sequencing was part of both projects presented in this work. As allele ratios are the result of a statistical counting process, the number of used genome equivalents determines the precision of measurement and has an effect on the limit of detection. High sensitivity and specificity are also important for early detection because, at these stages, low ctDNA levels on the background of cfDNA need to be detected. To reach these goals, we incorporated UMIs into our analysis. The location of the UMI within the sequencing read and the analysis method differed between the studies on retinoblastoma (3.1) and uveal melanoma (3.2.2) presented in this work. In the following, the impact of the UMIs in the two approaches will be first characterized and then compared.

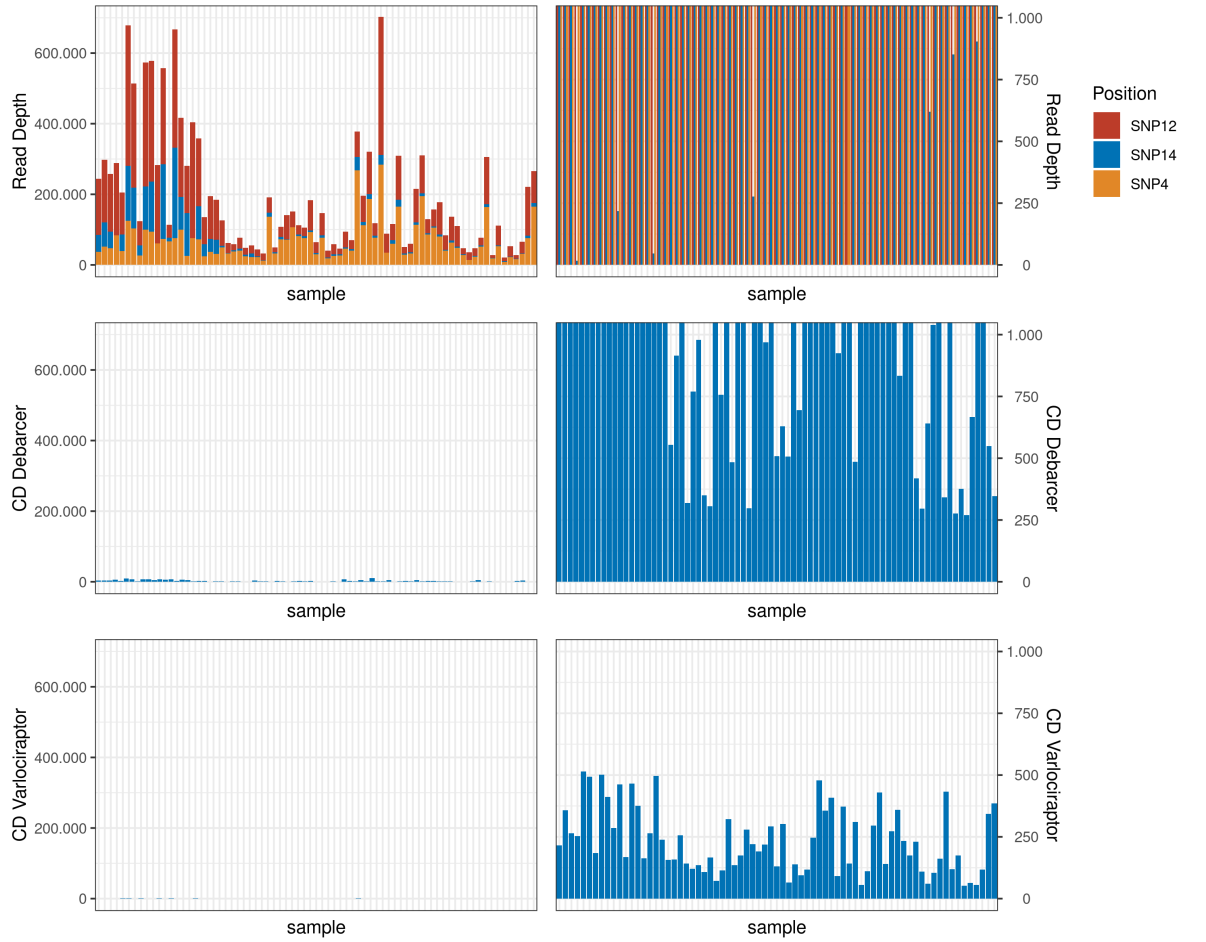

Figure 48: Comparison of read depth and consensus depths calculated with debarcer and varlociraptor. Read depth calculated by freebayes per SNP position in the first row; consensus depth calculated by debarcer in the second row; consensus depth after UMI consensus calling and varlociraptor analysis in the bottom row. Figures to the left: read depth range [0,700,000], figures to the right: read depth range [0,1000]. SNP: Single Nucleotide Polymorphism, UMI: Unique Molecular Identifier, CD: Consensus Depth.

4.4.1 Impact of UMIs as used in 3.1

To detect LOH in the Rb-cohort, we used the SiMSen-seq method that includes barcodes in the forward primer. For analysis of these data, we performed either UMI correction only (debarcer) or UMI correction (consensus calling pipeline) and uncertainty-aware variant calling via varlociraptor. Figure 48 displays a comparison of read depth (upper plots), consensus depth after UMI correction by debarcer (plots in the middle), and UMI grouping via the consensus calling pipeline and uncertainty-aware variant calling via varlociraptor (lower plots). The plots on the right side are magnifications of the plots on the left side, with the y-axis being limited to 1.000 reads. The read depth is shown in the upper row and amounts to an average of 64.233 reads, almost all samples tested show a read depth of more than 1.000 reads.

The consensus depth generated via the debarcer UMI pipeline displayed in the middle part of figure 48 is much lower than the read depth due to the UMI correction, but still more than half of the samples show a consensus depth higher than 1.000 reads, and all samples are covered by at

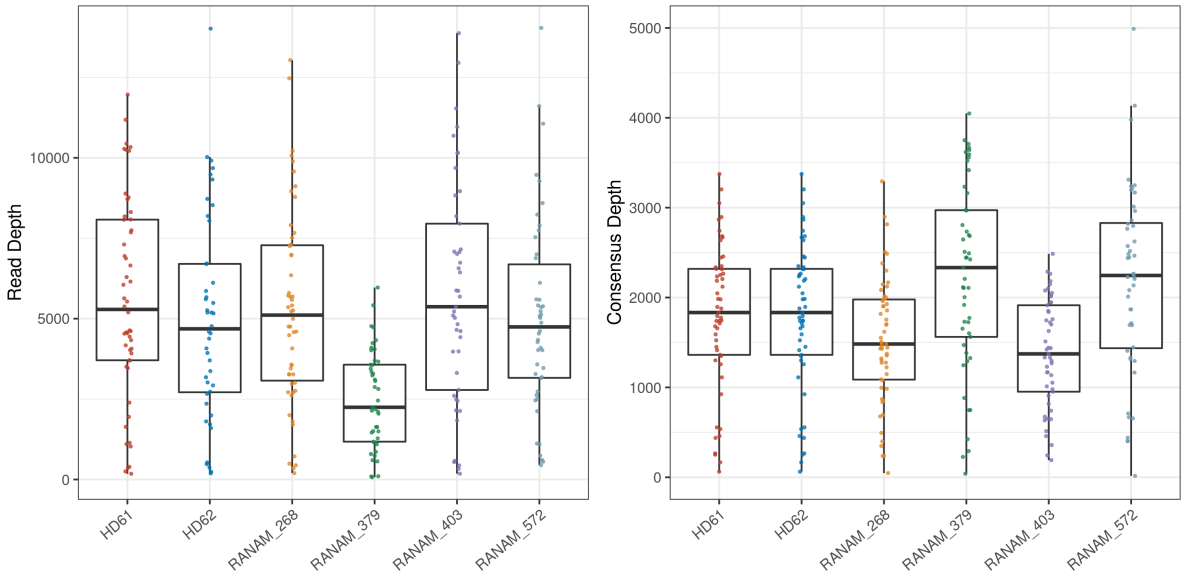

Figure 49: Comparison of read depth and consensus depth after UMI correction. Read depth calculated by freebayes, consensus depth calculated by UMI consensus calling. UMI: Unique Molecular Identifier, RANAM: UM patient who participated in a study named RANAM, HD: Healthy Donor.

least 250 consensus reads. This pipeline overcomes the PCR inflation and removes sequencing errors via UMIs, but does not consider any other biases or uncertainties.

Comparing the raw depth with the consensus depth after analysis with varlociraptor a read reduction of around 800-fold can be observed. For none of the samples, the consensus depth reached 1.000 reads, and the majority of samples have a consensus depth of fewer than 250 reads, with the mean consensus depth being 80 reads. This massive decrease of reads is due to the UMI correction performed via the consensus calling pipeline and the high level of filtering that is appllied by varlociraptor. The latter eliminates all sources of uncertainty as described in Köster et al. (2020). Compared to the debarcer pipeline, the consensus-calling varlociraptor pipeline leads to an additional decrease in read depth of around 10-fold. This emphasizes that besides UMI correction, there is a need for additional filtering and error correction that holds a high potential for a further increase of variant calling accuracy and calculation of VAFs.

4.4.2 Impact of UMIs as used in 3.2.2

For the detection of chromosome 3 status, we used the SureSelect$^{XT\ HS}$ Target Enrichment System, which includes UMIs in the i5 index read, and analyzed the results using the consensus calling pipeline for UMI correction. This approach consisted of UMI correction via the consensus calling pipeline only and was used to determine allelic ratios of SNPs in order to detect monosomy 3. For deep targeted sequencing of *GNAQ* and *GNA11* with the aim to analyze proportions of ctDNA, no UMIs were used. Figure 49 displays the comparison between the read depth determined via the analysis pipeline used for ctDNA determination and the consensus depth after UMI correction using the UMIs introduced by the SureSelect$^{XT\ HS}$ Target Enrichment System (Agilent). The consensus depth is around 2.5-fold smaller than the read depth.

4.4.3 Comparison of the two approaches

When comparing the read and consensus depth after target enrichment and consensus calling with those calculated by the debarcer pipeline after sequencing using the SiMSen-seq method, the read depth is smaller, but the consensus depth is higher. Hence, the impact of UMIs is smaller when using the target enrichment system and the consensus calling pipeline than when performing SiMSen-seq and using the debarcer pipeline for analysis. But what needs to be considered is that the read depth shown in figure 49 in 4.4.2 was calculated using a pipeline that uses already includes some error correction steps like merging of matched forward and reverse reads. The read depth presented in 4.4.2, on the contrary, was calculated using variant calling via freebayes only without any additional attempts for error correction.

Additionally, higher amounts of cfDNA were used for the approach to detect monosomy 3 than for the analysis of SNPs in the *RB1* gene. Furthermore, target enrichment as performed by the SureSelect$^{\text{XT HS}}$ Target Enrichment System (Agilent) is technically distinct from target amplification as performed via SiMSen-seq. Consequently, although the impact of UMIs is comparable only to a limited extent, their impact is significant in both use cases.

One source of errors when using UMIs has to be noted. Sequencing errors occurring within UMIs are very rare but have a fatal impact on the analysis if they occur. If the sequencing error creates a spurious barcode that is not present in any other read then the read with the erroneous barcode is just filtered out. But if the mistake results in a barcode that is already present, then the accompanying read is grouped with the other reads with the same barcode and hence affects the consensus sequence generated for this read group. Especially for rare variant detection, this might have an impact on the overall result and needs to be covered by the analysis pipeline that performs the UMI correction (Smith, Heger, and Sudbery 2017; Alborelli et al. 2019).

5 Abstract

Biomarkers are of great interest in applied medical research, specifically in oncology. Here, applications of biomarker analysis include the detection of primary disease processes as well as metastasis and tumor recurrence, prediction of therapy response, and prognosis of disease outcome. Most often, the analytical target of biomarker analysis in oncology is DNA. From the technical point of view, an essential advantage of this biomolecule is the availability of analytical methods for the detection of characteristics of DNA, such as sequence variation, methylation, and abundance, even if only a few molecules of the DNA of interest are present.

From the biological point of view, it is advantageous that these DNA characteristics are often tightly linked to the disease process or its root cause. Moreover, as DNA is present in many body liquids, this biomolecule may be available for analysis by taking samples of these fluids (liquid biopsies). Establishing a DNA-based biomarker analysis for some intended use is a multistep process that starts with identifying the specific DNA-characteristic that can serve as a biomarker. It ends with validating the complete examination procedure, i.e., confirming that it is apt for the intended use. The work presented here aimed to develop biomarker analyses for two applications, namely i) a diagnostic biomarker test for detecting second neoplasms in patients with heritable retinoblastoma and ii) a prognostic test for uveal melanoma.

A diagnostic biomarker test for detecting second neoplasms in patients with heritable retinoblastoma

Heritable retinoblastoma (Rb) is an autosomal-dominant tumor predisposition syndrome caused by pathogenic variants of the *RB1* gene. Rb-survivors have a high risk to develop a second primary malignancy (SPM). Development of retinoblastoma is often initiated by genetic mechanisms that result in loss of heterozygosity (LOH). It is to be expected that LOH is frequent in SPMs as well. We examined if LOH can be used as a biomarker for non-invasive early detection of SPMs in Rb-survivors.

We analyzed DNA derived from extracellular vesicles (EV-DNA) and cell-free DNA (cfDNA) extracted from blood plasma. DNA released by tumor cells with LOH at the *RB1* locus is expected to skew the ratio of *RB1* alleles in EV-DNA and cfDNA. We determined the allelic ratio of multiple Single Nucleotide Polymorphisms (SNPs) by Next-Generation Sequencing of cf-DNA. The assay was established for six SNPs located in the *RB1* gene on the same linkage group.

We evaluated the suitability of EV-DNA and cfDNA for our liquid biopsy examination, with the criterion for suitability being the number of effective genome equivalents (GEs) needed for the detection of at least 5 % of ctDNA. The number of GEs in EV-DNA was insufficient, but cfDNA was suitable to detect around 10 % ctDNA, which may still be clinically relevant as there are no other biomarker screening tests available for SPMs in Rb-survivors. For test validation, we

generated reference samples with tumor DNA admixtures. Tumor fractions of as little as 1% were detectable.

We applied our method to cfDNA from an Rb-cohort to review if the analytical procedure is suitable for the intended use. Contrary to our expectation, the assay was applicable to only one-third of patients because the proportion of patients being constitutionally heterozygous for the selected SNPs was lower in the cohorts from the cooperating countries. Due to the number of GEs measured in cfDNA, we expected a limit of detection (LoD) of 10 % ctDNA . The weighted arithmetic mean variant allele fraction (VAF) of two Rb-survivors and three SPM patients was above this threshold. However, these results need to be considered false positives as none of these patients had an SPM at the time of blood draw or in an appropriate period of time around the blood collection. Four patient samples collected at the time of diagnosis of SPM showed a VAF below the LoD and might be false negative.

Conclusively, we established a highly sensitive assay that allows the detection of 1 % tumor DNA in genomic DNA, but it was not applicable to the cfDNA samples collected within the European NIRBTEST study because of low DNA levels due to low sample volumes. However, this could not be adjusted during the project duration due to international standardization of sample collection and local ethical restrictions. As a next step, the suitability of the assay for the intended use should be evaluated using cfDNA reference material or patient blood samples of higher volumes.

A prognostic test for uveal melanoma

Uveal Melanoma (UM) is a rare cancer but still the most common primary intraocular tumor in adults. Most UMs fall in one of two classes that show distinct genetic features and are highly correlated with prognosis. Monosomy 3, a distinctive feature of UM class two, is strongly associated with a poor prognosis. Currently, testing this biomarker in smaller tumors requires a tissue biopsy. The sampling procedure of tumor tissue is invasive and may cause side effects like bleeding, retinal detachment, or tumor cell seeding. Therefore, less invasive methods to obtain tumor-derived DNA (ctDNA) are desirable. The source of ctDNA that can be obtained least invasively is blood, but it has been shown that at diagnosis of UM the proportion of ctDNA in cfDNA from blood is mostly too low for reliable biomarker analysis (Le Guin et al. 2021).

We performed a feasibility study to test if cfDNA from aqueous humor or vitreous body aspirate contains sufficient amounts of ctDNA for genetic analyses. cfDNA was isolated from both specimens, which were obtained from eyes after enucleation. The amount of tumor-derived DNA was determined by deep amplicon sequencing targeting oncogenic variants in *GNAQ* and *GNA11*, which are both highly specific for UM. For analysis of sequencing data, we developed a Snakemake pipeline that includes `bwa-mem` (alignment) and `freebayes` (variant calling) to determine the fraction of alleles specific for tumor variants. In seven of nine vitreous body samples and five of 14 samples from aqueous humor *GNAQ* or *GNA11* variants were detected with VAFs ranging from 3.7 % to 37.5 %.

To determine chromosome 3 dosage alterations in cfDNA, we developed an assay which is based on sequence enrichment of around 100 SNPs distributed over the whole chromosome 3. A balanced allelic ratio of informative SNPs is expected in cfDNA of healthy individuals or UM tumors with disomy 3, while an unbalanced allele ratio was expected for monosomy 3 tumors. We evaluated if this characteristic can serve as an indicator for chromosome 3 loss and, hence, as a prognostic biomarker for UM patients.

Testing the assay on cfDNA from plasma of healthy donors and UM patients, we found the VAF to be highly scattered around the expected VAF of 0.5. The LoD of the assay was highly above the targeted LoD of 5 % ctDNA and therefore needs to be optimized before the assay can be applied to cfDNA from AH and VB.

Taken together, cfDNA derived from AH or VB is a very promising analytical target for diagnostic and prognostic biomarker analysis as it contains high levels of ctDNA at the time of diagnosis. Future studies on cfDNA from AH and VB from small tumors collected from non-enucleated eyes will show if these liquid biopsies can be used to detect the chromosome 3 status as a prognostic biomarker.

6 Zusammenfassung

Biomarker sind in der angewandten medizinischen Forschung, insbesondere in der Onkologie, von großem Interesse. Zu den Anwendungsbereichen gehören die Erkennung von primären Krankheitsprozessen, Metastasen oder Tumorrezidiven, die Vorhersage des Therapieerfolgs, sowie die Prognose des Krankheitsverlaufs. In der Onkologie wird meist DNA für die Analyse von Biomarkern verwendet. Aus technischer Sicht hat die Verwendung von DNA den Vorteil, dass eine Vielzahl von Analysemethoden zur Verfügung stehen. Diese ermöglichen den Nachweis von diversen Eigenschaften der DNA wie Sequenzvariationen, Methylierung oder Häufigkeit, selbst wenn nur wenige Moleküle der zu analysierenden DNA vorhanden sind.

Aus biologischer Sicht ist es von Vorteil, dass diese DNA-Merkmale oft eng mit dem Krankheitsprozess oder seiner Ursache verbunden sind. Da viele Körperflüssigkeiten DNA enthalten, genügt die Entnahme von Proben dieser Flüssigkeiten (Flüssigbiopsie), um sie analysieren zu können. Die Etablierung einer DNA-basierten Biomarker-Analyse für einen vorgesehenen Verwendungszweck ist ein mehrstufiger Prozess, der mit der Identifizierung eines spezifischen DNA-Merkmals, welches als Biomarker dienen kann, beginnt. Der Prozess endet mit der Validierung des gesamten Untersuchungsverfahrens, also mit der Feststellung, dass das gewählte Merkmal für den vorgesehenen Verwendungszweck geeignet ist. Das Ziel dieser Arbeit war es, Biomarker-basierte Analysemethoden für zwei verschiedene Anwendungszwecke zu entwickeln. Diese waren zum einen ein diagnostischer Biomarker-Test zum Nachweis von Zweitneoplasien bei Patienten mit erblichem Retinoblastom und zum anderen ein prognostischer Test für Aderhautmelanome.

Ein diagnostischer Biomarker-Test zum Nachweis von sekundären Neoplasien bei Patienten mit erblichem Retinoblastom

Das erbliche Retinoblastom (Rb) ist ein autosomal-dominant vererbtes Tumorprädispositionssyndrom, das durch pathogene Varianten des *RB1*-Gens verursacht wird. Rb-Überlebende haben ein hohes Risiko, einen Zweittumor zu entwickeln. Die Entstehung eines Retinoblastoms wird meistens durch genetische Mechanismen initiiert, die zu einem Verlust der Heterozygotie (*loss of heterozygosity*, LOH) führen. Es ist zu erwarten, dass auch SPMs häufig durch LOH entstehen. Ziel dieser Arbeit war es zu untersuchen, ob LOH als Biomarker für die nichtinvasive Früherkennung von Zweittumoren bei Rb-Überlebenden verwendet werden kann.

DNA aus extrazellulären Vesikeln (EV-DNA) und zellfreie DNA (*cell-free DNA*, cfDNA) aus Blutplasmaproben. Es ist anzunehmen, dass das Verhältnis der *RB1*-Allele in EV-DNA und cfDNA durch von Tumorzellen mit LOH am *RB1*-Lokus freigesetzte DNA verändert wird. Das Allelverhältnis mehrerer Einzelnukleotid-Polymorphismen (*Single Nucleotide Polymorphisms*, SNPs) wurde durch *Next-Generation-Sequencing* (NGS) von cf-DNA bestimmt. Die Methode wurde für sechs SNPs im *RB1*-Gen auf derselben Kopplungsgruppe etabliert.

Die Eignung von EV-DNA und cfDNA für die Flüssigbiopsieuntersuchung wurde bewertet, wobei das Kriterium für die Eignung die Anzahl der effektiven Genomäquivalente war, die für den Nachweis von mindestens 5 % zirkulierender Tumor-DNA (*circulating tumor DNA*, ctDNA) erforderlich sind. Die Anzahl der Genomäquivalente in EV-DNA war für die vorgesehene Analyse nicht ausreichend, cfDNA war jeodch geeignet, um ctDNA Anteile von etwa 10 % nachzuweisen. Da noch kein Test zur Früherkennung von Zweittumoren bei Rb-Überlebenden entwickelt wurde, könnte auch ein solcher Test klinisch relevant sein. Zur Validierung der Methode wurden Referenzproben mit bekannten Anteilen an Tumor-DNA hergestellt, Tumoranteile von nur 1 % waren nachweisbar.

Die Methode wurde auf aus Blutproben unserer Patientenkohorte stammende cfDNA angewendet, um zu überprüfen, ob das Analyseverfahren für den vorgesehenen Verwendungszweck geeignet ist. Entgegen unserer Erwartungen war die Methode nur auf ein Drittel der Patienten anwendbar, denn in den Kohorten aus den kooperierenden Ländern war der Anteil an für Patienten, die konstitutionell heterozygot für die gewählten SNPs waren, geringer. Aufgrund der Anzahl der in cfDNA gemessenen Genomäquivalente wurde eine Bestimmungsgrenze von 10 % ctDNA erwartet. Das gewichtete arithmetische Mittel der Allelfrequenz lag bei zwei Rb-Überlebenden und drei Patienten mit Zweittumor über dem Schwellenwert. Diese Ergebnisse sind als falsch positiv zu bewerten, da keiner dieser Patienten zum Zeitpunkt der Blutentnahme, oder in einem relevanten Zeitraum einen Zweittumor entwickelt hat. Auch die in den Proben von Patienten mit Zweittumor detektierten Ergebnisse sind als falsch-positiv zu betrachten, da die betreffenden Patienten zwei Jahre vor bzw. 15 Monate nach der Blutentnahme einen Zweittumor aufwiesen. In den vier Proben von Patienten, die zum Zeitpunkt der Blutentnahme einen Zweittumor hatten, wurde keine Abweichung des Allelverhältnisses oberhalb der Bestimmungsgrenze detektiert, diese Ergebnisse könnten falsch negativ sein.

Im Rahmen dieser Arbeit wurde eine hochsensible Methode entwickelt, die den Nachweis von 1 % Tumor-DNA in genomischer DNA ermöglicht. Diese war jedoch auf die im Rahmen der europäischen NIRBTEST-Studie entnommenen cfDNA-Proben nicht anwendbar, da die DNA Mengen aufgrund des geringen Blutvolumens zu klein waren. Wegen der internationalen Standardisierung der Probenentnahme und aufgrund lokaler Ethik-Richtlinien konnte dies im Rahmen dieses Projektes nicht verändert werden. In einem nächsten Schritt sollte die Eignung der Methode für den vorgesehenen Verwendungszweck anhand von cfDNA-Referenzmaterial oder Patientenblutproben mit größerem Volumen weiter evaluiert werden.

Ein prognosticher Test für Patienten mit Aderhautmelanom

Das Aderhautmelanom (AM) ist eine seltene Tumorerkrankung, jedoch der häufigste primäre intraokulare Tumor bei Erwachsenen. Die meisten AM lassen sich einer von zwei Tumorklassen zuordnen. Beide Klassen unterscheiden sich bezüglich ihrer genetische Merkmale und sind in hohem Maße mit der Prognose der Patienten korreliert. Monosomie 3 ist ein charakteristisches Merkmal der zweiten Tumorklasse, die mit einer schlechten Prognose assoziiert ist. Die Bestim-

mung der Prognose erfordert die Untersuchung des Tumorgewebes, an dem die prognostischen Marker erhoben werden können. Bei kleineren Tumoren, die nicht enukleiert werden, ist hierfür eine Gewebebiopsie erforderlich. Das Verfahren zur Entnahme einer Biopsie ist invasiv und kann Nebenwirkungen wie Blutungen, Netzhautablösung oder Tumorzellaussaat verursachen. Daher sind weniger invasive Methoden zur Gewinnung von Tumor-DNA wünschenswert. Die Entnahme von Blut als Quelle für zirkulierende Tumor-DNA ist am wenigsten invasiv, aber es hat sich gezeigt, dass zum Zeitpunkt der Diagnose von Aderhautmelanomen der Anteil der ctDNA an der cfDNA aus Blut meist zu gering für eine zuverlässige Biomarkeranalyse ist (Le Guin et al. 2021).

Im Rahmen der vorliegenden Arbeit wurde eine Machbarkeitsstudie durchgeführt, um zu testen, ob cfDNA aus Vorderkammerwasser oder Glaskörperaspirat ausreichende Mengen an ctDNA für genetische Analysen enthält. cfDNA wurde aus diesen Aspiraten, die aus enukleierten Augen gewonnen wurden, isoliert. Die Menge der ctDNA wurde durch *Deep-Amplicon-Sequencing* von Aderhautmelanom-spezifischen onkogenen Varianten in den Genen *GNAQ* und *GNA11* bestimmt. Um den Anteil der vom Tumor stammenden Allele anhand der spezifischen Varianten zu bestimmen, wurde eine Snakemake-Pipeline entwickelt, die ein Alignment mittels `bwa-mem`, sowie *variant calling* mittels `freebayes` umfasst. In sieben von neun Glaskörperaspiratproben und fünf von 14 Proben aus dem Kammerwasser wurden *GNAQ*- oder *GNA11*-Varianten gefunden, die auf das Vorhandensein von ctDNA hinweisen. Die Anteile der varianten Allele lagen zwischen 3,7 % und 37,5 %.

Darüber hinaus wurde eine Methode zum Nachweis von Chromosom-3-Dosierungsveränderungen in cfDNA entwickelt. Die Methode basiert auf der Anreicherung und Sequenzierung einer Reihe von SNPs , die über das gesamte Chromosom 3 verteilt sind. Die *deep amplicon* Sequenzierung dient der Quantifizierung der Allelverhältnisse. In cfDNA von gesunden Personen oder Aderhautmelanomen mit Disomie 3 ist ein ausgeglichenes Allelverhältnis informativer SNPs zu erwarten, wohingegen bei Tumoren mit Monosomie 3 ein unausgeglichenes Allelverhältnis zu erwarten ist. Es wurde untersucht, ob dies als Indikator (oder Biomarker) für den Chromosom-3-Verlust und damit als prognostischer Biomarker für Aderhautmelanompatienten dienen kann.

Die Methode wurde mit cfDNA aus dem Plasma von gesunden Spendern und UM-Patienten getestet. Es zeigte sich eine starke Streuung der gemessenen Allelverhältnisse um den Erwartungswert von 0,5. Die Bestimmungsgrenze der Methode lag weit über dem angestrebten Wert von 5 % ctDNA und muss daher optimiert werden, damit die Methode auf cfDNA aus Kammerwasser und Glaskörperaspirat anwendbar ist.

Insgesamt ist cfDNA aus Kammerwasser oder Glaskörperaspirat eine sehr vielversprechende Matrix für Biomarker-basierte diagnostische und prognostische Tests, da sie zum Zeitpunkt der Diagnose hohe Mengen an ctDNA enthält. Künftige Studien zu cfDNA aus Kammerwasser und Glaskörperaspirat von kleinen Tumoren, die aus nicht enukleierten Augen entnommen wurde, werden zeigen, ob diese Flüssigbiopsien tatsächlich zum Nachweis des Chromosom-3-Status als prognostischer Biomarker verwendet werden können.

7 Bibliography

Abramson, D. H. et al. (1984). "Second Nonocular Tumors in Retinoblastoma Survivors: Are They Radiation-induced?" In: *Ophthalmology* 91.11, pp. 1351–1355. ISSN: 0161-6420. URL: https://www.sciencedirect.com/science/article/pii/S0161642084341276.

Açikbas, I. et al. (2002). "Detection of LOH of the RB1 Gene in Bladder Cancers by PCR-RFLP". In: *Urol Int* 68.3, pp. 189–192. DOI: 10.1159/000048448.

Akbar, N. et al. (Dec. 2019). "Extracellular vesicles in metabolic disease." In: *Diabetologia* 62 (12), pp. 2179–2187. DOI: 10.1007/s00125-019-05014-5.

Akgul, H. et al. (2011). "Intraocular biopsy using special forceps: a new instrument and refined surgical technique". In: *Br J Ophthalmol* 95.1, p. 79. DOI: 10.1136/bjo.2008.148395.

Alberry, M. S. et al. (Mar. 2021). "Non invasive prenatal testing (NIPT) for common aneuploidies and beyond." In: *European journal of obstetrics, gynecology, and reproductive biology* 258, pp. 424–429. DOI: 10.1016/j.ejogrb.2021.01.008.

Alborelli, I. et al. (2019). "Cell-free DNA analysis in healthy individuals by next-generation sequencing: a proof of concept and technical validation study". In: *Cell death & disease* 10.7, p. 534. DOI: 10.1038/s41419-019-1770-3.

Alix-Panabières, C. and K. Pantel (2021). "Liquid Biopsy: From Discovery to Clinical Application". In: *Cancer Discov* 11.4, pp. 858–873. DOI: 10.1158/2159-8290.CD-20-1311.

Allawi, H. T. and J. J. SantaLucia (Aug. 1997). "Thermodynamics and NMR of internal G.T mismatches in DNA." In: *Biochemistry* 36 (34), pp. 10581–94. DOI: 10.1021/bi962590c.

Andersson, D. et al. (2020). "Circulating cell-free tumor DNA analysis in pediatric cancers". In: *Molecular Aspects of Medicine* 72. Liquid biopsy analysis in cancer diagnostics, p. 100819. DOI: 10.1016/j.mam.2019.09.003.

Aronow, M. E., A. K. Topham, and A. D. Singh (2018). "Uveal Melanoma: 5-Year Update on Incidence, Treatment, and Survival (SEER 1973-2013)." In: *Ocular oncology and pathology* 4 (3), pp. 145–151. DOI: 10.1159/000480640.

Augsburger, J. J., Z. M. Corrêa, and N. Trichopoulos (Mar. 2013). "Prognostic implications of cytopathologic classification of melanocytic uveal tumors evaluated by fine-needle aspiration biopsy." In: *Arquivos brasileiros de oftalmologia* 76 (2), pp. 72–9. DOI: 10.1590/s0004-27492013000200004.

Bakhoum, S. F. et al. (Jan. 2018). "Chromosomal instability drives metastasis through a cytosolic DNA response." In: *Nature* 553 (7689), pp. 467–472. DOI: 10.1038/nature25432.

Balaj, L. et al. (Feb. 2011). "Tumour microvesicles contain retrotransposon elements and amplified oncogene sequences." In: *Nature communications* 2, p. 180. DOI: 10.1038/ncomms1180.

Barbany, G. et al. (2019). "Cell-free tumour DNA testing for early detection of cancer - a potential future tool". In: *J Intern Med* 286.2, pp. 118–136. DOI: 10.1111/joim.12897.

Bauer, J. et al. (Sept. 2009). "Oncogenic GNAQ mutations are not correlated with disease-free survival in uveal melanoma." In: *British journal of cancer* 101 (5), pp. 813–5. DOI: 10.1038/sj.bjc.6605226.

Becker, A. et al. (2016). “Extracellular Vesicles in Cancer: Cell-to-Cell Mediators of Metastasis”. In: *Cancer cell* 30.6, pp. 836–848. DOI: 10.1016/j.ccell.2016.10.009.

Benedict, W. F., Y.-k. T. Fung, and A. L. Murphree (1988). “The gene responsible for the development of retinoblastoma and osteosarcoma”. In: *Cancer* 62.S1, pp. 1691–1694. DOI: 10.1002/1097-0142(19881015)62:1+<1691::aid-cncr2820621306>3.0.co;2-5.

Berman, S. D. et al. (Aug. 2008). “Metastatic osteosarcoma induced by inactivation of Rb and p53 in the osteoblast lineage.” eng. In: *Proceedings of the National Academy of Sciences of the United States of America* 105 (33), pp. 11851–6. DOI: 10.1073/pnas.0805462105.

Berry, J. L. et al. (2017). “Potential of Aqueous Humor as a Surrogate Tumor Biopsy for Retinoblastoma”. In: *JAMA Ophthalmol* 135.11, pp. 1221–1230. ISSN: 2168-6165. URL: https://doi.org/10.1001/jamaophthalmol.2017.4097.

Bettegowda, C. et al. (2014). “Detection of Circulating Tumor DNA in Early- and Late-Stage Human Malignancies”. In: *Science Translational Medicine* 6.224, 224ra24–224ra24. DOI: 10.1126/scitranslmed.3007094.

Blomquist, T. et al. (2015). “Control for stochastic sampling variation and qualitative sequencing error in next generation sequencing”. In: *Special Issue: Advanced Molecular Diagnostics for Biomarker Discovery - Part I* 5, pp. 30–37. DOI: 10.1016/j.bdq.2015.08.003.

Bonzheim, I. et al. (2022). “The molecular hallmarks of primary and secondary vitreoretinal lymphoma”. In: *Blood Adv* 6.5, pp. 1598–1607. ISSN: 2473-9529. DOI: 10.1182/bloodadvances.2021004212.

Bornfeld, N. et al. (Feb. 2018). “The Interdisciplinary Diagnosis and Treatment of Intraocular Tumors.” In: *Deutsches ärzteblatt international* 115 (7), pp. 106–111. DOI: 10.3238/arztebl.2018.0106.

Bortner, C. D., N. B. Oldenburg, and J. A. Cidlowski (1995). “The role of DNA fragmentation in apoptosis”. In: *Trends in Cell Biology* 5.1, pp. 21–26. DOI: 10.1016/s0962-8924(00)88932-1.

Brady, P. et al. (2016). “Clinical implementation of NIPT - technical and biological challenges”. In: *Clin Genet* 89.5, pp. 523–530. DOI: 10.1111/cge.12598.

Bronkhorst, A. J. et al. (2021). “Towards systematic nomenclature for cell-free DNA.” In: *Human genetics* 140 (4), pp. 565–578. DOI: 10.1007/s00439-020-02227-2.

Burke, J. R., A. J. Deshong, et al. (2010). “Phosphorylation-induced Conformational Changes in the Retinoblastoma Protein Inhibit E2F Transactivation Domain Binding”. In: *Journal of Biological Chemistry* 285.21, pp. 16286–16293. DOI: 10.1074/jbc.m110.108167.

Burke, J. R., G. L. Hura, and S. M. Rubin (June 2012). “Structures of inactive retinoblastoma protein reveal multiple mechanisms for cell cycle control.” In: *Genes & development* 26 (11), pp. 1156–66. DOI: 10.1101/gad.189837.112.

Butler, T. M., P. T. Spellman, and J. Gray (2017). “Circulating-tumor DNA as an early detection and diagnostic tool”. In: *Current Opinion in Genetics & Development* 42. Cancer genomics, pp. 14–21. DOI: 10.1016/j.gde.2016.12.003.

Cabel, L. et al. (Aug. 2017). "Circulating tumor DNA changes for early monitoring of anti-PD1 immunotherapy: a proof-of-concept study." In: *Annals of oncology : official journal of the European Society for Medical Oncology* 28 (8), pp. 1996–2001. DOI: 10.1093/annonc/mdx212.

Caby, M.-P. et al. (May 2005). "Exosomal-like vesicles are present in human blood plasma". In: *International Immunology* 17.7, pp. 879–887. DOI: 10.1093/intimm/dxh267.

Cai, J. et al. (2016). "Functional transferred DNA within extracellular vesicles". In: *Experimental Cell Research* 349.1, pp. 179–183. DOI: 10.1016/j.yexcr.2016.10.012.

Califf, R. M. (2018). "Biomarker definitions and their applications". In: *Experimental Biology and Medicine* 243.3. PMID: 29405771, pp. 213–221. DOI: 10.1177/1535370217750088.

Carlson, E. A. and R. J. Desnick (1979). "Mutational mosaicism and genetic counseling in retinoblastoma". In: *Am. J. Med. Genet.* 4.4, pp. 365–381. DOI: 10.1002/ajmg.1320040408.

Caruso, S. and I. K. H. Poon (2018). "Apoptotic Cell-Derived Extracellular Vesicles: More Than Just Debris." eng. In: *Frontiers in immunology* 9, p. 1486. DOI: 10.3389/fimmu.2018.01486.

Casbon, J. A. et al. (July 2011). "A method for counting PCR template molecules with application to next-generation sequencing." In: *Nucleic acids research* 39 (12), e81. DOI: 10.1093/nar/gkr217.

Cavenee, W. K. et al. (1983). "Expression of recessive alleles by chromosomal mechanisms in retinoblastoma". In: *Nature* 305.5937, pp. 779–784. DOI: 10.1038/305779a0.

Chauveinc, L. et al. (2001). "Osteosarcoma following retinoblastoma: Age at onset and latency period". In: *null* 22.2, pp. 77–88. DOI: 10.1076/opge.22.2.77.2228.

Cirillo, D. and A. Valencia (2019). "Big data analytics for personalized medicine". In: *Systems Biology • Nanobiotechnology* 58, pp. 161–167. DOI: 10.1016/j.copbio.2019.03.004.

Couch, Y. et al. (Dec. 2021). "A brief history of nearly EV-erything - The rise and rise of extracellular vesicles." In: *Journal of extracellular vesicles* 10 (14), e12144. DOI: 10.1002/jev2.12144.

Daumann, L. M. et al. (2020). "Interdisziplinäre Behandlung des Retinoblastoms". In: *Onkologie heute* 6, pp. 41–50.

Decatur, C. L. et al. (July 2016). "Driver Mutations in Uveal Melanoma: Associations With Gene Expression Profile and Patient Outcomes." In: *JAMA ophthalmology* 134 (7), pp. 728–33. DOI: 10.1001/jamaophthalmol.2016.0903.

Di Fiore, R. et al. (2013). "RB1 in cancer: Different mechanisms of RB1 inactivation and alterations of pRb pathway in tumorigenesis". In: *Journal of Cellular Physiology* 228.8, pp. 1676–1687. DOI: doi.org/10.1002/jcp.24329. eprint: https://onlinelibrary.wiley.com/doi/pdf/10.1002/jcp.24329.

Di Vizio, D. et al. (2012). "Large Oncosomes in Human Prostate Cancer Tissues and in the Circulation of Mice with Metastatic Disease". In: *The American Journal of Pathology* 181.5, pp. 1573–1584. DOI: 10.1016/j.ajpath.2012.07.030.

Dick, F. A. and S. M. Rubin (2013). “Molecular mechanisms underlying RB protein function”. In: *Nature Reviews Molecular Cell Biology* 14.5, pp. 297–306. DOI: 10.1038/nrm3567.

Dimaras, H. et al. (2012). “Retinoblastoma”. In: *The Lancet* 379.9824, pp. 1436–1446. DOI: 10.1016/S0140-6736(11)61137-9.

Dommering, C. J. et al. (June 2012). “RB1 mutations and second primary malignancies after hereditary retinoblastoma.” In: *Familial cancer* 11 (2), pp. 225–33.

Dong, L. et al. (2018). “Evaluation of droplet digital PCR and next generation sequencing for characterizing DNA reference material for KRAS mutation detection”. In: *Scientific Reports* 8.1, p. 9650. DOI: 10.1038/s41598-018-27368-3.

Doyle, L. M. and M. Z. Wang (July 2019). “Overview of Extracellular Vesicles, Their Origin, Composition, Purpose, and Methods for Exosome Isolation and Analysis.” eng. In: *Cells* 8 (7). DOI: 10.3390/cells8070727.

Draper, G. J., B. M. Sanders, and J. E. Kingston (May 1986). “Second primary neoplasms in patients with retinoblastoma.” In: *British journal of cancer* 53 (5), pp. 661–71. DOI: 10.1038/bjc.1986.110.

Droste, M. and A. Büscher (June 2020). “Biomarkers derived from extracellular vesicles – the next generation of diagnostics in pediatric renal disease? (German)”. In: *Nieren- und Hochdruckkrankheiten* 49, pp. 279–284. DOI: 10.5414/NHX02099.

Duvvuri, B. and C. Lood (2019). “Cell-Free DNA as a Biomarker in Autoimmune Rheumatic Diseases.” In: *Frontiers in immunology* 10, p. 502. DOI: 10.3389/fimmu.2019.00502.

Elzanowska, J., C. Semira, and B. Costa-Silva (2021). “DNA in extracellular vesicles: biological and clinical aspects”. In: *Molecular Oncology* 15.6, pp. 1701–1714. DOI: 10.1002/1878-0261.12777.

Erdbrügger, U. and T. H. Le (2016). “Extracellular Vesicles in Renal Diseases: More than Novel Biomarkers?” In: *Journal of the American Society of Nephrology* 27.1, pp. 12–26. DOI: 10.1681/ASN.2015010074.

Fallico, M. et al. (Apr. 2021). “Current molecular and clinical insights into uveal melanoma (Review).” In: *International journal of oncology* 58 (4). DOI: 10.3892/ijo.2021.5190.

FDA-NIH Biomarker Working Group (2016). *BEST (Biomarkers, EndpointS, and other Tools) Resource*. 11/2021. Food, Drug Administration (US), and National Institutes of Health (US).

Fenech, M. et al. (Jan. 2011). “Molecular mechanisms of micronucleus, nucleoplasmic bridge and nuclear bud formation in mammalian and human cells”. In: *Mutagenesis* 26.1, pp. 125–132. DOI: 10.1093/mutage/geq052.

Fernando, M. R. et al. (Aug. 2017). “New evidence that a large proportion of human blood plasma cell-free DNA is localized in exosomes”. In: *PLOS ONE* 12.8, pp. 1–15. DOI: 10.1371/journal.pone.0183915.

Feugeas, O. et al. (1996). “Loss of heterozygosity of the RB gene is a poor prognostic factor in patients with osteosarcoma.” In: *JCO* 14.2, pp. 467–472. DOI: 10.1200/jco.1996.14.2.467.

Fischer, S. et al. (2016). “Indication of Horizontal DNA Gene Transfer by Extracellular Vesicles”. In: *PloS one* 11.9, e0163665. DOI: 10.1371/journal.pone.0163665.

Flores, M. and D. W. Goodrich (2022). “Retinoblastoma Protein Paralogs and Tumor Suppression.” eng. In: *Frontiers in genetics* 13, p. 818719. DOI: 10.3389/fgene.2022.818719.

Fox, E. J. et al. (2014). “Accuracy of Next Generation Sequencing Platforms.” In: *Next generation, sequencing & applications* 1. DOI: 10.4172/2469-9853.1000106.

Francis, J. H. et al. (Sept. 2021). “RB1 Circulating Tumor DNA in the Blood of Patients with Unilateral Retinoblastoma: Before and after Intra-arterial Chemotherapy.” eng. In: *Ophthalmology science* 1 (3), p. 100042. DOI: 10.1016/j.xops.2021.100042.

Friend, S. H. et al. (1986). “A human DNA segment with properties of the gene that predisposes to retinoblastoma and osteosarcoma.” In: *Nature* 323 (6089), pp. 643–6. DOI: 10.1038/323643a0.

Frizziero, L. et al. (July 2019). “Uveal Melanoma Biopsy: A Review.” In: *Cancers* 11 (8). DOI: 10.3390/cancers11081075.

Fu, G. K. et al. (2011). “Counting individual DNA molecules by the stochastic attachment of diverse labels”. In: *Proceedings of the National Academy of Sciences* 108.22, pp. 9026–9031. DOI: 10.1073/pnas.1017621108.

Gahan, P. B. and M. Stroun (2010). “The virtosome-a novel cytosolic informative entity and intercellular messenger.” In: *Cell biochemistry and function* 28 (7), pp. 529–38. DOI: 10.1002/cbf.1690.

Gallenga, C. E. et al. (2022). “Genetic Basis and Molecular Mechanisms of Uveal Melanoma Metastasis: A Focus on Prognosis.” In: *Frontiers in oncology* 12, p. 828112. DOI: 10.3389/fonc.2022.828112.

Gandham, S. et al. (2020). “Technologies and Standardization in Research on Extracellular Vesicles”. In: *Trends in Biotechnology* 38.10. Special Issue: Therapeutic Biomanufacturing, pp. 1066–1098. DOI: 10.1016/j.tibtech.2020.05.012.

García-Silva, S., M. Gallardo, and H. Peinado (2021). “DNA-Loaded Extracellular Vesicles in Liquid Biopsy: Tiny Players With Big Potential?” In: *Frontiers in Cell and Developmental Biology* 8. DOI: 10.3389/fcell.2020.622579.

Garrison, E. and G. Marth (July 17, 2012). “Haplotype-based variant detection from short-read sequencing”. In: arXiv: 1207.3907v2 [q-bio.GN].

Gentleman, R. C. et al. (Sept. 2004). “Bioconductor: open software development for computational biology and bioinformatics”. In: *Genome Biology* 5.10, R80. DOI: 10.1186/gb-2004-5-10-r80.

Ghanam, J. et al. (2022). “DNA in extracellular vesicles: from evolution to its current application in health and disease”. In: *Cell & Bioscience* 12.1, p. 37. DOI: 10.1186/s13578-022-00771-0.

Gielis, E. M. et al. (2015). “Cell-Free DNA: An Upcoming Biomarker in Transplantation”. In: *American Journal of Transplantation* 15.10, pp. 2541–2551. DOI: 10.1111/ajt.13387.

Ginini, L. et al. (Apr. 2022). “Insight into Extracellular Vesicle-Cell Communication: From Cell Recognition to Intracellular Fate.” eng. In: *Cells* 11 (9). DOI: 10.3390/cells11091375.

Ginkel, van et al. (2017). “Droplet digital PCR for detection and quantification of circulating tumor DNA in plasma of head and neck cancer patients”. In: *BMC Cancer* 17.1, p. 428. DOI: 10.1186/s12885-017-3424-0.

Global Retinoblastoma Study Group (May 2020). “Global Retinoblastoma Presentation and Analysis by National Income Level”. In: *JAMA Oncology* 6.5, pp. 685–695. DOI: 10.1001/jamaoncol.2019.6716.

Gnirke, A. et al. (Feb. 2009). “Solution hybrid selection with ultra-long oligonucleotides for massively parallel targeted sequencing”. In: *Nature Biotechnology* 27.2, pp. 182–189. DOI: 10.1038/nbt.1523.

Goossens, N. et al. (2015). “Cancer biomarker discovery and validation”. In: *Translational Cancer Research; Vol 4, No 3 (June 2015): Translational Cancer Research (Application of Genomic Technologies in Cancer Research)*. DOI: 10.3978/j.issn.2218-676X.2015.06.04.

Grabuschnig, S. et al. (2020). *Putative Origins of Cell-Free DNA in Humans: A Review of Active and Passive Nucleic Acid Release Mechanisms*. DOI: 10.3390/ijms21218062.

Guescini, M. et al. (2009). “Astrocytes and Glioblastoma cells release exosomes carrying mtDNA”. In: *Journal of Neural Transmission* 117.1, p. 1. DOI: 10.1007/s00702-009-0288-8.

Guo, Q.-M. et al. (2019). “Detection of Plasma EGFR Mutations in NSCLC Patients with a Validated ddPCR Lung cfDNA Assay.” In: *Journal of Cancer* 10 (18), pp. 4341–4349. DOI: 10.7150/jca.31326.

Gurunathan, S. et al. (2019). “Review of the Isolation, Characterization, Biological Function, and Multifarious Therapeutic Approaches of Exosomes”. In: *Cells* 8.4. DOI: 10.3390/cells8040307.

Gustafson, D., S. Veitch, and J. E. Fish (2017). “Extracellular Vesicles as Protagonists of Diabetic Cardiovascular Pathology”. In: *Frontiers in Cardiovascular Medicine* 4. DOI: 10.3389/fcvm.2017.00071.

Hager, M. H. et al. (2012). “DIAPH3 governs the cellular transition to the amoeboid tumour phenotype”. In: *EMBO Molecular Medicine* 4.8, pp. 743–760. DOI: 10.1002/emmm.201200242.

Hagstrom, S. A. and T. P. Dryja (1999). “Mitotic recombination map of 13cen-13q14 derived from an investigation of loss of heterozygosity in retinoblastomas”. In: *Proceedings of the National Academy of Sciences* 96.6, pp. 2952–2957. DOI: 10.1073/pnas.96.6.2952.

Han, A., T. J. Purwin, and A. E. Aplin (June 2021). “Roles of the BAP1 Tumor Suppressor in Cell Metabolism.” In: *Cancer research* 81 (11), pp. 2807–2814. DOI: 10.1158/0008-5472.can-20-3430.

Harbour, J. W. et al. (Dec. 2010). “Frequent mutation of BAP1 in metastasizing uveal melanomas.” In: *Science (New York, N.Y.)* 330 (6009), pp. 1410–3. DOI: 10.1126/science.1194472.

Harding, S. M. et al. (2017). “Mitotic progression following DNA damage enables pattern recognition within micronuclei.” In: *Nature* 548 (7668), pp. 466–470. DOI: 10.1101/156414.

Hartwig, T. S. et al. (2017). "Discordant non-invasive prenatal testing (NIPT) - a systematic review". In: *Prenat Diagn* 37.6, pp. 527–539. DOI: 10.1002/pd.5049.

Hermann, D. M. et al. (2022). "Emerging roles of extracellular vesicle-associated non-coding RNAs in hypoxia: Insights from cancer, myocardial infarction and ischemic stroke". In: *Theranostics*. DOI: 10.7150/thno.73931.

Hindson, B. J. et al. (2011). "High-Throughput Droplet Digital PCR System for Absolute Quantitation of DNA Copy Number". In: *Anal. Chem.* 83.22, pp. 8604–8610. DOI: 10.1021/ac202028g.

Holdenrieder, S. et al. (2001). "Circulating Nucleosomes in Serum". In: *Annals of the New York Academy of Sciences* 945.1, pp. 93–102. DOI: 10.1111/j.1749-6632.2001.tb03869.x.

Hong, F. D. et al. (1989). "Structure of the Human Retinoblastoma Gene". In: *Proceedings of the National Academy of Sciences of the United States of America* 86.14, pp. 5502–5506.

Hong, J. and D. Gresham (2017). "Incorporation of unique molecular identifiers in TruSeq adapters improves the accuracy of quantitative sequencing". In: *BioTechniques* 63.5, pp. 221–226. ISSN: 0736-6205. DOI: 10.2144/000114608.

Hu, T., J. Wolfram, and S. Srivastava (2021). "Extracellular Vesicles in Cancer Detection: Hopes and Hypes". In: *Trends in Cancer* 7.2, pp. 122–133. DOI: 10.1016/j.trecan.2020.09.003.

Huber, W. et al. (Feb. 2015). "Orchestrating high-throughput genomic analysis with Bioconductor". In: *Nature Methods* 12.2, pp. 115–121. DOI: /10.1038/nmeth.3252.

Ignatiadis, M., G. W. Sledge, and S. S. Jeffrey (2021). "Liquid biopsy enters the clinic – implementation issues and future challenges". In: *Nature Reviews Clinical Oncology* 18.5, pp. 297–312. DOI: 10.1038/s41571-020-00457-x.

Ilié, M. and P. Hofman (Aug. 2016). "Pros: Can tissue biopsy be replaced by liquid biopsy?" In: 5 (4), pp. 420–3. DOI: 10.21037/tlcr.2016.08.06.

Im, D. H. A. U. P. et al. (2022). "Potential of Aqueous Humor as a Liquid Biopsy for Uveal Melanoma". In: *International Journal of Molecular Sciences* 23.11. DOI: 10.3390/ijms23116226.

Jacobs, B. K. M., E. Goetghebeur, and L. Clement (2014). "Impact of variance components on reliability of absolute quantification using digital PCR". In: *BMC Bioinformatics* 15.1, p. 283. DOI: 10.1186/1471-2105-15-283.

Jager, M. J. et al. (2020). "Uveal melanoma". In: *Nature Reviews Disease Primers* 6.1, p. 24. DOI: 10.1038/s41572-020-0158-0.

Jeppesen, D. K. et al. (2019). "Reassessment of Exosome Composition". In: *Cell* 177.2, 428–445.e18. DOI: 10.1016/j.cell.2019.02.029.

Jiménez, I. et al. (Sept. 2021). "Molecular diagnosis of retinoblastoma by circulating tumor DNA analysis". In: *European Journal of Cancer* 154, pp. 277–287. ISSN: 0959-8049. DOI: 10.1016/j.ejca.2021.05.039.

Jin, E. and J. V. Burnier (2021). "Liquid Biopsy in Uveal Melanoma: Are We There Yet?" In: *Ocul Oncol Pathol* 7.1, pp. 1–16. DOI: 10.1159/000508613.

Jumper, J. et al. (2021). “Highly accurate protein structure prediction with AlphaFold”. In: *Nature* 596.7873, pp. 583–589. DOI: 10.1038/s41586-021-03819-2.

Kaatsch, P. (2018). *Pädiatrische Hämatologie und Onkologie*. Vol. 2. Auflage. Charlotte Niemeyer, Angelika Eggert. ISBN: 978-3-662-43685-1.

Kahlert, C. et al. (2014). “Identification of double-stranded genomic DNA spanning all chromosomes with mutated KRAS and p53 DNA in the serum exosomes of patients with pancreatic cancer”. In: *The Journal of biological chemistry* 289.7, pp. 3869–3875. DOI: 10.1074/jbc.C113.532267.

Kamat, A. A. et al. (2010). “Plasma cell-free DNA in ovarian cancer”. In: *Cancer* 116.8, pp. 1918–1925. DOI: 10.1002/cncr.24997.

Kanber, D. et al. (Dec. 2009). “The human retinoblastoma gene is imprinted.” In: *PLoS genetics* 5 (12), e1000790. DOI: 10.1371/journal.pgen.1000790.

Karpman, D., A.-l. Ståhl, and I. Arvidsson (2017). “Extracellular vesicles in renal disease”. In: *Nature Reviews Nephrology* 13.9, pp. 545–562. DOI: 10.1038/nrneph.2017.98.

Kawamura, Y. et al. (2017). “Extracellular vesicles as trans-genomic agents: Emerging roles in disease and evolution”. In: *Cancer science* 108.5, pp. 824–830. DOI: 10.1111/cas.13222.

Keller, L. et al. (Jan. 2021). “Clinical relevance of blood-based ctDNA analysis: mutation detection and beyond.” In: *British journal of cancer* 124 (2), pp. 345–358. DOI: 10.1038/s41416-020-01047-5.

Ketteler, P., I. Hülsenbeck, et al. (2020). “The impact of RB1 genotype on incidence of second tumours in heritable retinoblastoma.” In: *European journal of cancer (Oxford, England : 1990)* 133, pp. 47–55. DOI: 10.1016/j.ejca.2020.04.005.

Ketteler, P., M. Yiallouros, and D. med. Ch. Jurklies (2022). “Kurzinformation zum Retinoblastom: Allgemeine Informationen, Diagnose und Therapieplanung, Therapie, Prognose”. In: *unpublished*.

Kim, R. S. et al. (Feb. 2017). “Histopathologic Analysis of Transvitreal Fine Needle Aspiration Biopsy Needle Tracts for Uveal Melanoma.” In: *American journal of ophthalmology* 174, pp. 9–16. DOI: 10.1016/j.ajo.2016.10.019.

Kim, S. A., M. Brossard, et al. (Nov. 2019). “gpart: human genome partitioning and visualization of high-density SNP data by identifying haplotype blocks.” In: *Bioinformatics (Oxford, England)* 35 (21), pp. 4419–4421. DOI: 10.1093/bioinformatics/btz308.

Kim, S. A. and Y. J. Yoo (2021). “gpart: Human genome partitioning of dense sequencing data by identifying haplotype blocks. R package version 1.13.0.” In:

Kisurina-Evgenieva, O. P., O. I. Sutiagina, and G. E. Onishchenko (2016). “Biogenesis of micronuclei”. In: *Biochemistry (Moscow)* 81.5, pp. 453–464. DOI: 10.1134/S0006297916050035.

Kivioja, T. et al. (2011). “Counting absolute numbers of molecules using unique molecular identifiers”. In: *Nature Methods* 9.1, pp. 72–74. DOI: 10.1038/nmeth.1778.

Knaus, B. J. and N. J. Grünwald (2017). “vcfr: a package to manipulate and visualize variant call format data in R”. In: *Mol Ecol Resour* 17.1, pp. 44–53. DOI: 10.1111/1755-0998.12549.

Knudson, A. G. (1971). “Mutation and Cancer: Statistical Study of Retinoblastoma”. In: *Proceedings of the National Academy of Sciences* 68.4, pp. 820–823. DOI: 10.1073/pnas.68.4.820.

Koopmans, A. E. et al. (2014). “Clinical significance of immunohistochemistry for detection of BAP1 mutations in uveal melanoma”. In: *Modern Pathology* 27.10, pp. 1321–1330. ISSN: 1530-0285. DOI: 10.1038/modpathol.2014.43.

Köster, J. et al. (2020). “Varlociraptor: enhancing sensitivity and controlling false discovery rate in somatic indel discovery”. In: *Genome Biology* 21.1, p. 98. DOI: 10.1186/s13059-020-01993-6.

Kovac, M. et al. (2015). “Exome sequencing of osteosarcoma reveals mutation signatures reminiscent of BRCA deficiency”. In: *Nature Communications* 6.1, p. 8940. DOI: 10.1038/ncomms9940.

Kustanovich, A. et al. (2019). “Life and death of circulating cell-free DNA”. In: *null* 20.8, pp. 1057–1067. DOI: 10.1080/15384047.2019.1598759.

Kwapisz, D. (2017). “The first liquid biopsy test approved. Is it a new era of mutation testing for non-small cell lung cancer?” In: *Annals of translational medicine* 5 (3), p. 46. DOI: 10.21037/atm.2017.01.32.

Lázaro-Ibáñez, E., C. Lässer, et al. (2019). “DNA analysis of low- and high-density fractions defines heterogeneous subpopulations of small extracellular vesicles based on their DNA cargo and topology.” In: *Journal of extracellular vesicles* 8 (1), p. 1656993. DOI: 10.1080/20013078.2019.1656993.

Lázaro-Ibáñez, E., A. Sanz-Garcia, et al. (2014). “Different gDNA content in the subpopulations of prostate cancer extracellular vesicles: apoptotic bodies, microvesicles, and exosomes.” In: *The Prostate* 74 (14), pp. 1379–90. DOI: 10.1002/pros.22853.

Le Guin, C. H. D., N. Bornfeld, et al. (Sept. 2021). “Early detection of metastatic uveal melanoma by the analysis of tumor-specific mutations in cell-free plasma DNA.” In: *Cancer medicine* 10 (17), pp. 5974–5982. DOI: 10.1002/cam4.4153.

Le Guin, C. H. D., K. A. Metz, et al. (Mar. 2019). “Chromosome 3 is a valid marker for prognostic testing of biopsy material from uveal melanoma later treated by brachytherapy.” In: *Biomarkers : biochemical indicators of exposure, response, and susceptibility to chemicals* 24 (2), pp. 134–140. DOI: 10.1080/1354750x.2018.1517827.

Lee, C. et al. (Dec. 2002). “Structural basis for the recognition of the E2F transactivation domain by the retinoblastoma tumor suppressor.” In: *Genes & development* 16 (24), pp. 3199–212. DOI: 10.1101/gad.1046102.

Lee, T. H., S. Chennakrishnaiah, E. Audemard, et al. (2014). “Oncogenic ras-driven cancer cell vesiculation leads to emission of double-stranded DNA capable of interacting with target cells”. In: *Biochemical and Biophysical Research Communications* 451.2, pp. 295–301. DOI: 10.1016/j.bbrc.2014.07.109.

Lee, T. H., S. Chennakrishnaiah, B. Meehan, et al. (Aug. 2016). "Barriers to horizontal cell transformation by extracellular vesicles containing oncogenic H-ras." In: *Oncotarget* 7 (32), pp. 51991–52002. DOI: 10.18632/oncotarget.10627.

Lees, J. A. et al. (1991). "The retinoblastoma protein is phosphorylated on multiple sites by human cdc2." eng. In: *The EMBO journal* 10 (13), pp. 4279–90. DOI: 10.1002/j.1460-2075.1991.tb05006.x.

Lefèvre, S. H. et al. (2001). "Genome instability in secondary solid tumors developing after radiotherapy of bilateral retinoblastoma." In: *Oncogene* 20 (56), pp. 8092–9. DOI: 10.1038/sj.onc.1205009.

Leitão, E. et al. (2018). "Locus-Specific DNA Methylation Analysis by Targeted Deep Bisulfite Sequencing". In: *Epigenome Editing: Methods and Protocols*. New York, NY: Springer New York, pp. 351–366. DOI: 10.1007/978-1-4939-7774-1_19.

Leon, S. A. et al. (1977). "Free DNA in the serum of cancer patients and the effect of therapy." In: *Cancer research* 37 (3), pp. 646–50.

Li, B. et al. (2022). "Tumor-derived extracellular vesicles shuttle c-Myc to promote gastric cancer growth and metastasis via the KCNQ1OT1/miR-556-3p/CLIC1 axis". In: *Cell Death & Disease* 13.3, p. 217. ISSN: 2041-4889. DOI: 10.1038/s41419-021-04446-5.

Li, H. and R. Durbin (July 2009). "Fast and accurate short read alignment with Burrows-Wheeler transform." In: *Bioinformatics (Oxford, England)* 25 (14), pp. 1754–60. DOI: 10.1093/bioinformatics/btp324.

Lo, Y. M. et al. (1997). "Presence of fetal DNA in maternal plasma and serum." In: *Lancet (London, England)* 350 (9076), pp. 485–7. DOI: 10.1016/s0140-6736(97)02174-0.

Machiela, M. J. and S. J. Chanock (2015). "LDlink: a web-based application for exploring population-specific haplotype structure and linking correlated alleles of possible functional variants." In: *Bioinformatics (Oxford, England)* 31 (21), pp. 3555–7. DOI: 10.1093/bioinformatics/btv402.

Malkin, E. Z. and S. V. Bratman (2020). "Bioactive DNA from extracellular vesicles and particles". In: *Cell Death & Disease* 11.7, p. 584. DOI: /10.1038/s41419-020-02803-4.

Mandel, P. and P. Metais (1948). "[Nuclear Acids In Human Blood Plasma]." fre. In: *Comptes rendus des seances de la Societe de biologie et de ses filiales* 142 (3-4), pp. 241–3.

Martin, M. et al. (2013). "Exome sequencing identifies recurrent somatic mutations in EIF1AX and SF3B1 in uveal melanoma with disomy 3." In: *Nature genetics* 45 (8), pp. 933–6. DOI: 10.1038/ng.2674.

Martin-Marcos, P. et al. (2017). "eIF1A residues implicated in cancer stabilize translation preinitiation complexes and favor suboptimal initiation sites in yeast". In: *eLife* 6. Ed. by N. Sonenberg, e31250. DOI: 10.7554/eLife.31250.

McCormick, F. (2020). "Sticking it to KRAS: Covalent Inhibitors Enter the Clinic". In: *Cancer Cell* 37.1, pp. 3–4. DOI: 10.1016/j.ccell.2019.12.009.

McIntyre, R. S. et al. (2014). “Advancing biomarker research: utilizing ‘Big Data’ approaches for the characterization and prevention of bipolar disorder”. In: *Bipolar Disord* 16.5, pp. 531–547. DOI: 10.1111/bdi.12162.

Meddeb, R., E. Pisareva, and A. R. Thierry (2019). “Guidelines for the Preanalytical Conditions for Analyzing Circulating Cell-Free DNA”. In: *Clinical Chemistry* 65.5, pp. 623–633. DOI: 10.1373/clinchem.2018.298323. eprint: https://academic.oup.com/clinchem/article-pdf/65/5/623/33899781/clinchem0623.pdf.

Metz, C. H. D. et al. (2013). “Ultradeep sequencing detects GNAQ and GNA11 mutations in cell-free DNA from plasma of patients with uveal melanoma”. In: *Cancer medicine* 2.2, pp. 208–215. DOI: 10.1002/cam4.61.

Michel, P. O. et al. (2012). “A NanoDrop-based method for rapid determination of viability decline in suspension cultures of animal cells”. In: *Analytical Biochemistry* 430.2, pp. 138–140. ISSN: 0003-2697. DOI: 10.1016/j.ab.2012.08.028.

Midena, E. et al. (2020). “In vivo intraocular biomarkers”. In: *Medicine* 99 (38), e22091. DOI: 10.1097/md.0000000000022091.

Miguel Pérez, D. de et al. (2020). “Extracellular vesicle-miRNAs as liquid biopsy biomarkers for disease identification and prognosis in metastatic colorectal cancer patients”. In: *Scientific Reports* 10.1, p. 3974. DOI: 10.1038/s41598-020-60212-1.

Minciacchi, V. R., M. R. Freeman, and D. Di Vizio (2015). “Extracellular vesicles in cancer: exosomes, microvesicles and the emerging role of large oncosomes.” eng. In: *Seminars in cell & developmental biology* 40, pp. 41–51. DOI: 10.1016/j.semcdb.2015.02.010.

Möhrmann, L. et al. (2018). “Liquid Biopsies Using Plasma Exosomal Nucleic Acids and Plasma Cell-Free DNA Compared with Clinical Outcomes of Patients with Advanced Cancers”. In: *Clinical cancer research* 24.1, pp. 181–188. DOI: 10.1158/1078-0432.CCR-17-2007.

Mölder, F. et al. (2021). “Sustainable data analysis with Snakemake [version 2; peer review: 2 approved]”. In: *F1000Research* 10.33. DOI: 10.12688/f1000research.29032.2.

Moss, J. et al. (2018). “Comprehensive human cell-type methylation atlas reveals origins of circulating cell-free DNA in health and disease.” In: *Nature communications* 9 (1), p. 5068. DOI: 10.1101/448142.

Mouliere, F. and A. R. Thierry (2012). “The importance of examining the proportion of circulating DNA originating from tumor, microenvironment and normal cells in colorectal cancer patients”. In: *Expert Opinion on Biological Therapy* 12.sup1, S209–S215. DOI: 10.1517/14712598.2012.688023.

Nathan, P. et al. (2021). “Overall Survival Benefit with Tebentafusp in Metastatic Uveal Melanoma”. In: *N Engl J Med* 385.13, pp. 1196–1206. DOI: 10.1056/nejmoa2103485.

Negri, G. L. et al. (2019). “Integrative genomic analysis of matched primary and metastatic pediatric osteosarcoma”. In: *J. Pathol.* 249.3, pp. 319–331. DOI: 10.1002/path.5319.

Németh, A. et al. (2017). "Antibiotic-induced release of small extracellular vesicles (exosomes) with surface-associated DNA". In: *Scientific Reports* 7.1, p. 8202. DOI: 10.1038/s41598-017-08392-1.

New England Bioland GmbH (2022). *NEBioCalculator*. URL: https://nebiocalculator.neb.com/#!/qPCRlibQnt.

Oellerich, M. et al. (2017). "Using circulating cell-free DNA to monitor personalized cancer therapy." In: *Critical reviews in clinical laboratory sciences* 54 (3), pp. 205–218. DOI: 10.1080/10408363.2017.1299683.

Olmedillas-López, S., M. García-Arranz, and D. García-Olmo (2017). "Current and Emerging Applications of Droplet Digital PCR in Oncology." In: *Molecular diagnosis & therapy* 21 (5), pp. 493–510. DOI: 10.1007/s40291-017-0278-8.

Onken, M. D., L. A. Worley, D. H. Char, et al. (2012). "Collaborative Ocular Oncology Group report number 1: prospective validation of a multi-gene prognostic assay in uveal melanoma." In: *Ophthalmology* 119 (8), pp. 1596–603. DOI: 10.1016/j.ophtha.2012.02.017.

Onken, M. D., L. A. Worley, J. P. Ehlers, et al. (2004). "Gene expression profiling in uveal melanoma reveals two molecular classes and predicts metastatic death." In: *Cancer research* 64 (20), pp. 7205–9. DOI: 10.1158/0008-5472.can-04-1750.

Otandault, A. et al. (2019). "Recent advances in circulating nucleic acids in oncology". In: *Annals of Oncology* 30.3, pp. 374–384. ISSN: 0923-7534. DOI: 10.1093/annonc/mdz031.

Otterson, G. A. et al. (1997). "Incomplete penetrance of familial retinoblastoma linked to germline mutations that result in partial loss of RB function." In: *Proceedings of the National Academy of Sciences of the United States of America* 94 (22), pp. 12036–40. DOI: 10.1073/pnas.94.22.12036.

Pedersen, T. L. (2022). *patchwork: The Composer of Plots*. https://patchwork.data-imaginist.com, https://github.com/thomasp85/patchwork.

Poulet, G., J. Massias, and V. Taly (2019). *Liquid Biopsy: General Concepts*. DOI: 10.1159/000499337.

Prescher, G. et al. (1996). "Prognostic implications of monosomy 3 in uveal melanoma." In: *Lancet (London, England)* 347 (9010), pp. 1222–5. DOI: 10.1016/s0140-6736(96)90736-9.

Ptolemy, A. S. and N. Rifai (2010). "What is a biomarker? Research investments and lack of clinical integration necessitate a review of biomarker terminology and validation schema". In: *Scandinavian Journal of Clinical and Laboratory Investigation* 70.sup242, pp. 6–14. DOI: 10.3109/00365513.2010.493354.

Qu, X. et al. (Nov. 2020). "Extracellular Vesicles in Head and Neck Cancer: A Potential New Trend in Diagnosis, Prognosis, and Treatment." eng. In: *International journal of molecular sciences* 21 (21). DOI: 10.3390/ijms21218260.

Ragusa, M. et al. (2015). "miRNA profiling in vitreous humor, vitreal exosomes and serum from uveal melanoma patients: Pathological and diagnostic implications." In: *Cancer biology & therapy* 16 (9), pp. 1387–96. DOI: 10.1080/15384047.2015.1046021.

Rahat, B. et al. (2020). "Circulating Cell-Free Nucleic Acids as Epigenetic Biomarkers in Precision Medicine." In: *Frontiers in genetics* 11, p. 844. DOI: 10.3389/fgene.2020.00844.

Raposo, G. and W. Stoorvogel (Feb. 2013). "Extracellular vesicles: Exosomes, microvesicles, and friends". In: *Journal of Cell Biology* 200.4, pp. 373–383. DOI: 10.1083/jcb.201211138.

Reichstein, D. A. and A. L. Brock (2021). "Radiation therapy for uveal melanoma: a review of treatment methods available in 2021." eng. In: *Current opinion in ophthalmology* 32 (3), pp. 183–190. DOI: 10.1097/icu.0000000000000761.

Reschke, M. et al. (2021). *Eye Tumors in Childhood as First Sign of Tumor Predisposition Syndromes: Insights from an Observational Study Conducted in Germany and Austria*. DOI: 10.3390/cancers13081876.

Riely, G. J., J. Marks, and W. Pao (2009). "KRAS Mutations in Non-Small Cell Lung Cancer". In: *Proc Am Thorac Soc* 6.2, pp. 201–205. DOI: 10.1513/pats.200809-107lc.

Robertson, A. G. et al. (2017). "Integrative Analysis Identifies Four Molecular and Clinical Subsets in Uveal Melanoma". In: *Cancer Cell* 32.2, 204–220.e15. DOI: 10.1016/j.ccell.2017.07.003.

Rodríguez-Martín, C. et al. (2020). "Frequency of low-level and high-level mosaicism in sporadic retinoblastoma: genotype-phenotype relationships". In: *Journal of Human Genetics* 65.2, pp. 165–174. DOI: 10.1038/s10038-019-0696-z.

Roy, S., F. H. Hochberg, and P. S. Jones (2018). "Extracellular vesicles: the growth as diagnostics and therapeutics; a survey". In: *Journal of Extracellular Vesicles* 7.1. PMID: 29511461, p. 1438720. DOI: 10.1080/20013078.2018.1438720. eprint: https://doi.org/10.1080/20013078.2018.1438720.

Rubin, S. M. (2013). "Deciphering the retinoblastoma protein phosphorylation code". In: *Trends in Biochemical Sciences* 38.1, pp. 12–19. DOI: 10.1016/j.tibs.2012.10.007.

Rubin, S. M. et al. (2005). "Structure of the Rb C-Terminal Domain Bound to E2F1-DP1: A Mechanism for Phosphorylation-Induced E2F Release". In: *Cell* 123.6, pp. 1093–1106. ISSN: 0092-8674. DOI: 10.1016/j.cell.2005.09.044.

Rushlow, D. E. et al. (2013). "Characterisation of retinoblastomas without RB1 mutations: genomic, gene expression, and clinical studies". In: *The Lancet Oncology* 14.4, pp. 327–334. DOI: 10.1016/s1470-2045(13)70045-7.

Saeki, H. et al. (2011). "Copy-Neutral Loss of Heterozygosity at the p53 Locus in Carcinogenesis of Esophageal Squamous Cell Carcinomas Associated with p53 Mutations". In: *Clin Cancer Res* 17.7, pp. 1731–1740. DOI: 10.1158/1078-0432.CCR-10-1996.

Sakai, T. et al. (Sept. 1991). "Oncogenic germ-line mutations in Sp1 and ATF sites in the human retinoblastoma gene". In: *Nature* 353.6339, pp. 83–86. DOI: 10.1038/353083a0.

Salk, J. J., M. W. Schmitt, and L. A. Loeb (2018). "Enhancing the accuracy of next-generation sequencing for detecting rare and subclonal mutations". In: *Nature Reviews Genetics* 19.5, pp. 269–285. DOI: 10.1038/nrg.2017.117.

Sanchez, C. et al. (2021). “Circulating nuclear DNA structural features, origins, and complete size profile revealed by fragmentomics”. In: *JCI Insight* 6.7. DOI: 10.1172/jci.insight.144561.

Sanger, F., S. Nicklen, and A. R. Coulson (1977). “DNA sequencing with chain-terminating inhibitors.” In: *Proceedings of the National Academy of Sciences of the United States of America* 74 (12), pp. 5463–7. DOI: 10.1073/pnas.74.12.5463.

Sato, A. et al. (2018). “Investigation of appropriate pre-analytical procedure for circulating free DNA from liquid biopsy.” eng. In: *Oncotarget* 9 (61), pp. 31904–31914. DOI: 10.18632/oncotarget.25881.

Schaiquevich, P. et al. (2022). “Treatment of Retinoblastoma: What Is the Latest and What Is the Future”. In: *Frontiers in Oncology* 12. DOI: 10.3389/fonc.2022.822330.

Schefler, A. C. and R. S. Kim (2021). “Recent advancements in the management of retinoblastoma and uveal melanoma.” In: *Faculty reviews* 10, p. 51. DOI: 10.12703/r/10-51.

Sellam, A. et al. (Feb. 2016). “Fine Needle Aspiration Biopsy in Uveal Melanoma: Technique, Complications, and Outcomes.” In: *American journal of ophthalmology* 162, 28–34.e1. DOI: 10.1016/j.ajo.2015.11.005.

Selleck, M. J., M. Senthil, and N. R. Wall (2017). “Making Meaningful Clinical Use of Biomarkers.” In: *Biomarker insights* 12. DOI: 10.1177/1177271917715236.

Sharma, A. et al. (2019). “BHARAT: An Integrated Big Data Analytic Model for Early Diagnostic Biomarker of Alzheimer’s Disease.” In: *Frontiers in neurology* 10, p. 9. DOI: 10.3389/fneur.2019.00009.

Shulman, D. S. et al. (2018). “Detection of circulating tumour DNA is associated with inferior outcomes in Ewing sarcoma and osteosarcoma: a report from the Children’s Oncology Group”. In: *British Journal of Cancer* 119.5, pp. 615–621. DOI: 10.1038/s41416-018-0212-9.

Singh, A. D., M. E. Turell, and A. K. Topham (2011). “Uveal Melanoma: Trends in Incidence, Treatment, and Survival”. In: *Ophthalmology* 118.9, pp. 1881–1885. DOI: 10.1016/j.ophtha.2011.01.040. URL: https://www.sciencedirect.com/science/article/pii/S016164201100073X.

Singh, R. R. (2020). “Next-Generation Sequencing in High-Sensitive Detection of Mutations in Tumors: Challenges, Advances, and Applications”. In: *The Journal of Molecular Diagnostics* 22.8, pp. 994–1007. DOI: 10.1016/j.jmoldx.2020.04.213.

Sippel, K. C. et al. (1998). “Frequency of somatic and germ-line mosaicism in retinoblastoma: implications for genetic counseling.” In: *American journal of human genetics* 62 (3), pp. 610–9. DOI: 10.1086/301766.

Smith, T., A. Heger, and I. Sudbery (2017). “UMI-tools: modeling sequencing errors in Unique Molecular Identifiers to improve quantification accuracy”. In: *Genome Research* 27.3, pp. 491–499. DOI: 10.1101/gr.209601.116.

Snakemake-Workflows Contributors (2017). *Snakemake-Workflows*. URL: https://github.com/snakemake-workflows/.

Ståhlberg, A. et al. (2017). “Simple multiplexed PCR-based barcoding of DNA for ultrasensitive mutation detection by next-generation sequencing”. In: *Nature protocols* 12.4, pp. 664–682. DOI: 10.1038/nprot.2017.006.

Takahashi, A. et al. (2017). “Exosomes maintain cellular homeostasis by excreting harmful DNA from cells”. In: *Nature Communications* 8.1, p. 15287. DOI: 10.1038/ncomms15287.

Temming, P., M. Arendt, A. Viehmann, L. Eisele, C. H. D. Le Guin, M. M. Schündeln, E. Biewald, K. Astrahantseff, et al. (2017). “Incidence of second cancers after radiotherapy and systemic chemotherapy in heritable retinoblastoma survivors: A report from the German reference center”. In: *Pediatric blood & cancer* 64.1, pp. 71–80. DOI: 10.1002/pbc.26193.

Temming, P., M. Arendt, A. Viehmann, L. Eisele, C. H. D. Le Guin, M. M. Schündeln, E. Biewald, J. Mäusert, et al. (2016). “How Eye-Preserving Therapy Affects Long-Term Overall Survival in Heritable Retinoblastoma Survivors”. In: *JCO* 34.26, pp. 3183–3188. DOI: 10.1200/jco.2015.65.4012.

Temming, P., A. Viehmann, et al. (2015). “Pediatric second primary malignancies after retinoblastoma treatment”. In: *Pediatr Blood Cancer* 62.10, pp. 1799–1804. ISSN: 1545-5009. DOI: 10.1002/pbc.25576.

Tewhey, R. et al. (Oct. 2009). “Enrichment of sequencing targets from the human genome by solution hybridization”. In: *Genome Biology* 10.10, R116. DOI: 10.1186/gb-2009-10-10-r116.

Thakur, B. K. et al. (2014). “Double-stranded DNA in exosomes: a novel biomarker in cancer detection”. In: *Cell Research* 24.6, pp. 766–769. DOI: 10.1038/cr.2014.44.

Thermo Fischer (2022). “Tm Calculator”. In: URL: https://www.thermofisher.com/de/de/home/brands/thermo-scientific/molecular-biology/molecular-biology-learning-center/molecular-biology-resource-library/thermo-scientific-web-tools/tm-calculator.html.

Thierry, A. R. et al. (2016). “Origins, structures, and functions of circulating DNA in oncology”. In: *Cancer and Metastasis Reviews* 35.3, pp. 347–376. DOI: 10.1007/s10555-016-9629-x.

Thomas, S. et al. (2012). “Prognostic significance of chromosome 3 alterations determined by microsatellite analysis in uveal melanoma: a long-term follow-up study”. In: *British Journal of Cancer* 106.6, pp. 1171–1176. DOI: 10.1038/bjc.2012.54. URL: https://doi..

Tivey, A. et al. (2022). “Circulating tumour DNA – looking beyond the blood”. In: *Nature Reviews Clinical Oncology* 19.9, pp. 600–612. DOI: /10.1038/s41571-022-00660-y.

Tschentscher, F. et al. (2003). “Tumor Classification Based on Gene Expression Profiling Shows That Uveal Melanomas with and without Monosomy 3 Represent Two Distinct Entities”. In: *Cancer Res* 63.10, pp. 2578–2584.

Untergasser, A. et al. (2012). “Primer3–new capabilities and interfaces.” In: *Nucleic acids research* 40 (15), e115. DOI: 10.1093/nar/gks596.

Vagner, T. et al. (2018). “Large extracellular vesicles carry most of the tumour DNA circulating in prostate cancer patient plasma”. In: *Journal of extracellular vesicles* 7.1, p. 1505403. DOI: 10.1080/20013078.2018.1505403.

van Niel, G., G. D'Angelo, and G. Raposo (2018). "Shedding light on the cell biology of extracellular vesicles". In: *Nature reviews. Molecular cell biology* 19.4, pp. 213–228. DOI: 10.1038/nrm.2017.125.

Van Raamsdonk, C. D., V. Bezrookove, et al. (Jan. 2009). "Frequent somatic mutations of GNAQ in uveal melanoma and blue naevi." In: *Nature* 457 (7229), pp. 599–602. DOI: 10.1038/nature07586.

Van Raamsdonk, C. D., K. G. Griewank, et al. (2010). "Mutations in GNA11 in uveal melanoma." In: *The New England journal of medicine* 363 (23), pp. 2191–9. DOI: 10.1056/NEJMoa1000584.

VanLiere, J. M. and N. A. Rosenberg (Aug. 2008). "Mathematical properties of the r^2 measure of linkage disequilibrium." In: *Theoretical population biology* 74 (1), pp. 130–7. DOI: 10.1016/j.tpb.2008.05.006.

Varadi, M. et al. (2022). "AlphaFold Protein Structure Database: massively expanding the structural coverage of protein-sequence space with high-accuracy models". In: *Nucleic Acids Res* 50.D1, pp. D439–D444. DOI: 10.1093/nar/gkab1061.

Váraljai, R. et al. (2019). "Application of Circulating Cell-Free Tumor DNA Profiles for Therapeutic Monitoring and Outcome Prediction in Genetically Heterogeneous Metastatic Melanoma". In: *JCO Precision Oncology* 3, pp. 1–10. DOI: 10.1200/PO.18.00229.

Velez, G. et al. (2021). "Liquid biopsy proteomics of uveal melanoma reveals biomarkers associated with metastatic risk". In: *Molecular Cancer* 20.1, p. 39. DOI: 10.1186/s12943-021-01336-4.

Virgili, G. et al. (2007). "Incidence of Uveal Melanoma in Europe". In: *Ophthalmology* 1.12, 2309–2315.e2. DOI: 10.1016/j.ophtha.2007.01.032.

Volckmar, A.-L. et al. (Mar. 2018). "A field guide for cancer diagnostics using cell-free DNA: From principles to practice and clinical applications." In: *Genes, chromosomes & cancer* 57 (3), pp. 123–139. DOI: 10.1002/gcc.22517.

Wadayama, B.-i. et al. (1994). "Mutation Spectrum of the Retinoblastoma Gene in Osteosarcomas1". In: *Cancer Res* 54.11, pp. 3042–3048.

Wan, J. C. M. et al. (2017). "Liquid biopsies come of age: towards implementation of circulating tumour DNA". In: *Nature reviews. Cancer* 17.4, pp. 223–238. DOI: 10.1038/nrc.2017.7.

Wang, B. et al. (2017). "An adaptive decorrelation method removes Illumina DNA base-calling errors caused by crosstalk between adjacent clusters". In: *Scientific Reports* 7.1, p. 41348. DOI: 10.1038/srep41348.

Wang, X. et al. (Sept. 2022). "A pilot study of the use of dynamic analysis of cell-free DNA from aqueous humor and vitreous fluid for the diagnosis and treatment monitoring of vitreoretinal lymphomas." eng. In: *Haematologica* 107 (9), pp. 2154–2162. DOI: 10.3324/haematol.2021.279908.

White, V. A., B. K. McNeil, and D. E. Horsman (1998). "Acquired Homozygosity (Isodisomy) of Chromosome 3 in Uveal Melanoma". In: *Cancer Genetics and Cytogenetics* 102.1, pp. 40–45. DOI: 10.1016/s0165-4608(97)00290-2.

Wickham, H. (2016). *ggplot2: Elegant Graphics for Data Analysis*. Springer-Verlag New York. URL: https://ggplot2.tidyverse.org.

Wickham, H. et al. (2019). "Welcome to the tidyverse". In: *Journal of Open Source Software* 4.43, p. 1686. DOI: 10.21105/joss.01686.

Wierenga, A. P. A. et al. (2019). "Aqueous Humor Biomarkers Identify Three Prognostic Groups in Uveal Melanoma". In: *Invest. Ophthalmol. Vis. Sci.* 60.14, pp. 4740–4747. DOI: 10.1167/iovs.19-28309.

Willey, J. C. et al. (2021). "Advancing NGS quality control to enable measurement of actionable mutations in circulating tumor DNA". In: *Cell Reports Methods* 1.7, p. 100106. DOI: 10.1016/j.crmeth.2021.100106.

Willms, E. et al. (2018). "Extracellular Vesicle Heterogeneity: Subpopulations, Isolation Techniques, and Diverse Functions in Cancer Progression." In: *Frontiers in immunology* 9, p. 738. DOI: 10.3389/fimmu.2018.00738.

Wit, S. de et al. (2019). "Single tube liquid biopsy for advanced non-small cell lung cancer". In: *International journal of cancer* 144.12, pp. 3127–3137. DOI: 10.1002/ijc.32056.

Witwer, K. W. et al. (2017). "Updating the MISEV minimal requirements for extracellular vesicle studies: building bridges to reproducibility". In: *Journal of Extracellular Vesicles* 6.1, p. 1396823. DOI: 10.1080/20013078.2017.1396823.

Wu, C.-C. and J. A. Livingston (2020). "Genomics and the Immune Landscape of Osteosarcoma". In: *Current Advances in the Science of Osteosarcoma*. Cham, pp. 21–36. DOI: /10.1007/978-3-030-43085-6_2.

Wyllie, A. H. (Apr. 1980). "Glucocorticoid-induced thymocyte apoptosis is associated with endogenous endonuclease activation". In: *Nature* 284.5756, pp. 555–556. DOI: 10.1038/284555a0.

Xu, L. et al. (Aug. 2020). "Chromosome 6p Amplification in Aqueous Humor Cell-Free DNA Is a Prognostic Biomarker for Retinoblastoma Ocular Survival." eng. In: *Molecular cancer research : MCR* 18 (8), pp. 1166–1175. DOI: 10.1158/1541-7786.mcr-19-1262.

Yáñez-Mó, M. et al. (2015). "Biological properties of extracellular vesicles and their physiological functions". In: *Journal of extracellular vesicles* 4, p. 27066. DOI: 10.3402/jev.v4.27066.

Yang, Q. et al. (2022). "Role of extracellular vesicles in osteosarcoma." eng. In: *International journal of medical sciences* 19 (8), pp. 1216–1226. DOI: 10.7150/ijms.74137.

Ye, P. et al. (2021). "The diagnostic accuracy of digital PCR, ARMS and NGS for detecting KRAS mutation in cell-free DNA of patients with colorectal cancer: A systematic review and meta-analysis". In: *PLOS ONE* 16.3, e0248775. DOI: 10.1371/journal.pone.0248775.

Yokoi, A. et al. (2019). "Mechanisms of nuclear content loading to exosomes". In: *Science Advances* 5.11. DOI: 10.1126/sciadv.aax8849.

Zentrum für Krebsregisterdaten und Gesellschaft der epidemiologischen Krebsregister in Deutschland e.V. (2021). *Krebs in Deutschland für 2017/2018*. Robert Koch Institut.

Zhai, Y. L. et al. (Dec. 1999). “Frequent occurrence of loss of heterozygosity among tumor suppressor genes in uterine leiomyosarcoma.” In: *Gynecologic oncology* 75 (3), pp. 453–9. DOI: 10.1006/gyno.1999.5629.

Zhang, H. et al. (2018). “Identification of distinct nanoparticles and subsets of extracellular vesicles by asymmetric flow field-flow fractionation”. In: *Nature Cell Biology* 20.3, pp. 332–343. ISSN: 1476-4679. DOI: 10.1038/s41556-018-0040-4.

Zhang, Y. et al. (2017). “Total DNA input is a crucial determinant of the sensitivity of plasma cell-free DNA EGFR mutation detection using droplet digital PCR.” In: *Oncotarget* 8 (4), pp. 5861–5873. DOI: 10.18632/oncotarget.14390.

8 Appendix

8.1 Oligonucleotides

Table 12: Oligonucleotides for PCR amplification and Sanger sequencing

Primer	Sequence (5' - 3')
N1_RB_SNP1/1_fw	AAAGCCACCCAATCATCACC
N2_RB_SNP1/1_rev	TGACTGTGAGGATTGGCTCAC
N3_RB_SNP1/2_fw	CCACCCAATCATCACC
N4_RB_SNP1/2_rev	TAACACTACTGCCTCCTGACTG
N5_RB_SNP4/1_fw	ACCCAACTCTAGCATTCCATCC
N6_RB_SNP4/1_rev	CGTCTTCACTCCAGTTTCTCTC
N7_RB_SNP4/2_fw	TTCCATCCTGAGTGTCTGC
N8_RB_SNP4/2_rev	CCGTTCGTCTTCACTCCAGTTTCTC
N9_RB_SNP6/1_fw	GGCAACCAAGAAAGTGACTCAG
N10_RB_SNP6/1_rev	TGGAAAGTGCTGCCCAAGTC
N11_RB_SNP7/1_fw	GGCAACCAAGAAAGTGACTCAG
N12_RB_SNP7/1_rev	TGGAAAGTGCTGCCCAAGTC
N13_RB_SNP8/1_fw	ACAAAGTCACTGGCGTTG
N14_RB_SNP8/1_rev	GCTTGCATGGTAAGTC
N15_RB_SNP9/1_fw	AGCAGGTTGGAAGAGATC
N16_RB_SNP9/1_rev	GACAAGAGCAAGACCCCATC
N17_RB_SNP14/1_fw	TGGAGGTTTGGGAGAC
N18_RB_SNP14/1_rev	GCCTTTCCCCAATCCTAACC
N19_RB_SNP5/1_fw	TGAGAACACTTGTGGAG
N20_RB_SNP5/1_rev	TCCAGTACCCGAGATATGAACTG
GNAQ_Q209fw	CTTGCTTCCTGGCACGAGATGATAGAGGTGACATTTTCAAAGC
GNAQ_Q209rev	CAGGAAACAGCTATGACAATATGAGTATTGTTAACCTTGCAGAA
GNA11_Q209fw	CTTGCTTCCTGGCACGAGTGTGTCCTTTCAGGATGGTG
GNA11_Q209rev	CAGGAAACAGCTATGACGCGACGAGAAACATGATGG
GNAQ_R183fw	CTTGCTTCCTGGCACGAGACTTGGACCGCGTAGCTG
GNAQ_R183rev	CAGGAAACAGCTATGACAAGTCAAAGGGGTATTCGATGA
GNA11_R183fw	CTTGCTTCCTGGCACGAGATCGCCACCTTGGGCTAC
GNA11_R183rev	CAGGAAACAGCTATGACTGATGTTCTCCAGGTCGAAA
F-Tag	CTTGCTTCCTGGCACGAG
R-Tag	CAGGAAACAGCTATGAC

Table 13: Target primer for NGS using SiMSen-seq

Primer	Sequence (5' - 3')
N_rs9535007#1_fw_A	AAAGCCACCCAATCATCACC
N_rs9535007#1_rev_A	TGCTAATTATCTTAAAGCCACCCA
N_rs9535007#1_fw_B	TGACTGTGAGGATTGGCTCA
N_rs9535007#1_rev_B	ACAAGAAGTGAGTACGAAGACA
N_rs2254423#2_fw_A	ACACTTTGCATTTGGTTGCT
N_rs2254423#2_rev_A	TGGCAGGAAGGTAGAGACAGA
N_rs2254423#2_fw_B	TGCATTTGGTTGCTATATCCCT
N_rs2254423#2_rev_B	AAATGGCAGGAAGGTAGAGAC
N_rs9568029#4_fw_A	TCCATCCTGAGTGTCTGCAG
N_rs9568029#4_rev_A	ACACTCAGGCTCTGTTTTCTACA
N_rs9568029#4_rev_B	TCTACAGAACCCAGGCTAAAAG
N_rs11360969#5_fw_A	ACTTGTGGAGTCAAATTTGCAA
N_rs11360969#5_rev_A	CCGAGATATGAACTGTGTAGACT
N_rs11360969#5_fw_B	GTGAGAACACTTGTGGAGTCA
N_rs11360969#5_rev_B	TGAACTGTGTAGACTTTTAGAGAGT
N_SNP#6_&_#7_fw_A	GTTTGTACTGGGGGCAGTGA
N_SNP#6_&_#7_fw_B	GTGCTGCCCAAGTCAAACAG
N_SNP#6_&_#7_rev_A	CAGTTTGTACTGGGGGCAG
N_SNP#6_&_#7_rev_B	ATGGAAAGTGCTGCCCAAGT
N_rs1981434#8_fw_A	ACATTTACTTTCCTTCACAGAAGTGT
N_rs1981434#8_rev_A	TTTGCTTGCATGGTAAGTCAAA
N_rs1981434#8_fw_B	GCTATTACATTTACTTTCCTTCACAGA
N_rs1981434#8_rev_B	TTGCTTGCATGGTAAGTCAAATAT
N_rs9535016#11_rev_A	ACCTAACTTGTTGAGAGTTTTCATCA
N_rs9535016#11_fw_A	TCCAGAAAAAGTGTTTGACAAAACT
N_rs9535016#11_fw_B	AGATCCAGAAAAAGTGTTTGACAA
N_rs9535016#11_rev_B	ACTTGTTGAGAGTTTTCATCATGAA
N_rs4151450#12_fw_A	AGCCTATGGATGGGTCAGGT
N_rs4151450#12_rev_A	AGGAATTATACCAAAGCAGCTAACT
N_rs4151450#12_fw_B	TGGACAGCCTATGGATGGGT
N_rs4151450#12_rev_B	TGTATAAGGAATTATACCAAAGCAGCT
N_rs198619#14_fw_A	TGGAAGACCAAAGAATACCATATAAAA
N_rs198619#14_rev_A	GCCTTTCCCCAATCCTAACCA
N_rs2252544#15_fw_A	GATCCGTCCTCGCCAGGG
N_rs2252544#15_rev_A	TTCTGCAGACGCTCCGCC
Target TP7 forward	CCTGGAGTCTTCCAGTGTGATG
Target TP7 reverse	GACTGTACCACCATCCACTACAAC

Table 14: Barcode primer for NGS using SiMSen-seq

Primer	Sequence (5' - 3')
N_SNP4_A_Barcode_fw	GGACACTCTTTCCCTACACGACGCTCTTCCGATCTNNNNNNNNNNNNNNATGGGAAAGAGTGTCCTCCATCCTGAGTGTCTGCAG
N_SNP4_B_Barcode_rev	GTGACTGGAGTTCAGACGTGTGCTCTTCCGATCTTCTACAGAACCCAGGCTAAAAG
N_SNP5_A_Barcode_fw	GGACACTCTTTCCCTACACGACGCTCTTCCGATCTNNNNNNNNNNNNNNATGGGAAAGAGTGTCCACTTGTGGAGTCAAATTTGCAA
N_SNP5_A_Barcode_rev	GTGACTGGAGTTCAGACGTGTGCTCTTCCGATCTCCGAGATATGAACTGTGTAGACT
N_SNP5_B_Barcode_fw	GGACACTCTTTCCCTACACGACGCTCTTCCGATCTNNNNNNNNNNNNNNATGGGAAAGAGTGTCCGTGAGAACACTTGTGGAGTCA
N_SNP5_B_Barcode_rev	GTGACTGGAGTTCAGACGTGTGCTCTTCCGATCTTGAACTGTGTAGACTTTTAGAGAGT
N _SNP8_B_Barcode_fw	GGACACTCTTTCCCTACACGACGCTCTTCCGATCTNNNNNNNNNNNNNNATGGGAAAGAGTGTCCGCTATTACATTTACTTTCCTTCACAGA
N_SNP8_B_Barcode_rev	GTGACTGGAGTTCAGACGTGTGCTCTTCCGATCTTTGCTTGCATGGTAAGTCAAATAT
N_SNP11_B_Barcode_fw	GGACACTCTTTCCCTACACGACGCTCTTCCGATCTNNNNNNNNNNNNNNATGGGAAAGAGTGTCCAGATCCAGAAAAAGTGTTTGACAA
N_SNP11_B_Barcode_rev	GTGACTGGAGTTCAGACGTGTGCTCTTCCGATCTACTTGTTGAGAGTTTTCATCATGAA
N_SNP12_B_Barcode_fw	GGACACTCTTTCCCTACACGACGCTCTTCCGATCTNNNNNNNNNNNNNNATGGGAAAGAGTGTCCTGGACAGCCTATGGATGGGT
N_SNP12_B_Barcode_rev	GTGACTGGAGTTCAGACGTGTGCTCTTCCGATCTTGTATAAGGAATTATACCAAAGCAGCT
N_SNP14_A_Barcode_fw	GGACACTCTTTCCCTACACGACGCTCTTCCGATCTNNNNNNNNNNNNNNATGGGAAAGAGTGTCCTGGAAGACCAAAGAATACCATATAAAA
N_SNP14_A_Barcode_rev	GTGACTGGAGTTCAGACGTGTGCTCTTCCGATCTGCCTTTCCCCAATCCTAACCA
Barcode TP7 forward	GGACACTCTTTCCCTACACGACGCTCTTCCGATCTNNNNNNNNNNNNNNATGGGAAAGAGTGTCCCCTGGAGTCTTCCAGTGTGATG
Barcode TP7 reverse	GTGACTGGAGTTCAGACGTGTGCTCTTCCGATCTGACTGTACCACCATCCACTACAAC

Table 15: Adaptor primer for NGS

Primer	Sequence(5' - 3')
NSE 501	AATGATACGGCGACCACCGAGATCTACACTAGATCGCACACTCTTTCCCTACACGAC GCTCTTCCGATCTTATAGCCTTGCTTCCTGGCACGAG
NSE 502	AATGATACGGCGACCACCGAGATCTACACCTCTCTATACACTCTTTCCCTACACGAC GCTCTTCCGATCTATAGAGCTTGCTTCCTGGCACGAG
NSE 503	AATGATACGGCGACCACCGAGATCTACACTATCCTCTACACTCTTTCCCTACACGAC GCTCTTCCGATCTCCTATC CTTGCTTCCTGGCACGAG
NSE 504	AATGATACGGCGACCACCGAGATCTACACAGAGTAGAACACTCTTTCCCTACACGAC GCTCTTCCGATCTGGCTCT CTTGCTTCCTGGCACGAG
N701	CAAGCAGAAGACGGCATACGAGATTCGCCTTAGTGACTGGAGTTCAGACGTGTGCT CTTCCGATCTCAGGAAACAGCTATGAC
N702	CAAGCAGAAGACGGCATACGAGATCTAGTACGGTGACTGGAGTTCAGACGTGTGCT CTTCCGATCTCAGGAAACAGCTATGAC
N703	CAAGCAGAAGACGGCATACGAGATTTCTGCCTGTGACTGGAGTTCAGACGTGTGCT CTTCCGATCTCAGGAAACAGCTATGAC
N704	CAAGCAGAAGACGGCATACGAGATGCTCAGGAGTGACTGGAGTTCAGACGTGTGCT CTTCCGATCTCAGGAAACAGCTATGAC
N705	CAAGCAGAAGACGGCATACGAGATAGGAGTCCGTGACTGGAGTTCAGACGTGTGCT CTTCCGATCTCAGGAAACAGCTATGAC
N706	CAAGCAGAAGACGGCATACGAGATCATGCCTAGTGACTGGAGTTCAGACGTGTGCT CTTCCGATCTCAGGAAACAGCTATGAC
N707	CAAGCAGAAGACGGCATACGAGATGTAGAGAGGTGACTGGAGTTCAGACGTGTGCT CTTCCGATCTCAGGAAACAGCTATGAC
N708	CAAGCAGAAGACGGCATACGAGATCCTCTCTGGTGACTGGAGTTCAGACGTGTGCT CTTCCGATCTCAGGAAACAGCTATGAC
N709	CAAGCAGAAGACGGCATACGAGATAGCGTAGCGTGACTGGAGTTCAGACGTGTGCT CTTCCGATCTCAGGAAACAGCTATGAC
N710	CAAGCAGAAGACGGCATACGAGATCAGCCTCGGTGACTGGAGTTCAGACGTGTGCT CTTCCGATCTCAGGAAACAGCTATGAC
N711	CAAGCAGAAGACGGCATACGAGATTGCCTCTTGTGACTGGAGTTCAGACGTGTGCT CTTCCGATCTCAGGAAACAGCTATGAC
N712	CAAGCAGAAGACGGCATACGAGATTCCTCTACGTGACTGGAGTTCAGACGTGTGCT CTTCCGATCTCAGGAAACAGCTATGAC

Adaptor Primer used for NGS Sequencing with the SiMSen-seq method were taken from the corresponding publication Ståhlberg et al. 2017 and can be found in the Supplementary material thereof.

8.2 SNPs selected for detection of chromosome 3 status

Table 16: SNPs selected for detection of chromosome 3 status

rs Number	Start Position	Stop Position
rs735931	10483411	10483412
rs4684740	10863006	10863007
rs2697159	10932740	10932741
rs2246543	11033816	11033817
rs34313323	110361743	110361744
rs13080207	110434034	110434035
rs9867550	110513909	110513910
rs9834281	110537208	110537209
rs1512533	110598149	110598150
rs11715699	110603225	110603226
rs4362750	110665038	110665039
rs4682018	110677584	110677585
rs6773379	112006558	112006559
rs7651349	11620845	11620846
rs3856802	11626239	11626240
rs2030066	11691649	11691650
rs6762358	11692586	11692587
rs305499	11949563	11949564
rs6439255	130800571	130800572
rs56090776	130826829	130826830
rs9810476	131658263	131658264
rs11706180	131658774	131658775
rs1077391	131909336	131909337
rs2091650	132090150	132090151
rs9827510	132096206	132096207
rs6792743	132217866	132217867
rs2177148	150622326	150622327
rs9880339	151248704	151248705
rs9815520	151259622	151259623
rs62283021	151286091	151286092
rs7617677	151287025	151287026
rs6787801	151381952	151381953
rs1491974	151384663	151384664
rs17504	151398245	151398246
rs11716560	151838421	151838422
rs7624902	160286237	160286238
rs4680576	160303892	160303893
rs7629202	160451408	160451409
rs17826438	160922506	160922507
rs62280303	160930102	160930103
rs778649	160991588	160991589
rs6769642	161045680	161045681
rs7615592	161263759	161263760
rs336561	161407516	161407517
rs6444958	171046594	171046595

rs Number	Start Position	Stop Position
rs6799025	171307458	171307459
rs4955596	171046838	171046839
rs11917336	171252340	171252341
rs2088885	171253501	171253502
rs13099460	171298963	171298964
rs7621422	171404830	171404831
rs12631813	171408344	171408345
rs1316415	171770430	171770431
rs9866788	190315330	190315331
rs10937431	190376746	190376747
rs6444459	190774845	190774846
rs186064	191378003	191378004
rs186065	191378169	191378170
rs415149	191382386	191382387
rs392311	191388122	191388123
rs13090846	192012499	192012500
rs1388397	192015101	192015102
rs6550374	20154547	20154548
rs978928	20175199	20175200
rs4462985	20650875	20650876
rs9835460	21063375	21063376
rs9835881	21063538	21063539
rs141920290	21165524	21165525
rs341835	21381589	21381590
rs9871863	21612524	21612525
rs2878597	21691718	21691719
rs2679803	40131748	40131749
rs9311256	41011014	41011015
rs62259232	41071164	41071165
rs10490823	41082243	41082244
rs386132	41101084	41101085
rs6772565	41115775	41115776
rs417183	41127360	41127361
rs9816052	41591835	41591836
rs4973974	41592827	41592828
rs1060330	52254928	52254929
rs7629072	52271616	52271617
rs2276834	52291742	52291743
rs7622851	52299654	52299655
rs9311474	52304835	52304836
rs4434138	52522873	52522874
rs7638808	52538039	52538040
rs6445528	52538430	52538431
rs1133415	52541814	52541815
rs4425219	70238974	70238975
rs13089371	70260573	70260574
rs1996818	70263632	70263633
rs4677611	71358738	71358739

rs Number	Start Position	Stop Position
rs13060421	71467705	71467706
rs11706279	71468491	71468492
rs35483362	71482315	71482316
rs13327339	71484226	71484227
rs305499	11951484	11951485

8.3 Workflows

8.3.1 Snakemake Workflow for mutation detection in *GNAQ* and *GNA11*

```
# A snakefile
import pandas as pd
configfile: 'config.yml'

df_fastq_files = pd.read_csv("Fastq_files_df.csv", sep=",",
                             index_col="Sample")

rule all:
    input:
      result_all_samples = "data_tables/all_vcf_dataframe.pdf"

rule vsearch_merge_R1_R2:
  input:
    read_1 = lambda wildcards: df_fastq_files.loc[wildcards.sample, 'R1'],
    read_2 = lambda wildcards: df_fastq_files.loc[wildcards.sample, 'R2']
  output:
    "merged_reads/{sample}.fastq"
  conda:
    "envs/vsearch.yaml"
  shell:
    """
    vsearch --fastq_mergepairs {input[0]} \
    --reverse {input[1]} \
    --fastq_allowmergestagger\
    --fastqout {output}
    """

rule vsearch_fastx_filter:
  input:
    "merged_reads/{sample}.fastq"
  output:
    "filtered_reads/{sample}.fastq"
  conda:
    "envs/vsearch.yaml"
  shell:
    """
    vsearch --fastx_filter {input} \
```

```
    --fastq_stripleft 40 \
    --fastq_stripright 40 \
    --fastqout {output}
    """

rule bwa_mem:
  input:
    reads=["filtered_reads/{sample}.fastq"]
  output:
    "mapped_reads/{sample}.bam"
  log:
    "logs/bwa_mem/{sample}.log"
  params:
    index=config["reference"],
    sorting="samtools",
    sort_order="coordinate"
  threads: 16
  wrapper:
    "0.80.2/bio/bwa/mem"

rule samtools_index:
  input:
    "mapped_reads/{sample}.bam"
  output:
    "mapped_reads/{sample}.bam.bai"
  log:
    "logs/samtools_index/{sample}.log"
  threads: 16
  wrapper:
    "0.80.2/bio/samtools/index"

rule freebayes:
  input:
    ref = config["reference"],
    ref_indexed = config["reference_indexed"],
    samples="mapped_reads/{sample}.bam",
    indexes="mapped_reads/{sample}.bam.bai",
    regions="GNAX.bed"
  output:
    "calls/{sample}.vcf",
  log:
    "logs/freebayes/{sample}.log",
  params:
    extra="-F␣0.001␣--report-monomorphic",
    chunksize=100000,
    normalize=False,
  threads: 16
  wrapper:
    "0.80.2/bio/freebayes"
```

```
rule vcf_analysis_R_all:
  input:
    expand("calls/{sample}.vcf", sample = df_fastq_files.index)
  output:
    "data_tables/all_vcf_dataframe.pdf"
  script:
    "scripts/Analyze_all_vcf.R"
```

8.3.2 Snakemake Workflow for determination of UMI corrected VAFs via debarcer

```
# A snakefile

import pandas as pd
configfile: 'config.yml'

df_reads = pd.read_csv("SampleIDtofastq.tsv",sep="\t",index_col='SampleID')
df_regions_no_index = pd.read_csv("SampleID_to_Region.tsv", sep="\t")

wildcard_constraints:
sample_id="[^/]+"

rule all:
  input:
    expand("VCFfiles/Repaired_for_R/{sample_id}_{region}.repaired.vcf", zip,
      sample_id = df_regions_no_index.iloc[:,0],
      region = df_regions_no_index.iloc[:,1]),

rule debarcer_preprocess:
  input:
    read_1 = lambda wildcards: df_reads.loc[wildcards.sample_id, 'R1'],
    read_2 = lambda wildcards: df_reads.loc[wildcards.sample_id, 'R2']

  output:
  "{sample_id}/{sample_id}.incorrect_reads.R1.fastq.gz",
    "{sample_id}/{sample_id}.incorrect_reads.R2.fastq.gz",
    "{sample_id}/{sample_id}.umi.reheadered_R1.fastq.gz",
    "{sample_id}/{sample_id}.umi.reheadered_R2.fastq.gz"
  params:
    output_dir = "./{sample_id}/",
    prepfile = "config/library_prep_types.ini"
  conda:
    "envs/debarcer.yaml"
  shell:
    """
    debarcer preprocess -o {params.output_dir} -r1 {input.read_1} \
    -r2 {input.read_2} -p "SIMSENSEQ-PE" -pf {params.prepfile} \
    -c config/NB_config_beeUbuntu_v2.ini -px {wildcards.sample_id}
```

```
    """

rule bwa_index:
  input:
    config["reference"]
  output:
    "refs/hg19-ucsc/hg19.amb",
    "refs/hg19-ucsc/hg19.ann",
    "refs/hg19-ucsc/hg19.bwt",
    "refs/hg19-ucsc/hg19.pac",
    "refs/hg19-ucsc/hg19.sa"
  log:
    "logs/bwa_index/hg19.log"
  params:
    prefix="hg19",
    algorithm="bwtsw"
  wrapper:
    "0.68.0/bio/bwa/index"

rule bwa_mem:
  input:
    reads = ["{sample_id}/{sample_id}.umi.reheadered_R1.fastq.gz",
        "{sample_id}/{sample_id}.umi.reheadered_R2.fastq.gz"]
  output:
    bam="{sample_id}/{sample_id}.sorted.bam"
  log:
    "logs/bwa_mem/{sample_id}.log"
  params:
    index="/media/nicole/Data/NGS_data/Reference_genome/hg19_bwa_index",
    sort="samtools",
    sort_order="coordinate",
    sort_extra=""
  threads: 8
  wrapper:"0.68.0/bio/bwa/mem"

rule samtools_index:
  input:
    "{sample_id}/{sample_id}.sorted.bam"
  output:
    "{sample_id}/{sample_id}.sorted.bam.bai"
  params:
    ""
  wrapper:
    "0.68.0/bio/samtools/index"

rule debarcer_group:
  input:
    bam_file = "{sample_id}/{sample_id}.sorted.bam",
    bam_index_file = "{sample_id}/{sample_id}.sorted.bam.bai"
```

```
  output:
    "{sample_id}/Umifiles/{region}.json",
    "{sample_id}/Datafiles/datafile_{region}.csv",
    "{sample_id}/Stats/Mapped_read_counts_{region}.json",
    "{sample_id}/Stats/UMI_relationships_{region}.txt",
    "{sample_id}/Stats/Umis_{region}_before_grouping.json"
  params:
    region_on_chr = "{region}",
    output_dir = "./{sample_id}/",
    config = "config/NB_config_beeUbuntu_v2.ini"
  conda:
    "envs/debarcer.yaml"
  shell:
    """
    debarcer group -o {params.output_dir} \
                -r {params.region_on_chr} \
    -b {input.bam_file} -c {params.config}
    """

rule debarcer_collapse:
  input:
    umi_file = "{sample_id}/Umifiles/{region}.json",
    bam_file = "{sample_id}/{sample_id}.sorted.bam",
    ref_file = config["reference"]
  output:
    cons_file = "{sample_id}/Consfiles/{region}.cons",
    final_cons_file = "ConsFiles/{sample_id}_{region}.cons"
  params:
    output_dir = "./{sample_id}/",
    region_on_chr = "{region}",
    famsize = "3",
    count_treshold = "1",
    percent_treshold = "50",
    max_depth = "1000000",
    truncate = "False",
    ignore_orphans = "False",
    stepper = "nofilter",
    config = "config/NB_config_beeUbuntu_v2.ini"
  conda:
    "envs/debarcer.yaml"
  shell:
    """
    debarcer collapse -b {input.bam_file} -u {input.umi_file} \
      -rf {input.ref_file} -o {params.output_dir} -r {params.region_on_chr} \
      -f {params.famsize} -ct {params.count_treshold} \
      -pt {params.percent_treshold} -m {params.max_depth} \
      -t {params.truncate} -i {params.ignore_orphans} \
      -stp {params.stepper} -c {params.config}
    touch {output.cons_file}
```

```
    cp -r {output.cons_file} {output.final_cons_file}
    exitcode=$?
      if [ $exitcode -eq 1 ]
      then
          exit 0
       else
          exit 0
      fi
    """

rule debarcer_call:
  input:
    cons_file = "{sample_id}/Consfiles/{region}.cons",
    ref_file = config["reference"]
  output:
    vcf_file = "{sample_id}/VCFfiles/{region}.cons_famsize_3.vcf",
    final_output = "VCFfiles/{sample_id}_{region}.cons_famsize_3.vcf"
  params:
    output_dir = "./{sample_id}/",
    famsize = "3",
    ref_threshold = "95",
    alt_threshold = "2",
    filter_threshold = "10"
  conda:
    "envs/debarcer.yaml"
  shell:
    """
    set +e
      debarcer call -rf {input.ref_file} -o {params.output_dir} \
        -f {params.famsize} -rt {params.ref_threshold} \
        -at {params.alt_threshold} -ft {params.filter_threshold} \
        -cf {input.cons_file}
    touch {output.vcf_file}
    cp -r {output.vcf_file} {output.final_output}
    exitcode=$?
      if [ $exitcode -eq 1 ]
      then
          exit 0
       else
          exit 0
      fi
    """


rule debarcer_report:
  input:
    expand("{sample_id}/VCFfiles/{region}.cons_famsize_3.vcf", zip,
      sample_id = df_regions_no_index.iloc[:,0],
      region = df_regions_no_index.iloc[:,1])
```

```
  output:
    "{sample_id}/Report/debarcer_report.html"
  params:
    sample_report = "{sample_id}_fam3_report"
  conda:
    "envs/debarcer.yaml"
  shell:
    """
    debarcer plot -d {wildcards.sample_id}/ -s {params.sample_report}
    """

rule vcf_repair:
  input:
    "VCFfiles/{sample_id}_{region}.cons_famsize_3.vcf"
  output:
    "VCFfiles/Repaired_for_R/{sample_id}_{region}.repaired.vcf"
  shell:
    """
    ./vcf-repair.py {input} {output}
    """
```

8.3.3 Snakemake Workflow for consensus calling and varlociraptor analysis

```
# A snakefile

import pandas as pd

sample_sheet = pd.read_csv("dataset_v3.csv", sep="\t").set_index("SampleID")
SAMPLES = sample_sheet.index.unique().to_list()


ruleorder: samtools_sort > merge_consensus_reads
ruleorder: samtools_sort > merge_replicates
ruleorder: varlociraptor_call > varlociraptor_preprocess


rule all:
    input:
        final="results/tables_plots/all_vcf_dataframe.pdf",


# Prerequisites:perform bcl2fastq using this command:
# bcl2fastq -R /path/to/RunFolder/ --create-fastq-for-index-reads \
        --use-bases-mask Y12N16,Y123,I6,Y151 --barcode-mismatches 0 \
        --mask-short-adapter-reads 0

# Getting and indexing reference
rule get_genome:
```

```
    output:
        "resources/genome.fa",
    params:
        species="homo_sapiens",
        datatype="dna",
        build="GRCh38",
        release="108",
    log:
        "logs/get_genome.log",
    cache: True  # between workflow caching
    wrapper:
        "v1.19.1/bio/reference/ensembl-sequence"

rule bwa_index:
    input:
        "resources/genome.fa",
    output:
        idx=multiext("resources/genome.fa",".amb",".ann",
        ".bwt",".pac",".sa"),
    log:
        "logs/bwa_index/hg38.log",
    params:
        algorithm="bwtsw",
    wrapper:
        "v1.19.1/bio/bwa/index"

rule genome_faidx:
    input:
        "resources/genome.fa",
    output:
        "resources/genome.fa.fai",
    log:
        "logs/genome.log",
    params:
        extra="",  # optional params string
    wrapper:
        "v1.19.1/bio/samtools/faidx"

# get input files for aligment, needed because of replicate analysis
def get_bwa_input(wc):
    if wc.replicate == "Rep1":
        return [sample_sheet.loc[wc.sample, read]
    for read in ["R1_noUMI", "R2_noUMI"]]
    else:
        return [sample_sheet.loc[wc.sample, read]
    for read in ["R1_2_noUMI", "R2_2_noUMI"]
        ]

# Generate aligment
```

```
rule bwa_mem:
    input:
        reads=get_bwa_input,
        idx=multiext("resources/genome.fa",".amb",".ann",
        ".bwt",".pac",".sa"),
    output:
        "results/mapped/{sample}_{replicate}.bam",
    wildcard_constraints:
        replicate="Rep1|Rep2",
    log:
        "logs/bwa_mem/{sample}_{replicate}.log",
    params:
        extra=r"-R␣'@RG\tID:{sample}\tSM:{sample}'",
        sorting="samtools",
        sort_order="coordinate",
        sort_extra="",  # Extra args for samtools/picard.
    threads: 8
    wrapper:
        "v1.19.1/bio/bwa/mem"

# needed because of replicate analysis
def get_umi(wc):
    if wc.replicate == "Rep1":
        umi = "UMI"
    else:
        umi = "UMI_2"
    return sample_sheet.loc[wc.sample, umi]

# consensus calling pipeline starts
rule annotate_umis:
    input:
        bam="results/mapped/{sample}_{replicate}.bam",
        umi=get_umi,
    output:
        "results/mapped/{sample}_{replicate}.annotated.bam",
    resources:
        mem_gb="10",
    log:
        "logs/fgbio/annotate_bam/{sample}_{replicate}.log",
    wrapper:
        "v1.19.1/bio/fgbio/annotatebamwithumis"

rule mark_duplicates:
    input:
        bams=["results/mapped/{sample}.annotated.bam"],
    output:
        bam="results/dedup/{sample}.bam",
        metrics="results/qc/dedup/{sample}.metrics.txt",
    log:
```

```
        "logs/picard/dedup/{sample}.log",
    params:
        extra="--BARCODE_TAG RX --TAG_DUPLICATE_SET_MEMBERS true",
    wrapper:
        "v1.19.1/bio/picard/markduplicates"

module consensus_reads:
    meta_wrapper:
        "v1.19.1/meta/bio/calc_consensus_reads"
    config:
        config

use rule * from consensus_reads

use rule calc_consensus_reads from consensus_reads with:
    input:
        "results/dedup/{sample}.bam",

def merge_replicates_input(wc):
    return [
        f"results/consensus/{wc.sample}_{replicate}.sorted.bam"
        for replicate in ["Rep1", "Rep2"]
    ]
#consensus calling pipeline ends

rule merge_replicates:
    input:
        lambda wc: merge_replicates_input(wc),
    output:
        "results/consensus_merged/{sample}.bam",
    log:
        "logs/samtools_merge/{sample}.log",
    threads: 8
    wrapper:
        "v1.19.1/bio/samtools/merge"


rule samtools_sort:
    input:
        "results/{folder}/{sample}.bam",
    output:
        "results/{folder}/{sample}.sorted.bam",
    log:
        "logs/sort/{folder}/{sample}.log",
    params:
        extra="-m 4G",
    wildcard_constraints:
        folder="consensus|consensus_merged",
    threads: 8
```

```
    wrapper:
        "v1.19.1/bio/samtools/sort"


rule samtools_index:
    input:
        "results/consensus_merged/{sample}.sorted.bam",
    output:
        "results/consensus_merged/{sample}.sorted.bam.bai",
    log:
        "logs/samtools_index/{sample}.log",
    params:
        extra="",  # optional params string
    threads: 8  # This value - 1 will be sent to -@
    wrapper:
        "v1.19.1/bio/samtools/index"


# Variant Calling using Freebayes to obtain candidates for Varlociraptor
rule freebayes:
    input:
        ref="resources/genome.fa",
        ref_index="resources/genome.fa.fai",
        samples="results/consensus_merged/{sample}.sorted.bam",
        indexes="results/consensus_merged/{sample}.sorted.bam.bai",
        regions="SNPs.bed",
    output:
        "results/calls/{sample}.vcf",
    log:
        "logs/freebayes/{sample}.log",
    params:
        extra="",
        chunksize=100000,
        normalize=False,
    threads: 16
    wrapper:
        "v1.19.1/bio/freebayes"

# variant calling via Varlociraptor
rule varlociraptor_preprocess:
    input:
        ref="resources/genome.fa",
        bam="results/consensus_merged/{sample}.sorted.bam",
        bam_index="results/consensus_merged/{sample}.sorted.bam.bai",
        bcf="results/calls/{sample}.vcf",
    output:
        bcf="results/varlociraptor/{sample}.bcf",
    log:
        "logs/varlociraptor_preprocess/{sample}.log",
```

```
    conda:
        "envs/varlociraptor.yaml"
    shell:
        """
        varlociraptor preprocess variants {input.ref} --bam {input.bam} \
       --candidates {input.bcf} > {output.bcf} 2> {log}
        """

rule varlociraptor_call:
    input:
        obs="results/varlociraptor/{sample}.bcf",
        ref="resources/genome.fa",
        scenario="Scenario.yaml",
    output:
        "results/varlociraptor/{sample}_calls.bcf",
    params:
        mode="generic",
        bias="--omit-alt-locus-bias --omit-read-orientation-bias \
       --omit-read-position-bias --omit-softclip-bias \ --omit-strand-bias"
    log:
        "logs/varlociraptor_call/{sample}.log",
    conda:
        "envs/varlociraptor.yaml"
    shell:
        """
        varlociraptor call variants {params.bias} --output {output} \
        {params.mode} --scenario {input.scenario} \
        --obs blood={input.obs} 2> {log}
        """

rule bcf_to_vcf:
    input:
        "results/varlociraptor/{sample}_calls.bcf",
    output:
        "results/varlociraptor/{sample}_calls.vcf",
    log:
        "logs/bcf_to_vcf/{sample}.log",
    wrapper:
        "v1.19.1/bio/bcftools/view"

#use external R script for further analysis of vcf files
rule vcf_analysis_R_all:
    input:
        expand("results/varlociraptor/{sample}_calls.vcf", sample=SAMPLES),
    output:
        "results/tables_plots/all_vcf_dataframe.pdf",
        "results/tables_plots/Probability_LOH_groups.png",
        "results/tables_plots/Scores_posterior_odds.png",
    conda:
```

```
        "envs/R.yaml"
    script:
        "scripts/Analyze_results_v4.R"
```

8.4 Supplementary Figures

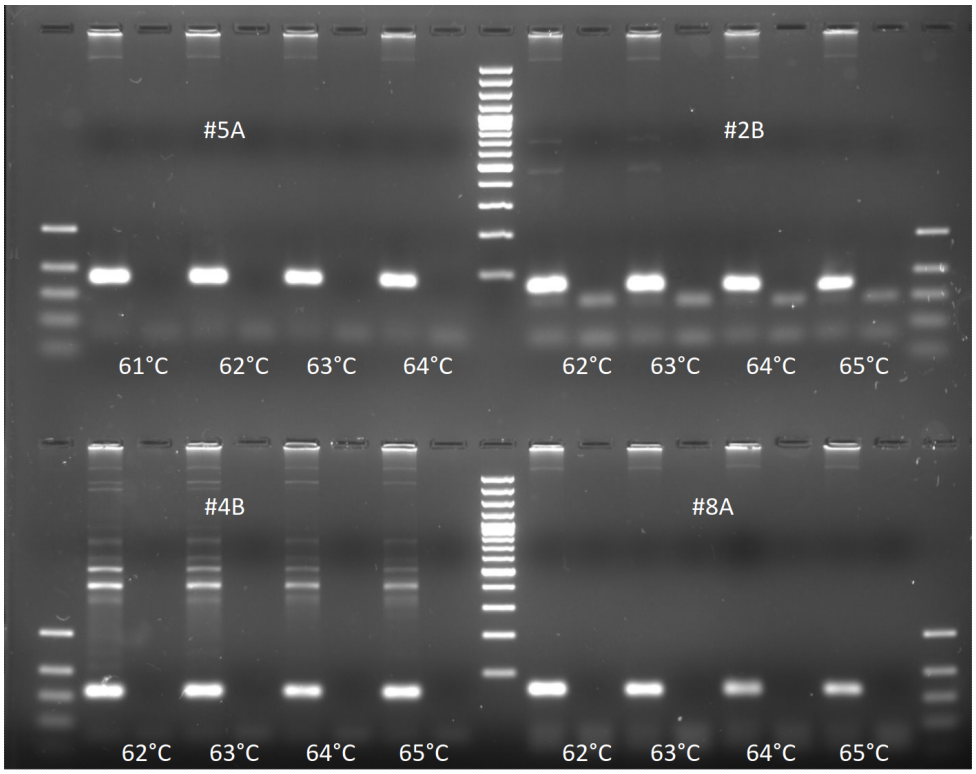

Figure 50: Optimization of annealing temperature for PCR using standard primers. Temperatures indicate the annealing temperature, numbers after # indicate the SNP and the A or B indicates the primer set used. Genomic DNA from a healthy donor was used for this test. Analysis was performed via agraose gel electrophoresis.

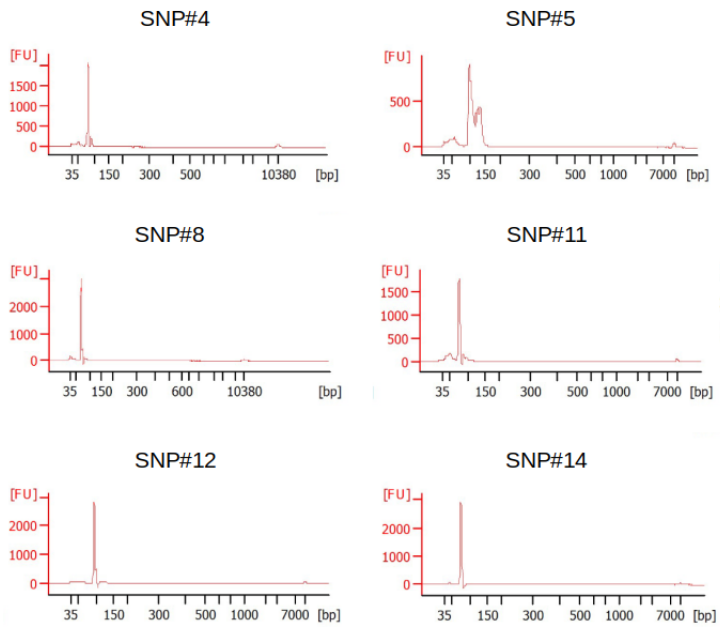

Figure 51: Fragment analysis for testing of target primers. Analysis was performed using a Bioanalyzer (Agilent) and a High Sensitivity Reagent Kit (Agilent). Genomic DNA from a healthy donor was used for this test.

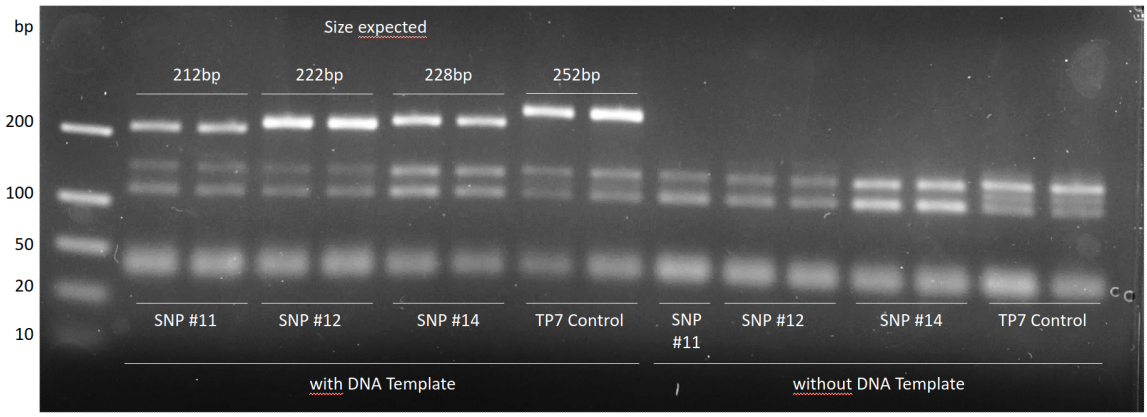

Figure 52: Analysis of fragment sizes of adapter PCR products. Analysis was performed via agraose gel electrophoresis. The expected product size is indicated on the top. Genomic DNA from a healthy donor was used for this test. Analysis was performed via agraose gel electrophoresis.

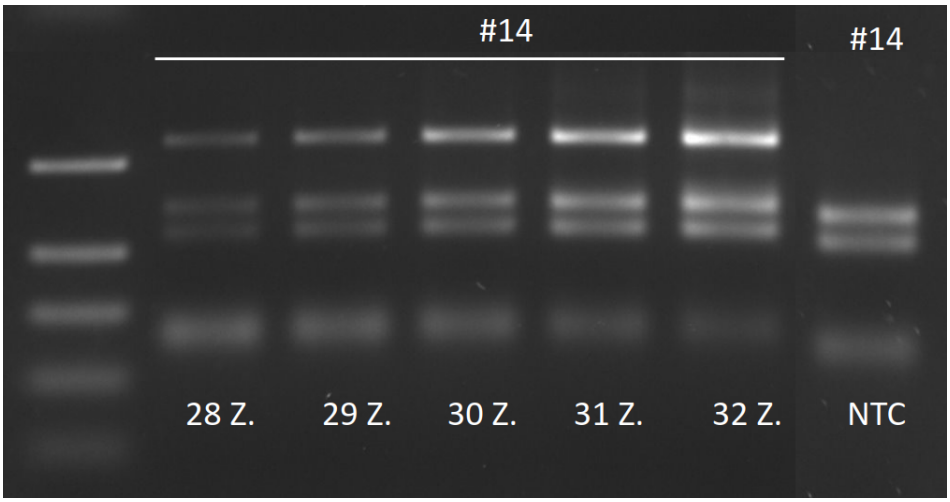

Figure 53: Optimization of number of cycles of adaptor PCR. Analysis was performed via agraose gel electrophoresis and based on SNP14. Genomic DNA from a healthy donor was used for this test. The number of cycles of Adaptor PCR is indicated on the bottom of the figure.

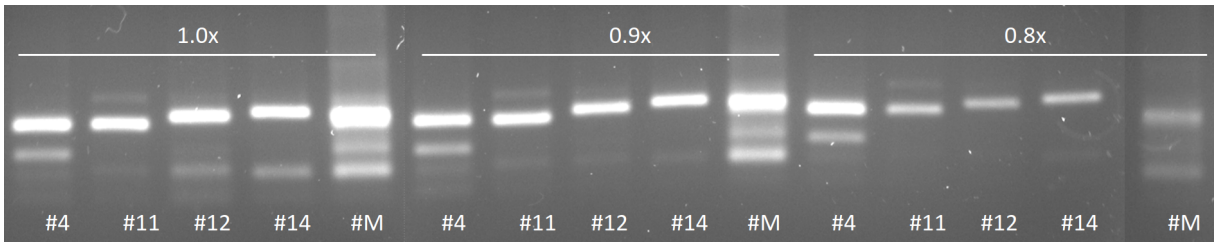

Figure 54: Bead ratio test Analysis was performed via agraose gel electrophoresis and based on SNPs 11,12 and 14 as indicated on the bottom of the figure. Genomic DNA from a healthy donor was used for this test. The bead ratios tested are indicated on the top of the figure. Library preparation and bead purification were performed according to Ståhlberg et al. (2017).

8.5 Glossary

Term	Definition
component	In the context of liquid biopsies, the cellular or cellfree part of the primary sample.
subcomponent	Element of a component of a liquid biopsy. For example, tumor cells and normal cells as subcomponents of the cellular component.
biomolecule	A molecule of biological origin. In the context of biomarker testing, quantitative and/or qualitative characteristics of this molecule can be used as a biomarker.
biomarker	"A defined characteristic that is measured as an indicator of normal biological processes, pathogenic processes, or biological responses to an exposure or intervention, including therapeutic interventions. Biomarkers may include molecular, histologic, radiographic, or physiologic characteristics. A biomarker is not a measure of how an individual feels, functions, or survives." (FDA-NIH Biomarker Working Group 2016)
Variant allele fraction	The number of reads of an alternate allele at a given locus devided by the total number of reads at that locus.
liquid biopsy	A primary sample consisting of any kind of body fluid.
liquid biosy examination	The complete process of analysis of a liquid biopsy.
prognostic biomarker	"A biomarker used to identify likelihood of a clinical event, disease recurrence or progression in patients who have the disease or medical condition of interest."(FDA-NIH Biomarker Working Group 2016)
diagnostic biomarker	"A biomarker used to detect or confirm presence of a disease or condition of interest or to identify individuals with a subtype of the disease."(FDA-NIH Biomarker Working Group 2016)
EV-DNA	Double-stranded DNA that is located inside extracellular vesicles or attached to their surface.

cfDNA	DNA contained in the cellfree component of a liquid biopsy.
incomplete penetrance	A reduced likelihood that a phenotype is expressed if a particular genotype is present (e.g., absence of tumor in an individual with a heritable predisposition to tumor development).
analyt	The part of a sample, that is investigated in an analysis.
measurand	A characteristic to be measured.
validation	of an examination procedure: Confirming that an analytical procedure is suitable for the intended use. of an analytical result: Providing objective evidence that the result is correct, for example by reproducing the result with indepentend methods.
informative SNP	A single nucleotide polymorphism locus that is heterozygous in a given individual (i.e. has an allelic ratio other than 0 or 1).
primary sample	A sample that is directly obtained from a patient.

List of Figures

List of Tables

List of abbreviations

AH	aqueous humor
ASXL1	ASXL transcriptional regulator 1
BAP1	BRCA1-associated protein 1
bp	basepairs
BRAF	B-Raf Protooncogene
cfDNA	cell-free DNA
CTCs	Circulating Tumor Cells
ctDNA	cell-free tumour DNA
DAG	Directed Acyclic Graph
ddPCR	Droplet Digital PCR
dsDNA	Double-stranded DNA
EGFR	Epidermal Growth Factor Receptor
EIF1AX	Eukaryotic Translation Initiation Factor 1A
EpCAM	epithelial cell adhesion molecule
EV-DNA	extracellular vesicle derived DNA
EVs	Extracellular vesicles
FNA	fine needle aspiration
GEs	genome equivalents
GNA11	guanine nucleotide-binding protein, alpha-11
GNAQ	guanine nucleotide-binding protein, Q polypeptide
ILVs	intraluminal vesicles
kbp	kilo basepairs
KRAS	KRAS Protooncogene
LD	Linkage Disequilibrium
LoD	limit of detection

LOH	Loss of heterozygosity
MBp	Mega Basepairs
mtDNA	mitochondrial DNA
MVBs	multivesicular bodies
MVEs	multivesicular endosomes
MVs	microvesicles
MYCN	MYCN Proto-Oncogene
NCBI	National Center for Biotechnology Information
NGS	Next generation sequencing
NSCLC	non-small cell lung cancer
PBS	Phosphate-buffered saline
PCR	Polymerase Chain Reaction
PEG	polyethylene glycol
qPCR	quantitative Real Time PCR
RB1	RB transcriptional co-repressor 1
RT	room temperature
SCNAs	Somatic copy number alteration
SEC	size exclusion chromatography
SF3B1	splicing factor 3B, subunit 1
SiMSen-seq	Simple, multiplexed, PCR-based barcoding of DNA for sensitive mutation detection using sequencing
STR	Short Tandem Repeat
TP53	tumor protein 53
UC	ultracentrifugation
UCH	ubiquitin C-terminal hydrolase
uEVs	urine derived extracellular vesicles
UM	uveal melanoma

UMIs	unique molecular identifiers
VAF	Variant Allele Fraction
VB	vitreous body
vcf-file	variant call format file
WGS	Whole Genome Sequencing

Danksagung

Als ich meine Promotion im Dezember 2018 begann hatte ich eine Menge über Bienengenetik gelernt, nicht aber über Humangenetik oder Bioinformatik. Heute, vier Jahre später stehe ich am Ende meiner Promotion und hinter mir liegt eine Zeit, in der ich unfassbar viel gerlent habe, in der meine Frustrationstoleranz weiter gestiegen ist und in der ich einmal mehr gelernt habe Herausforderungen zu meistern und niemals aufzugeben. An dieser Stelle möchte ich mich bei all denjenigen bedanken, die mich in den letzten vier Jahren begleitet und unterstzützt haben.

Herrn Prof. Dr. Dietmar Lohmann danke ich für die Übernahme des Erstgutachtens, Frau Prof. Dr. Anke Hinney danke ich für die Übernahme des Zweitgutachtens.

Das im Rahmen dieser Arbeit durchgeführte NIRBTEST Projekt wurde vom Transcan Netzwerk und dem Bundesministerium für Bildung und Forschung finanziert und von der Kinderaugenkrebsstiftung unterstützt. Hierfür möchte ich mich herzlich bedanken.

Ich bedanke mich bei Prof. Dr. Dietmar Lohmann und PD. Dr. Petra Ketteler für die Betreuung meiner Doktorarbeit, die Möglichkeit meine Dissertation am Institut für Humangenetik sowie in der Kinderklinik des Universitätsklinikums Essen anfertigen zu dürfen und die Bereitstellung des sehr interessanten Forschungsprojektes. Vielen Dank für all die Anregungen, die Kritik, die wissenschaftlichen Diskussionen, eure Ideen und die Möglichkeit an Konferenzen teilzunehmen.

Lieber Dietmar, danke für alles was ich in dieser Zeit lernen durfte, insbesondere im puncto Statistik und Bioinformatik. Danke, dass du mich Holzwege hast beschreiten lassen und dass ich meine eigenen Erfahrungen sammeln durfte. Danke auch für sehr bereichernde Gespräche über Bienen, Fotografie oder nordische Länder. Auch für das zur Verfügung stellen der benötigten Rechenpower und die Unterstzützung bei technischen Problemen danke ich dir. Liebe Petra, vielen Dank dass du trotz deines Sabbaticals immer Zeit für mich hattest und mich unterstzützt hast wo du nur konntest. Danke für alles was ich von dir lernen durfte und für all deine Bemühungen, insbesondere bei der Patientenrekrutierung.

So groß wie die Herausforderungen waren, die das Thema dieser Arbeit mit sich brachte, so viel habe ich bei der Bearbeitung gelernt und so sehr konnte ich mein Methodenspektrum erweitern. Danke für den vielen Freiraum, den ihr mir gewährt habt und dass ich selbstständig und eigenverantwortlich arbeiten durfte, aber immer auf eure Unterstzützung bei der Entscheidungsfindung bauen konnte. Das hohe Maß an Vertrauen, dass ihr mir entgegengebracht habt war für mich nie selbstverständlich. Auch Zwischenmenschlich hattet ihr stets ein offenes Ohr und sehr viel Verständnis, vielen Dank dafür!

Herrn Dr. Michael Zeschnigk danke ich für die herzliche Aufnahme, die Bereitstellung des sehr interessanten Themas zum Aderhautmelanom und die Übernahme der Co-Betreuung. Lieber Michael, vielen Dank, dass du mich auch bei meinem Rb-Projekt jederzeit unterstützt hast wo du nur konntest. Danke, dass ich das Aderhautmelanom-Projekt mit dir starten durfte, es hat mir wirklich sehr viel Spaß gemacht daran zu arbeiten und ich habe sehr viel dabei gelernt.

Herrn Prof. Dr. Bernhard Horsthemke und Herrn Prof. Dr. Frank Kaiser danke ich für die Möglichkeit meine Arbeit am Institut für Humangenetik durchzuführen. Danke für die anregende Kritik und die bereichernden wissenschaftlichen Diskussionen.

Herrn Dr. Johannes Köster und Herrn Felix Mölder danke ich für die Unterstützung bei der Etablierung der Snakemake-Pipelines. Lieber Johannes, vielen Dank für deine Unterstützung bei meinem Projekt, für die Zeit die du dir genommen hast, für die Diskussionen, die meine Arbeit sehr bereichert haben und die Erklärungen, die mir Snakemake und die Bioinformatik im Allgemeinen näher gebracht haben. Lieber Felix, vielen Dank für die Zeit, die du geopfert hast und die Geduld, die du mit mir hattest. Herrn Dr. Christopher Schröder danke ich für die bereichernden Gespräche und das zur Verfügung stellen der Abbildung zur ctDNA. Herrn Dr. Fabian Kilpert danke ich für die Hilfe bei technischen und bioinformatischen Fragen. Lieber Christo, lieber Fabian, ich möchte euch auch für den Zugang zu eurem Server und dem Netzwerk der Genominformatik danken, ihr habt mir das Leben mit Pinguin sehr viel leichter gemacht.

Bei den Patienten, die an der NIRBTEST Studie teilgenommen haben bedanke ich mich herzlich für ihr Teilnahme, ihr Engagement und die Bereitschaft zur Blutspende. Ohne Ihren Beitrag wäre dieses Forschungsprojekt nicht möglich gewesen.

Bei den Kooperationspartnern, die an dem NIRBTEST Projekt beteiligt waren bedanke ich mich für die tolle Zusammenarbeit und den bereichernden wissenschaftlichen Austausch. Es war großartig Teil eines eropäischen Projektes sein zu dürfen. Bei Frau Dr. Armida Fabius bedanke ich mich für die Projektkoordination.

Frau Maren Wagemanns und allen Mitarbeitern des Rb-Registers danke ich für die unermüdliche Dokumentation der Patiendaten und die Unterstützung bei den Blutentnahmen. Liebe Maren, danke auch für den Austausch von Doktorandin zu Doktorandin und die tolle Zusammenarbeit.

Der Augenklinik am Universitätsklinikum Essen danke ich für die Zusammenarbeit bei der Patientenrekrutierung und Probenentnahme. Frau Dr. Saskia Ting aus dem Institut für Pathologie danke ich für die Hilfe bei der Sammlung von pathologischem Probenmaterial.

Herrn Dr. Thakur und Frau Dr. Kontopoulo danke ich für die Unterstzützung bei der Arbeit mit extrazellulären Vesikeln.

Herrn Prof. Dr. Nils von Neuhoff danke ich für die Zurverfügungstellung der Droplet Digital PCR. Herrn Prof. Dr. Bernd Giebel danke ich für die Bereitstellung des ZetaView und der Ultrazentrifuge. Der Genomics and Transcriptomics Facility danke ich für die Möglichkeit den MiSeq und das RealTime PCR Gerät zu nutzen. Lieber Herr Dr. Scholtysik, vielen Dank für Ihre Unterstzützung und die sehr lehrreichen Diskussionen. Liebe Frau Senkel, liebe Frau Kruse, danke dass Sie all meine Sonderwünsche ermöglicht haben.

Bei Martina Fleuringer, Martina Klutz, Lars Maßhöfer und Nina Bludau möchte ich mich für die tatkräftige Unterstützung bei meinem Projekt bedanken. Danke für zahlreiche DNA Isolationen, die Unterstzützung bei Sequenzierungen aller Art und die Einwiesung in jegliche Laborabläufe und SOPs. Danke aber auch, dass ihr mich so herzlich aufgenommen habt und ich bei euch eine so tolle und freundschaftliche Arbeitsatmosphäre erfahren durfte.

Dr. Theresa Kühnel, Julia Wöstefeld, Dr. Deniz Kanber und Dr. Jasmin Beygo danke ich für die Beantwortung jeglicher Fragen, die anregenden Diskussionen und die großartige Hilfsbereitschaft. Auch möchte ich euch für die tolle Aufnahme am Institut für Humangenetik, den ein oder anderen Escape Room und die gemeinsamen Essen bedanken, es hat mir sehr viel Spaß gemacht mit euch.

Liebe Julia, liebe Theresa, danke auch für eure Unterstützung im Labor, eure Freundschaft und die Hilfe bei unseren Hochzeitsvorbereitungen. Ich freue mich schon auf die nächste Wonder Wafell mit euch. Liebe Julia, danke für deine Unterstützung und Motivation während des Schreibprozesses. Es war schön diesen letzten Teil des Weges nicht alleine gehen zu müssen und jemanden zu haben, der einem in den tiefen Tälern der Achterbahn sagt, dass es auch wieder nach oben gehen wird.

Allen Mitarbeitern des Instituts für Humangenetik danke ich für die herzliche Aufnahme, die ständige Hilfsbereitschaft, die tolle Arbeitsatmosphäre, das Interesse an und die Unterstützung bei meiner Arbeit.

Meinen Freunden danke ich für die Unterstützung in allen Lebenslagen, die Motivation und den Ausgleich zum Arbeitsalltag. Besonders bedanken möchte ich mich bei Lisa, Janine, Patti und Jacky, ihr seid großartig, bitte bleibt genau so wie ihr seid. Danke für die Brettspielabende, den spontanen Besuch aus Münster, die Nervennahrung und die Escape Rooms. Liebe Jacky, liebe Lisa, danke auch für die Korrektur meiner Arbeit.

Ich bedanke mich bei meinen Eltern, die mich mein Leben lang unterstzützt und mir stets mit Rat und Tat zur Seite gestanden haben. Ohne euch wäre ich nicht so weit gekommen, aber noch viel wichtiger: Ohne euch wäre ich nicht der Mensch, der ich heute bin. Ihr seid mein Ursprung, mein Vertrauen, meine Insel und mein Schatz. Mein Mund formt euer Lachen, mein Herz schlägt euren Takt.

Ich danke meinem Mann für alles, was er für mich getan hat. Insbesondere für sein Feedback zu meiner Arbeit und für die Hilfe bei Python und LaTeX und anderen informatischen Problemen. Du hast mir geholfen diese vier Jahre mit all ihren Höhen und Tiefen durchzustehen und niemals aufzugeben. Du bist mein Ankerplatz, mein Ruhepol und mein Refugium. Ich kann mir ein Leben ohne dich nicht mehr vorstellen und bin glücklich dich für immer an meiner Seite zu wissen. Danke, dass es dich gibt.

Curriculum Vitae

Der Lebenslauf ist in der Online-Version aus Gründen des Datenschutzes nicht enthalten.

Eidesstattliche Erklärung

Erklärung

Hiermit erkläre ich, gem. § 7 Abs. (2) d) + f) der Promotionsordnung der Fakultät für Biologie zur Erlangung des Dr. rer. nat., dass ich die vorliegende Dissertation selbständig verfasst und mich keiner anderen als der angegebenen Hilfsmittel bedient, bei der Abfassung der Dissertation nur die angegeben Hilfsmittel benutzt und alle wörtlich oder inhaltlich übernommenen Stellen als solche gekennzeichnet habe.

Essen, den _____ _____

Doktorandin

Erklärung

Hiermit erkläre ich, gem. § 7 Abs. (2) e) + g) der Promotionsordnung der Fakultät für Biologie zur Erlangung des Dr. rer. nat., dass ich keine anderen Promotionen bzw. Promotionsversuche in der Vergangenheit durchgeführt habe und dass diese Arbeit von keiner anderen Fakultät/-Fachbereich abgelehnt worden ist.

Essen, den _____ _____

Doktorandin

Erklärung

Hiermit erkläre ich, gem. § 6 Abs. (2) g) der Promotionsordnung der Fakultät für Biologie zur Erlangung der Dr. rer. nat., dass ich das Arbeitsgebiet, dem das Thema „Analysis of biomarkers in liquid biopsies for prognostic and diagnostic testing in patients with retinoblastoma and uveal melanoma“ zuzuordnen ist, in Forschung und Lehre vertrete und den Antrag von Nicole Barwinski befürworte.

Essen, den _____ _____

Prof. Dr. med. Dietmar Lohmann